Dynamic model for the formation and evolution of the Pannonian Basin:

The link between tectonics and sedimentation

Een dynamisch model voor de vorming en evolutie van het Pannoonse Bekken:

Het verband tussen tektoniek en sedimentatie

(met een samenvatting in het Nederlands)

Proefschrift

ter verkrijging van de graad van doctor aan de Universiteit Utrecht op gezag van de rector magnicus, prof.dr. G.J. van der Zwaan, ingevolge het besluit van het college voor promoties in het openbaar te verdedigen op donderdag 6 juli 2017 des avonds te 6.00 uur

door

Attila Balázs

geboren op 20 januari 1989 te Szeged, Hongarije

Promotoren:	Prof. dr. S.A.P.L. Cloetingh
	Prof. dr. F. Horváth
Copromotor:	Dr. L.C. Matenco

This study was financially supported by the Netherlands Research Centre for Integrated Solid Earth Sciences.

"*Most events and phenomena are connected, caused by, and interacting with a huge number of other pieces of a complex universal puzzle.*"

Albert-László Barabási

"*I see injustice beyond reason*
And then I find hope in Nature's reasoned chaos"

Bilal Haq

Members of the Reading Committee:

Prof. Dr. T. Gerya	Swiss Federal Institude of Technology (ETH) Zürich
Prof. Dr. C. Gaina	University of Oslo, Norway
Prof. Dr. M. Scheck-Wenderoth	GFZ Helmoltz Centre Potsdam, Germany
Prof. Dr. G.V. Bertotti	Delft University of Technology, the Netherlands
Dr. D. Granjeon	IFP Energies Nouvelles, France

The research presented in this thesis was carried out at:

- Tectonics Research Group, Department of Earth Sciences, Faculty of Geosciences, Utrecht University, the Netherlands;
- Department of Geophysics and Space Sciences, Institute of Geography and Earth Sciences, Eötvös Loránd University, Budapest, Hungary;
- Department of Geology-Geophysics-Geochemistry, IFP Energies Nouvelles, Rueil-Malmaison, France.

This is Utrecht Studies in Earth Sciences volume 132

ISBN: 978-90-6266-474-0

Printed in the Netherlands

Cover: Coherency seismic attribute map calculated on a 3D seismic time slice from the Great Hungarian Plain. Red colour shows similar seismic channels, while brown and grey colours highlight discontinuities related to sedimentary channels and faults.

Contents

1. Introduction

Extensional basins play a prime role in the spectrum of sedimentary basins covering large areas of the Earth and containing important energy resources. Quantifying their thermo-mechanical properties, tectonic and sedimentary processes that exert first-order control on basin formation and evolution is important for understanding the dynamics of System Earth. The formation and evolution of extensional basins and associated differential vertical movements are primarily controlled by the overall crustal and lithospheric thinning linked to their rheological layering, amount and rates of extension, and also linked to surface processes, in terms of erosion and sedimentation coupled with climatic variations (e.g., *Burov and Poliakov*, 2003, *Cloetingh and Haq*, 2015). Furthermore, deep mantle processes may have a strong impact in modifying their evolution by creating dynamic topography (*Cloetingh and Willett*, 2013; *Faccenna et al.*, 2014) and change the overall basin stratigraphy (e.g., *Petersen et al.*, 2010). Thanks to the existing advanced knowledge from the Pannonian Basin (Figure 1.1) and the surrounding Alpine-Carpathian-Dinaridic system (*Horváth et al.*, 2006, 2015; *Cloetingh et al.*, 2006; *Ustaszewski et al.*, 2008; *Matenco et al.*, 2016 and references therein), this region provides a key natural laboratory for the development and verification of a new generation of tectono-sedimentary models for extensional basins formed in a back-arc setting.

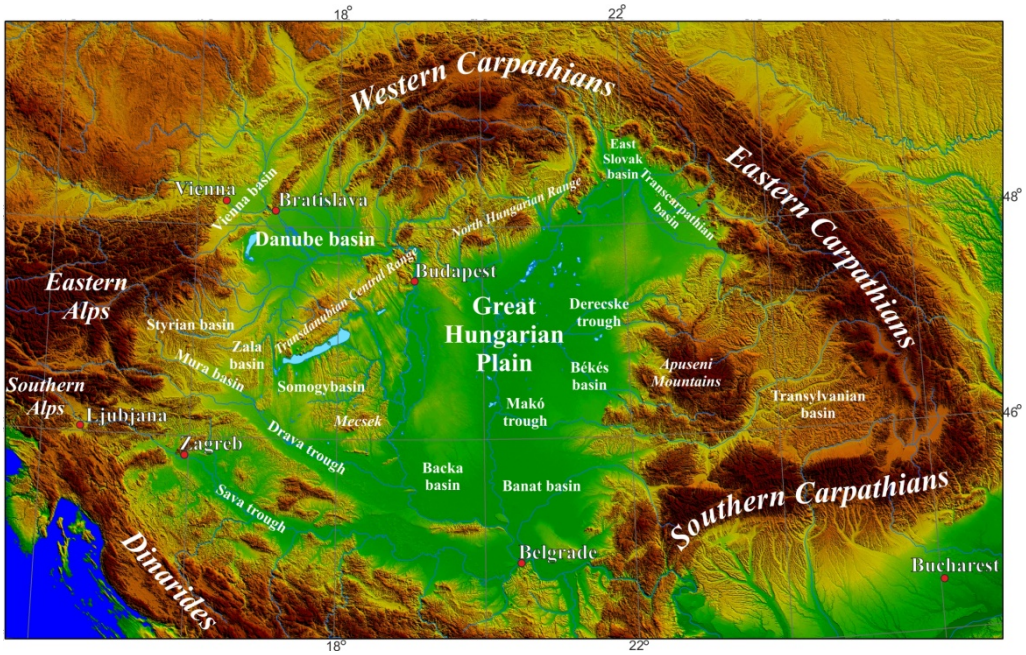

Figure 1.1: Digital elevation model of the Pannonian Basin and surrounding orogens (after *Horváth et al.*, 2015).

1.1 The Pannonian Basin system within the Alpine-Mediterranean region

The Mediterranean region is a wide zone of convergence between the Eurasian and African plates. A noteworthy feature of this setting is the abundance of extensional basins overlying former orogenic structures. Their formation was coupled with oroclinal bending, block rotations and orogen-parallel displacement of tectonic units (Figure 1.2; *Dewey*, 1980; *Horváth and Berckhemer*, 1982). These extensional back-arc basins are associated with roll-back of oceanic slabs and the retreat of the subduction fronts where the rate of subduction is higher than the convergence velocity. The Pannonian Basin of Central Europe has always been considered to be a typical example of such a continental extensional back-arc basin, extensively studied with a large number of seismic, well and other geophysical data on subsurface geology and lithospheric structure. The first seismic experiments that studied the crustal structure of the Pannonian region already showed that the Moho below the Great Hungarian Plain is located at a considerably shallow position at ca. 22 km (e.g., *Gálfi and Stegena*, 1955). Similar geophysical data acquisition campaigns and available well data enabled the Pannonian Basin to be amongst the first natural laboratories to test classical stretching models and their subsequent modifications (*Sclater et al.*, 1980). Such 1D thermo-mechanical models implied that extension in the region was associated with pronounced crustal thinning, and locally, extremely high lithospheric mantle thinning values (~10-50, *Horváth et al.*, 1988; *Lenkey*, 1999; *Horváth et al.*, 2015). This heterogeneous extension is reflected by the variety of deep sub-basins and basement highs in the Pannonian Basin (Figure 1.2). Their complex tectonic settings are reflected in the calculated basin subsidence histories (Figure 1.3).

1.2 Research objectives

Building on the large amount of geological and geophysical information available in the Pannonian Basin and its analogues elsewhere, this thesis aims to improve our understanding on the connections between tectonic and surface processes in extensional back-arc basins. Classical models on the extension of the Pannonian Basin (e.g., *Horváth and Royden*, 1988) described fixed boundaries for its syn-rift and post-rift evolution. However, more recent studies (e.g., *Matenco and Radivojević*, 2012; *Balázs et al.*, 2013; *Fodor et al.*, 2013; *ter Borgh*, 2013; *Horváth et al.*, 2015) proposed a more dynamic evolution for the main extensional events.

The focus of this thesis is to understand the dynamics of basin evolution in areas characterized by migration of extensional events in time and space, their implications for the associated syn- and post- rift sedimentation and the interplay with other external and internal forcing factors, such as climate, external sediment influx, sourcing by uplifting footwalls, creation of diachronous and synchronous

unconformities and sedimentation cycles. This research aims to define phenomenological evolutionary models of basin evolution from lithospheric to local basin-scale and subsequently quantify the main controlling factors by conducting a series of numerical models.

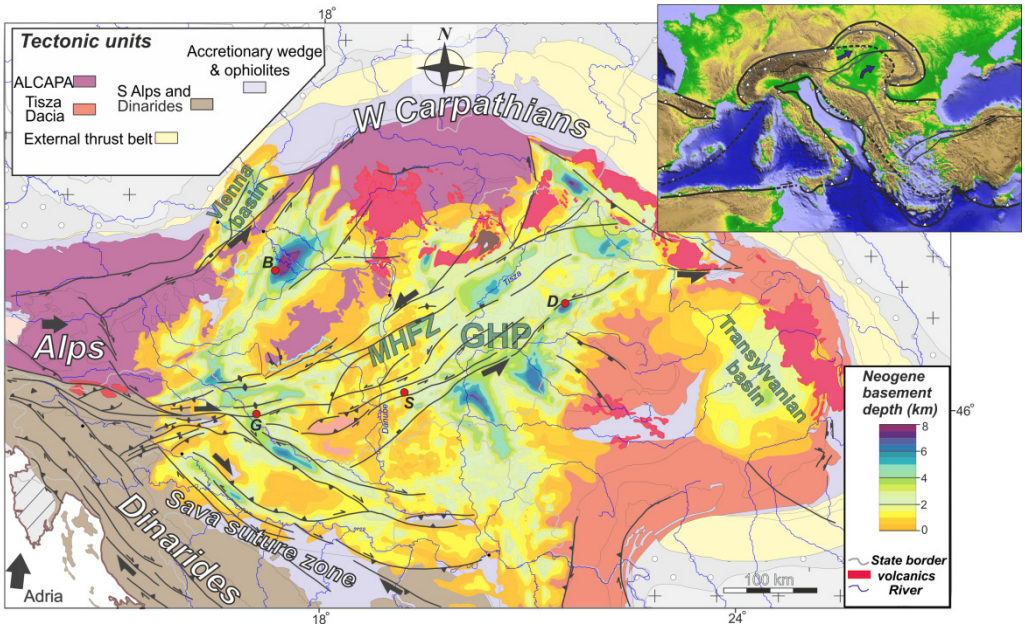

Figure 1.2: Simplified tectonic map (after *Schmid et al.*, 2008) showing the main neotectonic fault pattern (modified after *Bada et al.*, 2007) and the present-day Miocene-Quaternary sedimentary thickness in the Pannonian, Vienna and Transylvanian basins. The ALCAPA mega-unit in the north (in purple) is an Adriatic-derived unit, while Tisza-Dacia in the south (in orange) is a unit with mixed affinities. In between, the Mid-Hungarian Fault Zone (MHFZ) accommodated the change in polarity from the southward subduction of the Alpine Tethys in the Alps-Carpathians to the northward subduction of the Neotethys in the Dinarides (*Balla*, 1986; *Csontos and Nagymarosy*, 1998; *Handy et al.*, 2015). GHP – Great Hungarian Plain. Red circles indicate well locations of Figure 1.3. B – Bősárkány well of the Danube Basin, G – Gyékényes well from the northernmost Dráva sub-basin, D - Derecske sub-basin, S – Soltvadkert well from the Danube-Tisza interfluve.

The observation of a thin syn-rift and thick post-rift sedimentary fill in the centre of the Pannonian Basin has been interpreted as a consequence of depth-dependent stretching, necking depth, or intraplate stresses (e.g., *Royden and Dövényi*, 1988; *Lankreijer et al.*, 1995; *Horváth and Cloetingh*, 1996; *Huismans et al.*, 2001). A large number of new, deep well data enables the re-calculation of basement and tectonic subsidence histories (Figure 1.3) from the main sub-basins together with detailed seismic and wells interpretation. This has demonstrated a migration of tectonic and sedimentological events in time and space during and after the observed rifting moments. Such high-resolution observations enable the application of a wide range of numerical modelling techniques, such as lithospheric-scale thermo-

mechanical or basin-scale stratigraphic modelling that are able to couple the deep and surface processes during basin evolution.

Previous observations and large-scale modelling have shown that back-arc extension post-dates at relatively short times the orogenic nappe stack contraction by often reactivating thrust contacts or suture zones and exhumes rocks previously buried at high depth (e.g., *Brun and Faccenna*, 2008). The Pannonian Basin provides an appropriate natural laboratory to study such major tectonic reactivations (e.g., *Fodor et al*., 2005; *Windhoffer et al.*, 2005), where extensional reactivation of suture zones or nappe contacts was often observed in particular at its southern and western margins (*Horváth and Rumpler*, 1984; *Tari et al.*, 1992; *Ustaszewski et al.*, 2010; *Matenco and Radivojević*, 2012). This provides an appropriate opportunity to understand the effects of lithospheric-scale rheological heterogeneities and their role in basin formation.

Classical sequence stratigraphy has been developed in passive-margin settings (e.g., *Vail et al.*, 1977; *van Wagoner*, 1990), where the rates and variability of tectonic subsidence is minor in comparison with active rift basins or in back-arc areas (e.g., *Prosser et al*., 1993; *Nottvedt et al*., 1995; *Martins-Neto and Catuneanu*, 2010). Sediment cyclicity and the overall sedimentary architecture of asymmetric extensional basins, driven by the activity of one major normal fault or detachment and associated with footwall exhumation, is less understood. This understanding is important in the context of the formation of tectonically and climatically controlled rift cycles, and their links to external and footwall-derived sediment sources with the overall asymmetric tectonic subsidence.

These outstanding questions are addressed in this thesis by starting from an observational model for the syn- and post-rift evolution of the Pannonian extensional back-arc basin. This model is built by the interpretation of a dense network of 2D and 3D seismic data calibrated by well data and supported by other geophysical and geological constraints. This model crosses the spatial scales by studying both the regional lithospheric to crustal geometries and their upscaling in high-resolution sedimentation, coupled with their evolution with time. Furthermore, process-oriented numerical modelling techniques have been applied to build and validate tectonic and stratigraphic concepts by quantifying the effects of different geometries, boundary conditions and forcing factors.

Figure 1.3 (facing page): Subsidence history curves from Pannonian sub-basins. For well location see Figure 1.2. SA – sediment burial, TSW – water loaded tectonic subsidence history, TSR – tectonic subsidence rate. Note the migration of active depocentres and the variable subsidence and uplift rates.

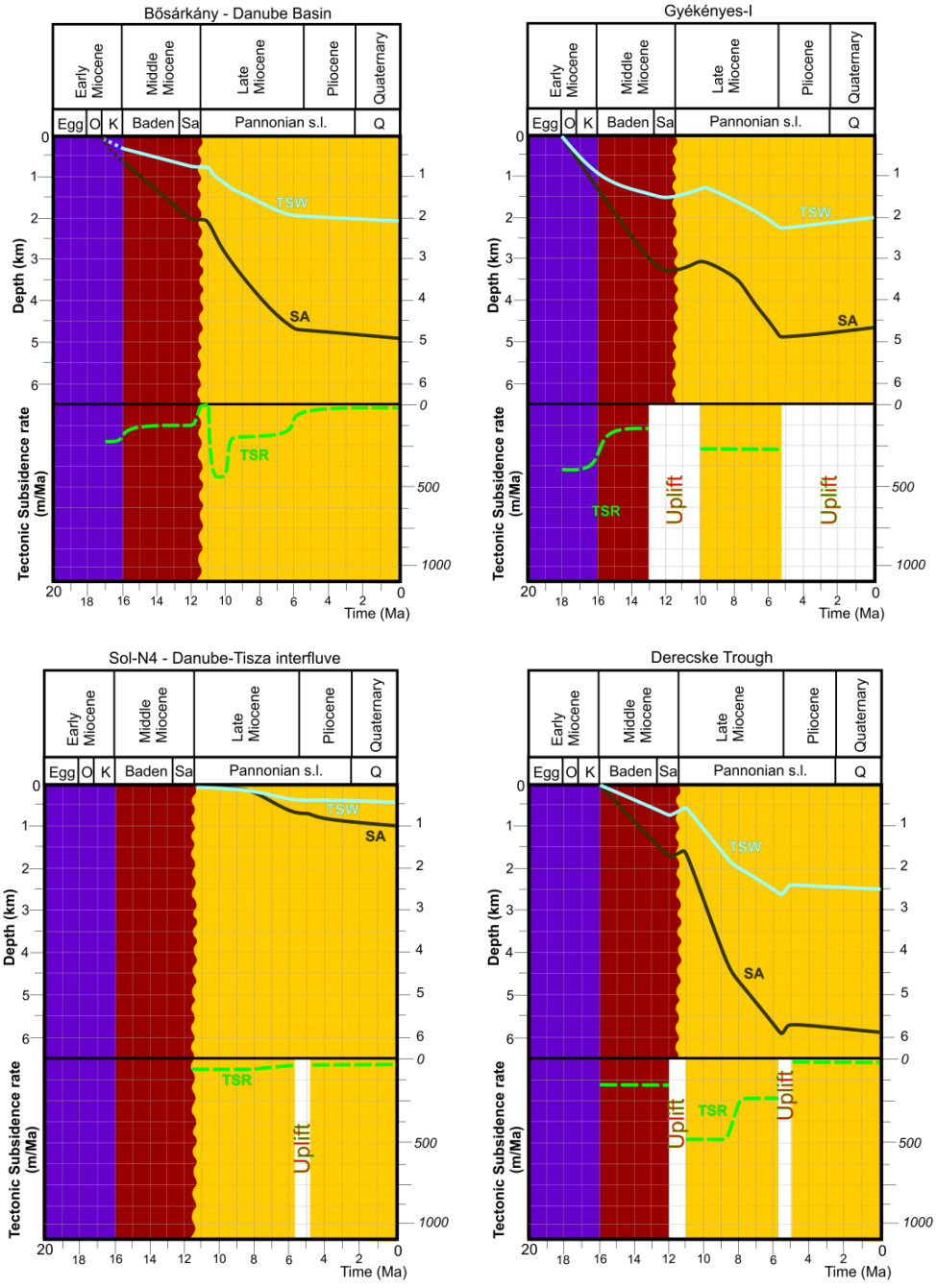
Bősárkány - Danube Basin
Gyékényes-I
Sol-N4 - Danube-Tisza interfluve
Derecske Trough
Early Miocene
Middle Miocene
Late Miocene
Pliocene
Quaternary
Egg
O
K
Baden
Sa
Pannonian s.l.
Q
TSW
SA
TSR
Uplift
Depth (km)
Tectonic Subsidence rate (m/Ma)
Time (Ma)

1.3 Outline of the thesis

Following this introduction, Chapter 2 provides a detailed analysis of the tectono-sedimentary evolution of the Pannonian Basin by means of interpretation of seismic and well data from the Great Hungarian Plain part of the basin. A novel kinematic, seismic and well sequence stratigraphic interpretation allow the quantification of the link between the formation of half-grabens and coeval sedimentation in the Great Hungarian Plain. Our interpretation of temporal and spatial migration of extension during the entire Miocene times explains the contrasting present-day strike of various sub-basins as a result of their gradual clockwise rotation. The link between tectonics and sedimentation has allowed the definition of a novel model of sedimentation in asymmetric basins that can be applied in other natural scenarios of similarly hyperextended continental back-arc basins observed elsewhere.

Chapter 3 focuses on the post-rift sedimentation in Lake Pannon, an initial underfilled, then balance fill and finally overfilled large paleo-lake by the interpretation of 2D and 3D seismic dataset corroborated with calibrating wells. The Late Miocene-Pliocene lake persisted for about 7-8 Myr and was progressively filled by clastic material sourced by the surrounding mountain chains and transported by large rivers, such as the paleo-Danube and paleo-Tisza. We combined sedimentological observations with a backstripping methodology facilitated by well lithology and porosity data to gradually remove the sediment overburden. This has resulted in a morphological reconstruction of the former depositional surfaces with special focus on the prograding shelf-margin slopes. Calculations show that the paleobathymetric differences in the lake were clearly larger than 1000 metres in the deepest sub-basins of the Great Hungarian Plain. The large amount of compaction associated with lateral variations of Neogene sediment thicknesses has created non-tectonic normal fault offsets and folds. These features have important consequences for fluid migration and hydrocarbon trapping. We furthermore compare the geometries and effects of such non-tectonic features with the activity of larger offset sinistral strike-slip zones by the analysis of 3D seismic attributes.

The following two chapters contain analyses by process-oriented forward numerical modelling of the tectonic and sedimentary infill in extensional basins at different spatial scales. Chapter 4 focuses on the effects of lithospheric-scale rheological heterogeneities on the extension of an over-thickened, hot lithosphere. Pre-existing orogenic suture zones localize extensional deformation resulting in asymmetric basins. Such crustal geometries are often in contrast with the more symmetrical regional lithospheric structure observed beneath extensional basins. We study such (a)symmetries and their controlling parameters by conducting a series of 2D thermo-mechanical numerical experiments. The modelling shows that syn-rift subsidence rates are low to moderate creating asymmetric half-grabens where

extension migrates in space and time, grouped in an overall symmetrical appearance on a larger scale. The initial lithospheric mantle asymmetry is attenuated by lateral heat conduction and further dynamic evolution of the thermal anomaly during the "post-rift" phase, resulting in differential vertical movements of the crust including additional 2-3 km subsidence in the basin centre. The modelling shows that the initial crustal and lithospheric thicknesses, rate of extension and surface processes strongly control the thermo-mechanical evolution of the extensional system.

Chapter 5 describes the results of 3D stratigraphic numerical forward modelling at the scale of individual half-grabens, controlled by one major normal fault focussing the coeval sedimentation in the hanging wall and comparable uplift of its footwall. The numerical experiments were performed with the 3D deterministic forward modelling software Dionisos. This model accounts for spatially and temporally variable subsidence and erosion rates, sediment flux composed of different lithologies, compaction, eustasy, water discharge and transport processes. Our modelling applied to the Miocene syn-rift evolution of the Pannonian Basin highlighted the migration of active depocentres between Early to Late Miocene and its sedimentary responses. Our rift sequence model inspired by seismic and well data interpretation, described in Chapter 2 is analysed in detail with this numerical approach. Our modelling can discriminate the low-order tectonic and higher order sea-level and climatic-driven transgressive-regressive cycles from the auto-cyclic nature of the depositional system.

Finally, chapter 6 contains the synthesis of the inferred links between tectonics and sedimentation in extensional basins and their implications for the evolution of Pannonian Basin system. Consequences for the feedbacks between deep mantle processes, lithosphere dynamics, basin-scale tectonics and surface processes are highlighted, followed by an outlook on possible future research.

2. The link between tectonics and sedimentation in back-arc basins: new genetic constraints from the analysis of the Pannonian Basin[1]

[1]*This chapter is based on Balázs, A., Matenco, L., Magyar, I., Horváth, F., Cloetingh, S., 2016. Tectonics 35, 1526–1559.*

2.1 Introduction

The architecture of sedimentary basins reflects the relationship between accommodation space and sediment supply, their rates and localization are variable during basin evolution (e.g., *Cloetingh and Haq*, 2015; *Schlager*, 1993). The link between tectonics and associated surface processes in terms of erosion and sedimentation has been recognized as the critical feedback interaction influencing the final geometry of sedimentary basins, in particular relevant in extensional settings (e.g., *Burov and Guillou-Frottier*, 2005; *Burov and Poliakov*, 2003). Extensional back-arc basins, floored by oceanic or continental lithosphere, develop in the hinterland of orogenic arcs when the rate of subduction is higher than the convergence velocity (e.g., *Dewey*, 1980; *Royden and Burchfiel*, 1989; *Uyeda and Kanamori*, 1979). Although their position behind a magmatic arc is not always very clear, a large amount of back-arc basins were defined in the Mediterranean region, formed during Oligocene-Miocene times in response to the subduction retreat of the Aegean, Gibraltar, Calabrian or Vrancea slabs, in the hinterland of the highly arcuate Hellenides, Rif-Betics, Apeninnes and Carpathians orogens, respectively (*Faccenna et al.*, 2005; *Horváth et al.*, 2015; *Jolivet and Brun*, 2010; *Vergés and Fernàndez*, 2012; *Wortel and Spakman*, 2000). In all these situations extension post-dates at relatively short times the contraction and is juxtaposed over an inherited nappe stack, often reactivating thrust contacts and exhuming rocks previously deeply buried, such as in the Apennines or Aegean system (e.g., *Brun and Faccenna*, 2008). Such reactivations are recognized along major detachments, locally associated with the formation of large core-complexes or other extensional domes, or low-angle normal faults, as observed in the Rhodope or the Alboran domain (e.g., *Brun and Sokoutis*, 2007; *Vissers*, 2012). These structures controlled also the evolution of their hanging-wall half-grabens grouped along large extensional basins with amounts of cumulated extension in the order of hundreds of kilometers, such as in the Aegean or the Alboran Domain (*Comas et al.*, 1992; *van Hinsbergen et al.*, 2005). In other geodynamic settings, such large amounts of extension characterize hyper-extended passive continental margins (*e.g., Tugend et al.*, 2014). Such definitions are less understood in the case of extensional back-arc basins floored by continental lithosphere characterized by large amounts of extension (e.g., *Huismans and Beaumont*, 2003), in particular when analyzing the link between tectonics and sedimentation. Symmetry or asymmetry in extensional basins is used in many different ways. We use the term of asymmetric extension in a non-genetic way, i.e. for any extensional (sub-)basin that shows one major structure, normal fault or detachment, controlling the coeval sedimentation in the hanging-wall and at least comparable uplift of its footwall. Such a simple definition is independent of the controlling mechanics, from simple-shear in

single or multi-layered lithosphere to complex multi-stage hyper-extended basins (*Huismans and Beaumont*, 2003; *Manatschal et al.*, 2015; *Wernicke*, 1985).

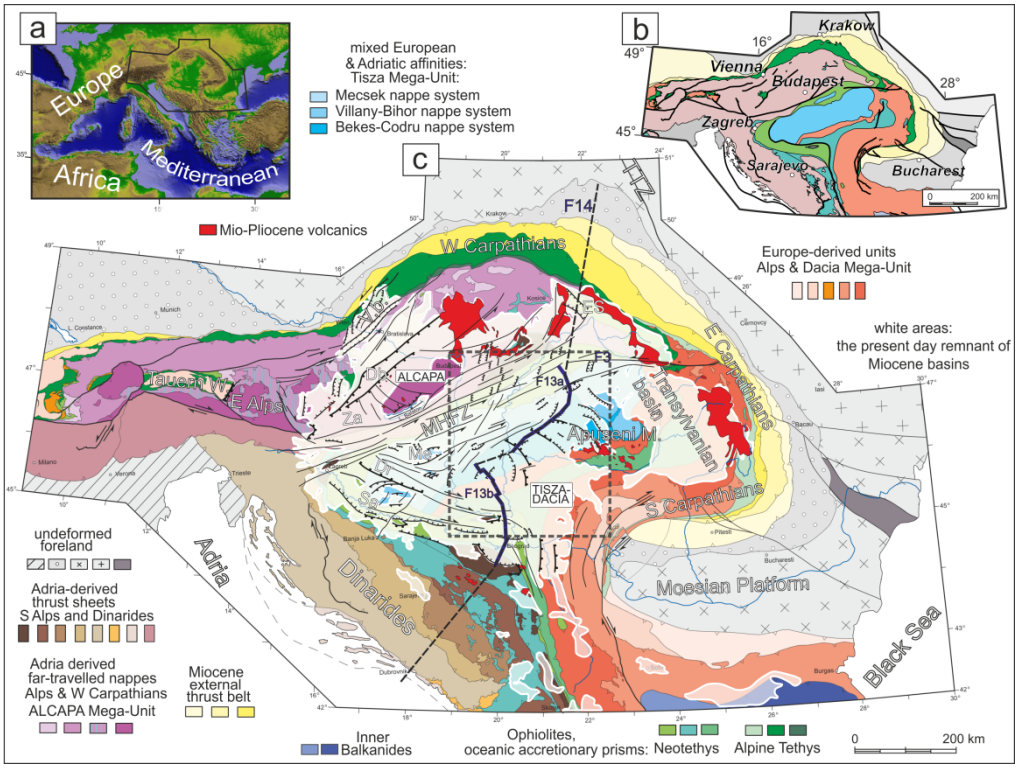

Figure 2.1: a) Location of the Pannonian Basin system. b) Main tectonic units of the Alps-Carpathians and Dinarides (simplified after *Schmid et al.*, 2008). The Tisza-Dacia contact is slightly modified. Note that the overlying Neogene basins in the intra-Carpathians area are ignored. c) Miocene - Quaternary tectonic map of the Pannonian Basin and the Alps-Carpathians-Dinarides system showing the present day extent of the Neogene sediment cover of the Pannonian, Vienna and Transylvanian basins overlying the pre-Neogene structures and showing the major Miocene to Quaternary faults (modified after *Horváth et al.*, 2015; *Schmid et al.,* 2008; *Ustaszewski et al.*, 2014 and the results of this study). Note that the present day geometry of these basins does not reflect their original position at the time of formation, some Neogene deposits were eroded in the Pannonian Basin or underthrust beneath the Carpathian nappe stack. The TTZ has served as a rheological contrast zone localising Miocene tectonics of the Carpathians (e.g., *Matenco et al*., 2016). Vb – Vienna Basin, Dr – Dráva sub-basin, Sa – Sava sub-basin, Za – Zala sub-basin, Me – Mecsek hill, Db – Danube basin, ES – East Slovakian basin, TTZ – Teisseyre-Tornquist Zone, MHFZ – Mid-Hungarian Fault Zone.

A typical example is the Pannonian Basin of Central Europe (Figure 2.1), where the large amount of extension is accommodated by the rapid roll-back of the Carpathians slab between 20-9 Ma (*e.g., Csontos*, 1995; *Fodor et al.*, 1999; *Horváth et al.*, 2006; *Matenco and Radivojević*, 2012; *Merten et al.*, 2010). The observation of a thin syn-rift and thick post-rift basin fill is usually interpreted as a consequence of

either depth dependent stretching, necking depth or intra-plate stresses (e.g., *Horváth and Cloetingh*, 1996; *Lankreijer et al.*, 1995). The 150-200 km of extension is associated with crustal thinning factors up to ~2.2, while the ones of mantle lithosphere have locally extreme values in the order of 5-50 (*Horváth et al.*, 2006; *Lenkey*, 1999; *Sclater et al.*, 1980). Such extreme values resemble the geometry controlled by detachments of other extensional Mediterranean back-arcs and/or the ones observed in hyper-extended continental passive margins (*Huismans and Beaumont*, 2011). The geometry of the Pannonian Basin is generally dominated by typical half-grabens, many of them being flanked by detachments with crustal-scale uplift of footwalls, such as observed in the western part of the basin or inferred along its eastern margin (*Ratschbacher et al.,* 1991; *Tari et al.*, 1992; *Tari et al.*, 1999). Some of these half-grabens show typical syn-kinematic patterns of deposition that are diagnostic for deriving moments of hanging-wall subsidence and, interestingly, of footwall uplift (e.g., *Matenco and Radivojević*, 2012; *Tari et al.*, 1992). Although the link between kinematics, exhumation and deposition in these extensional features is well studied near the western and southern margin of the basin, much less is known on such genetic features in the main part of the Pannonian Basin, i.e. the Great Hungarian Plain. Remarkable attention has been devoted recently to this area by seismic interpretation and deep geophysical studies (*e.g., Magyar et al., 2006; Matenco and Radivojević, 2012, Sztanó et al., 2013; Windhoffer et al., 2005*). In this part of the basin, we have used a large network of regionally distributed 2D and 3D seismic surveys to study the link between deformation and coeval sedimentation, in order to quantitatively analyze the genesis of the half-grabens filled by Miocene sedimentary and volcanic rocks. Starting from the Pannonian Basin case study, our analysis correlated with previously published data has allowed the definition of a coupled tectono-sedimentary model of highly extended back-arc basins.

2.2 Formation and evolution of the Pannonian Basin

The Miocene to Quaternary formation of the Pannonian Basin was proceeded by a pre-Neogene orogenic evolution that resulted from the opening and subsequent closure of two oceanic realms (Figure 2.1), the Triassic-Cretaceous Neotethys and Middle Jurassic – Tertiary Alpine Tethys that separated three continental units (e.g., *Csontos and Vörös*, 2004; *Schmid et al.*, 2008). In the NW, the ALCAPA Mega-Unit is an Adriatic-derived block that was sutured to Europe during the N-wards Cretaceous – Eocene closure of the Alpine Tethys (*Csontos*, 1995; *Schmid et al.*, 2004). To the E and SE, the Dacia unit separated from Europe during the late Jurassic opening of the Ceahlau-Severin Ocean (*Csontos and Vörös*, 2004; *Săndulescu*, 1988). In the center (Figure 2.1), Tisza is a unit with mixed affinities that drifted away from Europe during Middle Jurassic and was sutured to Dacia during the late Jurassic - late

Early Cretaceous closure of a NE branch of the Neotethys Ocean (i.e., Eastern Vardar, *Haas and Péró*, 2004; *Schmid et al.*, 2008). The final closure of the Neotethys Ocean by subduction and collision in latest Cretaceous-Eocene times has juxtaposed the, by now welded, Tisza-Dacia upper tectonic plate with the lower Dinaridic unit, the latter being build-up by thick-skinned thrust sheets deforming the former Adriatic continental margin (*Karamata*, 2006; *Schmid et al.*, 2008). The Neogene formation of the Pannonian Basin, coupled with the extrusion of the Eastern Alps has created a large amount of translations and opposite sense rotations (i.e., counterclockwise in ALCAPA and clockwise in Tisza-Dacia) accompanying the extension of these continental units (*Balla*, 1987; *Csontos*, 1995; *Márton and Fodor*, 2003). These units were juxtaposed along a major suture zone (Mid-Hungarian Fault Zone) that possibly accommodated the change in polarity from the southward subduction of the Alpine Tethys in the Alps-Carpathians to the northward subduction of the Neotethys in the Dinarides (*Balla*, 1986; *Csontos and Nagymarosy*, 1998; *Schmid et al.,* 2008).

2.2.1 Extension of the Pannonian Basin

Similar to other highly arcuated Mediterranean retreating subduction systems (*Faccenna et al.*, 2014), the Neogene extension of the Pannonian Basin was coeval with the contraction recorded at the exterior of the Carpathians (e.g., *Ellouz and Rocca,* 1994; *Roure et al.,* 1993). Extension in the ALCAPA Mega-Unit was accompanied by lateral extrusion from the Eastern Alps (e.g., *Ratschbacher et al.*, 1991) and large scale offsets along major transcurrent shear zones such as the Periadriatic Fault system and the Balaton line (e.g., *Balla*, 1987; *Csontos and Nagymarosy*, 1998; *Fodor et al.*, 1998; *Ustaszewski et al.,* 2008). This extension took place dominantly along extensional detachments exhuming deep crustal rocks in core-complexes located near the basin margins (*Tari et al.*, 1992; *Fodor et al.*, 1998). Much less is known about the extensional kinematics of the largest part of the Pannonian Basin, i.e. the Great Hungarian Plain, where such detachments are indirectly inferred near the Dinaridic or South Carpathians margins (*Matenco and Radivojević*, 2012; *Stojadinovic et al.*, 2013; *Ustaszewski et al.*, 2010). In contrast with the counterclockwise rotations accompanying E-ward translations in the ALCAPA unit (*Márton and Fodor*, 2003; *Márton et al.*, 2007), the overall clockwise up to 100° Paleogene-Miocene rotation of the Tisza-Dacia took place with a rotation pole situated near the SE junction between the Dinarides and Carpathians Mountains. This latter rotation was accommodated by contraction at the exterior of the East and SE Carpathians and by up to 100 km dextral offset of the curved Cerna-Timok fault system in the South Carpathians (*Balla*, 1987; *de Leeuw et al.*, 2013; *Fügenschuh and Schmid*, 2005; *Matenco et al.*, 2010; *Ratschbacher et al.,* 1993). The uplift of the Alpine – Himalayan mountainous belt has gradually fragmented the larger Tethys Ocean starting with the late Eocene times. The Pannonian Basin is part of the northern

branch, the Paratethys, which evolved in a semi-enclosed marine to lacustrine basin system. The Paratethys is characterized by a separate endemic biostratigraphy (Figure 2.2, see *Báldi,* 1986*; Nagymarosy and Müller*, 1988; *Piller et al.*, 2007; *Steininger and Rögl*, 1984).

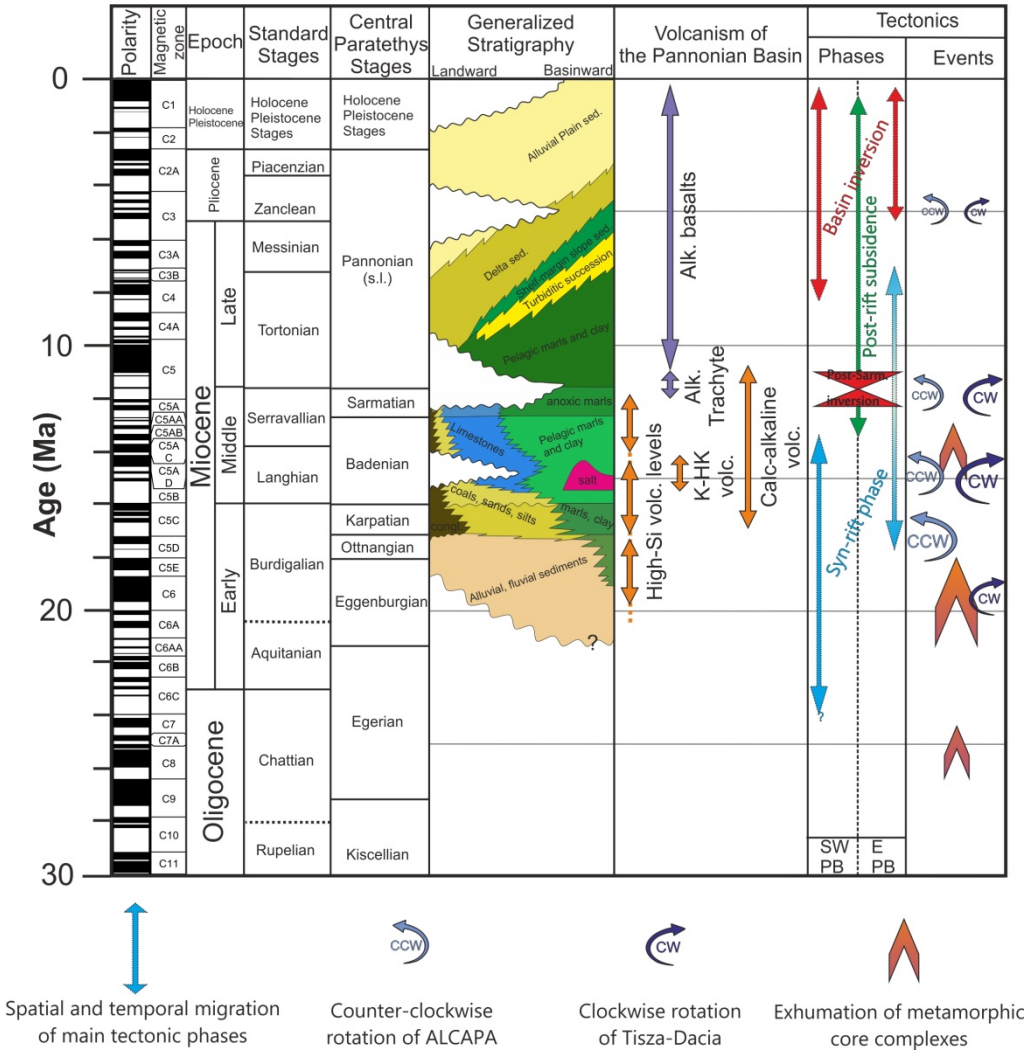

Figure 2.2: Tectono-stratigraphic chart of the Great Hungarian Plain part of the Pannonian Basin with biostratigraphic correlation of the standard and Central Paratethys stages (after *Pezelj et al.*, 2013; *Piller et al.,* 2007) and the generalized Miocene lithostratigraphy of the study area, the volcanic activity of the Pannonian Basin (after *Harangi and Lenkey*, 2007; *Pécskay et al.,* 2006) and the main tectonic phases and events (modified after *de Leeuw et al.* 2013; *Horváth et al*., 2006; *Márton and Fodor* 2003; *Márton et al.* 2007). Latest Miocene-Pliocene minor vertical axis rotations are connected to basin inversion. Note that the syn-rift/post-rift boundary and the onset of last stage of basin inversion appear to be older in the SW and progressively younger E-NE -wards.

Timing of the main extensional events of the basin (Figure 2.2) is constrained by the onset of extensional magmatism, absolute age dating of exhumation in the footwall of extensional detachments that outcrop near the basin margin and, more importantly, by the timing of syn- and post-rift sediments. In the Hungarian part of the basin, the extension is connected with successive volcanic events, mostly of rhyolites or rhyolitic tuffs (Figure 2.2; *Pécskay et al.*, 2006). The base of this volcanic sequence is intercalated in the lowermost part of the syn-rift sedimentation and was originally dated at ~20 Ma (K-Ar dating, *Hámor*, 1985). More recent dating of the tuff has indicated younger ages of ~17 Ma (Ar-Ar and U-Pb dating, *Pálfy et al.*, 2007). Widespread extensional magmatism creating intrusions or volcanic successions in the Dinarides or near their border with the Pannonian Basin have indicated ages spanning from 22-17 Ma (*Cvetkovic et al.*, 2007; *Koroneos et al.*, 2011; *Schefer et al.*, 2011). Large-scale calc-alkaline magmatism associated with the subduction at the exterior of the Carpathians followed subsequently by adakitic to alkaline magmatism related to post-collisional slab evolution is also recorded in the Pannonian Basin or its adjacent areas (Figure 2.2, *Harangi and Lenkey*, 2007; *Seghedi et al.*, 2011). Low-temperature thermochronology has shown that the peak exhumation occurred in the footwall of extensional detachments situated near the transition between the Alps and the Pannonian Basin (Rechnitz window, Pohorje structure and the detachments bordering the Tauern Window to the east and west) and the main activity of the Periadriatic Lineament span in the interval 23-10 Ma (*Dunkl et al.*, 1998; *Fügenschuh et al.*, 1997; *Fodor et al.*, 2008; *Scharf et al.*, 2013; *Tari et al.*, 1992). Near the margin with the Dinarides, in the southwestern periphery of the Pannonian Basin the exhumation in the footwall of extensional detachments has started already in the Oligocene at ~28 Ma and continued with a main peak at Middle Miocene times ~15-11 Ma (*Stojadinovic et al.*, 2013; *Toljić et al.*, 2013; *Ustaszewski et al.*, 2010). In agreement with thermochronology studies, the analysis of the basin fill and its syn-kinematic deposition has constrained the timing of the main extensional events of the basin to Early and Middle Miocene, the latter being the moment of peak extension in the entire basin (Figure 2.2, *Fodor et al.*, 1999; *Horváth et al.*, 2006; *Magyar et al.*, 1999; *Nagymarosy and Hámor*, 2012; *Tari et al.*, 1999). The kinematics indicates that in many situations extensional structures reactivate former pre-Neogene thrust contacts (e.g., *Tari et al.*, 1992; *Windhoffer et al.*, 2005).

Early Miocene depositional environments are dominantly characterized by fluvial, lacustrine and other continental sediments in our study area of the Great Hungarian Plain (*Matenco and Radivojević*, 2012; *Pavelić et al.*, 2001; *Saftić et al.,* 2003), while in the northwestern parts of the basin marine sediments deposited (*Nagymarosy and Hámor*, 2012). Transgression during the Middle Miocene (*Kováč et al.*, 2007) resulted in the deposition of deep basinal sediments in the center of extensional (half-) grabens, while deposition along their margins is dominated by

near-shore to shallow-marine sedimentation, including shallow water algal limestone (*Nagymarosy and Hámor*, 2012). Interestingly, in the center of the Great Hungarian Plain the late Middle Miocene (Sarmatian s.s.) deposition took place in a near shore environment overlying basement highs, but such sedimentation is absent in the adjacent deeper areas (*Szepesházy,* 1971; *Kőrössy,* 1992). This indicates that the basin topography was flatter, lacking significantly deep depressions in the center of the basin (*Magyar et al.*, 1999).

2.2.2 Post-extensional evolution

There is no consensus on a general onset of post-rift deposition across the basin, as this process appears to be diachronous. In several parts of the Pannonian Basin, but dominantly in the NW, an intra-Middle Miocene unconformity marks the cessation of significant normal faulting (~14.8 Ma, Figure 2.2, *Tari et al.*, 1999). In other parts of the Pannonian Basin, but dominantly in the Great Hungarian Plain, the onset of post-rift deposition is interpreted at the boundary between Middle and Late Miocene (11.63 Ma, *ter Borgh et al.*, 2013). This was associated with the development of an unconformity interpreted to be coeval with the peak of collision in the East Carpathians (Figure 2.2, first phase of basin inversion; *Horváth*, 1995), where thrusting ceased subsequently until 9Ma (*Matenco and Bertotti*, 2000; *Merten et al.*, 2010). In the Pannonian Basin, this unconformity removed parts of the upper Middle Miocene succession (Sarmatian strata, *Magyar et al.*, 1999). In contrast, near the Pannonian Basin margins (Vienna, East Slovakian, Transylvanian and Danube basins) the thickness of Sarmatian sediments is significant, locally exceeding 1 km. Other seismic interpretation studies in the SE part of the basin suggested that extensional deformation was diachronous across the basin and migrated in time and space from ~28 Ma near the Dinarides to 8-5.5 Ma NE- and E-wards (*Matenco and Radivojević*, 2012). This means that in a first stage the Dinaridic nappe contacts were reactivated as extensional detachments or low-angle normal faults. This was followed by a progressive migration of depocenters towards the present-day center and E-NE part of the Great Hungarian Plain. Late Miocene extensional structures with various offsets were observed by outcrop and seismic interpretation studies in the center of the Pannonian Basin (*Balázs et al.,* 2013; *Fodor et al.,* 2013).

The uplift of the Carpathians and the associated unconformity between the Middle and Late Miocene strata mark the disruption of connections with the remainder of the Paratethys realm. This coincides with the onset of a marked environmental and sedimentological change in the evolution of the Pannonian Basin, which was restricted to the size of a large isolated lake (Lake Pannon, *Magyar et al.*, 1999, 2013). An up to 7 km thick sedimentary succession was deposited in the Great Hungarian Plain during Late Miocene to recent times. The basin fill recorded an initial transgression followed by shelf margin and slope progradation driven by the

influx of sediments by a fluvial system resembling the present day Danube and Tisza rivers. This shelf margin prograded ~500 km in 6 Myr until ~4 Ma from the NW and NE in a ~S-SE direction while minor progradation was recorded in other directions (*Magyar et al.*, 2013; *ter Borgh et al.*, 2015; *Vakarcs et al.*, 1994; *Pogácsás et al.*, 1988). The coeval sedimentation reflects the deposition of a number of diachronous lithostratigraphic formations that mirror the various lithofacies associations of a deep lake depositional environment (Figure 2.2, *Bérczi et al.,* 1987; *Juhász*, 1991; *Sztanó et al.*, 2013). These associations are laterally variable (Figure 2.2) from deep hemi-pelagic deposition (Endrőd Formation), turbidites (Szolnok Formation), prograding shelf-margin slope (Algyő Formation) and delta (Újfalu Formation) to alluvial plain sediments (Zagyva Formation). Their typical expression in seismic lines provides an excellent lateral correlation of seismic facies. These diachronous associations are also correlated by magneto- and bio-stratigraphic studies calibrated by a limited number of absolute age measurements (*Magyar et al.*, 1999; *Magyar and Sztanó*, 2008; *Magyar et al.*, 2013).

The cessation of extension was followed by the onset of large scale inversion in the Pannonian Basin during late Miocene times (8-7.5 Ma) controlled by the counterclockwise rotation and push of the Adriatic micro-plate, which created large scale contractional structures near the Dinaridic margin and dominantly transcurrent kinematics elsewhere. This deformation event is still presently active (*Bada et al.*, 2007; *Dombrádi et al.*, 2010; *Fodor et al.*, 2005; *Horváth and Cloetingh*, 1996; *Jarosinski et al.*, 2011; *Pinter et al.*, 2005; *Uhrin et al.*, 2009). An unconformity is observed in the basin fill near the boundary between the Miocene and Pliocene

Figure 2.3 (facing page): Neogene basement isopach (in kilometers, compiled from *Haas et al.*, 2010; *Matenco and Radivojević*, 2012; *Rabagia*, 2009; *Tulucan*, 2007 and the data of this study) and tectonic map of the Great Hungarian Plain. The map indicates the main depocenters with their strike (dashed lines), age of rift climax system tract and the main direction of extensional tectonic transport in the various sub-basins (the same color-coded arrows). White lines show the locations of the interpreted seismic sections. Main sub-basins of the area: Nyí – Nyírség sub-basin, Ga – Galospetru-Mecentiu Depression, Ch – Chet Tamaseu Depression, De – Derecske Trough, Bor – Borod Depression, Bo – Bors Depression, Vé – Vésztő Trough, Be – Beius Depression, Dé – Dévaványa Trough, Já – Jászság Basin, Ör – Örkény Trough, Ad – Adony Basin, Ke – Kecskemét Depression, Tá – Tázlár Trough, So – Soltvadkert sub-basin, Ki – Kiskunhalas Trough, Kf – Kunfehértó sub-basin, Za – Zarand Depression, Gr – Graniceri Depression, Bk – Békés Basin, Mk – Makó Trough, Fö – Földeák sub-basin, Sze – Szeged Trough, He – Hercegszántó Trough, BM – Bački Monoštor Depression, BT – Bačka Topola Depression, Cn – Čantavir Depression, Tc – Tomnatec Depression, Sc – Srpska Crnja Depression, Sr – Srbobran Depression, Cg – Čurug Depression, Zr – Zrenjanin Depression, Tr – Temerin Depression, Mr – Morović Depression, Sf – Sefkerin Depression, Ss – Samoš Depression, Pc – Pančevo Depression, Pn – Plandište Depression, Zg – Zagajica Depression.

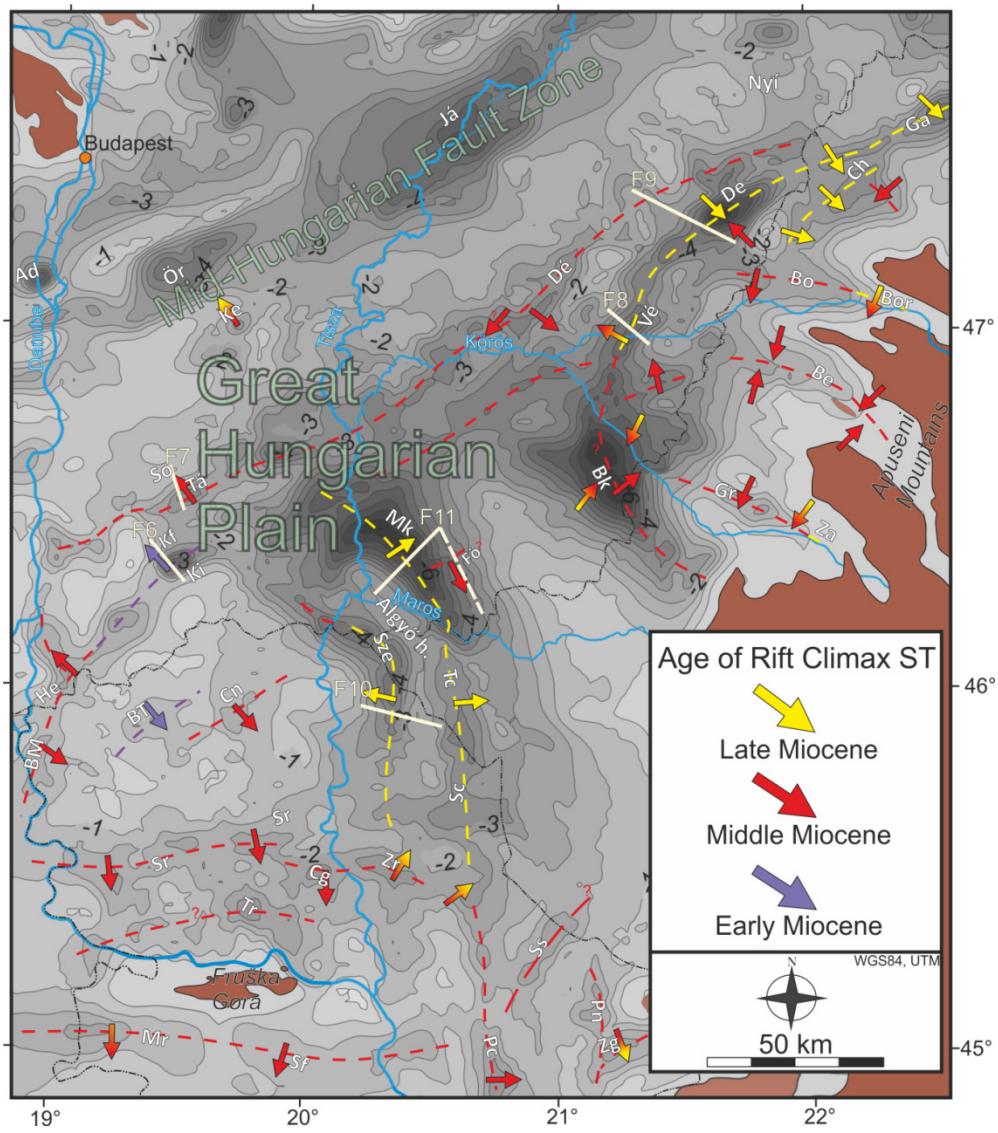

basin fill (e.g., *Vakarcs* et al., 1994). This unconformity is angular and locally erosional near the basin margins and passes to a correlative conformity towards the basin center. It is interpreted either related to basin inversion (*Magyar and Sztanó*, 2008; *Sacchi et al.*, 1999; *ter Borgh et al.*, 2015) or formed in response to the Messinian Salinity Crisis of the Paratethys (e.g., *Csató et al.*, 2015). One other slightly older unconformity formed at ~6.8 Ma is observed at depth in the Great Hungarian Plain (Figure 2.3). This has been interpreted as either the result of a significant water level fall of Lake Pannon (e.g., *Csató,* 1993, *Vakarcs et al.*, 1994) associated with the formation of large canyon incision in the center of the Great

Hungarian Plain (the Alpar Canyon of *Juhász et al.*, 2013), or a cross-over zones of different progradational directions (*Magyar and Sztanó*, 2008).

2.3 Methodology

We have analyzed the link between structures and sedimentation in the sub-basins located in the Great Hungarian Plain part of the Pannonian Basin mostly in Hungary, but also in Serbia, Slovakia and Romania (Figure 2.1 and 2.3). In Hungary, we have analyzed a large array of 2D and 3D seismic data calibrated by a dense network of exploration wells distributed regionally in the study area particularly in the studied sub-basins, but also on their flanks and connecting areas. The signal/noise ratio and resolution of the seismic sections are variable, driven by the variability from recent 3D seismic surveys to older 2D seismic lines. Although in this paper we present only a limited number of seismic transects usually oriented across the strike of various sub-basins, we used a much larger seismic and well database (including hundreds of 2D seismic lines and a few 3D seismic surveys). Well logs were tied to seismic sections using the standard VSP logs and checkshots commonly available in the exploration industry (e.g., *Mészáros and Zilahi-Sebess,* 2001). The interpretation was also assisted by Bouguer anomaly and vertical component magnetic anomaly data using maps available in the Pannonian Basin (*Kiss,* 2006*; Kiss and Gulyás,* 2006*; Tari et al.,* 1999). The reflectivity of the seismic data decreases substantially beneath the basin fill sedimentary rocks, thus the pre-Neogene interpretation relies dominantly on well data (*Haas et al.,* 2010) and the outcropping areas situated on the flanks of few sub-basins. The exceptions are the zones with increased reflectivity and correlation in seismic lines, such as the carbonatic cover in the Mesozoic sediments, which were correlated across the basin. This interpretation is in general agreement with the recent pre-Neogene interpretation based of the entire Hungarian well database (*Haas et al.,* 2010), but local details may vary. Outside Hungary, in the Pannonian Basin regions of Slovakia, Serbia and Romania, in the Dinarides of Serbia and Montenegro and in the Carpathians of Poland the regional interpretation used published studies (*Dimitrijevic,* 1997*; Ellouz and Rocca,* 1994*; Gagala et al.,* 2012; *Matenco and Radivojević,* 2012; *Pigott and Radivojević,* 2010*; Puchnerova et al.,* 2002*; Răbăgia,* 2009*; Schmid et al.,* 2008*; ter Borgh,* 2013*; Tulucan,* 2007).

The structural analysis followed the typical seismic interpretation methodology in defining reflector terminations, such as truncations, onlaps, toplaps, offlaps or downlaps. Our seismic stratigraphic interpretation used a combination of classical sequence stratigraphy and applied tectonic system tract methodology that is less known in available literature and requires more explanation.

Seismic facies unit	Seismic examples (vertical scale represents 100 ms)	Line drawing interpretations	Amplitude and frequency characteristics	Spatial distribution/ typical occurrence
Parallel discontinuous	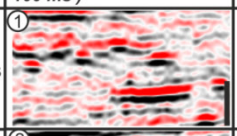		Low to high amplitude, medium frequency	Occurs at shallower depths (alluvial plain sed.)
Sub-parallel fairly continuous	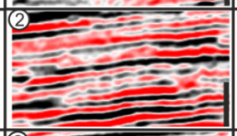		High amplitude, high frequency	Occurs above the prograding clinoforms (delta sed.)
Clinoform - Continuous, discontinuous alternating	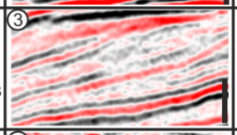		Medium to low amplitude, high frequency	Occurs between deep and shallow depth sediments (prograding shelf-margin slope)
Hummocky discontinuous	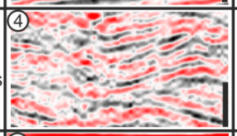		Medium to low amplitude, high frequency	Occurs between deep and shallow depth sediments (prograding shelf-margin slope)
(Sub-)parallel continuous	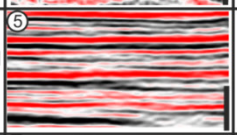		Medium to high amplitude, low to high frequency	Present within and just above of the half-graben infill
Sub-parallel discontinuous	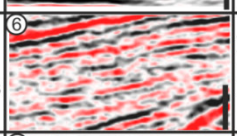		Low amplitude, medium to high frequency	Occurs within half-graben infill
Oblique	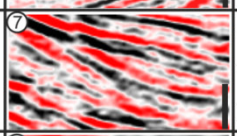		Variable amplitude, low to high frequency	Occurs within half-graben infill, usually prograding toward the basin center
Oblique hummocky	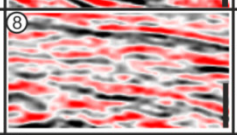		Low to high amplitude, low to medium frequency	Occurs within half-graben infill, near the flanks
Proximal lobe - hummocky to discontinuous	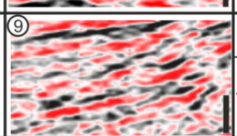		Low to medium amplitude, low frequency	Occurs within half-graben infill, next to boundary faults
Chaotic discontinuous	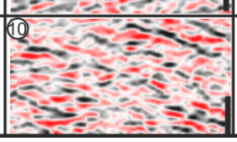		Low to medium amplitude	Occurs above the acoustic basement

Figure 2.4: Characteristic seismic facies units used in the seismic sequence stratigraphic interpretation.

Starting from the readily available principles of sequence stratigraphy that study the relationship between the accommodation space and sediment supply (*e.g., Catuneanu et al.,* 2009; *Catuneanu et al.,* 2011; *Posamentier and Allen,* 1993*; Schlager,* 1993*; Vail et al.,* 1977), the application to tectonically active basins (*e.g., van Wagoner et*

al., 1990) is less known. In active basins, the system tracts and sequences are linked to vertical movements; they can be related to individual events of fault activation and are independent from the known cyclicity timescales of the classical sequence stratigraphy (*e.g., Miall and Miall,* 2001).

In extensional basins, tectonic sequence stratigraphic models are available by correlating the sedimentation and the tectonic subsidence of hanging-walls (e.g*., Martins-Neto and Catuneanu,* 2010; *Nottvedt et al.,* 1995*; Prosser,* 1993*; Ravnås and Steel,* 1998; *van Wagoner et al.,* 1990), but these studies do not quantify the footwall uplift in asymmetric systems. Similar with other studies (e.g., *Hinsken et al.*, 2007; *Pereira and Alves*, 2012, *Răbăgia et al.*, 2011), we have used a combination of these readily available (seismic) sequence stratigraphic methodologies. The first order extensional cyclicity has been defined by using a seismic sequence stratigraphic model (*Nottvedt et al.,* 1995; *Prosser*, 1993). Among the limited availability of such approaches in existing literature, this model has the closest similarity in terms of geometries with the ones detected in our study and, therefore, provides the closest meaning of tectonic system tracts. A tectonic system tract is defined by linked depositional systems controlled dominantly by tectonics, bounded by key stratigraphic surfaces (e.g., *Prosser*, 1993). In such a definition, the rift initiation system tract records the first extensional pulses in the basin and is followed by a rift climax system tract, which reflects the moments of maximum fault activity and subsidence rates. The end of faulting marks the start of an immediate post-rift system tract, when the continued thermal sag subsidence resulted in the burial of the inherited rift topography, which is followed by a late post-rift system tract, when compaction and gradual slowing of subsidence drives a final stage of regressive basin fill. Differently from the original model, these system tracts have a different meaning by reflecting the specific evolution of half-grabens bounded by exhumed footwalls. Each system tract is associated with characteristic seismic facies associations grouping seismic facies units, reflecting the depositional environment. The burial in late post-rift stage may create differential compaction effects over the half grabens, such as synclinal geometries or compaction faults with increasing offsets towards the surface, in particular when the thickness of the overburden is high.

Figure 2.5 (facing page): Sequence stratigraphic well log interpretation from the Kiskunhalas sub-basin showing cyclicity of the Neogene basin fill. Generalized lithological column is based on well reports. Locations of the wells are displayed in Figure 2.6.

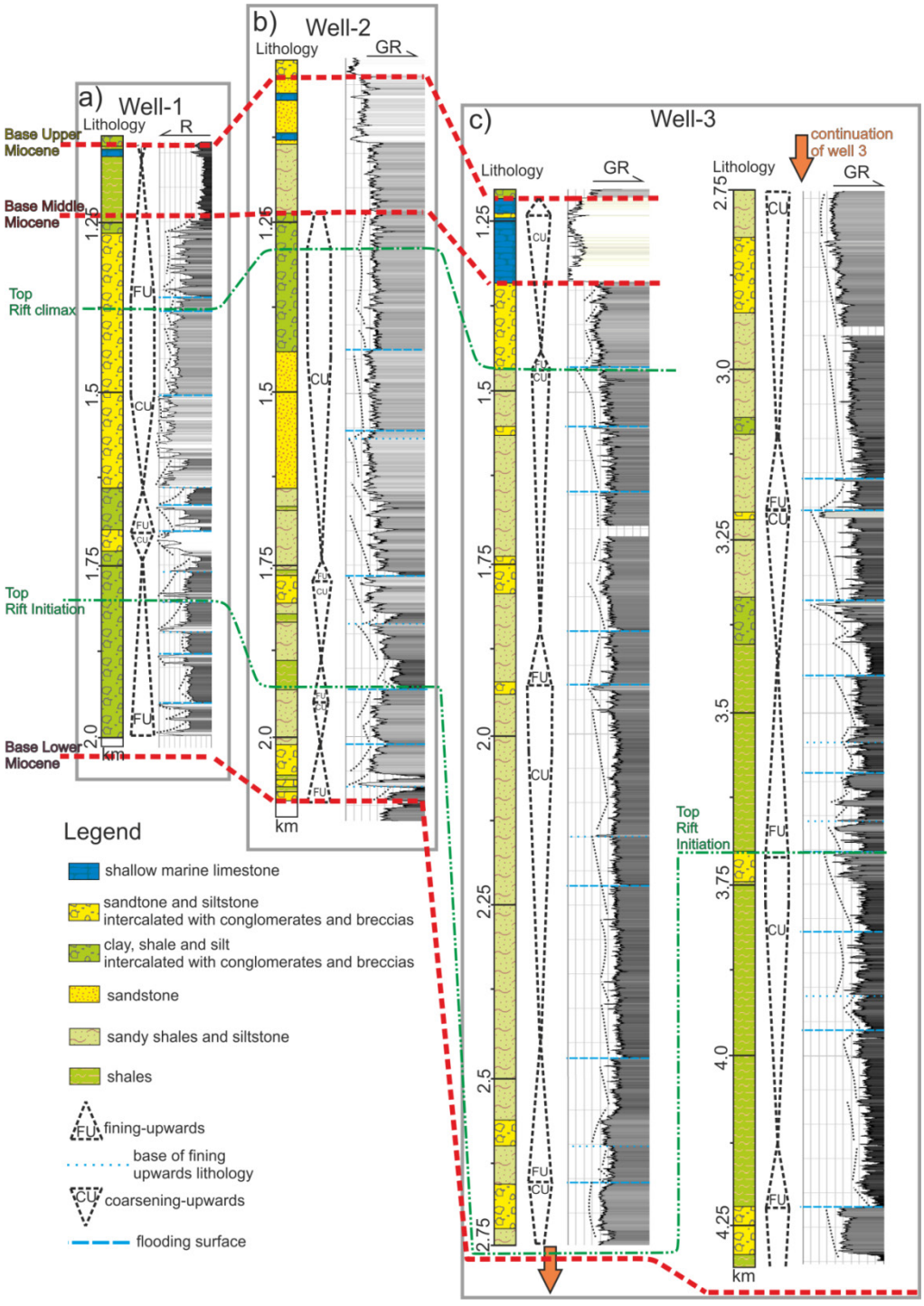

The large syn-kinematic sedimentation rate of the Pannonian Basin increased the time resolution of the seismic lines and enabled us to locally detect a higher order

sequence stratigraphic cyclicity also in the seismic data. This is generally related to individual episodes of normal faulting and was analyzed by defining transgressive – regressive sequences (*e.g., Catuneanu,* 2002*; Catuneanu et al.,* 2009; *Embry and Johannessen,* 1992*; Johnson and Murphy,* 1984). The amplitude, frequency, continuity, terminations and distribution of reflectors define various seismic facies units (Figure 2.4), which were subsequently grouped into seismic facies associations defining progradational, retrogradational or aggradational geometries. They are controlled by the rate of accommodation and the sediment supply (*Catuneanu et al.,* 2009). The specificity of asymmetric extensional systems is the footwall exhumation and erosion, and the migration of faulting in space and time. As long as the footwall is eroded, the coeval deposition and onlaps in the neighboring hanging-wall are coastal and therefore a direct interpretation of the progradational, retrogradational or aggradational geometries in stratigraphic sequences is possible. Footwall erosion, combined with the correlative maximum regression surface interpreted as classical sequence boundaries defined by the geometry of the seismic facies units, is an expression of the composite surface that bounds a Transgressive – Regressive (TR) sequence (*Embry and Johannessen,* 1992*; Johnson and Murphy,* 1984). Variations in paleobathymetries are available in published studies of Early and Middle Miocene basin evolution, although in the case of Late Miocene paleobathymetry, our model is more speculative (e.g.*, Báldi et al.,* 2002; *Lemberkovics,* 2014*; Pezelj et al.,* 2013*; Sztanó et al.,* 2013). The maximum flooding surface of a TR sequence is less controlled in older sediments located at the center of various sub-basins, where wells are less frequent. In these situations, the maximum flooding surface (MFS) has been taken as the boundary between retrogradational and progradational geometries. Although this is an important approximation in theory, its error does not affect significantly the practical interpretation of individual episodes of normal faulting.

Our seismic stratigraphic interpretation is also constrained by available well logs, such as resistivity and gamma ray logs (Figure 2.5). These logs provide the required validation of the prograding-retrograding facies associations and evolution of the sedimentary infill in the half-grabens of the Great Hungarian Plain. This integrated approach enables the analysis of the episodic tectono-sedimentary signature of the syn-kinematic basin fill at different scales (see also *Martins-Neto and Catuneanu*, 2010; *Pereira and Alves,* 2012). Although such well log interpretations are available in the entire study area of the Great Hungarian Plain, we have chosen to illustrate one well in the center of the Kiskunhalas sub-basin and two wells at its the flank (Figures 2.5 and 2.6). Their interpretation followed a standard well log sequence stratigraphic approach (*e.g., van Wagoner et al.,* 1990), the derived cyclicity is correlated and interpreted with the evolution of the seismic facies units and associations.

2.4 Structural and seismic sequence stratigraphic interpretations in the Great Hungarian Plain

The Miocene extension created a number of individual sub-basins in the Great Hungarian Plain (Figure 2.3). The main characteristic geometry of these sub-basins is the low-angle dip of their flanks (Figures 2.6-2.11), which is unusual for typical upper crustal normal faults. This geometry suggests the existence of large-scale low-angle normal faults or detachments, as interpreted in other areas in the upper crust of the Pannonian Basin (*Tari et al.*, 1992; *Tari et al.*, 1999). These structures flank sub-basins with low-angle dipping hanging-walls in overall half-graben geometries. Although antithetic normal faults with significantly lower offsets often cross cut these hanging-walls, the syn-kinematic basin fill shows that the structure is still highly asymmetric (e.g., Figure 2.6). These half-grabens frequently show an opposite polarity of low-angle normal faults, have decreasing offsets and are connected by transfer faults along their strikes (see also *Tari et al.*, 1992). The overall strike of these structures separated by basement highs is NE-SW in the central part of the study area, changing to E-W in the south near the Dinarides and to NW-SE in the eastern part of the GHP near the Apuseni Mountains (Figure 2.3). The overall low-angle dipping geometry of the normal faults and the lateral variations along their strike reflect in many situations the geometry and variability of the thrust kinematics in the nappe stack developed during the Cretaceous-Paleogene evolution of the Tisza-Dacia Mega-Unit.

2.4.1 Seismic facies units in the sub-basins of the Great Hungarian Plain

Ten seismic facies units have been differentiated in the Miocene basin fill of the Pannonian Basin (Figure 2.4). Although the seismic characteristics depend on the seismic acquisition and processing methodology of various seismic data, general pattern can be established. The first three facies units, large scale (sub-)parallel discontinuous, fairly continuous and clinoform are characteristic for the large scale progradation that took place during Pannonian (s.l.) times in the upper part of the basin fill, and in all cases they post-date the extension. The clinoform facies unit contains locally intercalated hummocky ones (i.e. fourth seismic facies unit), which are in fact either clinoforms cross-cut along their strike or local turbiditic bodies (Szolnok Formation). The spatial distribution and significance of these post-rift facies units are well documented elsewhere (*Juhász et al.,* 2007; *Magyar et al.*, 2013; *Sztanó et al.*, 2013). The syn-kinematic sedimentation in the various sub-basins is characterized by a combination between different seismic facies units (units 5-10, Figure 2.4). In the lower parts of the syn-kinematic basin fill a chaotic seismic facies (unit 10) characterizes the onset of extension. This unit is either buried at high depth in the center of the graben (e.g., Figure 2.6) or spatially shifted along its flanks (e.g.,

Figure 2.7 and 2.9). The sub-parallel continuous and discontinuous seismic facies (units 5 and 6) are the most common ones usually observed in the center of the basins at high distance from its flanks by onlapping previous unconformity surfaces and inter-fingering with other facies units. These units are (sub-)parallel or can be gently divergent due to coeval offsets along normal faults. The proximal and distal lobes seismic facies (units 9 and 8) are observed in contact with the flanks of sub-basins, in particular well developed against normal faults. The proximal lobes facies unit has a gravitational character with coarse deposition and reflects periods of erosion of the adjacent footwall or hanging-wall flank. The lobes are always in close spatial contact, either prograding toward the center of the basin, retrograding towards its margins or aggrading. In the lower parts of the basin fill, this facies shows rapid progradation or retrogradation, while these patterns become more attenuated in its upper part. The oblique facies (unit 7) reflects progradation and is bounded by downlap and toplap reflection terminations.

2.4.2 Structures with peak syn-kinematic deposition during the Early Miocene

The Kiskunhalas Trough, with limited extent along its strike, is a narrow and deep basin, with syn-kinematic sedimentation reaching more than 3 kilometers in thickness (Figure 2.6). The overall structural geometry is asymmetric, with one large listric normal fault dipping NW-wards and several lower offset antithetic normal faults (Figures 2.3 and 2.6). The minimum value of the total horizontal offset cumulated along all normal faults, calculated by displacements in the syn-kinematic hanging-walls deposition, is ~6-7 km. Note that such offset calculations do not quantify footwall exhumation affected by erosion and therefore provide a minimum estimate. This erosional geometry is visible in the Kiskunhalas Trough by seismic onlaps and is most likely sub-aerial (Figure 2.6). The drilled pre-Neogene sequence includes medium-grade metamorphic rocks, Triassic shallow-water carbonates and Cretaceous deposits that are diagnostic for the Tisza unit. These pre-Neogene rocks have been attributed to the Villány-Bihor nappe of the Tisza unit (*Haas et al*., 2010). Wells have penetrated in the deepest part of the basin a (volcano-) clastic lacustrine succession (Kiskunhalas Formation). This is correlated with a similar succession found elsewhere that contains poorly developed Lower Miocene (Karpatian) fauna (*Rumpler and Horváth*, 1988; *Kőrössy*, 1992).

Figure 2.6 (facing page): Non-interpreted (top) and interpreted (bottom) reflection seismic section from the Kiskunhalas Trough. Location is displayed in Figure 2.3. White arrows indicate the Miocene kinematics of faults, red arrows show the late Middle - early Late Miocene inversion of the structure.

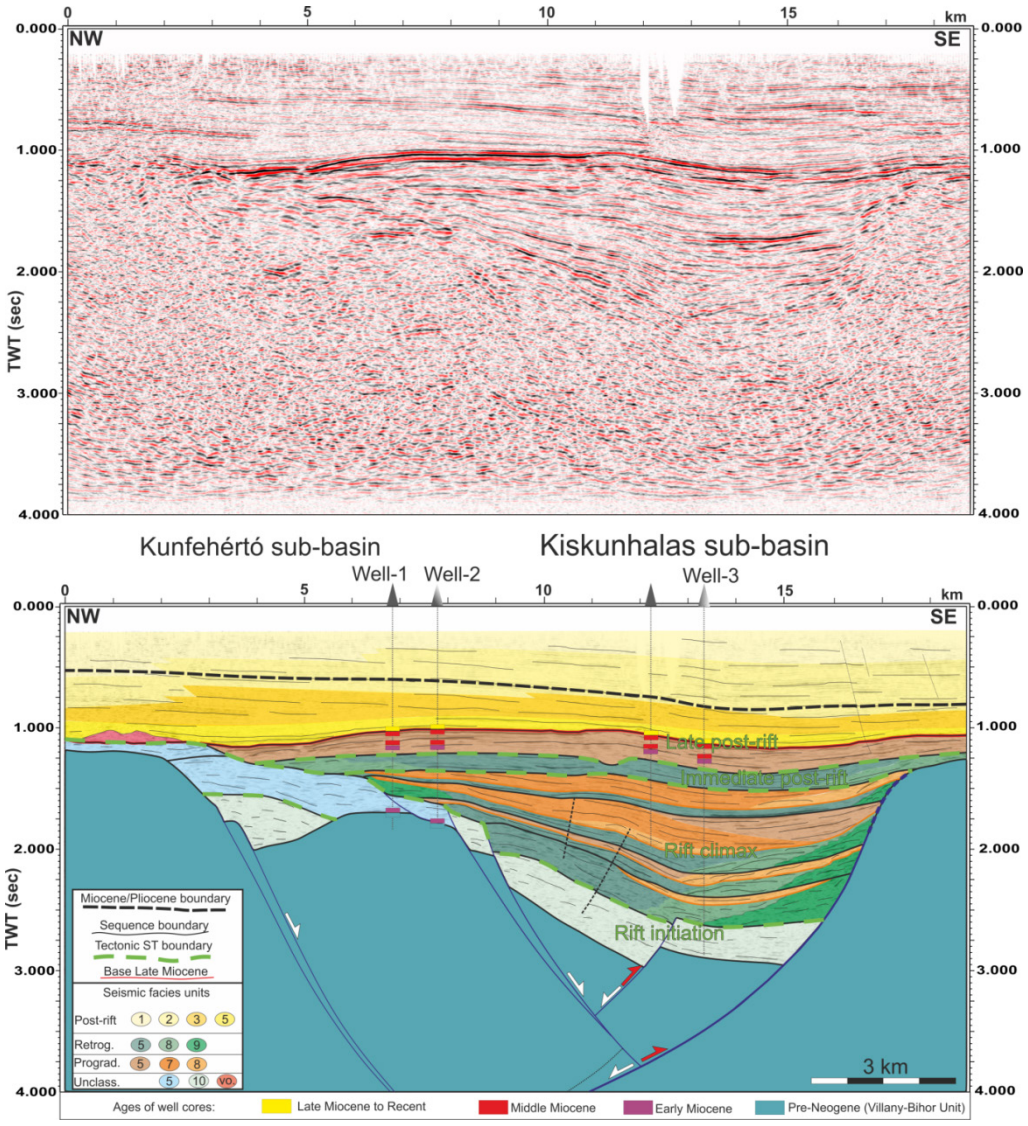

It is overlain by lower Middle Miocene (Badenian) carbonate and clastic rocks that are separated by an erosional unconformity from the overlying Pannonian sedimentary rocks. The lateral correlation of biostratigraphic ages observed in wells demonstrates that the age of the normal faults is Early Miocene. This unconformity is folded in a gentle anticline with Pannonian strata onlapping over its flanks. The entire upper Middle Miocene (Sarmatian) is missing or only a few meters thick below the unconformity (*Kőrössy,* 1992). This folded unconformity is the result of contraction (*Horváth,* 1995) that occurred during the late Middle Miocene or earliest Late Miocene and is associated with very low offset, high-angle reverse faults with south vergence located in the core of the anticline that could reactivate the earlier normal

faults (Figure 2.6). The overlying Late Miocene sequence is gently deformed and has thicknesses of about 1 km.

The seismic sequence interpretation of the Kiskunhalas sub-basin (Figure 2.6) shows a chaotic seismic facies unit in its lower part, interpreted as rift initiation system tract of Early Miocene in age. The overlying Early Miocene rift-climax sedimentation is composed of prograding and retrograding facies association units. Coeval erosion of the footwall indicates that the onlaps are coastal and the correlative maximum regression surface on the top of the prograding units is a regressive – trangressive sequence boundary. The rift climax system tract contains clastic lobes facies units that decrease gradually upwards in the stratigraphy, most likely as a result of the gradual footwall burial. The overall interpretation of Lower Miocene (Karpatian) sediments is in agreement with previous studies (*Lemberkovics*, 2014). The immediate post-rift system tract is in fact built up by one other Lower Miocene retrograding facies association that was followed by a latest Early - Middle Miocene prograding facies association during the onset of the post-rift system tract (Figure 2.5). The late post-rift deposition was interrupted by the contraction creating the erosional unconformity at the base of Late Miocene and its antiformal geometry (Figure 2.6). The overlying Pannonian sediments are part of the late post-rift system tract, which is sub-divided by an unconformity separating Miocene and Pliocene sediments (*Magyar and Sztan*ó, 2008). Near the NW margin of the structure hummocky to chaotic seismic facies units overlying the top Middle Miocene are likely Late Miocene basalts that are well studied in the nearby Kecel volcanic field (e.g. *Pécskay et al.,* 2006).

Our interpretation of the tectonic system tracts is in agreement with the sequence stratigraphic interpretation of well logs (Figures 2.5 and 2.6). The latter demonstrate a higher resolution cyclicity than the one depicted by the seismic lines, which is visible by high-resolution trends in the well logs (Figure 2.5). Along this first order pattern, the high-resolution prograding and/or retrograding trends can be grouped into a lower order cyclicity that matches the ones derived by the seismic interpretation. During the rift initiation, the coarse sedimentation along the NW flank is gradually replaced by lacustrine shales with periodic influxes of coarse alluvial sediments, more frequent near lower order sequence boundaries, which are likely controlled by the increase in accommodation space by normal faulting (Figure 2.6). One retrograding - prograding cycle can be observed in the rift-initiation system tract, likely underlain by one other beneath the depth investigation of the deepest well in the basin center (well 3, Figure 2.5). The rift climax is when coarser sedimentation is distributed throughout the entire basin, its variability matching the cyclicity observed in seismic lines by prograding-retrograding facies associations. Similarly with the seismic interpretation, well logs suggest four retrograding-prograding cycles that are gradually coarser upwards. Inside these sequences, the higher resolution cyclicity may

reflect tectonics or, most likely, higher order climatic or Milankovitch cyclicity. Also in accordance with the seismic interpretation, the immediate post-rift system tract is made up just by one trangressive facies association, followed by regression during the onset of the late stage post-rift, interrupted by the uplift, erosion and the formation of the regional Middle-Late Miocene unconformity.

2.4.3 Structures with peak syn-kinematic deposition during the Middle Miocene

To the north, the Kiskunhalas structure is adjacent to the Tázlár Trough (Figure 2.7). Wells penetrating the basement and the pre-Neogene sedimentary cover have shown that the Tázlár Trough overlies the thrust contact between the Villány-Bihor and Mecsek nappes (*Haas et al.*, 2010). The high-amplitude seismic reflectors observed in the pre-Neogene sequence along the NNW part and center of this structure are interpreted as the Triassic carbonatic cover of the Mecsek Unit, which was thrust by the SSE-ward located Paleozoic basement of the Villány-Bihor nappe (Figure 2.7). The overall structural geometry shows larger offset low-angle normal faults dipping NNW-wards which cross-cut the inherited Late Cretaceous Nappe contact and are associated with smaller offset antithetic normal faults dipping SSE-wards. The footwalls of the main NNW-dipping low-angle normal faults are highly eroded, suggesting exhumation and denudation during extension. The minimum value of the total horizontal offset cumulated along all normal faults is in the order of 4-5 km. The oldest stratigraphic age penetrated by wells in the SSE located main depocenter is lower Middle Miocene (Badenian), while the upper Middle Miocene (Sarmatian) is apparently missing. In this main depocenter the entire syn-kinematic sedimentation is interpreted as lower Middle Miocene (Badenian) in age, based on lateral correlation of well data available in the prolongation of the trough along its strike. One small offset normal fault cross cuts the Late Miocene sediments along the NNW flank of the main depocenter. This depocenter is flanked on the NNW by a smaller half-graben (locally named as the Soltvadkert sub-basin, Figure 2.7) filled with Lower Miocene (Karpatian) conglomerates and sandstones, which are separated from the overlying Pannonian sediments by an erosional unconformity, likely of sub-aerial origin. This half-graben is also slightly inverted by folding in a gentle anticline-syncline structure in a similar fashion as the Kiskunhalas sub-basin.

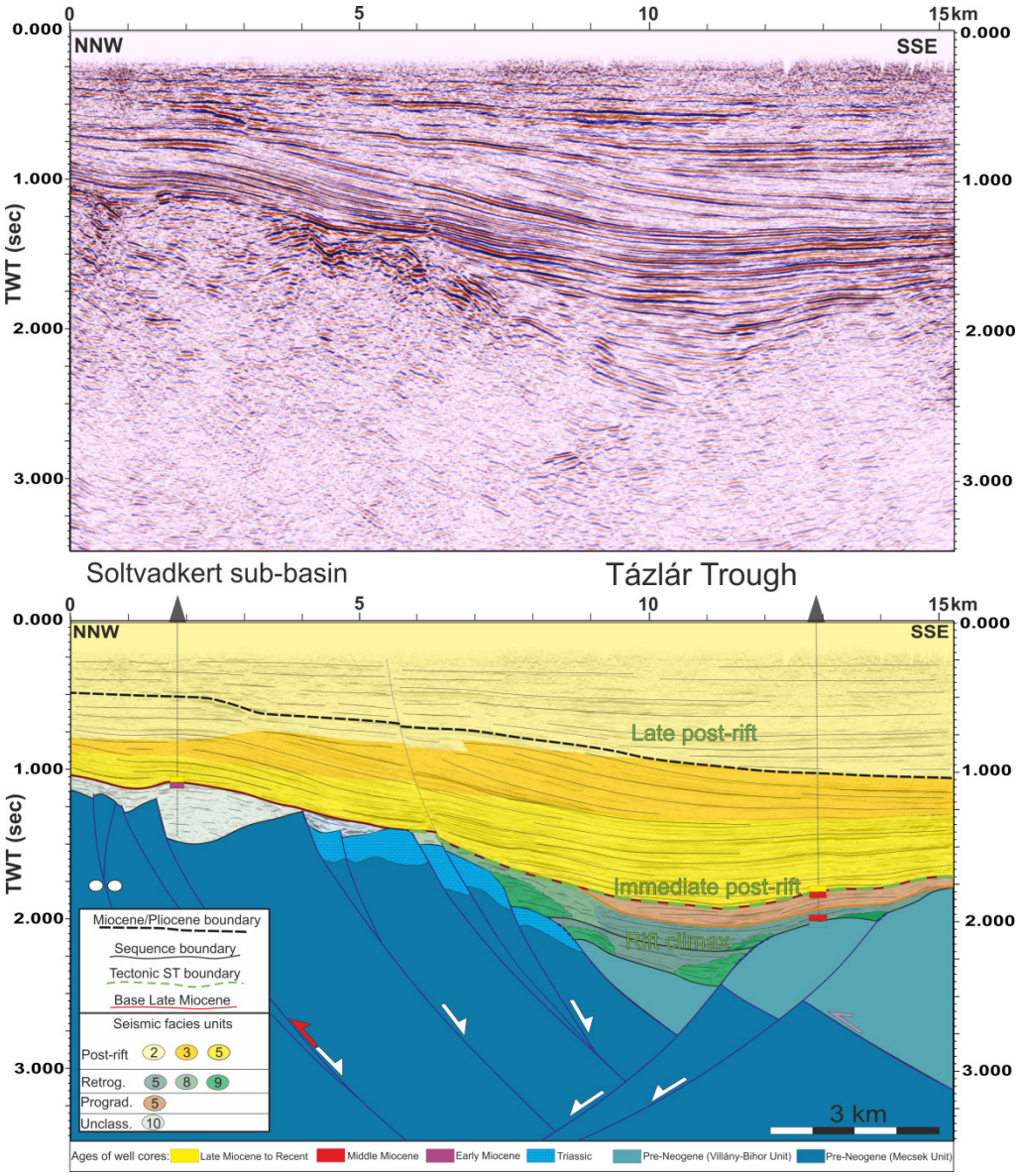

Figure 2.7: Non-interpreted (top) and interpreted (bottom) reflection seismic section from the Tázlár Trough. For location, see Figure 2.3. Grey arrow indicates Cretaceous thrust. White arrows indicate the Miocene kinematics of faults. Red arrow indicates the possible inversion of the fault of the small Soltvadkert sub-basin.

No clear rift-initiation could be identified in the main depocenter of the Tázlár Trough, where the sedimentation starts directly with a rift-climax system tract (Figure 2.7). A typical rift-initiation system tract with chaotic reflectors accompanying continental sedimentation is observed along the NNW located smaller Early Miocene half-graben. This geometry shows that the extension started with a rift initiation system tract located on the flank of the later basin followed by a migration of

deformation in the main depocenter where the rift climax is located. Such a spatial arrangement demonstrates a migration in space and time of structures and associated system tracts during extension. In the main depocenter, the rift climax system tract is made up by a retrograding facies association and a retrogradational-progradational cycle. The separating progradational facies association cannot be separated at seismic resolution. The immediate post-rift system tract is built up by Late Miocene (Pannonian) sediments. Similar with the Kiskunhalas structure, the erosion of the footwall in the Tázlár sub-basin indicates that these are genetic trangressive-regressive sequences. Overlying the rift climax system tract, the Upper Miocene sediments filled the depocenter during the late post-rift system tract. In fact the entire post-rift is part of the typical upper prograding shelf margin – slope clinoform system observed in the Great Hungarian Plain. A larger unconformity is observed within this latter sequence, where Pliocene sediments onlap the Miocene prograding slope clinoforms. Interpretation of additional seismic sections from this area shows that the height of the prograding clinoform is much higher above the former Middle-Miocene half-graben than above the flanking structural highs.

In the eastern part of the Great Hungarian Plain, near the Apuseni Mountains, a series of depocenters with arcuated shape connects a number of sub-basins, i.e. Békés, Vésztő and Derecske (Figure 2.3). The age of the syn-kinematic sediments is younger from SW to NE (i.e., from Békés to Derecske). In the SW, wells in the large Békés sub-basins have penetrated Middle-Miocene syn-kinematic sediments until ~5 km depth (see *Teleki et al.,* 1994). Beneath these deposits, the age near the base of the syn-kinematic succession in this up to 7 km thick sub-basin is still unknown.

The Vésztő Trough is a half-graben with low-angle normal faults dipping NW-wards (Figure 2.8). Although the number of wells penetrating this structure is relatively low, the lateral correlation from the neighboring Békés and Derecske sub-basins indicates that the syn-kinematic basin fill is Middle Miocene – earliest Late Miocene. This structure is typical for the overall Pannonian Basin, thin (~1.5 km) syn-kinematic deposition is overlain by remarkably thick (~3.5 km) post-rift sediments. The minimum total horizontal offset cumulated along all normal faults is in the order of 6 km. In the middle of the basin a low offset high-angle reverse fault inverted an earlier normal fault and is associated with a small anticline in the Middle Miocene sediments. Similar with elsewhere, the boundary of Middle and Late Miocene is an erosional unconformity, although less clearly observed and constrained. In the Vésztő Trough, the rift initiation system tract can be observed by the typical low amplitude, chaotic seismic facies both at the base of the main Miocene depocenter and along its flanks, being truncated by faults in the footwall or separated by an erosional unconformity in the hanging-wall (Figure 2.8).

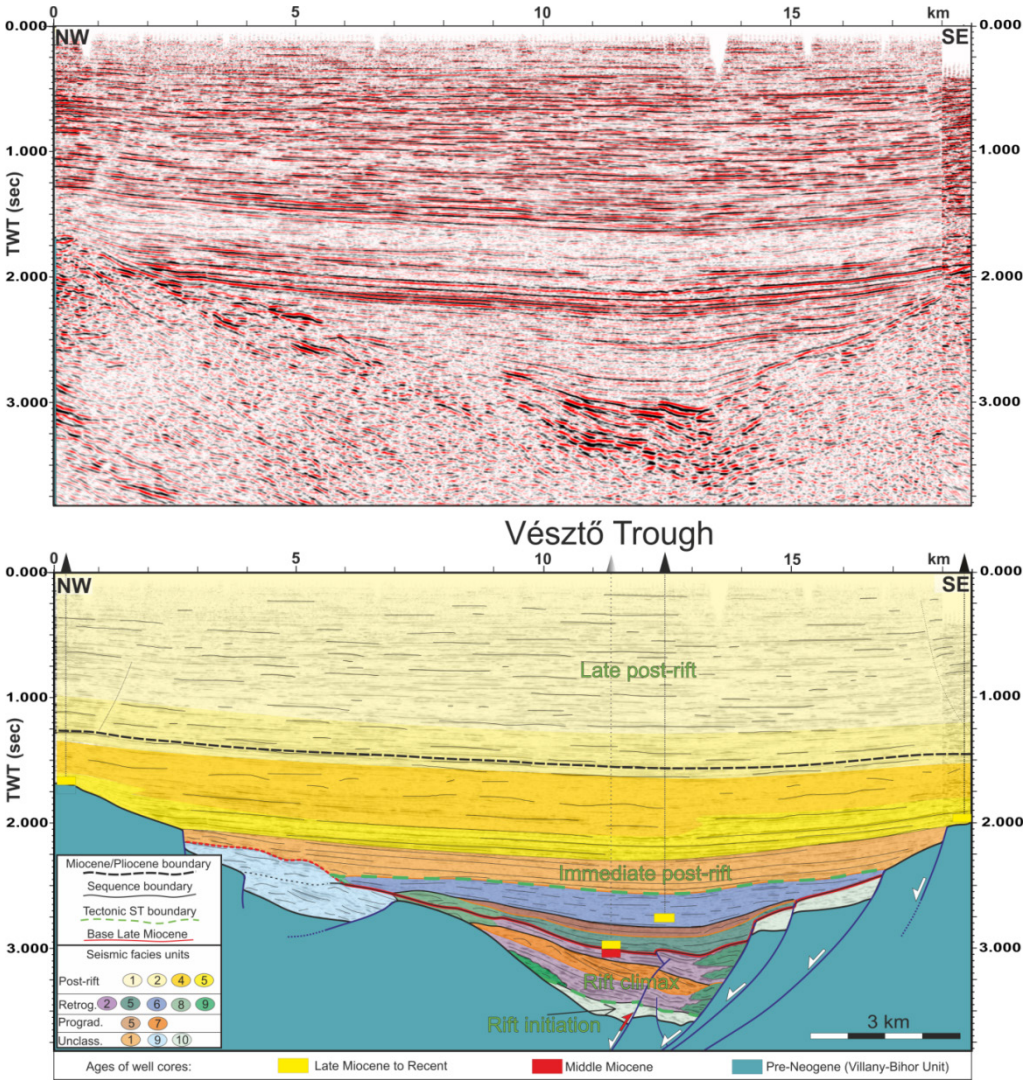

Figure 2.8: Non-interpreted (top) and interpreted (bottom) reflection seismic section from the Vesztő Trough. For location, see Figure 2.3. White arrows indicate the Miocene kinematics of faults. Red arrow indicates positive inversion of the Miocene normal fault during the earliest Pannonian times.

The rift climax system tract is built up by Middle and partly Upper Miocene sediments. In the main depocenter, three higher order transgressive-regressive cycles and a final retrograding cycle build up this rift climax system tract with clear lobe facies units near the flanks of the half-graben. Within the thinner second Middle Miocene cycle no progradation was observed, being likely either below seismic resolution or removed by erosion beneath the base Late Miocene unconformity. This unconformity separates the second from the third cycle and is associated with the small inversional structure. During the Late Miocene another retrogradational-

progradational and a final retrograding cycle is observed in the rift climax, overlain by the immediate post-rift and a thick late post-rift system tract. In the latter, the prograding shelf-margin slope (Algyő Formation) is observed by a typical low amplitude seismic facies, with a progradation direction perpendicular to the orientation of the section. The Miocene/Pliocene boundary is interpreted as a correlative conformity within the delta plain sediments of the late post-rift system tract (Figure 2.8).

2.4.4 Structures with peak syn-kinematic deposition during the Late Miocene

The Derecske Trough overlies the NW-verging contact between the Villány–Bihor and Mecsek nappes of the Tisza Mega-Unit emplaced during Cretaceous times (Figures 2.3 and 2.9). A deep exploration well has penetrated a structural contact where Mesozoic sediments affected by a Cretaceous greenschists metamorphic degree appear in a tectonic window from beneath the overall Paleozoic of the Villány-Bihor nappe. West of this window, this Paleozoic is also affected by this Cretaceous metamorphism, while eastward it retains only the original Paleozoic high degree of metamorphism (*Árkai et al.,* 1998). A number of thrust sheets have been identified to be associated with this tectonic contact that were reactivated by the Miocene extension when the ~6.5 km deep Derecske sub-basin was created (e.g. *Windhoffer et al.,* 2005). Interesting is that the Paleozoic and Cretaceous metamorphosed sediments are situated in the footwall of the large-offset normal fault system dipping E-wards (Figure 2.9). This implies that the exhumation of these footwall metamorphics is genetically related to the extension, likely along a low-angle detachment cross cut by a system of low-angle listric normal faults formed at later stages during exhumation. The age of these ESE-dipping faults gradually migrated in the same direction from Middle Miocene to Late Miocene times. These ESE dipping faults are associated with antithetic WNW dipping higher angle normal faults that migrate in age from Middle Miocene in the center of the sub-basin to Late Miocene along the ESE flank (Figure 2.9). The asymmetry of the syn-kinematic basin fill indicates higher cumulated offsets for the ESE-dipping system when compared with the WNW-dipping one. In the upper part of the syn-kinematic sediments, tilting of the reflectors gradually ceased within the Pannonian strata, suggesting the termination of the normal faulting during Late Miocene times at ~9 Ma. Minimum horizontal displacement of the extensional structures is ~12 km along the section.

Rift initiation sediments are made up of lower Middle Miocene (Badenian) chaotic seismic facies units drilled by wells in the main depocenter and in particular thicker overlying the WNW flank of the sub-basin (Figure 2.9).

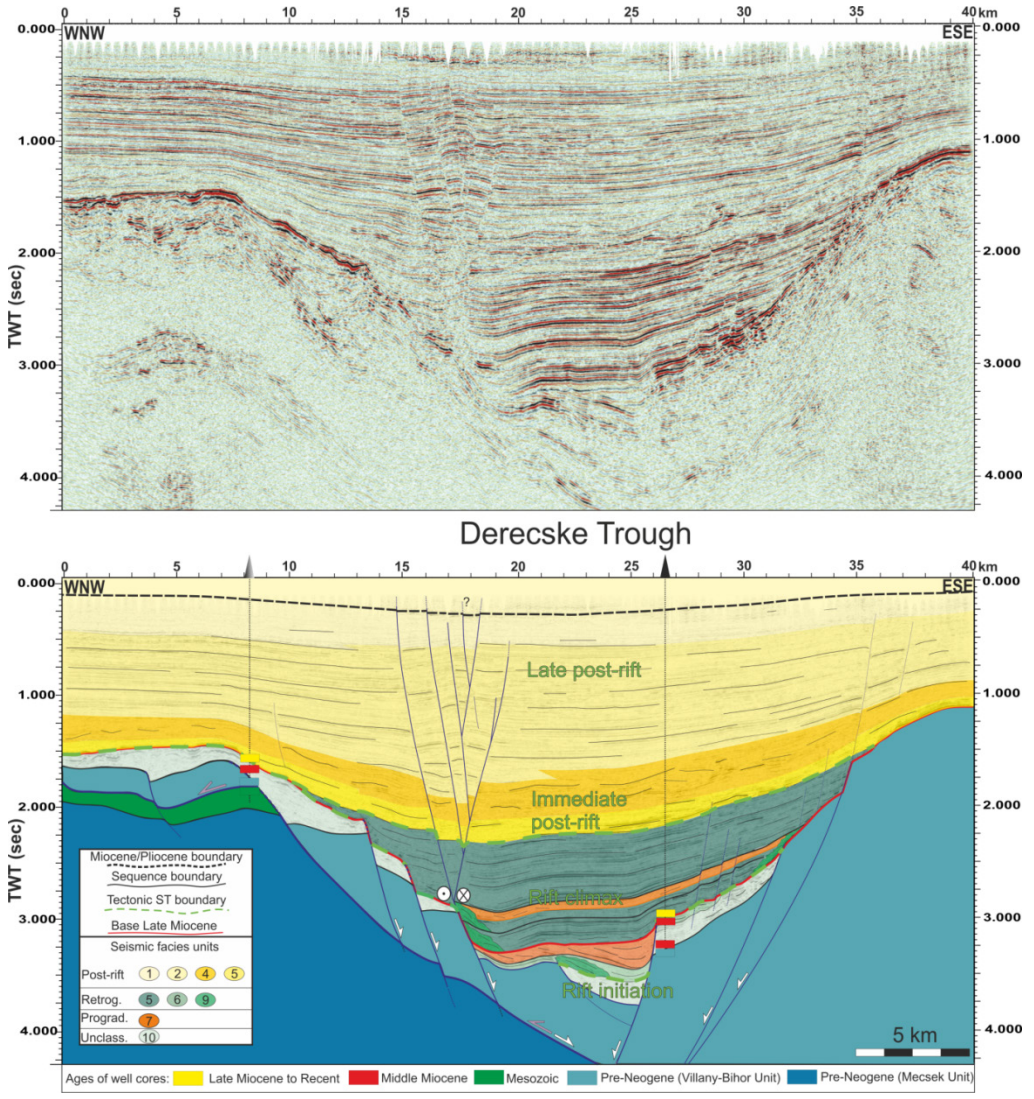

Figure 2.9: Non-interpreted (top) and interpreted (bottom) reflection seismic section from the Derecske Trough. For location, see Figure 2.3. Grey arrows indicate Cretaceous thrusts (after *Windhoffer et al*., 2005). White arrows indicate the Miocene normal faulting. The fault zone reactivated again during Pliocene - Quaternary times as a sinistral strike-slip zone creating the young negative flower structure.

This indicates a migration in time ESE-ward of the normal faulting during extension. The rift climax system tract is made up by a first retrograding-prograding sequence of hummocky and sigmoid facies units organized in an overall progradation that was interrupted by the Middle-Late Miocene unconformity. A second Late Miocene retrogradational, a retrograding-prograding and a final retrograding sub-cycle completes the rift-climax system tract. Immediate post-rift system tract is built up by progradation made up by the turbidites and clinoform facies units. The footwall of the

Middle-Late Miocene normal faults is highly eroded due to the gradual migration in space of normal faulting with time. Basin inversion starting around latest Miocene - Pliocene times has cross-cut and reactivated the inherited normal fault system as a sinistral negative flower structure. The horizontal displacement along individual fault segments is in the order of a few hundred meters (*Lemberkovics et al*., 2005). A few low offset normal faults are present near the ESE flank of the basin, most probably induced by differential compaction. The Miocene/Pliocene unconformity is situated only a few hundred metres below the surface indicating that there was limited amount of subsidence during the last ~5 Ma.

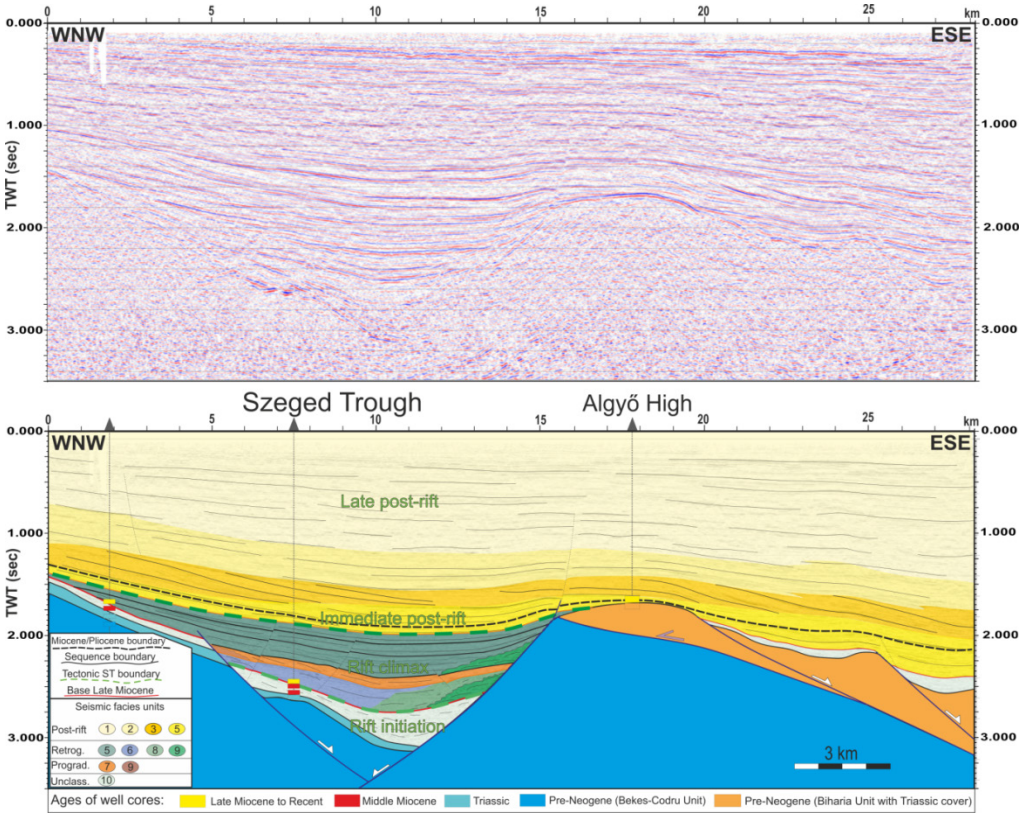

Figure 2.10: Non-interpreted (top) and interpreted (bottom) reflection seismic section from the Szeged (Banatsko Aranđelovo) Trough. For location, see Figure 2.3. Grey arrow indicates Cretaceous thrust of a piece of Dacia onto Tisza. White arrows indicate the Miocene kinematics of faults.

In the southeastern part of the Great Hungarian Plain three deep sub-basins developed in a relatively small area, i.e., Szeged, Makó and Tomnatec sub-basins (Figure 2.3). The Szeged Trough (or Banatsko Arandelovo in the Serbian prolongation) has a half-graben structural geometry with a low-angle normal fault dipping westwards and a smaller offset antithetic normal fault dipping eastwards

(Figure 2.10). The highly eroded footwall of the ESE fault bordering the Algyő-High suggests exhumation during extension. Two smaller offset low-angle normal faults might have inverted the former thrusts on the WSW flank of the neighboring Tomnatec sub-basin and are associated with Middle and Late Miocene syn-kinematic sedimentation. The minimum value of the horizontal extensional displacement along all these structures is in the order of 8 kilometers. The syn-kinematic sedimentation reached ~2.5 km in the center of the Szeged sub-basin. The wells drilled on the flanks of the basin have identified a sequence composed of early Middle Miocene (Badenian) shallow water limestones and Late Miocene clastics, while the upper Middle Miocene (Sarmatian) is missing (*Pigott and Radivojević*, 2010).

The seismic sequence interpretation of the Szeged sub-basin shows Middle-Miocene rift initiation in the main depocenter with chaotic, low amplitude seismic facies units that are also observed on the WSW flank of the neighboring Tomnatec sub-basin. Overlying the basal unconformity, a full retrograding-prograding cycle and three upper retrograding facies associations compose the Late Miocene rift climax system tract, in particular well visible by the evolution of lobe facies along both flanks of the sub-basin. The retrograding seismic facies units are separated by unconformities. Overlying the near shore Middle Miocene limestones and the subsequent Late Miocene lobe facies units an ESE-ward progradation pattern with downlap reflection terminations can be observed in the regressive facies association from WNW direction toward the basin which is coeval in time with footwall erosion along the opposite flank of the basin (Figure 2.10). This infers that the progradation took place in shallow water conditions. Overlying the upper retrograding facies associations, the immediate post-rift system tract has a progradational character that continues also during the late post-rift system tract. In fact the entire post-rift is part of the Pannonian prograding shelf margin – slope clinoform system that started during the immediate post-rift with the deposition of bottomsets at ~5 Ma (*Magyar et al*., 2013). The Pliocene late post-rift system tract reaches 1.5 km in thickness. The main fault bordering to the ESE the Szeged sub-basin has an offset upwards in the post-rift sequence. This is only apparent, as the offset is created by differential compaction. There are no contractional structures apparent in our seismic interpretation during the transition between Middle and Late Miocene. The overall thickening of the post-rift strata eastwards are likely related to the higher amount of extension observed in the neighboring Makó-Tomnatec structure. The Miocene/Pliocene boundary was correlated within the immediate post-rift turbiditic sediments in this sub-basin.

The Makó Trough of SE Hungary is one of the largest and deepest Neogene sub-basins of the Pannonian Basin, the center of the basin attaining a depth of about 7 km. It continues laterally along its strike to the SE and S with the Tomnatec sub-basin (Figure 2.3). Recent studies have suggested that the entire succession in the center of the basin is Upper Miocene and younger in age (*Magyar et al*., 2006; *Szuromi-Korecz*

et al., 2004). Middle Miocene sediments are observed discontinuously by wells drilled over the neighboring highs and are separated by unconformities in their lower and upper parts (*Magyar et al*., 2006).

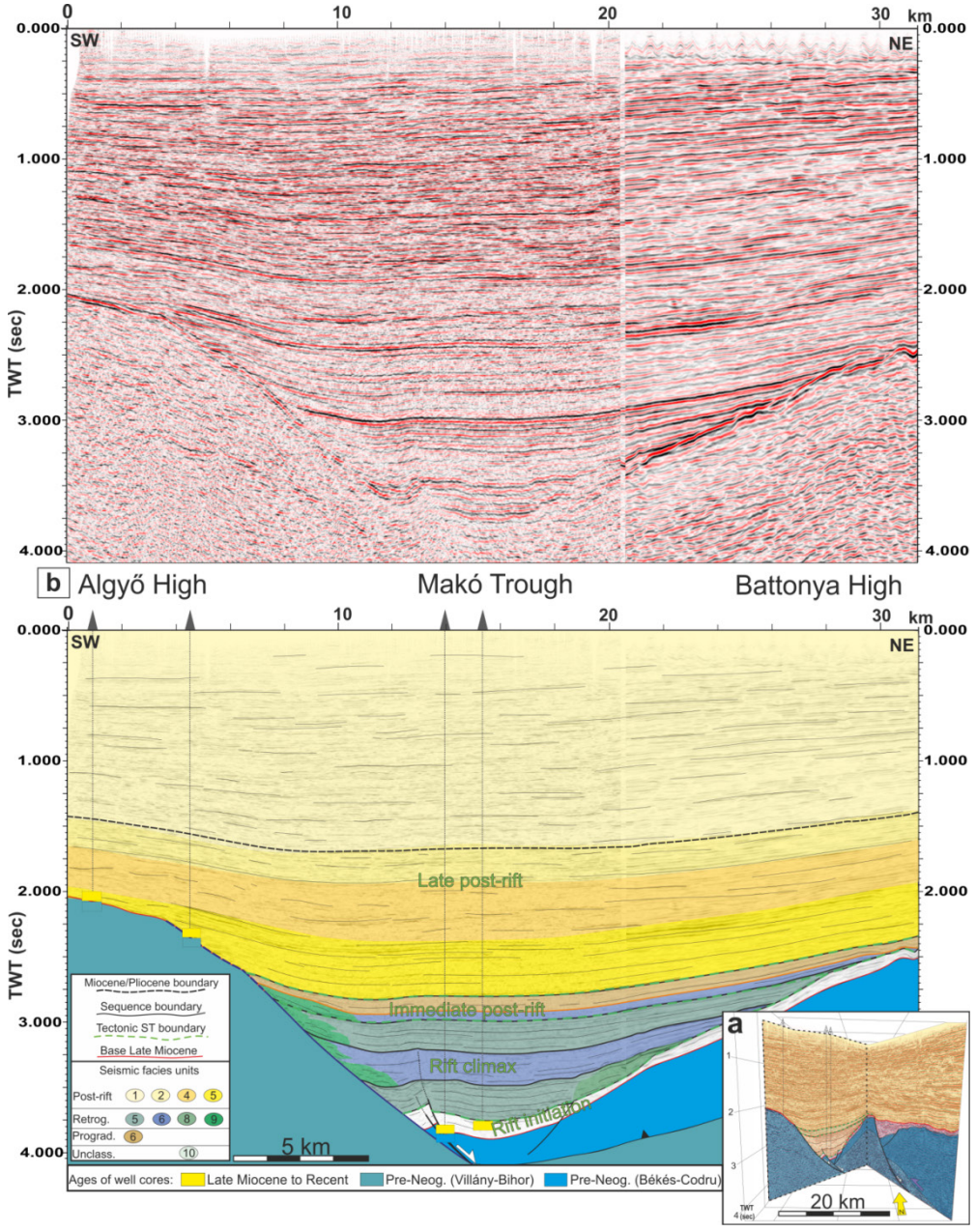

Figure 2.11: Seismic data from the vicinity of the Makó Trough. (a) Composite section from the sub-basins showing perpendicular extensional structures. (b) Non-interpreted (top) and interpreted (bottom) reflection seismic section from the Makó Trough. For location, see Figure 2.3. In our interpretation of the pre-Neogene basement and cover, the contact between Békés-Codru and Villány-Bihor units is a Late Cretaceous top NNW thrust contact. White arrows indicate the Miocene kinematics of faults.

In the center of the basin near its base, proximal conglomerates, likely related to normal faults activity, were drilled by the well Makó-6 and are of Late Miocene in age (based on nannoflora and dinoflagellates; see *Sztanó et al*., 2013). On the overall, the geometry of the pre-Neogene sub-basin flanks is remarkably symmetric. However, the real asymmetry is visible in the syn-kinematic basin fill. The main controlling structure is a low angle listric normal fault located in the SW side that accommodated the subsidence of the Makó sub-basin and the uplift of the adjacent Algyő footwall (Figure 2.11, see also *Tari et al*., 1999). Significantly smaller offsets normal faults can be observed near the center of the basin, either antithetic or synthetic. In the middle of the basin, one very gentle dipping anticline is likely associated with a minor inversion along a synthetic normal fault (*Sztanó et al*., 2013). The minimum value of the horizontal extensional displacement along all these structures is about 10 kilometers.

The rift initiation system tract in the Makó sub-basin is Pannonian in age, although the few hundred meters at the base of the depocenter are not yet drilled. It is made up of thin conglomerates and sandy siltstones (*Sztanó et al.,* 2013) and can be observed at the base of the sub-basin as overlain by an unconformity (Figure 2.11). Within the rift climax system tract three higher-order retrogradational sub-cycles can be distinguished based on the variable seismic facies and lobes seismic units near its flanks. Progradational features are absent or below the seismic resolution in the upper part of these sub-cycles. Sourcing to the half-graben with sediments eroded from the exhumed Algyő High during the rift climax system tract took place until ~9-8 Ma, when this high was submerged (*Magyar et al.*, 2006). This means that the higher order cycles of the rift climax system tract are in fact genetic TR sequences. The onset of the immediate post-rift system tract is interpreted as the first progradational facies association. The Makó sub-basin was ultimately filled by thick prograding shelf slope sediments at ~5.7 Ma (*Magyar et al.,* 2013; *Sztanó et al*., 2013), followed by deltaic and alluvial plain sedimentation. The Miocene/Pliocene boundary is a correlative conformity in the area of this sub-basin within the alluvial and delta plain environments.

The flanks of the NNW-SSE oriented Makó sub-basin is cross-cut by a smaller WSW-ENE oriented normal fault that created the smaller Földeák sub-basin filled most likely by syn-kinematic Middle Miocene sediments overlain unconformably by Upper Miocene deposits (Figure 2.11). These two orientations may be related to two extensional directions, the older Middle Miocene one reactivating a system of WSW-ENE oriented Cretaceous thrusts with NNW vergence (*Tari et al*., 1999). In the older basin, the seismic facies is rather uniform and difficult to separate in individual units, characterized by high amplitude, discontinuous reflectors.

2.5 Seismic sequence stratigraphy in the Great Hungarian Plain and phenomenological inferences

The spatial and temporal distribution of seismic facies units is conditioned by episodic activity of normal faults in various sub-basins (Figure 2.12). The chaotic seismic facies make up the rift-initiation system tract in the oldest unit observed either at the base of the entire syn-kinematic succession (e.g., Early Miocene rift initiation of the Kiskunhalas and Middle Miocene rift initiation of the Szeged sub-basins, Figures 2.6 and 2.10, respectively) or over the flanks of the separating highs (e.g., Tázlár and Derecske sub-basins, Figures 2.7 and 2.9, respectively). The latter position is absent in typical sequence stratigraphic models of extensional grabens (e.g., *Martins-Neto and Catuneanu*, 2010; *Prosser*, 1993) and is a result of gradual migration of extension in time from the position of the present-day flank to the center of the sub-basin (Figure 2.12). The sedimentological environment of the rift-initiation system tract in our observed extensional sub-basins is also different when compared with these earlier models. Continental conditions are observed only when the rift-initiation system tract is entirely of Lower Miocene in age (e.g., Soltvadkert sub-basin, Figure 2.7), when the Central Paratethys domain of the Pannonian Basin was separated from the marine realm. Wherever the onset of extension took place during Middle – Late Miocene, the rift initiation system tract contains the record of a rapid transition from continental to shallow marine conditions (e.g., the Szeged sub-basin, Figure 2.10). This means that the sedimentological environment of the rift initiation system tract is dependent on the regional presence or absence of connections between the half-graben and the marine realm, rather than the evolution of the local sub-basin. No retrograding - prograding (and therefore no transgressive - regressive) cyclicity could be defined in the rift initiation sequence at the seismic details, most likely because the organization of sediments in these cycles is beneath the seismic resolution. However, such patterns are rather clear in the well logs seismic stratigraphy (Figure 2.4) that shows cyclicity also within the rift initiation system tract.

The evolution of sedimentation during the rift climax system tract (Figure 2.12) is directly controlled by normal fault offsets, creating gravity driven deposits in proximal areas, such as lobes seismic facies units, derived directly from the exhumed hanging wall and, more importantly, from the erosion of the uplifting footwalls. The progradational, retrogradational or aggradational character of these lobes is one major criteria to distinguish the high resolution cyclicity. In more distal positions, (sub-) parallel to divergent seismic facies units characterize the basin fill associated with sigmoidal seismic facies units during periods of regression. In the final part of the rift-climax system tract the footwall subsides and is gradually covered by sediments, decreasing its importance as a source area. Finally, during Late Miocene times the sub-parallel to hummocky turbiditic seismic facies units fill the large accommodation

space created by a subsidence that is more regional than the scale of individual sub-basins, followed by the deposition of the clinoform seismic facies units of the prograding shelf-margin slope. The (sub-) parallel continuous and fairly continuous seismic facies units in the upper part of the basin indicate the gradual fill of the basin and deltaic and alluvial plain sediments (Figure 2.12).

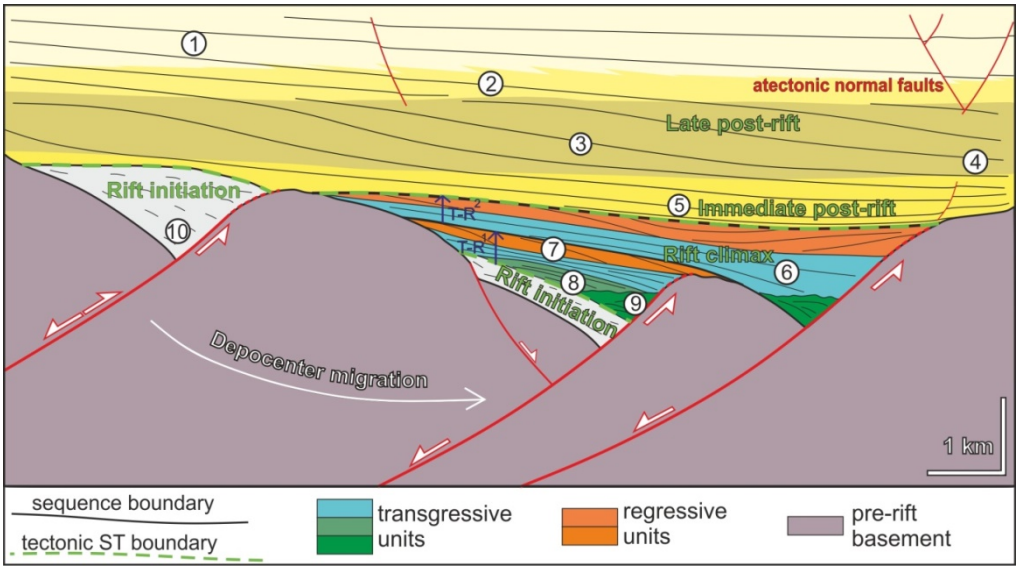

Figure 2.12: Simplified stratigraphic model of the half-grabens of the Pannonian Basin (modified after *Prosser,* 1993; *ter Borgh,* 2013). Numbers represent the characteristic seismic facies units of a half-graben, cf. Figure 2.4. The characteristic retrograding and prograding seismic facies units are grouped into transgressive-regressive cycles. These cycles are grouped into lower order tectonic system tracts, representing phases of basin evolution such as rift initiation, rift climax, immediate post-rift and late post-rift. Note the features of these half-grabens, such as migration of depocenters and the exhumation and erosion of the footwalls of active low angle listric normal faults.

Footwall erosion was coeval with the deposition of almost all retrogradational -progradational cycles. This indicates that erosion combined with the correlative maximum regression surface defined by the geometry of the seismic facies units is an expression of the composite surface that bounds a transgressive – regressive (TR) sequence (Figure 2.12). The exception is locally the last retrogradation of the rift climax or the subsequent progradation of the immediate post-rift system tracts, where footwall erosion was reduced or absent. The transgressive facies associations are made by (sub-)parallel to divergent continuous to hummocky seismic facies units onlapping both the footwall and hanging-wall, intercalated with large amounts of lobe seismic facies units. The latter results from the large rate of displacement along normal faults creating high-dip slopes. Periods of reduced rate of offset along normal faults are associated with the regressive facies associations, made up mainly by offlaps and prograding seismic reflection patterns. In the case of Kiskunhalas, Vesztő

and Szeged sub-basins (Figures 2.6, 2.8 and 2.10), delta systems can be observed prograding over the hanging-wall towards the center of the sub-basins during the deposition of the regressive facies associations. The transgressive - regressive sequence boundaries are marked by toplap and overlying downlap reflection terminations. This higher order transgressive-regressive cyclicity is characteristic for the Early and Middle Miocene rift climax sequences, but apparently less developed within Late Miocene rift climax deposits.

In the central part of the Great Hungarian Plain the late Middle Miocene (Sarmatian) sediments are very thin or completely missing beneath the Middle-Late Miocene unconformity, which has an erosional character outside the deepest Middle-Miocene (half) grabens. The unconformity is often associated with contractional structures showing N-S compressional direction, such as gentle symmetric anticlines of small inversion of earlier normal faults (e.g., Kiskunhalas or Vésztő sub-basins). On the contrary, the late Middle Miocene is thick near the Pannonian basin margins bordering the Serbian Dinarides, Alps and the Carpathians (Figure 2.14, *Magyar et al*., 1999; *Pavelić*, 2001; *Kováč et al*., 1995).

Starting from the erosional unconformity at the Middle/Late Miocene boundary, the water depth of Lake Pannon increased during the early Late Miocene, as indicated by the height of the subsequent prograding Pannonian shelf margin slopes (*Magyar et al.*, 2013). Previous calculations indicate several hundreds of meters, possibly up to 1 km paleobathimetries (*Balázs et al*., 2013). In the peripheral areas of the Pannonian Basin, like the Nyírség sub-basin in the NE and in the vicinity of the southern coastline of Lake Pannon, delta and alluvial plain environments remained characteristic during the entire Late Miocene – Pliocene evolution, where sedimentation kept pace with the rate of creating accommodation space (Figures 2.3 and 2.13). This means that in the deepest Late Miocene half-grabens, situated further away from source areas, shallow water sediments build up only the oldest Pannonian syn-kinematic succession. The rate of creating accommodation space (i.e. rapid relative lake-level rise) was significantly higher when compared with the rate of sediment supply. Therefore, these thick Late Miocene rift climax system tracts situated in a distal position in the Great Hungarian Plain relative to the source area (e.g., Derecske and Makó Trough; Figures 2.9 and 2.11) are mainly built up by transgressive cycles. In such situations, it is possible that the bulk of the Pannonian sedimentation post-dated the normal faulting, burying the normal faults with such deep water deposition during post-kinematic times.

The immediate post-rift system tract was coeval with the cessation of fault offsets, with the rate of sediment supply being generally higher than the rate of creating accommodation space. This can be recognized by sub-parallel, fairly continuous, occasionally gently divergent reflections (Figure 2.5). The onset of post-

rift deposition was diachronous in the various sub-basins and is not marked by a clear erosional unconformity marking a transition to post-rift sedimentation. Driven by regional contractional processes (*Horváth*, 1995), the juxtaposition of the Middle/Late Miocene regional unconformity with a general syn-rift/post-rift boundary would be a coincidence, but this was not observed in every studied sub-basin.

The late post-rift system tract deposits of the Pannonian Basin are made up by turbiditic deposits, prograding shelf margin slope, and alluvial plain and delta sediments (Figures 2.5 and 2.12). During the late post-rift system tract the cyclicity was controlled by other regional processes than the local scale of the extensional sub-basins, such as absolute lake level variations or the late stage basin inversion (*Csató et al*., 2015; *Magyar and Sztanó,* 2008; *Sacchi et al.*, 1999). Interesting is that the large scale Pannonian progradation contains thicker prograding clinoforms above the former extensional basins, most likely due to differential compaction being active during deposition. This compaction creates also offsets in the post-rift sequence overlying the earlier normal faults (e.g. *Teleki et al*., 1994), which typically increase upwards in the stratigraphy.

2.6 Discussion

Our study demonstrates that the Pannonian Basin system has undergone multiple phases of extension and basin inversion during its Miocene evolutionary history. Different sub-basins were affected by different amounts of deformation at various times, as a function of rheological variations, inherited weakness zones and degree of extensional asymmetry (Figure 2.14).

Figure 2.13 (facing page): Interpreted composite reflection seismic transects from the Pannonian Basin showing the main tectonic and stratigraphic features of the area. For location, see Figure 2.1. Note the striking difference of the thickness of Early to Middle Miocene and Late Miocene deposits. Late Miocene succession is subdivided based on the characteristic time transgressive environments of Lake Pannon (age of the prograding shelf-edges derives from *Magyar et al*., 2013). a) Section from the eastern part of the Pannonian Basin is modified after *Balázs et al.* (2013). It shows Middle- and Upper Miocene syn-kinematic deposition in the (half) grabens. Bouguer gravity anomalies imply the asymmetry of the highly extended Makó Trough and Békés Basin, where local gravity minimum corresponds to the basement high, while positive values characterize the deep basins (for detailed modeling see *Szafián and Horváth*, 2006; *Király et al.*, 2012; *Tari et al.,* 1999). b) Section from the southern and western parts of the Pannonian Basin is modified after *Matenco and Radivojević* (2012), where syn-tectonic deposition is Lower to Middle Miocene. Neotectonic inversional structures have formed, for instance, at offset 80, 135 and 170 kilometers in section b. At the southern part of this section the low Bouguer anomaly values correspond to the crustal "root" of the Dinarides.

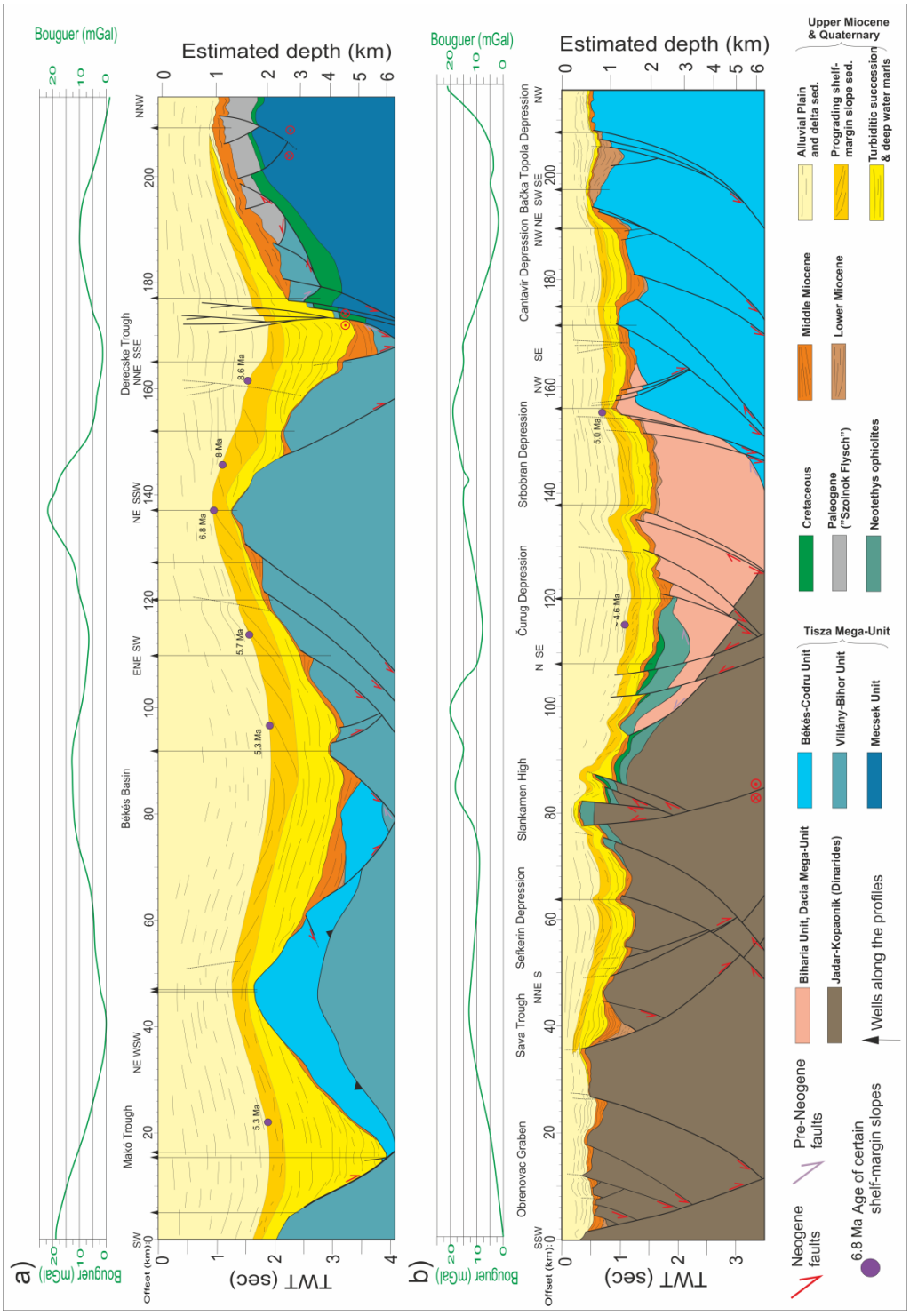
a)
b)
Bouguer (mGal)
Estimated depth (km)
TWT (sec)
Offset (km)
Mako Trough
Békés Basin
Derecske Trough
Sava Trough
Selkerin Depression
Slankamen High
Čurug Depression
Srbobran Depression
Cantavir Depression
Bačka Topola Depression
Obrenovac Graben
5.3 Ma
5.7 Ma
6.8 Ma
8 Ma
8.6 Ma
~4.6 Ma
5.0 Ma
Upper Miocene & Quaternary
Alluvial Plain and delta sed.
Prograding shelf-margin slope sed.
Turbiditic succession & deep water marls
Middle Miocene
Lower Miocene
Cretaceous
Paleogene ("Szolnok Flysch")
Neotethys ophiolites
Tisza Mega-Unit
Békés-Codru Unit
Villány-Bihor Unit
Mecsek Unit
Biharia Unit, Dacia Mega-Unit
Jadar-Kopaonik (Dinarides)
Neogene faults
Pre-Neogene faults
6.8 Ma Age of certain shelf-margin slopes
Wells along the profiles

2.6.1 Tectono-sedimentary evolutionary model of a highly extended back-arc basin

The seismo-stratigraphic interpretation infers a clear interplay between sedimentation and tectonics during the Miocene syn-kinematic deposition in the Great Hungarian Plain part of the Pannonian Basin. The type and amount of sedimentation was variable in time and space and resulted in different sedimentary facies units deposited at first in continental alluvial to lacustrine, shallow marine to pelagic and locally deep-water environments, and ultimately back to continental lacustrine to alluvial sedimentation. Although discussed in previous studies, our analysis is the first basin-scale demonstration that the extension in the Great Hungarian Plain part of the Pannonian Basin migrated in time and space throughout the Miocene.

The activity of the extensional sub-basins and associated detachments started near or in the Dinarides already during Early Miocene times, possibly even earlier during Oligocene (*e.g., Toljic et al*., 2013), extensional detachments being accompanied by the deposition of thin continental alluvial to lacustrine sediments (*Krstic et al*., 2003; *Matenco and Radivojević*, 2012). Interestingly, the amplitude of extensional exhumation of the footwalls was much higher than the tectonic subsidence of the associated sub-basins during the Early Miocene. Our data show that the Early Miocene direction of extension was NW – SE oriented (Figure 2.3), such as observed in the Kiskunhalas sub-basin. In agreement with all previous studies, our data show that the Middle Miocene was the peak period of syn-rift subsidence of the Pannonian Basin, most of the half-grabens of the Great Hungarian Plain accommodating maximum hanging-wall deposition. The extension had variable offsets and extensional directions, in general N –S in the southern and westernmost parts and NW – SE in the central part (Figure 2.3). The variable extensional directions were likely related to coeval vertical axis clockwise rotations during the overall NE to E-ward translations (Figure 2.15).

The anomalous pattern of the distribution of late Middle Miocene (Sarmatian) sediments might be related to different processes, but one interesting feature is its ~400 km of wavelength. This geometry can be interpreted either as complete removal of late Middle Miocene strata by the inversion in the central part of the basin (*Horváth*, 1995), or by gradual footwall exhumation leading to erosion and/or non-deposition as suggested in areas near the Dinarides (*Matenco and Radivojević*, 2012). This can be also interpreted as an effect of basin scale uplift in the center of the Great Hungarian Plain and coeval subsidence of its peripheral areas. This interpretation is in agreement with the observation that in the center part of the Pannonian Basin shallow water environment was dominant in contrast to the early Middle Miocene higher water depth. Contractional structures are also present, but their amplitude cannot justify the erosional removal of a km-thick sequence. Therefore, the unconformity formed likely as a combination between the previously mentioned mechanisms. The

N-S oriented direction of contraction is in contrast with the inferred E-ward coeval movement of Carpathian units. This is also the peak moment of coeval clockwise rotations in the Tisza-Dacia units (Figure 2.2), whose effects in the various sub-basins of the Great Hungarian Plain are largely unknown.

The extension continued during the Late Miocene times. Although various normal faults with variable offsets have been previously described (*Fodor et al*., 2013; *Balázs et al.*, 2013; *ter Borgh,* 2013) our study demonstrates that this extension had major effects by creating or significantly enlarging some of the deepest sub-basins in the Great Hungarian Plain, such as Makó, Szeged or Derecske with an average E-W extensional transport direction. This was followed by large-scale post-rift subsidence that was diachronous and buried most of the sub-basins beneath 2-3 km thick deposition of sediments.

The overall extensional directions presently observed in the Great Hungarian Plain were obviously affected by the gradual clockwise rotation of the Tisza-Dacia block (e.g., *Balla*, 1987). Earlier Miocene structures recorded larger amounts of rotation when compared with the later ones. In fact, there is just one main ENE-WSW extensional direction in the entire Great Hungarian Plain that becomes more N-S near the Dinarides and more E-W near the Apuseni Mountains (*Csontos and Nagymarosy*, 1998; *Fodor et al*., 1999) following the clockwise geometry of their relative rotations. All other orientations reflect subsequent rotations after deformation (Figure 2.15). This also explains why different orientations are observed in the same area, such as the early Miocene NE-SW strike of Kiskunhalas or Földeák sub-basin versus the NW-SE strike of Late Miocene Szeged or Makó sub-basins (Figure 2.3 and 2.11a). Such high degrees of vertical axis rotation during extension are also observed in other back-arc basins, for instance, at the Alboran domain of the Gibraltar arc, the Aegean Sea at the Hellenic Trench or the Caribbean region at the Lesser Antilles Trench (*Faccenna et al.*, 2014; *Govers and Wortel*, 2005).

The first structures of the last stage of tectonic inversion formed during the latest Miocene times near the Dinarides such as in the SW Zala Basin (Figure 2.1, *Uhrin et al*., 2009) or in the southern Serbian part (Figure 2.13b) at ~7.5 – 8 Ma. This means that when extension was still active in the eastern part of the Pannonian Basin (Szeged, Makó, Derecske), when the onset of contractional deformation took place near the Dinarides. Therefore, the last stage of inversion also migrated in space and time from the S and SW margin of the Dinarides N-wards (i.e. from the Adriatic indenter) towards the central Pannonian Basin. The peak contractional event took place at the end of Miocene or earliest Pliocene, caused likely by the northward drift and CCW rotation of the Adriatic microplate (*Pinter et al*., 2005). It has resulted in a clear unconformity near the Miocene/Pliocene boundary with major angular aspect in

various places in the basin (e.g., Tázlár sub-basin, Figure 2.7), being replaced laterally with a correlative conformity in deeper sub-basins (*Magyar and Sztanó*, 2008).

2.6.2 Extensional detachments versus low angle normal faults in the Great Hungarian Plain

One interesting feature of the Pannonian extensional structures is the relative low-angle dip of fault planes that is variable from ~20° (Makó sub-basin) to ~30° (Szeged sub-basin), or up to ~40° (Derecske sub-basin). This was facilitated by the reactivation of the former low-angle Cretaceous thrusts as observed by seismic and well data in our and previous studies (e.g., the Derecske sub-basin, Figure 2.9, see also *Windhoffer et al*., 2005). This is in particular obvious for the presently NW-ward vergent Turonian nappe contacts of Tisza unit. The extensional mechanism is clearly asymmetric, being linked with the activity of controlling low-angle normal faults or extensional detachments that resulted in significant erosion during the relative uplift of footwalls. In other situations, the low-angle normal faults crosscut pre-existing thrusts (such as the Tazlar sub-basin, Figure 2.7), most likely because the inherited thrusting geometry was not favorable for reactivation. Extensional detachments are widely known near the Pannonian Basin margins with or inside the Eastern Alps or the Dinarides (e.g., *Ustaszewski et al.,* 2010; *van Gelder et al.*, 2015). Such detachments exhumed in their footwall previously metamorphosed Mesozoic rocks during the Cretaceous - Paleogene nappe stacking. In the studied area of the Great Hungarian Plain, only the WNW part of the Derecske sub-basin shows such Paleozoic - Mesozoic basement and sediments affected by a Cretaceous greenschists metamorphic degree (*Árkai et al.*, 1998; Figure 2.9). This area may satisfy the possible conditions of a ductile shear zone exposed in the footwall of an extensional detachment that could eventually define a core-complex type of structure. All other sub-basins show non-metamorphosed Mesozoic or Paleogene sediments in the immediate footwall of the controlling structures and, therefore, such structures should be called low angle normal faults with footwall exhumation controlling half-grabens.

Such an interpretation includes likely the Algyő High that is situated in the footwall of the controlling structure in both the Szeged and Makó sub-basins (e.g., Figure 2.10), previously interpreted as a Miocene metamorphic core complex based on a preliminary Early Miocene zircon fission track age (*Tari et al*., 1999). Wells penetrating this high have identified a non-metamorphic Triassic carbonatic sequence that is in structural contact with rocks metamorphosed during Cretaceous times (*Lelkes-Felvári et al*., 2005), while the wells penetrating the pre-Neogene sequence on the western flank of the Szeged sub-basin have penetrated Paleozoic metamorphics and a Triassic sequence of the Békés-Codru nappe of the Tisza unit. The Cretaceous metamorphosed rocks were assigned to the Biharia nappe of the Apuseni Mountains, thrusted probably during Turonian times over the neighboring Békés-Codru nappe

that retains a Variscan age metamorphism and is covered by a non-metamorphosed Mesozoic sequence (Figure 2.10; *Schmid et al*., 2008). The alternative interpretation suggests that Algyő High contains a part of Tisza overprinted by a pressure-dominated eo-Alpine, amphibolite facies metamorphism, likely a window of a deeper nappe unit (*Lelkes-Felvári et al.*, 2005), probably a tectonic window of Villány-Bihor unit (Figure 2.11). Whichever interpretation is favored, these all assume large exhumation of metamorphic units in the Algyő High pre-dating the Miocene extension. This was subsequently followed by ~7-8km of Miocene exhumation, which is roughly above the 220° ZFT annealing temperature and below the metamorphic threshold, given the high geothermal gradient of the Pannonian Basin. Alternatively, the Cretaceous metamorphism of the Algyő High may be explained as a Miocene extensional tectonic window beneath a detachment, but such an interpretation is difficult to accommodate in the current image of the basement structure.

Such significant exhumation can be derived in the footwall of all main controlling structures of the studied sub-basins, obviously controlled by the asymmetry of extension. Given the amounts of footwall erosion, block tilting and correlation markers across these structures, we can estimate the amount of exhumation between 2-7 km, significantly higher in the case of the Derecske detachment, where a minimum of ~10 km is a reasonable estimation. These amounts of exhumation are locally comparable or higher than thickness of the syn-kinematic basin fill deposited in their hanging-walls. This type of exhumation increases in local detachments and core-complexes towards the Eastern Alps and Dinarides margins of the Pannonian Basin. Therefore, the amount of extension along various controlling structures is in reality much higher than looking solely on the syn-kinematic basin fill. The 150-180 km of extension estimates in the Tisza-Dacia part of the Great Hungarian Plain are based on a subsidence restoration procedure that took into account only the syn-kinematic sedimentation combined with crustal and lithospheric attenuation (*Lenkey*, 1999). This means that the amount of crustal extension in the Pannonian basin is much higher than previously thought, at least with 50% given the 20-40° average normal faults dip. This leads to a total amount in the order of 220-270 km along a NE-SW transect that crosses the deepest sub-basins (Figures 2.13 and 2.14). Such rough calculations can become quantitative whenever thermochronology would become more widely available in the footwall of controlling extensional structures.

2.6.3 Inferences for the regional geodynamics

The subduction roll-back of the Carpathian and possibly the Dinaridic slab was associated with dynamic mantle evolution and associated topography in the Pannonian Basin (e.g., *Burov and Cloetingh*, 2009; *Horvath et al.*, 2015).

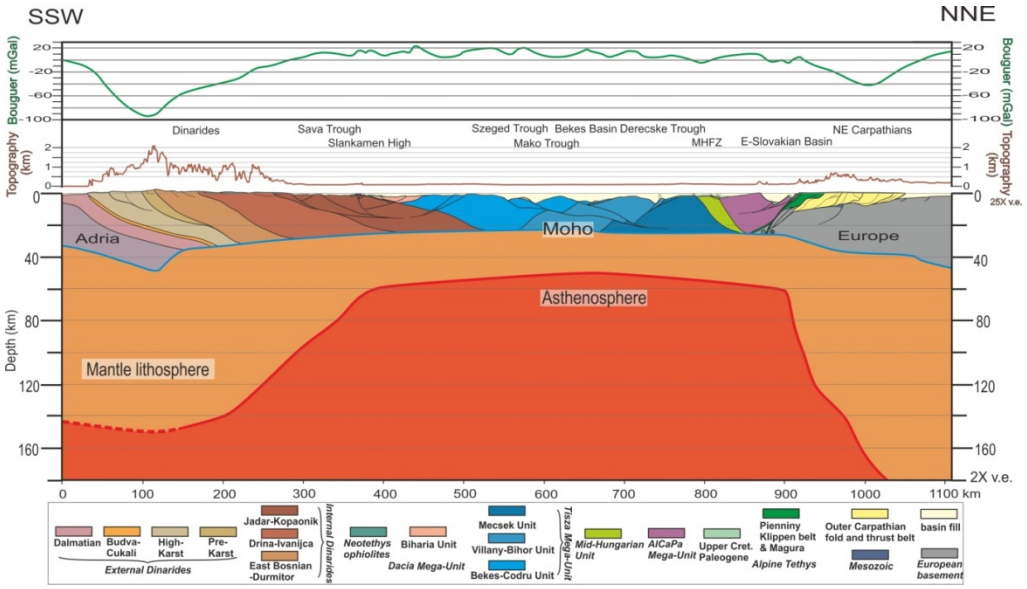

Figure 2.14: Generalized lithospheric scale cross section over the Dinarides – Pannonian Basin – NW Carpathians. Lithosphere-asthenosphere boundary compiled from *Artemieva et al.* (2006), *Tari et al.* (1999), *Tasarova et al.* (2009). Moho depth derives from *Horváth et al.* (2006), *Janik et al.* (2011) and *Sumanovac* (2010). Tertiary tectonic interpretation is based on this study and *Csontos and Vörös* (2004), *Gagala et al.* (2012), *Matenco and Radivojević* (2012), *Roure et al.* (1993) and *Schmid et al*. (2008).

Beyond possible heterogeneities created by the inherited nappe structure, the anti-correlation of the basement depth with the Bouguer gravity anomaly (Figure 2.13a) has been previously observed (*Szafián and Horváth*, 2006). In our view, such anti-correlation does not reflect a heterogeneous mantle structure, but rather the lateral shift of stretching at various crustal or upper lithospheric mantle depths, controlled by detachments and/or low angle normal faults. Such geometry is anyway required at the crustal level by the observed detachments near the Eastern Alps and Dinarides (*Tari et al.,* 1992; *Ustaszewski et al.*, 2010).

When combining our study of the Great Hungarian Plain with the regional structure of the Dinarides and Carpathians along a NE-SW oriented transect (Figure 2.14), a number of critical inferences can be derived. The Carpathians kinematics assume that the upper units translated NE- and E- wards during Miocene times in the absence of absolute plate motions, the shortening at the exterior being accommodated entirely by back-arc extension (*Horváth et al*., 2015; *Matenco et al.*, 2016). In other words, the Africa - Europe convergence in the Tisza-Dacia sector of the Pannonian Basin was retained entirely in the Dinarides during the extension of the Pannonian Basin. Further northwards, the un-stretched parts of the Tisza-Dacia units simply translated NE- and E-wards, shortening the external Carpathians nappes at the exterior and collapsing by extension of the Pannonian back-arc.

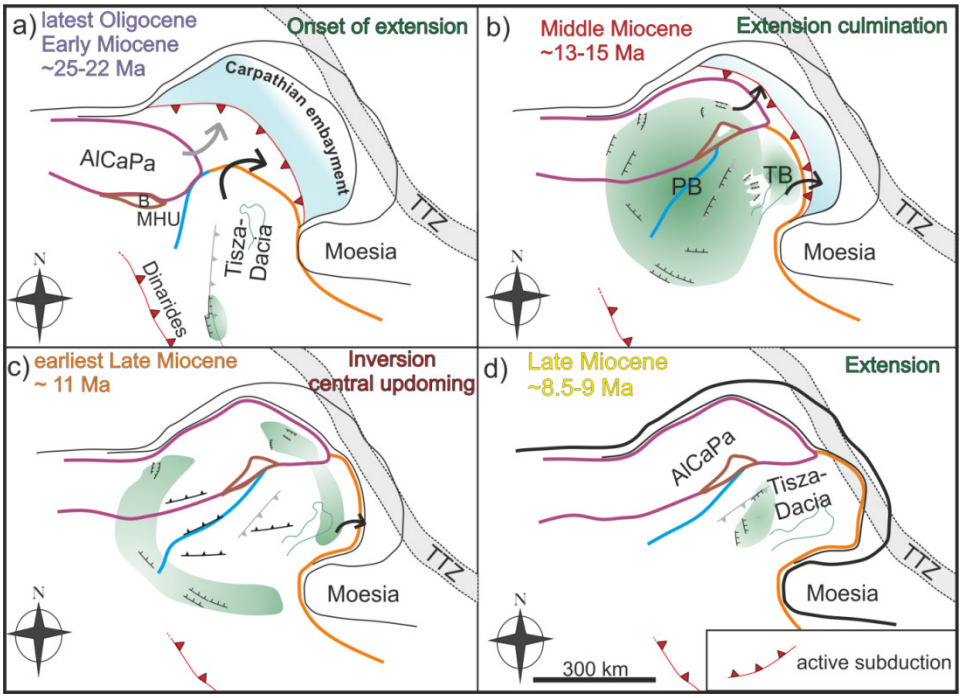

Figure 2.15: Simplified sketch showing the syn-rift evolution of the Pannonian Basin (after *Csontos and Nagymarosy*, 1998; *Faccenna et al*., 2014, *Fodor et al*., 1999; *Ustaszewski et al.*, 2008). Green color shows the area of syn-rift subsidence. Coeval vertical axis CW rotation of the Tisza-Dacia and CCW rotation of the ALCAPA Mega-Units and the Carpathians and Dinaridic slab roll back related extension resulted in several deep half-grabens in the Great Hungarian Plain with variable strikes during the Miocene. Internal deformation accommodated the different amounts of rotation in various parts of the mega-units. A short interruption in extension is inferred at the onset of the Late Miocene times, when N-S compressional structures are observed. Note the striking difference of subsiding areas during the early Middle Miocene (ca. 15-13 Ma) and the latest Middle Miocene to earliest Late Miocene (ca. 12-11 Ma). PB – Pannonian Basin, TB – Transylvanian Basin, B – Bükk Unit, MHU – Mid-Hungarian Unit, TTZ – Teisseyre-Tornquist Zone (Trans-European Suture Zone, location after *Malinowski et al*., 2013; *Pharaoh*, 1999).

In such a restricted lithospheric configuration (Figure 2.14) there is no space for significant amounts of oceanic subduction accommodating absolute plate convergence. The overall shortening, collision and extension must have affected dominatly a continental lithospheric domain. These processes were obviously driven by the evolution of inherited subducted slabs, as derived by teleseismic tomography (e.g., *Benett et al.*, 2008; *Martin and Wenzel*, 2006; *Wortel and Spakman*, 2000).

The overall pattern of large-scale erosion in the center of the Pannonian Basin and significant subsidence and deposition near its margins during the transition from Middle to Late Miocene has a large-scale wavelength with hundreds of kilometers that suggests deep lithospheric mechanism. One can speculatively link this with

dynamic topography mechanisms, such as an active mantle upwelling creating a 3D lithospheric folding in the Pannonian basin. This would result in accelerated subsidence rates in the peripheral areas and updoming in the central parts, thus decreasing the accommodation space in the Great Hungarian Plain. Such a mantle upwelling can be related to subduction induced poloidal mantle flow, created by the Carpathian slab (e.g. *Funiciello et al*., 2006), or a passive extension induced upper mantle upwelling (*Huismans et al*., 2001) or can be the effect of a deeper mantle plume (e.g., *Burov and Cloetingh,* 2009). A clear discrimination of these mechanisms requires further process oriented modeling.

The latest Miocene - Quaternary inversion of the Pannonian Basin has higher amplitudes on individual fault structures in the western part of the Tisza-Dacia block, near the basin margins (Figure 2.13b). However, the regional pattern is the one of wide open antiforms and synforms at the scale of the entire Great Hungarian Plain (Figure 2.13a). The induced vertical movements created shallow positions of the Miocene syn-kinematic basin fill (e.g., Derecske Trough, Figure 2.9), but also their significant burial (such as in the Makó or Szeged sub-basins, Figures 2.11 and 2.10). Our study in the Great Hungarian Plain is in agreement with the previously inferred large scale lithospheric folding due to the northward push of the Adriatic indentation into the rheologically weak Pannonian Basin that created various wavelengths in contrasting rheologies (e.g., *Dombrádi et al.*, 2010; *Horváth and Cloetingh*, 1996; *Jarosinki et al.*, 2011).

2.7 Conclusions

Our interpretation of seismic data from the Great Hungarian Plain of the Pannonian Basin corroborated with calibrating wells and correlated with available studies has led to a novel image of the extensional mechanism in the Pannonian Basin. The back-arc extension took place at high rates with dominantly asymmetric mechanism and has resulted in the formation of a significant number of sub-basins separated by uplifted basement highs. Our study demonstrates for the first time that the extension of the entire Great Hungarian Plain was diachronous and migrated in space and time across the basin. It started during the Early Miocene and significant deformation was still taking place until 9 Ma. The evolution of these sub-basins was controlled by low-angle normal faults or detachments that resulted in significant footwall exhumation. The overall extensional direction remained roughly constant through time, presently observed as NNE-SSW near the Dinarides (e.g., Dráva and Sava sub-basins) to E-W in the eastern (e.g., Szeged sub-basin) and NW-SE in the northern-central Great Hungarian Plain (e.g., Derecske sub-basin). The gradual and large amount of clockwise rotation of the Tisza-Dacia Mega-Unit significantly modified the original geometry of the sub-basins. The extensional mechanism was

controlled by the pre-existence of the Cretaceous nappe stack that exerted a fundamental control on the (re-)activation of detachments or low-angle normal faults.

The combined seismic and well logs sequence stratigraphy has resulted in the novel definition of a tectonic system tracts model in the Pannonian asymmetric extensional basin. This model is able to detect in the syn-kinematic basin fill the succession of higher resolution individual offsets along major controlling extensional structures in the basin.

The combined kinematic and depositional model at the scale of the entire basin infers that the cumulated amounts of Miocene extension were much higher than previously thought, reaching ca. 220-270 km. The contraction and associated vertical movements observed near the limit between Middle and Late Miocene show differential distribution patterns in the upper crustal structure of the Pannonian Basin that indicate a dynamic topography response. Similar potential dynamic topography mechanisms (e.g., *Burov et al.*, 2009; *Houseman and Gemmer*, 2007; *Horváth et al*., 2015) have still to be quantified. The effects of the subsequent latest Miocene - Pliocene contraction migrated in space and time from the Adriatic to the Carpathian margins of the basin.

All these inferences show that in terms of the upper crustal geometry correlated with the overall lithospheric configuration, the Pannonian Basin should be considered rather a hyper-extended back-arc, its formation and evolution being strongly controlled by inherited orogenic asymmetries, subsequent slab dynamics and dynamic topography mechanics.

3. Morphology of a large paleo-lake: analysis of compaction in the Miocene-Quaternary Pannonian Basin[2]

[2]*This chapter is based on Balázs, A., Magyar, I., Matenco, L., Sztanó, O., Tőkés, L., Horváth, F., 2017. Submitted to Global and Planetary Change*

3.1 Introduction

Deep lake basins formed in intra-continental settings affected by large amounts of extension can record the deposition of kilometres thick sediments. Paleo-water depth and the sedimentary architecture are controlled by several external forcing factors; their effects and interactions show marked differences from open marine environments (*Katz*, 1990; *Martins-Neto and Catuneanu*, 2010; *Sztanó et al.*, 2013). Lakes are more sensitive to climate by the primary control of the local balance between precipitation and evapotranspiration (e.g., *Carroll and Bohacs*, 1999). In contrast to passive margins, the subsidence and/or uplift rates in intra-continental settings are also more variable (*Xie and Heller*, 2009). Lakes are also sensitive to episodic (dis)connections with other neighbouring basins at the separating gateways, which are controlled by tectonics and lake level variations (e.g, *Leever et al.*, 2011; *ter Borgh et al.*, 2013; *Matenco et al.*, 2016). This overall interplay between tectonics, lake level variations, sedimentation rates and transport routing results in spatially and temporally heterogeneous depositional environments (*Garcia-Castellanos et al.*, 2003; *de Leeuw et al.*, 2012; *ter Borgh et al.*, 2015).

A typical example where a high-resolution data set is available allowing the analysis of the formation and evolution of a paleo-lake is the Pannonian basin of Central Europe (Figure 3.1). The Paleo-Danube and paleo-Tisza rivers discharged large volumes of sediments into Lake Pannon during Late Miocene - Early Pliocene times in a sink area that roughly comprised the Vienna, Pannonian and Transylvanian basins. The lake persisted for 7-8 Myrs and was progressively filled by, and buried under, clastic material sourced by the surrounding mountain chains (e.g., *Magyar et al*. 2013). The long-standing hydrocarbon exploration activity of the basin has resulted in the availability of high-resolution geophysical data including well logs and 2D/3D seismic data (e.g., *Bérczi and Phillips*, 1985; *Royden and Horváth*, 1988; *Pogácsás et al*., 1988; *Juhász*, 1991; *Grow et al.*, 1994; *Vakarcs et al*., 1994; *Saftic et al.*, 2003; *Magyar et al.*, 2006; *Sztanó et al.*, 2013) that allow a high prospectivity for conventional and unconventional geo-resources, such as geothermal energy (e.g., *Cloetingh et al.*, 2010; *Horváth et al.*, 2015). Lacustrine organic-rich shales define good hydrocarbon source rocks, while deep-water turbidites, deltaic and fluvial sand bodies are important reservoirs (*Saftić et al.*, 2003; *Magyar et al.*, 2006; *Tari and Horváth*, 2006).

In order to understand the morphology of depositional surfaces and evolution of such a deeply buried lacustrine system, we have performed 2D and 3D seismic interpretation and backstripping in the up to ~7 km thick Pannonian Neogene sediments. Paleo-bathymetric estimates were derived by successive decompaction of

prograding shelf-margin slope clinoforms based on the available lithology and porosity data from wells in different regions of the Pannonian Basin.

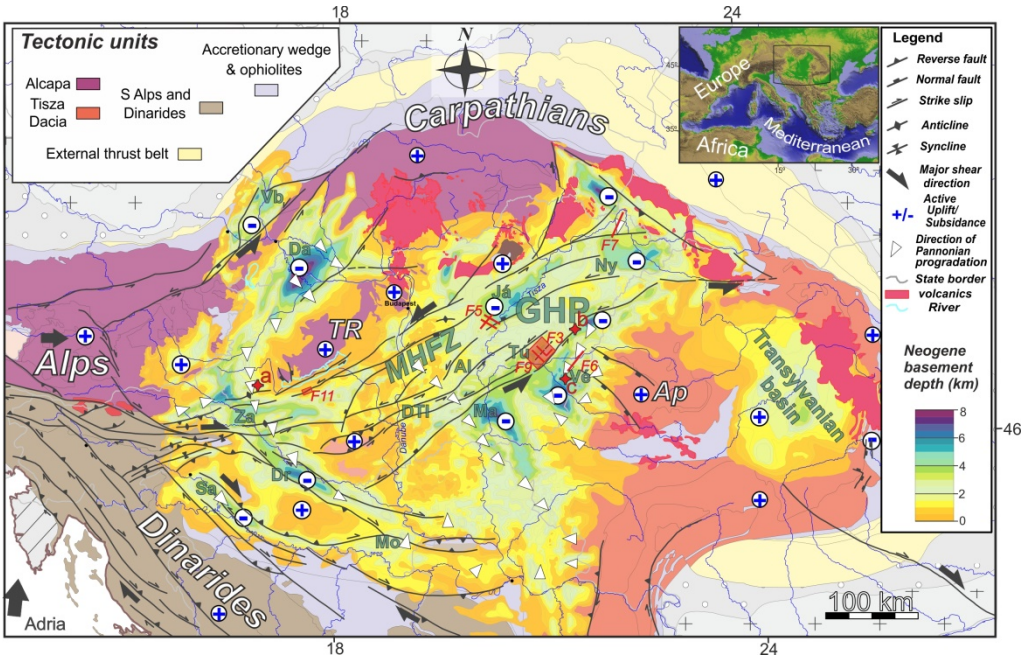

Figure 3.1: Tectonic map of the Pannonian Basin and adjacent areas showing the neotectonic fault pattern and active differential vertical movements (modified after *Bada et al.*, 2007) overlain by the depth of the pre-Neogene basement. The tectonic units of the pre-Tertiary basement outcropping on the flanks of the basin are simplified after Schmid et al. (2008). GHP – Great Hungarian Plain, Vb – Vienna basin, MHFZ – Mid-Hungarian Fault Zone, TR – Transdanubian Range, Ny – Nyírség sub-basin, Já – Jászság sub-basin, Al – Alpár sub-basin, Ma – Makó Trough, Vé – Vésztő Trough, Tú – Túrkeve Trough, DTI – Danube-Tisza interfluve, Da – Danube basin, Za – Zala sub-basin, Dr – Drava Trough, Sa – Sava Trough, Mo – Morovic depression, Ap – Apuseni Mountains. Well locations of Figure 3.3 (a,b,c) are marked by red cross symbols.

We have analysed the spatial and temporal variation of clinoform geometries and shelf-edge trajectories (e.g., *Helland-Hansen and Hampson*, 2009; *Henriksen et al.*, 2011) controlled by the interplay between high sediment fluxes, inherited pre-Neoegen basement geometries, paleo-water depth, the rate of subsidence interrupted by periods of tectonically-induced uplift and climatically controlled lake level variations. We have furthermore analysed the effects of the few kilometres thick overburden and the variable relief of the basin floor in creating large compaction effects, such as long wavelength folds and differential compaction induced faults (e.g., *Magara, 1978*; *Williams*, 1987; *Xu et al.*, 2015).

3.2 Evolution of the Pannonian Basin and Lake Pannon

The Pannonian basin of Central Europe is a Neogene continental back-arc basin, where the 220-290 km of Miocene extension is accommodated by the rapid roll-back of the Carpathians and Dinaridic slabs (Figure 3.1, *Ustaszewski et al.*, 2010; *Matenco and Radivojević*, 2012; *Horváth et al.*, 2015). Extensional basin formation followed a pre-Neogene orogenic evolution that resulted from the opening and subsequent closure of two oceanic realms, the Triassic-Cretaceous Neotethys and Middle Jurassic – Paleogene Alpine Tethys (e.g., *Schmid et al.*, 2008 and references therein).

Starting from the late Eocene times the uplift of the Alpine – Himalayan mountain belt has gradually fragmented the larger Tethys Ocean and formed the Paratethys branch. The Pannonian Basin was part of the Central Paratethys, a semi-enclosed marine to lacustrine basin system (*Báldi*, 1989; *Nagymarosy and Müller*, 1988; *Rögl and Daxner-Höck*, 1996). Lower Miocene sediments were deposited in fluvial, lacustrine and locally marine conditions (*Báldi*, 1986; *Nagymarosy and Hámor*, 2012). The Middle Miocene is the time when the subsidence associated with extension resulted in the deposition of deep basinal sediments in the centre of extensional (half) grabens, while deposition along their margins was dominated by near-shore to shallow-marine conditions (*Kováč et al.*, 2007; *Nagymarosy and Hámor*, 2012). The uplift of the Carpathians and Dinarides led to the formation of an unconformity between the Middle and Late Miocene strata marking the disruption of connections with the Paratethys Sea and development of the large, brackish, isolated Lake Pannon (Figure 3.2; *Magyar et al.*, 1999; *ter Borgh et al.*, 2013). An up to 7 km thick sedimentary succession was deposited during Late Miocene to recent times in the Great Hungarian Plain, the area recording most of the stretching in the Pannonian Basin (Figure 3.1, *Lenkey, 1999*). The basin fill recorded an initial transgression resulting in a period of underfilled stage. It was followed by shelf margin and slope progradation fed by the influx of sediments via fluvial systems resembling the present-day Danube and Tisza rivers. The largest spatial extension of Lake Pannon was at ~9.5 Ma (*Magyar et al.*, 1999), covering the Vienna, Pannonian and Transylvanian basins. The shelf-margin prograded about 500 km in 6 Myrs until the early Pliocene from the NW and NE in a ~S-SE direction, while minor progradation was recorded from other directions (*Pogácsás et al.*, 1988; *Vakarcs et al.*, 1994; *Magyar et al.*, 2013; *ter Borgh et al.*, 2015). The coeval sedimentation reflects the deposition of several diachronous lithostratigraphic formations that were deposited in response to the progradation from deep to shallow lake environments (Figure 3.2, *Bérczi and Phillips*, 1985; *Juhász*, 1991; *Sztanó et al.*, 2013). These associations are laterally variable from deep hemi-pelagic deposition (Endrőd Formation), turbidites (Szolnok Formation), shelf-margin slope (Algyő Formation) and delta (Újfalu

Formation) to alluvial plain sediments (Zagyva Formation). Their typical seismic expression provides an excellent lateral correlativity of seismic facies units.

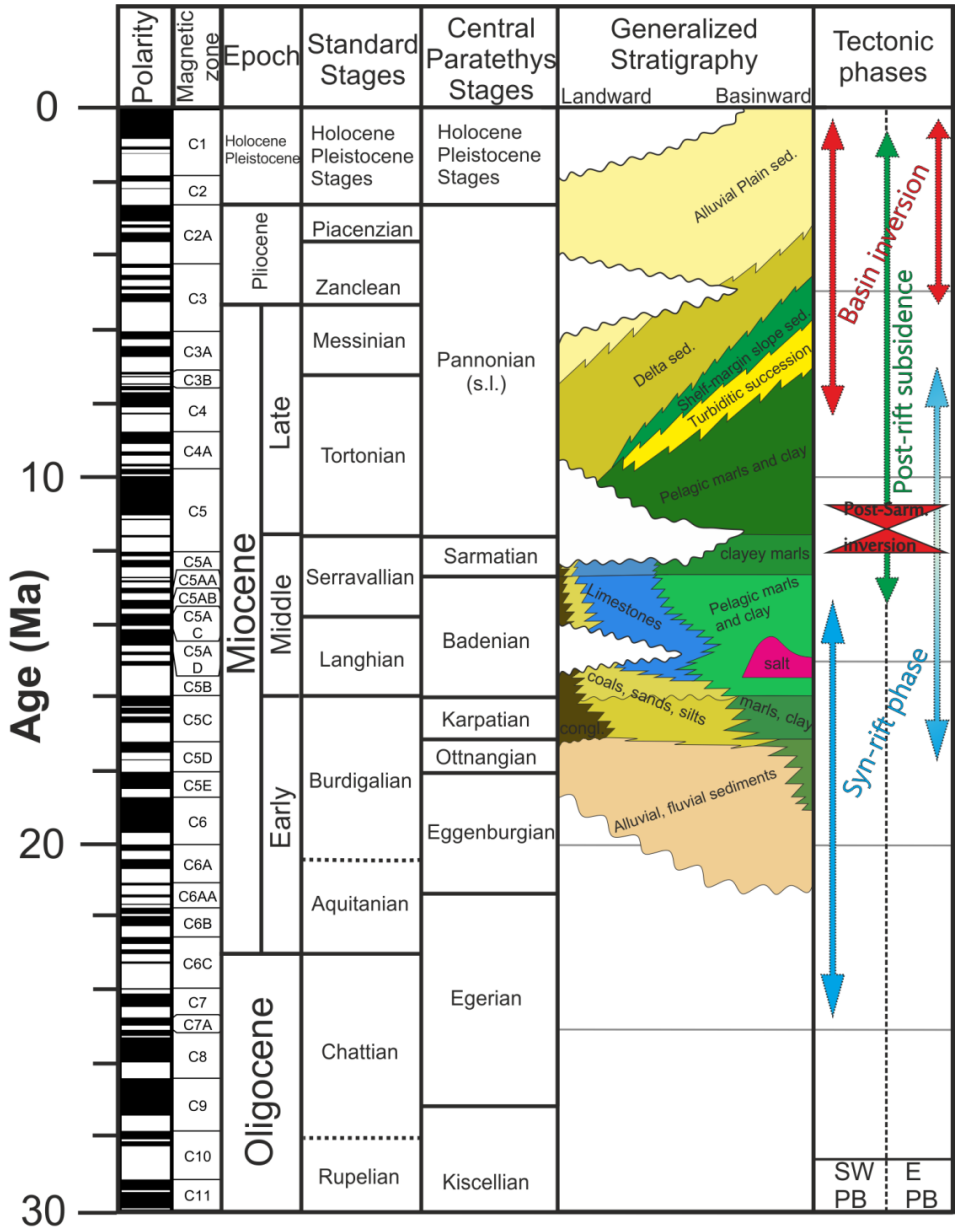

Figure 3.2: Tectono-stratigraphic chart of the Great Hungarian Plain part of the Pannonian Basin with biostratigraphic correlation of the standard and Central Paratethys stages, the generalized Miocene lithostratigraphy of the study area, the volcanic activity of the Pannonian Basin and the main tectonic phases affecting the basin (after *Balázs et al.*, 2016). Note that the syn-rift/post-rift boundary and the onset of the latest stage basin inversion are older in the SW and progressively younger E-NE -wards.

Extension and subsequent thermal subsidence in the Pannonian Basin was followed by a period of basin inversion that started at ~8 Ma (*Uhrin et al.*, 2009), observed by accelerated differential vertical movements and fault reactivations (*Horváth and Cloetingh*, 1996; *Fodor et al.*, 2005; *Ruszkiczay-Rüdiger et al.*, 2005; *Bada et al.*, 2007; *Dombrádi et al.*, 2010). Active sinistral faults with ENE-WSW strike are interpreted in the centre of the basin and dextral shear zones with WNW-ESE strike at its southern margin (Figure 3.1, *Horváth et al.*, 2006). Several unconformities are observed during these times in the basin fill (e.g., *Vakarcs et al.*, 1994). One unconformity, formed at ~6.8 Ma, is observed at depth in the basin fill. Another unconformity is observed near the boundary between the Miocene and Pliocene, which is angular and locally erosional near the basin margins and passes to a correlative conformity towards the basin centre. These unconformities are variably interpreted as either related to basin inversion (*Sacchi et al.*, 1999; *Magyar and Sztanó*, 2008), or formed in response to major lake level variations (*Csató et al.*, 2015), or representing cross-over zones of different progradational directions reflected by onlap patterns in slope deposits (*Magyar and Sztanó*, 2008).

3.3 Data and methods

We have analysed a large array of 2D and 3D seismic data calibrated by a dense network of exploration wells. This analysis is illustrated by the selection of several key seismic lines and wells, generally oriented parallel with the direction of sediment transport (e.g., Figure 3.3). The signal/noise ratio and resolution of the seismic sections are variable, and reflect the availability of data, from recent 3D seismic surveys to older 2D seismic lines; the vertical resolution averages 20-30 meters. Well-logs were tied to seismic sections using standard VSPs and check-shots, the error-bar is generally below the seismic resolution (see also *Mészáros and Zilahi-Sebess,* 2001).

Our interpretation is focused on the prograding shelf-margin slope clinoforms connecting the shelf with the deep part of the basin. The slope sediments are associated with a medium to low amplitude, continuous-discontinuous alternating, high frequency seismic facies grouped in overall clinoform foreset geometry (Figures 3.3-3.5, see also *Magyar et al.*, 2013). In seismic lines oriented perpendicular to the direction of progradation (Figure 3.5e) the seismic facies is rather hummocky to chaotic often showing incisions or canyons of variable magnitudes near the shelf or along the slope as well as turbidite channels and turbidite channel-levee complexes at the base of slope.

We have performed first a sedimentological and seismo-stratigraphic interpretation by detecting reflection terminations and separating seismic facies units (e.g., *Posamentier and Walker*, 2006), followed by calculating of a number of seismic

attributes in 3D seismics that allowed a better differentiation of faults and sedimentary features (e.g., *Cartwright and Huuse*, 2005; *Chopra and Marfurt*, 2005).

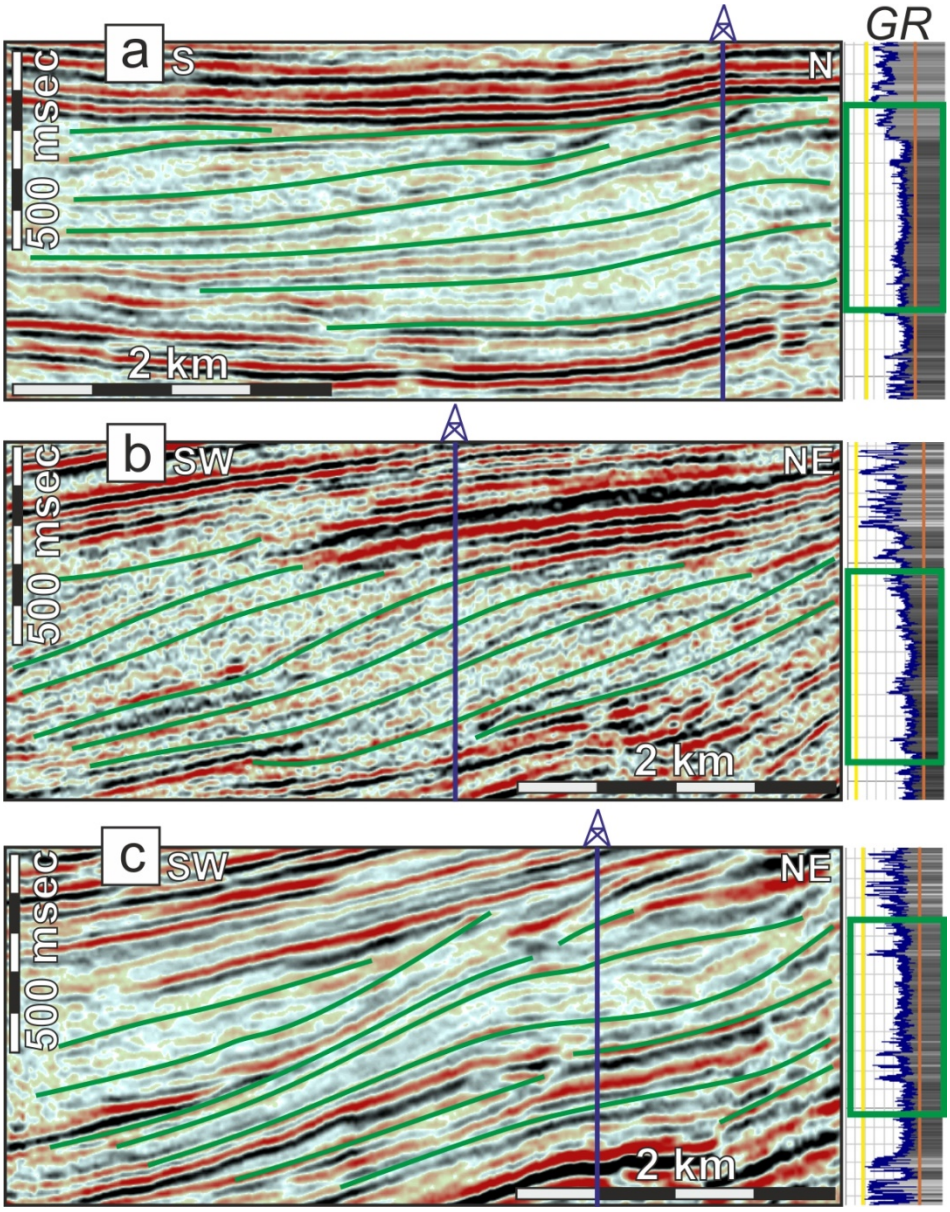

Figure 3.3: Seismic sections parallel with the direction of progradation and gamma ray logs showing the characteristic seismic facies and lithology of the prograding shelf-margin slope sediments. Slope clinoforms are indicated by green lines, green box indicates the interval of slope sediments on well logs. Note the low-amplitude seismic facies, fine grained lithology of the unit and the gentle tilting post-dating the deposition of the slope sediments. Well locations (a-c) are displayed in Figure 3.1.

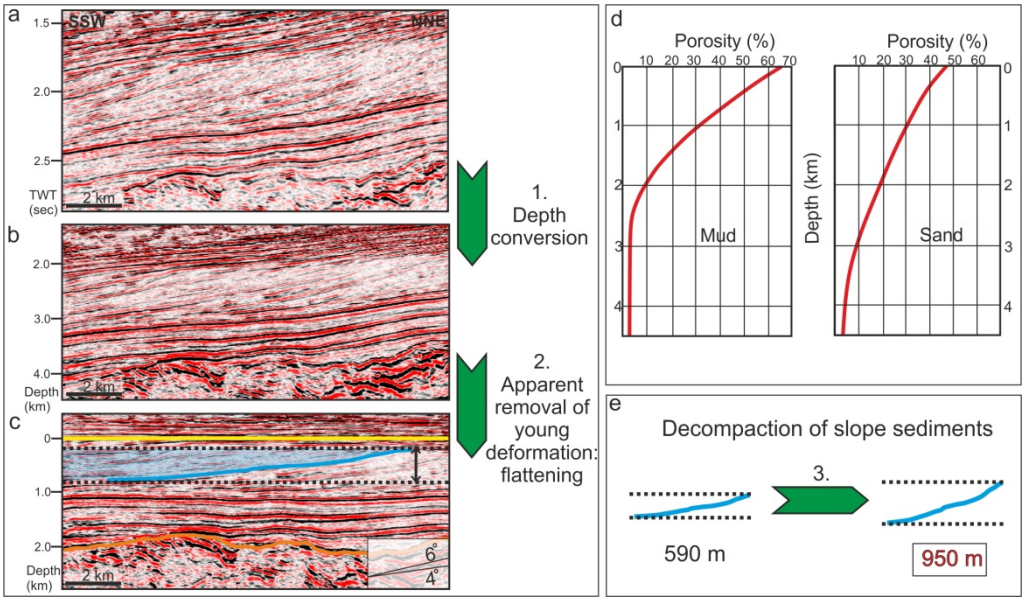

Figure 3.4: Methodology used for paleobathymetrical calculations. The TWT version of the seismic line (a) is converted to depth (b) and subsequently flattened (c) by using a horizon located immediately above the prograding clinoform sequence (in the overlying delta deposits). We use a lithology dependent porosity-depth function available for these sediments in the Pannonian Basin (d, after *Szalay*, 1982) to decompact sediments and calculate the shelf-margin slope (e). The distance between topset and bottomset is 590 m and 950 m before and after decompaction, resp.

Seismic attributes are particularly suitable to highlight paleo-geomorphological and structural features. We have used seismic amplitude values extracted on mapped horizons to highlight amplitude anomalies related to sharp acoustic impedance contrasts connected, for instance, to sharp lithological changes. We have also used spectral decomposition (e.g., *Partyka et al.*, 1999) to produce amplitude and phase spectra for targeted windows over horizons. Different discrete frequency values were RGB colour blended and displayed on the interpreted horizon. We have calculated coherency attribute cubes based on the cross-correlation of seismic traces in selected windows to highlight structural features.

The bottom morphology of Lake Pannon was derived in a gradual procedure (Figure 3.4). Seismic lines were converted to depth (i.e., from a vertical scale in two-way-travel-time seconds to a vertical scale in kilometres, e.g. Figure 3.4a to Figure 3.4b). Following the lacustrine evolution, the upper part of the basin fill is composed by delta and alluvial sediments deposited over a low and flat morphological relief (*Sztanó et al.*, 2007). These sediments are affected by a deformation generally characterized by large open folds locally affected by faults with small vertical offsets. The areas affected by local faulting were generally avoided for lake morphology calculations. The effects of the gentle folding were restored by flattening the seismic

lines to the first continuous reflector representing paleo-horizontal in the delta and alluvial sediments that is laterally continuous above the clinoforms along the seismic line. The distribution of these sediments (Újfalu and Zagyva Formations) in seismic lines is very well controlled by available wells, where these have characteristic well-log expressions (Figure 3.3, *Bérczi and Phillips*, 1985; *Juhász*, 1991). In seismic lines the first deposition of the delta deposits is observed as coherent high amplitude, low frequency continuous reflections facies overlying the topsets and clinoforms of the lacustrine progradation (Figure 3.4). Given the resolution of the seismic lines, this type of restoration is a very good approximation of the morphology of Lake Pannon, affected by the subsequent compaction. The seismo-stratigraphic interpretation has separated seismic facies units and seismic facies associations (e.g., Figure 3.5) in the prograding clinoforms, which were converted into lithological facies units based on available well-logs (mostly gamma-rays, e.g., Figure 3.3). The shelf-margin slope foresets are built up by about 80% mudstone combined with 20% sandstone (see also *Szalay and Szentgyörgyi*, 1988), only the upper and lowermost parts contain higher amounts of sand. Decompaction of the progradation geometry to derive the original morphology of Lake Pannon was achieved by a standard modelling technique (e.g., *Angevine et al*., 1990) based on the lithology dependent porosity-depth data available for the Great Hungarian Plain (*Szalay*, 1982; *Dövényi*, 1994). This 1D modelling was performed in successive places over the seismic line. Note that the first continuous reflector of the delta and alluvial seismic facies may be at different depth across one section, due to the progradation/aggradation geometries. In places where a smaller scale delta progradation was detected in the shelf facies, the flattening was performed at the first continuous reflector overlying this secondary progradation.

By connecting successive 1D decompacted geometries, the evolution of the lake morphology was reconstructed along each studied seismic line. This lake morphology gives a minimum estimation of the water depth. These calculations have a resolution close to the seismic one in the proximity of the lake shelf-margin slope, while at farther distances these estimates are less precise (*Steckler et al*., 1999). Following existing sedimentological interpretations (*Juhász*, 1991; *Sztanó et al*., 2013), an additional 0-75 m water-depth characterized the shelf of the lake (where part of the deltaic sedimentation is located), while at farther distances from the progradation our calculation are just minimum estimates, the paleo-bathymetry could have been much higher. It is likely that the overall paleo-bathymetry decreases with the approaching progradation by the distal infill of deep-water turbidites and more pelagic sedimentation.

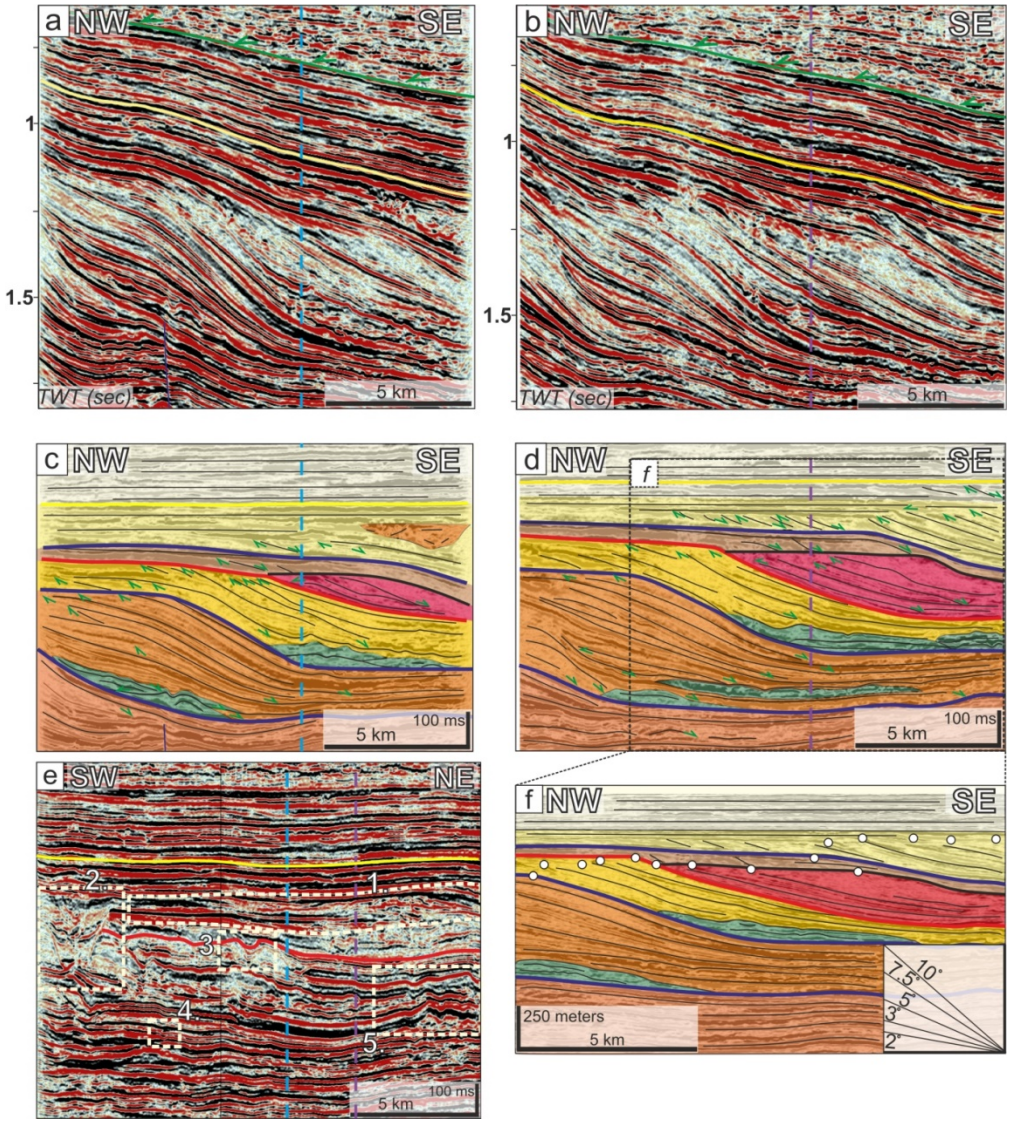

Figure 3.5: Seismic sections a) and b) oriented parallel with the direction of progradation in the Jászság sub-basin showing typical progradational (in orange), aggradational (in yellow), deposits during forced regression (red), and above retrogradational pattern in the Great Hungarian Plain (location in Figure 3.1). Note the turbidite complexes at the toe of slopes (in green). Green half-arrows are reflection terminations. Green line is the unconformity between Miocene and Pliocene sediments, yellow line is the flattening level; c) and d) are the flattened version of the seismic lines above; e) seismic section in the same area perpendicular to the direction of progradation. Vertical dashed lines are intersections with profiles displayed in Figures 3.5a and 3.5b. This seismic line shows (1) delta progradation over the shelf area; (2,3) large-scale incision (~200 meters deep) near the transition between the shelf and the slope; (5) stacked channel-levee systems (~30-60 m thick); (4) small turbidite channel within deep water sediments (see also *Sztanó et al*., 2013; *Juhász et al*., 2013); f) depth converted version of part of the seismic line in Figure 3.5d. Small circles denote the evolution of the shelf margin (i.e., shelf edge trajectories).

3.4 Paleobathymetry of Lake Pannon

The general extensional geometry of the Pannonian Basin is characterized by individual sub-basins filled by 1 - 3.5 km of Early to Late Miocene syn-kinematic deposits, furthermore overlain by a 1.5 - 3.5 km thick post-extensional sedimentary cover. Here we focus on the prograding shelf-margin slope clinoforms that post-date this syn-extensional sedimentation to derive the morphology of the Late Miocene to Pliocene Lake Pannon.

3.4.1 Paleobathymetric calculations

Based on the flattened height of the Upper Miocene to Pliocene prograding shelf-margin slope clinoforms, paleobathymetric estimations by decompaction have been carried out in 8 representative sub-basins (Figure 3.6, Table 3.1). Seismic section from the Nádudvar sub-basin of the central Great Hungarian Plain (Figure 3.6b) shows the initial distribution of Pannonian sediments by prograding shelf-margin slope and delta sediments over deep-water marls and turbidites. This was followed by a base level rise at ~8 Ma (*Juhász et al.*, 2007) associated with a major retrogradation and renewed deposition of deep-water sediments over the deltaic succession, overlain by renewed progradation and filling of the basin by deltaic and alluvial sediments in the upper part of the section (Figure 3.6b). The calculated evolution of the lake morphology indicates 650 meters for the older clinoforms, up to few tens of metres for the deltaic environment and 200 meters of paleo-bathymetry for the upper, younger clinoforms.

Seismic section from the central part of the Great Hungarian Plain between the present-day Danube and Tisza rivers (Figures 3.1 and 3.6c) shows a thin prograding sequence with decompacted paleo-bathymetries of ~130 m that is laterally slightly higher in the area above the Middle Miocene (half) grabens. To the northeast, seismic sections form the Alpár sub-basin (Figure 3.6d) show an inverted basement high to the NW, while the depth of this basement increases SE-wards. The calculated paleo-water depth is ~675 meters, the age of progradation in this area being 7-6.8 Ma (*Magyar et al.*, 2013). We note that multiple phases of inversion and strike-slip deformation observed in the sediments overlying the Alpár sub-basin have also created a large incised canyon system at ca. 6.8 Ma (*Juhász et al.*, 2013). Subsequently it was followed from ~5.3 Ma by continuous differential vertical movements creating the tilting observed in our seismic line (Figure 3.6d). To the southeast, the ~5.7 Ma progradation observed in the Makó Trough (*Sztanó et al.*, 2013) has ~750 m calculated paleobathymetries (Figures 3.1, 3.6e), in the centre of this very deep sub-basin, decreasing to 650 m over its flanks (*Balázs et al.,* 2015). In the western part of Lake Pannon, the SE-ward progradation of the paleo-Danube took place between 10-6.8 Ma (*Magyar et al.*, 2013). The calculated paleo-bathymetries for

this area are 550 m for the NW in the Danube basin (Figures 3.1, 3.6f), 600 m for the Zala (Figure 3.6g) and ~600 m for the Drava sub-basins (see also *Balázs et al.*, 2015). These values are in agreement with earlier predictions in this area (*Uhrin et al.*, 2009). In the southern part of the Pannonian Basin, paleo-bathymetric calculations in the Sava Trough and Morovic Depression (Figure 3.1, seismic lines in *Ustaszewski et al.*, 2014 and *ter Borgh et al.*, 2015, respectively), indicating E-wards prograding clinoforms paleobathymetries of 275 m and N-ward prograding clinoforms paleobathymetries of 525 m, respectively.

Location	Age (Ma)	Section (Figures)	Compacted height (m)	Decompacted height (m)
Jászság sb.	~ 7 Ma	F. 3.5	440	690
Jászság sb.	~ 7 Ma	F. 3.5	450	690
Jászság sb.	~ 7 Ma	F. 3.5	370	580
Túrkeve sb.	~ 5.7 Ma	F. 3.8, location a)	290	510
Túrkeve sb.	~ 5.7 Ma	F. 3.8, location b)	350	630
Túrkeve sb.	~ 5.7 Ma	F. 3.8, location c)	255	470
Túrkeve sb.	~ 5.7 Ma	F. 3.8, location d)	455	740
N Nyírség sb.	~ 10 Ma	F. 3.7, delta	48	70
N Nyírség sb.	~ 10 Ma	F. 3.7, slope	91	150
Makó Trough	~ 5.7 Ma	F. 3.6e	425	750
Nádudvar sb.	~ 8 Ma	F. 3.6b upper	180	200
Nádudvar sb.	~ 8.6 Ma	F. 3.6b lower	400	650
Danube Basin	~ 10 Ma	F. 3.6f	280	550
Zala Basin	~ 8 Ma	F. 3.6g	340	600
Alpár sb.	~ 7 Ma	F. 3.6d	420	675
Danube-Tisza if.	~ 7.5 Ma	F. 3.6c	75	130
Vésztő Trough	~ 5.3 Ma	F. 3.4	590	950
Sava Trough	~ 6.5? Ma	*	185	275
Morovic sb.	~ 4.5? Ma	*	350	525

Table 3.1: Height of the clinoforms before and after decompaction, the latter represents a minimum estimation of the paleo-water depth in different Pannonian sub-basins (sb.). *Seismic data used for our paleobathymetric estimation for the Sava Trough and Morovic sub-basin is used after Ustaszewski et al. (2014) and ter Borgh et al. (2015), respectively.

3.4.2 The paleo-morphology of Lake Pannon

The main observed mechanism of Late Miocene – Early Pliocene basin infill is the rapid progradation. However, the processes controlling the balance between the accommodation space and sediment supply in the Lake Pannon have similar orders of amplitude and create a local fine interplay with aggradational, progradational and retrogradational geometries as well (e.g., *Juhász et al.*, 2007; *Sztanó et al.*, 2013).

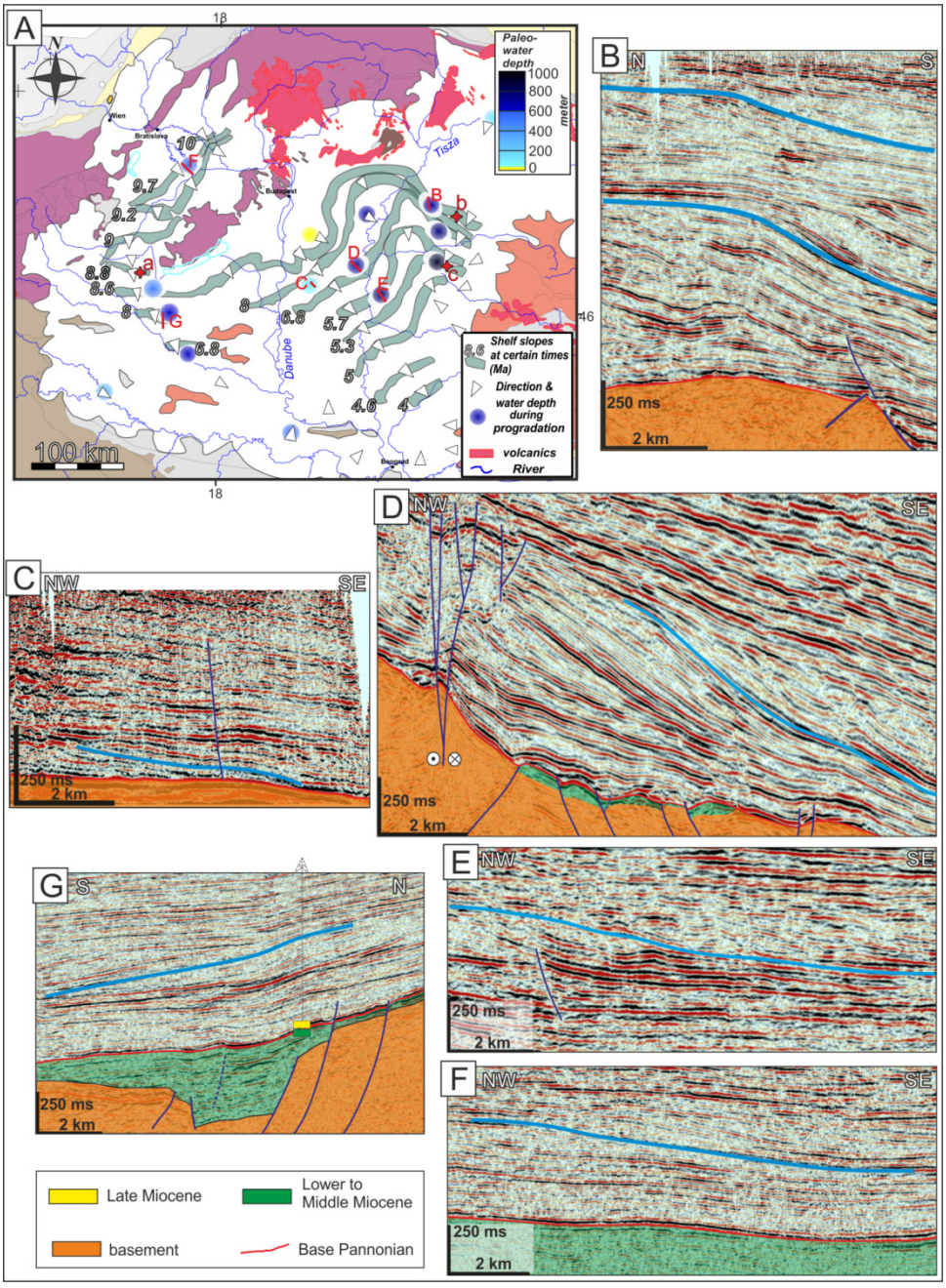

Figure 3.6: a) Positions of the prograding shelf-margin slopes during the Miocene – Pliocene sedimentation (modified after *Magyar et al.*, 2013). Blue circles indicate our calculated water depth values. Red cross symbols will small caps letters (a-c) show the well positions of Figure 3.3. B-F are the locations of the seismic sections in Figures 3.10b-f showing the shelf-margin slopes used for paleobathymetric estimations; b) Seismic line in the Nádudvar sub-basin; c) Seismic section in the Danube-Tisza interfluve; d) Seismic section in the Alpár sub-basin; e) Seismic section in the Makó Trough; f) Seismic section in the Danube Basin; g) Seismic section in the Zala Basin.

These processes are the Late Miocene – Quaternary thermal subsidence, climatic variations, the massive sourcing of sediments from the paleo-Danube and paleo-Tisza rivers, the inherited extensional morphology and the eventual connection at the separating gateways with other basins.

An appropriate place where this fine interplay can be observed is the Jászság sub-basin of the northern part of the Great Hungarian Plain (Figure 3.1). This sub-basin was filled by sediments transported by both the paleo-Danube from WNW and the paleo-Tisza from NE directions between ~8-6.8 Ma (*Magyar et al.*, 2013). Two seismic lines (Figures 3.5a,b) parallel with the local direction of progradation show the geometries of the shelf-margin slope, delta progradation on the shelf and toe of slope sediment complexes. An angular unconformity between the Miocene and Pliocene sediments (green line in Figures 3.5a,b) marks the boundary of delta and alluvial environments as well. Shelf-edge trajectories (Figure 3.5f) infer an interplay between normal regression, transgression and forced regression (reflecting base-level drop of ~ 80 m) and retrogradation (reflecting a base-level rise of ~200 m). Seismic lines perpendicular to the direction of progradation show that shelf incisions took place during both relative water-level rise and water-level fall (Figure 3.5e). This means that such observed incisions are not necessarily sub-aerial.

3.4.3 Effects of inherited extensional half-grabens on the paleobathymetry of Lake Pannon

The analysis of the syn-kinematic sedimentation in the diachronous extensional half-grabens is available in previous studies (e.g., *Matenco and Radivojević*, 2012; *ter Borgh et al.*, 2015; *Balázs et al.*, 2016). We illustrate here only on few typical examples of the structural history characterizing the evolution of the Pannonian Basin. Although our analysis has studied a much larger area, two specific zones are chosen to illustrate the overall tectono-sedimentary features of the lake: the Nyírség sub-basin in the north-eastern margin of the Great Hungarian Plain and the Túrkeve sub-basin from the deep central part.

The region of the Nyírség sub-basin in the NE part of the Great Hungarian Plain (Figure 3.1) contains significant amounts of upper Middle Miocene (Sarmatian) rhyolites, rhyodacites and dacites, dome-flow complexes and related tuffs (*Pécskay et al.*, 2006). The analysis of a seismic line in this sub-basin (Figure 3.7) shows such a buried Sarmatian volcanic geometry made up by extrusive flows, sills, and further intrusive complexes, surrounded by high amplitude reflectors located beneath the base Late Miocene unconformity. The Miocene depocentre is filled with Middle Miocene volcano-clastic sediments, which is a typical feature observed in many other sub-basins located in a similar tectonic position along the Mid-Hungarian Fault Zone (e.g., *Horváth et al.*, 2015).

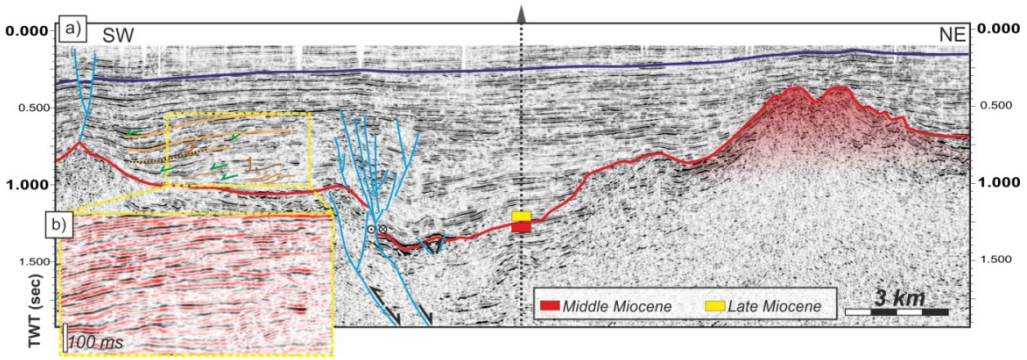

Figure 3.7: a) Interpreted seismic section located in the NE part of the Pannonian Basin. Location in Figure 3.1. The interpretation underlines a buried late Middle Miocene (Sarmatian) volcanic structure beneath the subsequent Late Miocene (Pannonian) sediments. The gentle anticline geometry of overlying Pannonian sediments (see arbitrary blue horizon) is created by differential compaction. The red line is the Middle- Upper Miocene unconformity. Small deltas indicated by numbers are used in Table 3.1; b) Detail of the same seismic line showing a prograding delta over the shelf, observed by evident downlap reflection terminations (green arrows).

These Middle Miocene syn-kinematic wedges were deposited against the controlling NE-dipping normal faults. The fault zone was likely reactivated during earliest Late Miocene times with low reverse and strike-slip offsets creating a flower structure. The entire Upper Miocene succession in the Nyírség sub-basin shows only deltaic and alluvial facies with no deeper shelf-margin slope clinoforms observed, suggesting that the rate of sedimentation has always kept pace with the local subsidence rate and the absence of inherited paleobathymetries. This is in agreement with observations in one well (Figure 3.7) penetrating the entire Late Miocene succession reporting frequent coal intercalations in the entire Upper Miocene sequence (*Székyné et al.*, 1985). Laterally to the SW in the analysed seismic lines 10s of meters thick deltaic clinoforms prograding over a shallow shelf are observed within the earliest Pannonian sediments. The height of these clinoforms increases further SW-ward in the direction of progradation and becomes the much larger shelf-margin slope clinoforms observed elsewhere in the basin. In other words, these clinoforms show the older onset of Late Miocene progradation in the basin that started with low amplitude clinoforms and that gradually increase in height with time indicating an increase of the paleo-water depth. The decompacted height of these initial clinoforms (Figure 3.7b, Table 3.1) is in the order of 70 to 150 meters and were deposited between 11.6 - 9 Ma. Note the gentle anticline geometry of the younger Pannonian to Quaternary horizons above the buried volcano that reflects differential compaction effect (Figure 3.7). The present-day Tisza river is changing its strike significantly around this anticline (Figure 3.1).

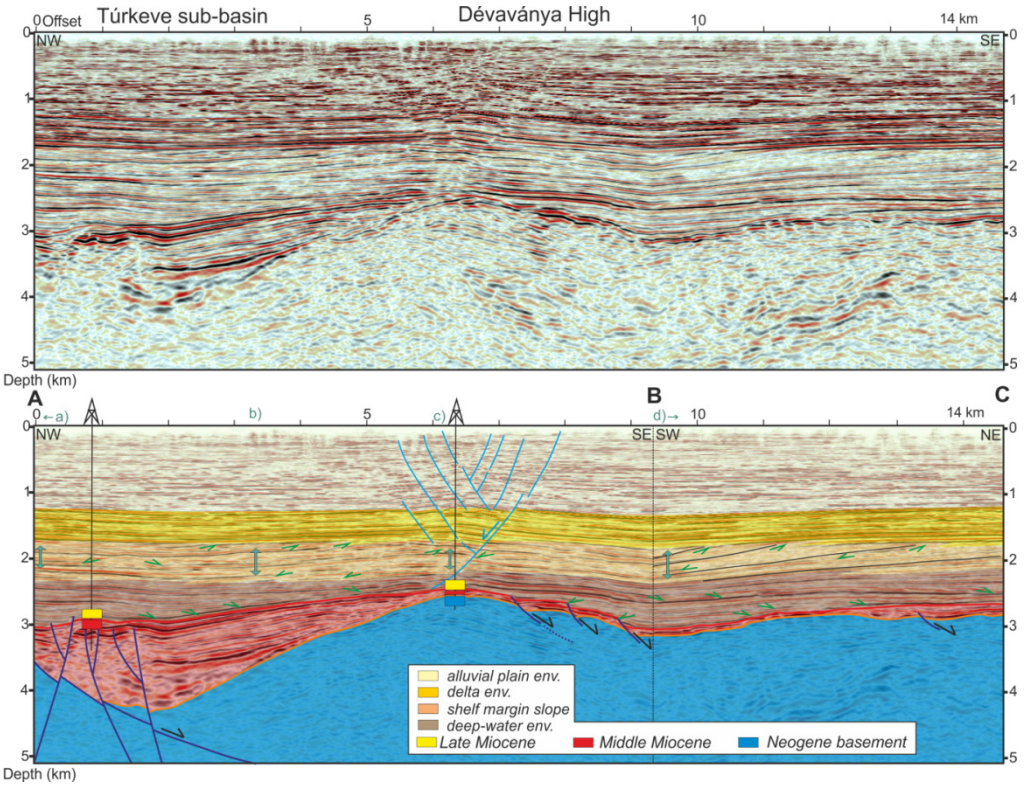

Figure 3.8: Non-interpreted (up) and interpreted (down) seismic depth-converted section from the central part of the Great Hungarian Plain (location in Figure 3.1) showing an Early to Middle Miocene sub-basin and typical Late Miocene seismic facies. Note that the trace of the section is a composite between a segment parallel with and one perpendicular to the direction of progradation (BC and AB, respectively). Note the wide segmented fault zone above the basement high that reflects differential compaction in the sub-basins above the basement high. Green arrows are reflection terminations. The four blue double arrows are locations of paleo-water depth calculations (a-d) within the slope environment.

A depth converted seismic section from the Túrkeve sub-basin (Figures 3.1, 3.8) shows a typical structure for the central part of the Great Hungarian Plain: a half-graben filled with Early to Middle Miocene syn-extensional sediments is overlain by ~3 km of Late Miocene post-kinematic deposits. The half-graben is controlled by a large offset SE-dipping low-angle normal fault, which is accompanied by lower offset normal faults. The half-graben is also slightly inverted by a positive flower structure and shows the typical unconformity also observed elsewhere in the Pannonian Basin at the transition between Middle and Late Miocene (Sarmatian to Pannonian). The structural style is otherwise similar to other such Early – Middle Miocene sub-basins (e.g., Kiskunhalas or Vésztő, see also *Balázs et al.*, 2016). The overlying strata show gentle anticline geometry over the Dévaványa basement high (Figure 3.8). The typical progradation of shelf-margin slope clinoforms is observed in the overlying Upper Miocene (Pannonian) sediments. The prograding shelf-margin slope reached this sub-

basin by prograding SW-wards at about 5.7 Ma (*Magyar et al*., 2013). The paleo-water depth was calculated in four points along the same spatially correlated timeline (or reflector, Figure 3.8, Table 3.1). These calculations show a variable bathymetry at the base of the slope ranging from 475m over the Dévaványa basement high to 630 and 740 m in the region overlying the depocentres. Our calculations thus demonstrate that paleo-bathymetries were controlled by the inherited extensional geometries, the base of the slope showing higher values over the various sub-basins when compared with intervening basement highs. This means that the deposition of deep-water pelagic sediments and distal turbidites were unable to compensate the inherited morphological differences from extensional times before the shelf-margin slope progradation arrived to a more proximal position.

3.5 Compaction-induced folds and faults

The centre of the gentle anticline overlying the Dévaványa basement high (Figure 3.8) is cross-cut by a wide normal fault zone truncating the Late Miocene - Quaternary sediments. This fault zone has been interpreted either as normal growth fault (e.g., *Grow et al.*, 1994), or a wide strike slip fault zone that is similar to other negative flower structures commonly interpreted in 2D seismic lines in many other areas of the Pannonian Basin (*Horváth et al.*, 2006; *Bada et al.*, 2007). Interestingly, the detailed analysis in this Túrkeve area shows that fault offsets gradually increase upwards from the basement high and furthermore decrease in the uppermost part of the section.

The mechanism of formation of this system of normal faults with variable offsets observed above the Dévaványa basement high can be studied in more details on a 3D seismic cube, where individual fault segments and marker horizons cross-cut by faults were mapped (Figures 3.9, 3.10). These faults truncate and offset Pannonian post-rift sediments. The fault with the largest offset dips SE-wards in the southern part of the studied area and changes to a NW-ward dip in the north, where the fault zone is wider (Figure 3.9). The offset analysis in the 3D cube confirms the observation of the 2D seismic lines of a gradual increase of offset upwards from the basement high and furthermore decrease in the uppermost part of the section (Figure 3.9). This is a typical attribute of faults related to salt movement and/or differential compaction effects (e.g., *Magara*, 1978; *Williams*, 1987; *Xu et al.*, 2015). The absence of salt bodies in our seismic observations and previous studies infer differential compaction effects. A much clearer discrimination from strike-slip deformation is provided by the analysis of horizontal offsets. We have calculated a large number of attribute maps that all show excellent expressions of the faults system and the sedimentology of variable fluvial-alluvial to deltaic environments, from meandering rivers (Figure 3.10a) to turbiditic channels on slopes (Figure 3.10e).

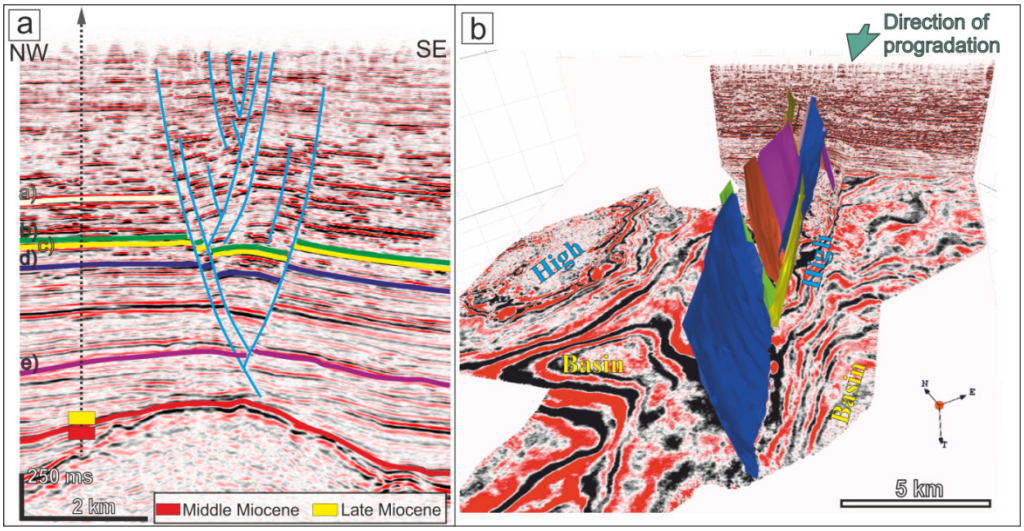

Figure 3.9: Interpreted seismic data from the central part of the Great Hungarian Plain. Location in Figure 3.1. a) The segmented Túrkeve Fault zone affecting Late Miocene to Quaternary sediments. Note the increase in offsets upwards in the stratigraphy. The horizons a) to e) were mapped in the seismic cube and are displayed as horizon maps in Figure 3.10. b) 3D image of the same Túrkeve Fault segments above the basement high, surrounded by deeper basins on either side.

Most of the larger channels are oriented parallel with the normal faults, which is also the strike of the neighbouring older extensional basins and the strike of the basement high. However, smaller channels often cross the various branches of the normal fault system but none of these sedimentary channels indicate any horizontal offset when crossing the various fault branches and, therefore, the strike-slip kinematics of this zone can be ruled out. We conclude that differential compaction is the primary mechanism creating such structures.

3.6 Discussion

3.6.1 Controls on water depth variations and progressive infill of Lake Pannon

Our calculations show spatially and temporally variable paleo-water depth values during the Late Miocene to Pliocene evolution of Lake Pannon. This variable morphology was created by a number of forcing factors, such as inherited bathymetries, tectonic subsidence and/or uplift rates, climatic driven water level changes, rates and transport modes of sediment supply. Their relative importance varied spatially through space and time.

The overall Early and Middle Miocene back-arc extension created heterogeneous basement morphology with uplifted footwalls and localized deep hanging walls in the centre of the (half-) grabens. The erosional unconformity at the base of Late Miocene

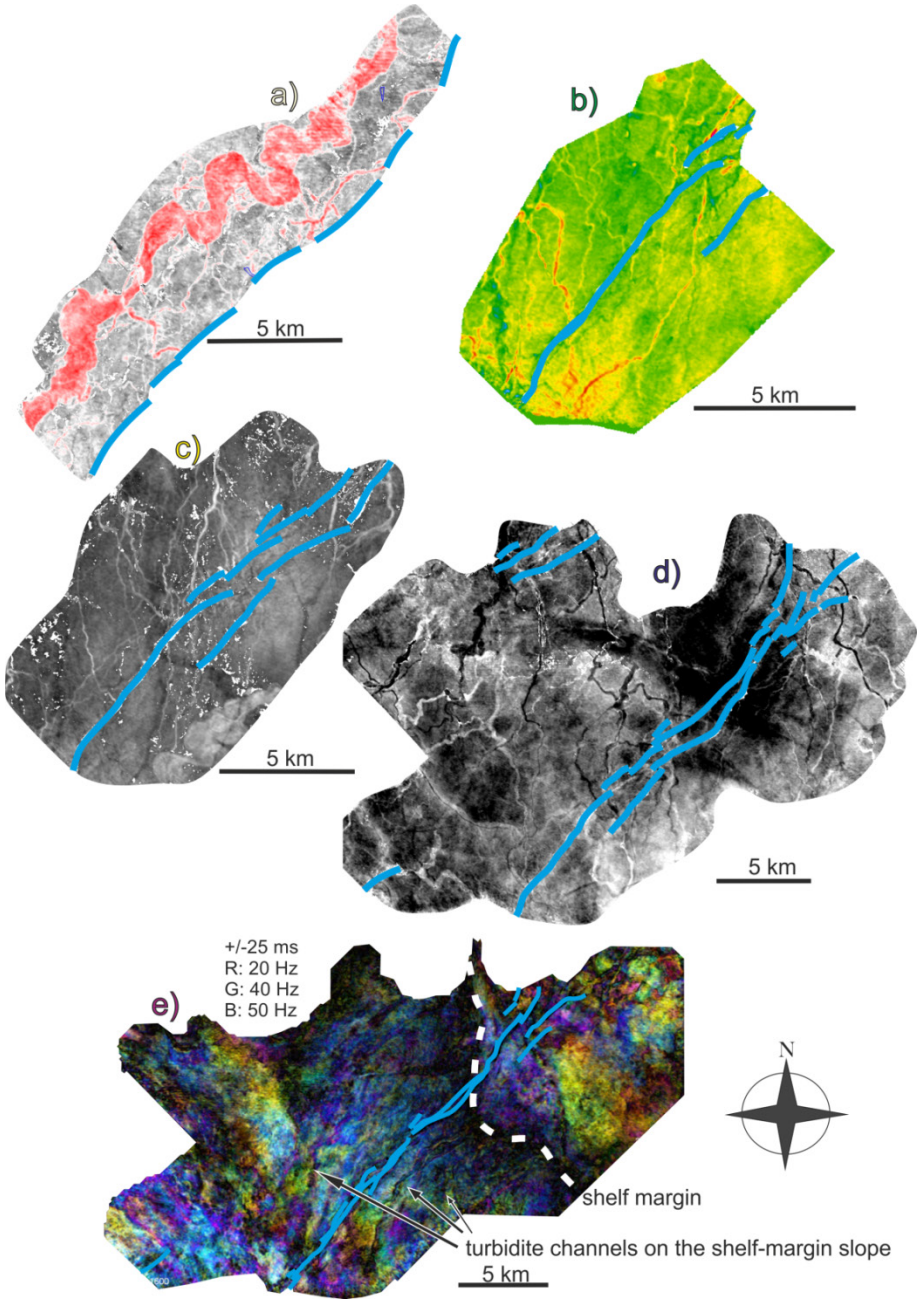

Figure 3.10: Interpreted seismic horizon maps. Blue lines indicate fault segments cross-cutting horizons. Figures a) to e) correspond to horizons a-e shown in Figure 3.9a. (a) Amplitude map of a horizon from the alluvial plain, illustrating a meandering river and smaller distributaries. (b-d) Amplitude maps of horizons from anastomosing delta plain environments showing meandering and anastomosing channels. (e) Spectral decomposition attribute map of a horizon through the shelf, shelf-margin, slope and deep water environments (see text for further explanations). Note that no channel is displaced horizontally by the fault segments and, therefore, these faults do not show strike-slip displacements.

sediments and the very thin or absent late Middle Miocene (Sarmatian) succession in the centre of the Pannonian Basin (*Magyar et al.*, 1999) suggests an overall low water depth or even sub-aerial environment during the onset of Late Miocene (Pannonian) times. Exceptions are recorded in the deepest Middle Miocene (half-)grabens, such as the Békés basin, and areas near the margins of the Pannonian Basin, like the Danube basin, where Middle Miocene subsidence outpaced sediment supply and, therefore, deep water environments could have continued. This asymmetry of shallow in the centre and deep bathymetry near the margins of the Pannonian Basin was created by the overall variability of the extensional mechanics (*Balázs et al*., 2016).

After a short break in extension during earliest Pannonian times, rapid subsidence continued in the Pannonian Basin (e.g., *Matenco and Radivojević*, 2012; *Horváth et al.*, 2015; *Balázs et al*., 2016). This subsidence was locally enhanced by the formation of other Late Miocene half-grabens, mostly concentrated in the E and SE parts of the Pannonian Basin until about 9-8 Ma. This subsidence has created a rapid transgression associated with the deposition of a deep-water facies recorded in most of the Pannonian and Transylvanian basins (e.g., *Krézsek et al.*, 2010). These have resulted in highly variable paleo-bathymetries during the evolution of Lake Pannon, as reflected by our calculated heights of the subsequent shelf-margin slope progradation (Figure 3.6). In the NW Danube basin, the water depth increased to a minimum 550 m and the basin was subsequently filled by 9 Ma with ~1.5 km thick deep water sediments. In the NE (e.g., the Nyírség sub-basin) the subsidence and water level rise kept pace with sedimentation, resulting in a small paleo-bathymetrical variability of consistently shallow water prograding – aggrading – retrograding delta and alluvial environments during the entire Late Miocene - Quaternary basin evolution with only a few localized exceptions (Figure 3.7). Southwards (near the Nádudvar sub-basin, Figure 3.6b), the prograding - retrograding pattern suggests that at 8-8.6 Ma, the rates of sediment supply and creation of accommodation space are roughly in balance (see also *Carroll and Bohacs*, 1999). In contrast, the rate of tectonic subsidence was lower in the western part of the Pannonian Basin resulting in a gradual basin fill by aggradation and progradation. In the centre of the Pannonian Basin (the Danube-Tisza interfluve, Figure 3.1) the subsidence rates were low during the entire evolution and represented a basement high, therefore, the paleo-bathymetry has never reached the few hundreds of meters observed elsewhere (Figure 3.6).

The subsidence rates and accommodation space continuously decreased with time after the initial Late Miocene transgression, but the rate of sedimentation remained high and, therefore, the entire Lake Pannon was finally filled by ~4 Ma (*Magyar et al.*, 2013). Smaller scale water level variations are observed by the analysis of the shelf-edge trajectories, interpreted to be climatically driven (*Uhrin and Sztanó*, 2011; *Sztanó et al.,* 2013). Our reconstructed paleobathymetries show that the lake reached the highest water depth values between 6.8 and 5 Ma of ~1000 m (Table 3.1, see also

Balázs et al., 2015). The asymmetry of the transport direction dominant from the NE and NW during the continuous subsidence has created higher paleo-bathymetries in the SE where the rapid progradation was recorded at later times (Figure 3.6a). By the same reasoning, these basins contain the largest thicknesses of deep water pelagic sedimentation and distal turbidites reaching thicknesses of 3.5 km (e.g., *Sztanó et al.*, 2013).

3.6.2 Shelf-margin morphology

Sediments previously deposited on the slope connecting the shelf with the deep-water basin of Lake Pannon are presently deeply buried in the Pannonian Basin. Our analysis shows that the width of the slope between the shelf-edge to the toe-slope varies between 5 and 15 km at decompacted heights between 200 and 1000 m. This results in slope angles between 3^0 and 8^0. Such values are similar to dip angles of marine slopes (*Porebski and Steel*, 2003; *Johanessen and Steel,* 2009; *Gong et al.*, 2016) that are controlled by lithology, grain size distribution or sediment influx from the source area (e.g, *Gvirtzman et al.*, 2014).

Our calculations demonstrate that paleo-bathymetries were controlled by the inherited extensional geometries, the base of the slope showing higher values (600-700 m) over the various sub-basins when compared with intervening basement highs (400-500 m). This means that the deposition of deep-water pelagic sediments and turbidites was unable to compensate all the inherited morphological differences from extensional times before the shelf-margin slope progradation arrived.

Our analysis of the shelf sedimentation (Figure 3.5) shows progradation of tens of meters thick deltas (see also *Uhrin and Sztanó*, 2011). Their position on the inner or outer shelf is controlled by lake water level variations that typically reach ~100 m during highstands, as observed in marine domains or semi-enclosed seas, such as the Black Sea (*Porebski and Steel*, 2003; *Matenco et al.*, 2016). Our interpretation of water-level variations infer periods of ascending, descending and stationary shelf-edge trajectories (Figure 3.5). Such an analysis does not necessarily take into account the small-scale variations of accommodation on the shelf, but in basins characterized by ongoing tectonic subsidence, such as the Miocene Pannonian Basin, even stationary shelf-edge trajectory indicates periods of climatically-driven water-level fall (cf., *Sztanó et al.*, 2013). Their rates are similar to the rate of basin subsidence. However, in our case their local amplitude is only in the order of tens of meters usually. In contrast with typical passive margin settings, back-arc extension has resulted in highly variable basement morphology, such as deep half-grabens, like for instance the Makó Trough or basement highs, like the Transdanubian Range (Figure 3.1). These structures also control locally the direction of sediment transport, such as in the Túrkeve sub-area, where the direction of progradation followed the strike of the

inherited Middle Miocene sub-basin (Figures 3.1, 3.8), the Sava Trough or south of the Transdanubian Range (*Törő et al.*, 2012).

The inherited relief, spatially variable subsidence rates and lake water level variations controlled the paleo-bathymetries and created tens of metres high deltaic clinoforms over the shelf and up to 1000 meters high shelf-margin slope clinoforms. Of course, between such end members the balance between the rate of sedimentation and progressively increasing base-level rise could result in the continuous transition from small scale deltas to high shelf-margin slopes (cf. *Sztanó et al.*, 2015). Such transitional slopes are observed in the Nyírség sub-basin (Figure 3.7) and its prolongation towards the deep Derecske Trough (*Balázs et al.*, 2016), or in the Danube-Tisza interfluve, water depths are in general higher above the former half (grabens) and lower above the separating basement highs.

The extension of the Pannonian Basin ceased at 8-9 Ma (e.g., *Matenco and Radivojević*, 2012; *Balázs et al.*, 2017). The subsequent evolution was controlled by post-rift thermal cooling and the basin-wide inversion during the Adriatic indentation creating differential vertical movements (Figure 3.1; *Sacchi et al.*, 1999; *Bada et al.*, 2007). Such inverted structures are well documented for instance at ~8 Ma in the western part of the Pannonian Basin (*Fodor et al.*, 2005; *Uhrin et al.*, 2009), at 6-8 Ma along the Mid-Hungarian Fault zone (Figure 3.6d, see also *Juhász et al.*, 2013). Our results show that effects of basin inversion should be taken into account significantly during the calculation of the paleo-bathymetries in the central and SE part of the basin as well. The observed contraction reached a peak at the transition between Miocene and Pliocene times, caused likely by the northward drift and CCW rotation of the Adriatic microplate (*Pinter et al.*, 2005). This peak contraction is the main mechanism creating the widespread unconformity observed at the transition between the Miocene and Pliocene in the Pannonian Basin (e.g., Figure 3.5), being replaced laterally by a correlative conformity in deeper sub-basins (*Magyar and Sztanó*, 2008). Our observations confirm that the Late Miocene to Recent evolution of the Pannonian Basin and associated subsidence/uplift pattern is mainly controlled by basin scale flexural effects superimposed on post-rift thermal sagging (*Horváth and Cloetingh*, 1996; *Dombrádi et al.*, 2010; *Jarosinski et al.*, 2011).

Previous interpretations assumed that the inversion was also associated with the (re)activation of strike slip zones along former structures (Figure 3.1; *Horváth et al.*, 2006, *Bada et al.*, 2007; *Visnovitz et al.*, 2015). Strike-slip kinematics are certainly significant in many parts of the Pannonian Basin, demonstrated by the observation of offsets and Riedel shears in 2D or 3D seismics (e.g., Figure 3.11, see also *Várkonyi et al.*, 2013). However, our study demonstrates for the first time that compaction effects creating fault systems such as the one quantified above the Dévaványa basement high are certainly significant in the sediments of the Pannonian Basin. The effects should

be similar elsewhere: by faults with variable offsets, increasing and subsequently decreasing towards the surface, reaching a maximum in the order of 150 m (Figures 3.8, 3.12).

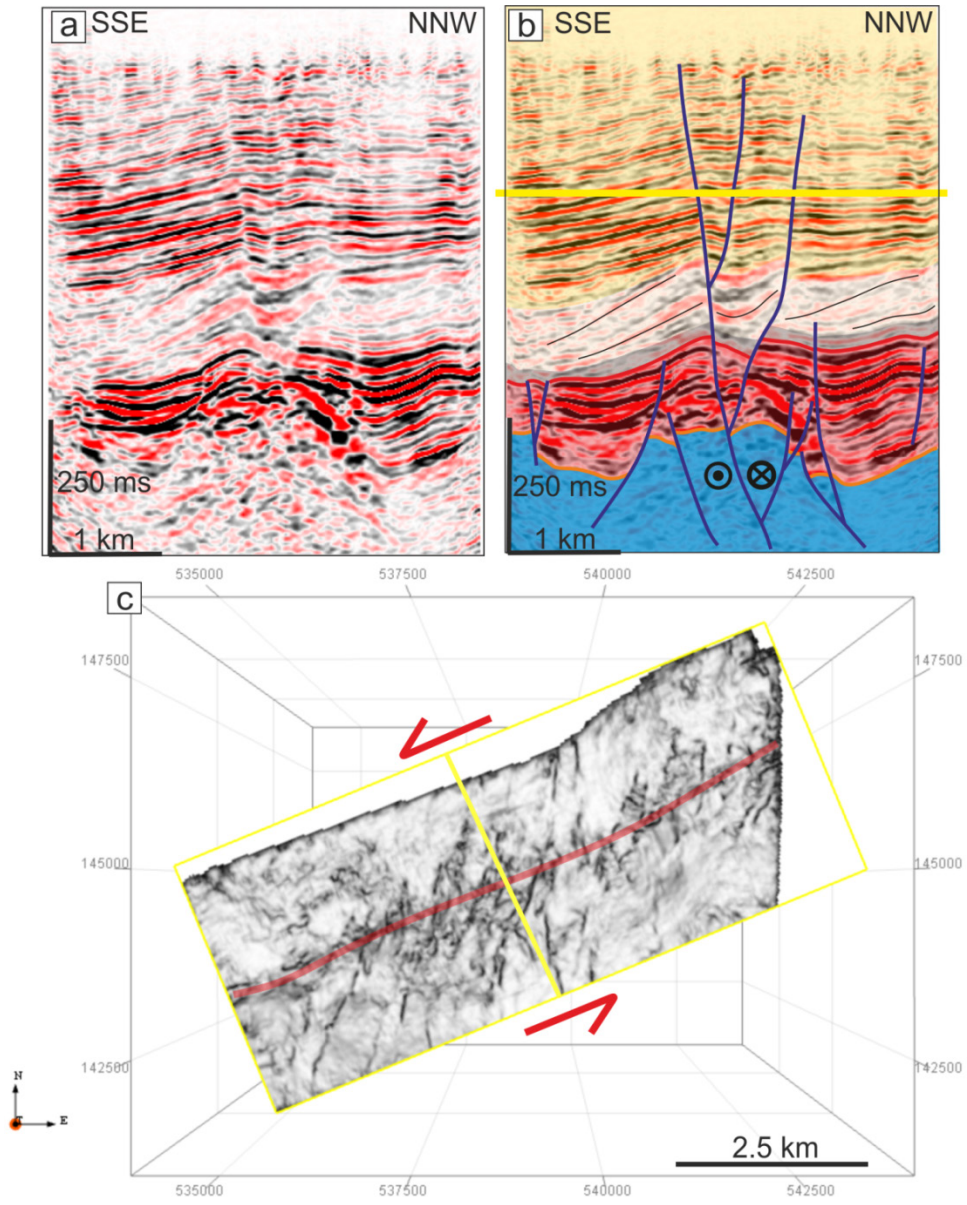

Figure 3.11: Non-interpreted (a) and interpreted (b) seismic section crossing the Balaton Fault zone, location in Figure 3.1; c) Coherency cube time slice highlighting the geometry of synthetic Riedel faults and demonstrating the sinistral strike-slip offset of this fault zone (see also *Várkonyi et al.*, 2013 and *Visnovitz et al.*, 2015).

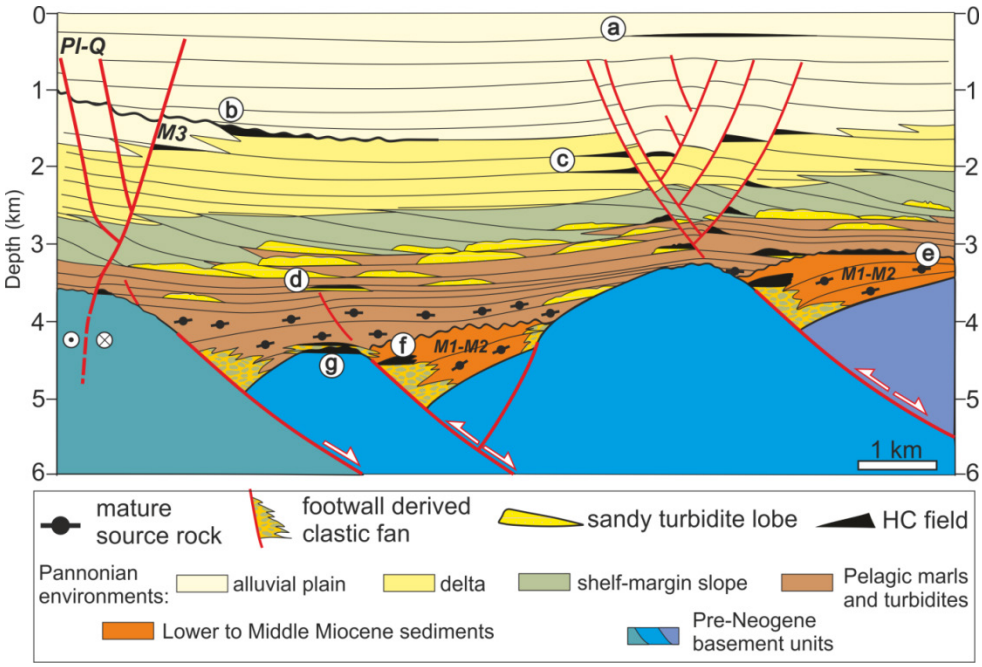

Figure 3.12: Conceptual model of filling the morphology of Lake Pannon in the Great Hungarian Plain that takes into account the inherited extensional structures and further effects, such as differential compaction over basement highs and neotectonic strike-slip fault zones (modified after *Tari and Horváth*, 2006). Figure also shows the main hydrocarbon play types of the basin: a) Biogenic and thermogenic fields in drape-folds above basement highs; b) delta sandstones and conglomerates in stratigraphic traps or connected to unconformites; c) delta or deep-water turbiditic sandstones affected by compaction induced normal faults; d) deep-water turbiditic sandstones in stratigraphic or structural traps. Differential compaction induced faults at the periphery of half grabens also provide migration pathways; e) Sandstones and conglomerates at the unconformity of inverted Early-, Middle- Miocene basins; f) footwall-derived fans along the boundary faults of half-grabens; g) basal conglomerates deposited onto the basement or the fractured Neogene-basement itself.

3.7 Conclusions

Our interpretation of 2D and 3D seismic data from the Late-Miocene to Quaternary sedimentary succession from Pannonian Basin correlated with wells shows the transition from an initial underfilled to a final stage of overfilled large lacustrine basin. Spatial and temporal variations of the external and internal forcing factors result in lateral changes of prograding – aggrading – retrograding shelf-margin slope geometries and paleo-water depths. Using decompacted thicknesses of the prograding shelf-margin slope clinoforms, our calculations indicate the variation of water depth values from ~75 m up to ~1 km. The shelf had paleo-bathymetries of up to 75 m with a high order variability controlled by climate.

Both water depth and sedimentary transport routes were primarily determined by inherited and/or local active tectonics, including the control of the Miocene shelf-margin progradation directions and Recent fluvial transport routes. Highest water depth values characterized the SE latest Miocene to Pliocene remnant of the lake due to the higher subsidence rates and more distal position from the main source areas.

Latest Miocene to Recent tectonic topography appears to be basin scale folding process. Areas of uplift were subject to denudation and the eroded material continuously overfilled the generated accommodation space. Sediments up to ~6 km have been affected by this still ongoing differential vertical movement and compaction creating gentle fold geometries and differential compaction induced fault offsets, playing a major role in hydrocarbon migration and trapping (Figure 3.12). 3D geometries of such atectonic compaction related faults above basement highs are compared with fault geometries from a sinistral strike-slip zone by the calculation and analysis of seismic attributes.

4. Symmetry during the syn- and post-rift evolution of extensional back-arc basins: the role of inherited orogenic structures[3]

[3]*This chapter is based on Balázs, A., Burov, E., Matenco, L., Vogt, K., Francois, T., Cloetingh, S., 2017. Earth and Planetary Science Letters 462, 86–98.*

4.1 Introduction

The evolution of extensional basins is controlled by multiple internal and external forcing factors and parameters, such as variable plate divergent rates, surface processes, coupled or decoupled crustal and lithospheric configurations, evolution of asthenospheric thermal anomalies and associated mantle dynamics (e.g., *Huismans and Beaumont*, 2003; *Burov*, 2007; *Liao and Gerya*, 2014). Moreover, rheology is a key parameter influencing the geometry of extension, strength contrasts and degree of brittle-ductile coupling (e.g., *Brun*, 1999; *Burov and Poliakov*, 2001). It also controls localisation of deformation and its subsequent evolution (*Dunbar and Sawyer*, 1988; *Sokoutis et al.*, 2007; *Li et al.*, 2011). The extension rates also control the style of extension, for instance low divergence rates or tectonic quiescence periods may lead to rift migration (*van Wijk and Cloetingh*, 2002; *Naliboff and Buiter*, 2015), critical for the formation of hyper-extended margins (*Brune et al*., 2014). Furthermore, low extension rates favour the formation of asymmetric basins, resulting in the creation of high lateral offsets between the locations of maximum crustal and lithospheric thinning (e.g., *Huismans and Beaumont*, 2003). Analogue models infer that different extension rates also have considerable impact on strain localisation. An increase of plate divergence rate increases the strength of the ductile layers and therefore enhances the coupling between the brittle and ductile layers resulting in more distributed extension (*Brun*, 1999; *Corti et al.*, 2003).

The symmetry of extension, in terms of crustal and lithospheric thinning and its evolution with time, and the degree of rheological coupling between different lithospheric layers are particularly important when extension affects a pre-existing nappe stack (e.g., *Ziegler and Cloetingh*, 2004). In orogenic settings, nappe contacts provide critical rheological contrasts. In particular, subduction and suture zones formed during the amalgamation of continents provide the possibility of large lithospheric scale reactivations (e.g., *Dunbar and Sawyer*, 1988; *Sokoutis et al.*, 2007). Such conditions are most often met in extensional back-arc domains, where asymmetric (i.e., simple shear) extension reactivates suture zones and nappe contacts shortly after orogenic build-up, affecting an overthickened, hot and weak lithosphere (*Le Pourhiet et al.*, 2004; *Tirel et al.*, 2008; *Huet et al.*, 2011; *Menant et al.*, 2016). Back-arc extension reactivates thrust contacts and exhumes rocks previously buried at great depths, such as in the Apennines or Aegean system (e.g., *Brun and Faccenna*, 2008). In these settings deformation occurs at high strain rates, controlled by the interplay between subduction and plate convergence velocities, such as typically observed in Mediterranean back-arcs. Extension was variable in time and space with average velocities of 2-3 cm/yr for the last 30 My, of course short periods of very slow and fast extensional pulses are inferred (*Faccenna et al.*, 2014).

The role of evolving thermal anomalies, phase transformations and migration of deformation in space and time associated with variable subsidence rates are important in understanding the evolution of extensional basins, in particular in back-arc settings (*Cloetingh et al.*, 2013; *Menant et al.*, 2016). Numerical models have demonstrated the close feedback between stretching, evolution of thermal anomalies and basin formation (*Huismans and Beaumont*, 2003; *Burov*, 2007). However, their relationship with the extensional back-arc basin infill, in terms of symmetry, evolution and migration of deformation in time and space, is less understood.

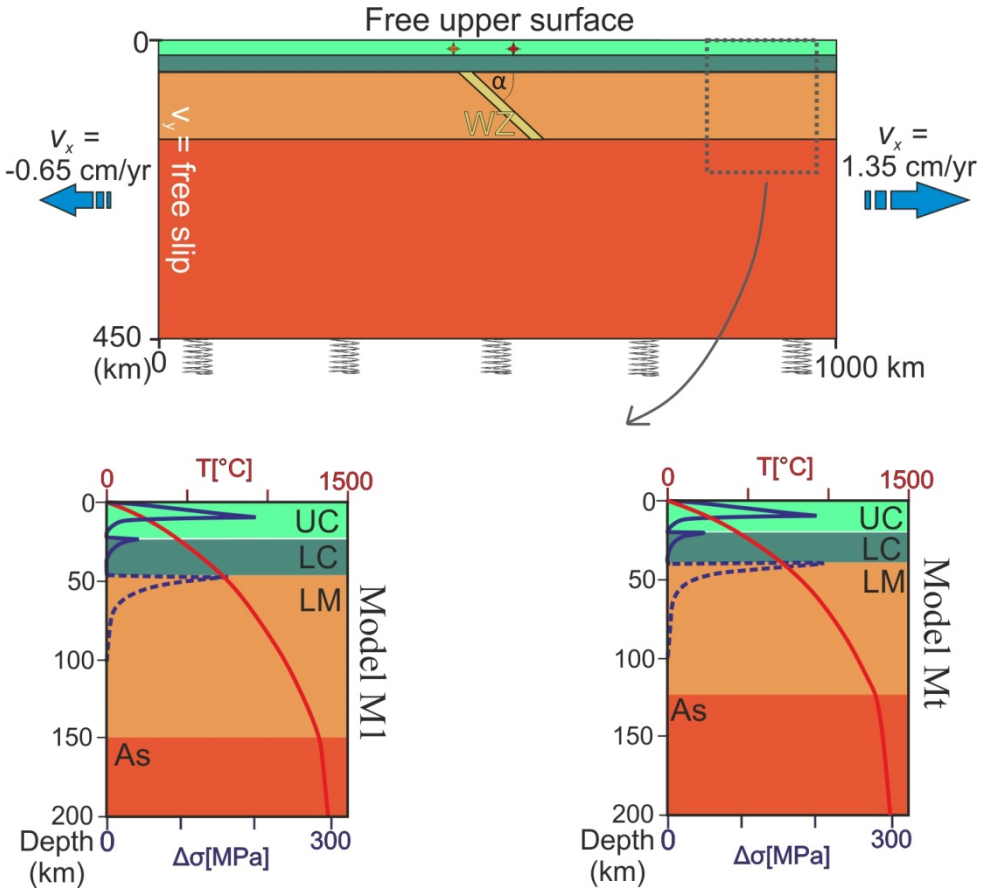

Figure 4.1: Initial setup of the numerical model. The upper model boundary is a free surface. Springs indicate lithostatic pressure (Winkler basement) applied at the base of the model. Constant lateral velocities are applied at the sides of the model (blue arrows). An initial tilted rheological weak zone (WZ) is defined in the lithospheric mantle. Two crustal marker points are plotted on the phase configuration showing the evolution of extension with time in Figure 4.2. The initial geotherms and strength profiles were calculated for model M1 (left) and Mt (right) based on the rheological parameters of Table 4.1. UC: upper crust, LC: lower crust, LM: lithospheric mantle, As: asthenosphere. The lithospheric mantle is relatively weak (dashed line) due to the high geotherm and has no strength at the weakness zone at such high temperature values.

In this study, we investigate the influence of large scale rheological weakness zones during the formation and evolution of back-arc extension using 2D thermo-mechanical numerical modelling calibrated by geological and geophysical observations. A key element in our model is the implementation of a lithospheric weakness zone, simulating the influence of a pre-existing suture or major nappe contact during extension. We conducted a series of numerical models to test the controls of key parameters, such as the initial crustal and lithospheric thicknesses, weakness zone geometry, extensional velocities applied at the model sides and rate of erosion and sedimentation. Our study focuses on analysing the influence of these parameters on the interplay between the extensional symmetric versus asymmetric crustal deformation and mantle structure, and the formation and evolution of the overlying sedimentary basins. Our numerical modelling results are compared to observations in two of Europe's largest extensional back-arc areas, the Pannonian and Aegean basins of the Mediterranean region.

4.2 Modelling methodology

Thermo-mechanical numerical modelling is particularly well suited to study the mechanics of extension and the evolution of associated sedimentary basins (e.g., *Burov and Poliakov*, 2001; *Huismans and Beaumont*, 2003). We have employed the thermo-mechanically coupled 2D finite element code Flamar v12 (e.g., *Francois et al.*, 2013; *Burov and Gerya*, 2014), based on the earlier Flac-Para(o)voz algorithm (e.g, *Poliakov et al.*, 1993). Because of its capability to solve for large strains and its free upper surface boundary condition, this method is especially suitable to monitor the surface vertical movements during basin (de)formation (Figure 4.1). The numerical algorithm explicitly takes into account elasto-visco-plastic properties of different lithospheric layers and the asthenosphere. The implemented constitutive laws include linear elasticity, Mohr–Coulomb failure criterion for brittle deformation (faults) and pressure–temperature and strain-rate dependent viscous deformation (*Ranalli*, 1995). Linear cohesion softening is used for effective localisation of plastic deformation (e.g., *Huismans and Beaumont*, 2003). Our modelling setups involve a 2D section of 1000 km wide and 450 km deep. Constant lateral velocities are applied at the sides, while the upper boundary is a free surface (*Burov and Poliakov*, 2001). Pliable lithostatic pressure (Winkler basement) is applied at the bottom of the model, which implies vertical normal stresses proportional to vertical displacement of the boundary, multiplied by the density contrast (see also *Burov and Cloetingh*, 1997; *Francois et al.*, 2013). The horizontal grid resolution is 2 km and the vertical grid resolution varies between 1.2 up to 3 km, with higher resolution in the upper part of the crust and the overlying sedimentary basin (Figure 4.1). The accuracy of vertical displacements is in the order of 10 meters based on a series of sensitivity analyses (see Appendix and *Francois et al.*, 2013).

Length of models x_L	1000 km
Amount of extension	190 – 260 km
Temperature at the base of the lithosphere	1300 °C
Radioactive heat production, H_s	1.5×10^{-9} W kg^{-1}
Radiogenic production decay length, h_r	10 km
Crustal thermal conductivity, k_c	2.5 W K^{-1} m^{-1}
Mantle thermal conductivity, k_m	3.3 W K^{-1} m^{-1}
Thermal diffusivity of mantle, χ	10^{-6} m^2 s^{-1}
Specific heat, C_p	1000 J K^{-1} kg^{-1}
Cohesion	20 MPa

	Upper Crust	Lower Crust	Mantle Lithosphere	Weak zone	Asthenosphere
Thickness (km)	24, 20	24, 20	102, 95	-	300, 315
Density, ρ_0 (kg m^{-3})	2750	2900	3330	3270	3330
Power law constant, A (MPa^{-n} s^{-1})	6.7×10^{-6}	6.3×10^{-2}	7×10^3	6.8×10^3	7×10^3
Creep activation energy, E (kJ mol^{-1})	156	276	520	276	510
Power law constant, n	2.4	3.05	3	4	3

Model	Erosion coeff. k_e (m^2 yr^{-1})	Extension velocity (cm yr^{-1})	Weak zone dip degrees	Lithospheric, crustal thickness (km)	Moho T (°C)
M1	500	-0.65 + 1.35	50	150, 48	740
Mf	500	-1 + 2	50	150, 48	740
Mf2	500	-1.33 + 2.66	50	150, 48	740
Ms	500	-0.5 + 1	50	150, 48	740
Mst	500	-0.5 + 1	50	135, 40	725
Mt	500	-0.65 + 1.35	50	135, 40	725
Mft	500	-1 + 2	50	135, 40	725
Mft2	500	-1.33 + 2.66	50	135, 40	725
M1le	250	-0.65 + 1.35	50	150, 48	740
M1he	750	-0.65 + 1.35	50	150, 48	740
M1ne	0	-0.65 + 1.35	50	150, 48	740
Mws	500	-0.65 + 1.35	65	150, 48	740
Mwg	500	-0.65 + 1.35	30	150, 48	740
Mwr	500	-0.65 + 1.35	-50	150, 48	740
Mwv	500	-0.65 + 1.35	90	150, 48	740
Mtp	500	-0.65 + 1.35	-	150, 48	740
Mo	500	-0.65 + 1.35	50	150, 48	585

Table 4.1: Basic parameters of the 17 presented model experiments. Rheological parameters are adapted from similar numerical experiments (upper crust: e.g., *Burov*, 2007; *Cloetingh et al.*, 2013; lower crust: e.g., *Francois et al.*, 2013; mantle: e.g., *Burov and Poliakov*, 2001; and *Ranalli* (1995). Model Mo with much lower geotherm is presented in Appendix A.

The experiments are specifically designed to simulate the fast extension of a hot and overthickened lithosphere that is common to many back-arc areas preceding extension, for instance in the Alpine-Carpathian region (Figure 4.1; *Faccenna et al.*, 2014). Our modelling procedure includes the implementation of a reference model (model M1, Table 4.1) and further analysis of the effects of variable parameters, such as rate of erosion and sedimentation, lithospheric weakness zone dip angle, initial crustal and lithospheric thickness and the rate of extension. A setup with an initial crustal thickness of 48 km, lithospheric thickness of 150 km, lithospheric weakness zone dip angle of 50 degrees with lateral velocities of 0.65 cm/yr left and 1.35 cm/yr right has been defined as a reference model for comparison with other scenarios (Figures 4.1 and 4.2, Table 4.1). Similar to other numerical models (*Burov and Poliakov*, 2001), surface processes in terms of erosion and sedimentation were simulated by a linear diffusion law, where different erosion coefficients (k_e) correspond to different erosion rates (Table 4.1). Such an approach allows us to consider the dependence of erosion and sedimentation rate on the smoothness of the relief (i.e. surface curvature). The influence of the surface processes is simulated by a variable erosion coefficient (k_e) between 0 to 750 m^2yr^{-1}.

The thermo-mechanical properties of each element of the numerical grid are defined by the temperature and pressure dependent density, the thermal and elasto-visco-plastic parameters of its material. An initial overthickened and thermally weakened orogenic lithosphere is simulated by a crustal thickness of 40-48 kilometres at Moho temperatures of 725-740 °C and lithospheric thickness variable between 135-150 kilometres (Figure 4.1). The initial thermal structure of the lithosphere is averaged from available observations in young orogens with 0°C on the surface and 1330 °C at the base of the lithosphere (Figure 4.1). Moho temperatures of ~ 740 °C are generally observed in young orogenic settings (*Tesauro et al.*, 2009). Our chosen rheological and thermal parameters are limited to one type that averages a typical young and hot orogen (Figure 4.1, and Table 4.1) where rheological decoupling of the crustal and lithospheric layers takes place in most cases and results in horizontal ductile flow in the intermediate or lower crust (*Burov*, 2011). In such a decoupled "jelly sandwich" type of rheology, the strength of the lithospheric mantle is especially weak due to the high temperature values. We have not implemented variable rheologies in our extensional model because their role is extensively discussed elsewhere (*Burov and Poliakov*, 2001; *Burov*, 2011).

Furthermore, a 15 km thick rheological weakness zone simulating an inherited subduction/suture zone or major lithospheric-scale thrust contact has been implemented in the centre of our models by decreasing the creep activation energy. This type of implementation is commonly successfully used in modelling to simulate rheological weakness zones (e.g., *Li et al.*, 2011; *Liao and Gerya*, 2014; *Sokoutis et al.*, 2007). We assume that the former subduction and subsequent collision phase have

resulted in a thickened crust and a weak suture zone in the mantle (Figure 4.1). The latter is attributed to fluids released during subduction, which causes a major rheological contrast in the mantle. While in nature series of thrusts are distributed over a larger area, their size and rheological contrast are less effective at our given resolution (*Burg and Gerya*, 2005). The angle of dip of the rheological weak zone has been tested in a number of models as a parameter influencing the geometry of extension (Figure 4.1). These experiments were also compared with one model without any weakness zone, where strain localisation occurred by an initial thermal anomaly of +50° C at the base of the lithospheric mantle at the beginning of the experiment. The implemented viscosity fields of our models are shown in Appendix A. A model with stronger coupling between the crust and lithospheric mantle is shown in Appendix A. Further details are available in Appendix B and previous publications using this numerical approach (e.g., *Burov and Poliakov*, 2001; *Francois et al*., 2013).

Divergent velocities on the sides of the model during the syn-rift phase simulate extension. Starting from the reference model, different lateral velocities were tested in subsequent models. When studying the effects of the extensional velocity, experiments with initial thicker lithosphere (150 km) were compared after the same amount of 240 km total extension. Models with a thinner configuration (initial crustal thickness of 40 km, lithospheric thickness of 135 km) were analyzed when the same amount of lithospheric thinning was obtained compared to the thicker scenarios. The overall values of total horizontal extension, extensional velocities and duration of syn- and post-rift basin evolution are taken from averages from observed values in Mediterranean back-arc basins (*Faccenna et al*., 2014). Zero velocities are applied during the subsequent post-rift evolution. In order to simulate the back-arc character of the extension, we have implemented different extensional velocities at the sides of our model, where the velocity at one boundary is double the value than on the opposite side (Figure 4.1). The higher velocity on one side of the model simulates the effect of slab retreat. Further subduction effects, such as slab sinking are ignored to discriminate them from the studied extensional kinematics. Most of our model setups include a weak zone dipping in the opposite direction relative to the direction of subduction during slab-retreat simulated in our models (i.e. dipping to the right relative to the retreat of a slab dipping to the left in Figure 4.1).

4.3 Numerical modelling results

Starting from a reference model (Figure 4.2) the influence of the extension velocities, erosion rates, the inclination of the rheological weak zone and the lithospheric/crustal thicknesses were tested and described in subsequent models (Figures 4.3-4.7). Note that the same amount of bulk stretching in our models creates different amounts of crustal and lithospheric thinning as a function of strain

localisation, surface processes and convective thermal erosion of the lithosphere. Model results are illustrated by lithospheric layering geometries (i.e. cross-section of phase configuration: upper crust, lower crust, lithospheric mantle and underlying asthenosphere), finite strain (Figures 4.2-4.4) and temperature distribution (Figure 4.6) at various times (Figures 4.2, 4.6 and 4.7). A comparison of different models is shown in Figures 4.3-4.5.

4.3.1 Reference model results

The reference model (M1, Figure 4.2, Table 4.1) simulates the extension of an overthickened orogenic structure affected by typical rates of extension observed in the Mediterranean area. It has initial thicknesses of 24 and 24 km for the upper and lower crust, respectively, 740°C Moho temperature and 150 km lithospheric thickness. An erosion coefficient of 500 m^2yr^{-1} is applied during the 13 Myr of extension and the subsequent 9 Myr of post-rift evolution. An initial dip of the lithospheric weakness zone of 50° was defined.

During the first 2-3 Myr, the extensional geometry is controlled by fast lithospheric mantle thinning resulting in an initial updoming in the centre of the model with very shallow and restricted accommodation space (Figure 4.2a). The crust is affected by low offset normal faulting when the underlying lithospheric mantle weakness zone is partly re-distributed over a larger area. This is followed by localisation of deformation, which creates deeper depocentres in individual half-grabens (1-4, Figure 4.2). These sub-basins form at first near the margins of the underlying and progressively re-distributed weakness zone. Subsequently the extension migrates with time towards the centre of the area overlying the re-distributed weakness zone. Therefore, younger depocentres are located more to the centre of the extensional area between older sub-basins (from 1 to 4, Figures 4.2b-d). The upper crustal thinning is accommodated by lower crustal ductile flow resulting in opposing thinning geometries (Figure 4.2c).

Figure 4.2 (facing page): Evolutionary model of the reference experiment (M1 in Table 4.1). Model results are illustrated by lithospheric layering geometries (i.e., phase configuration: upper crust, lower crust, lithospheric mantle and the underlying asthenosphere, yellow colour represents sedimentary basin fill) on the left and finite strain on the right panels. Two crustal marker points are plotted on the phase configuration showing the evolution of extension with time. The inherited weakness zone (WZ) controls the fast lithospheric mantle attenuation, while the style of crustal thinning evolves from an initial stage (a) to a localised, migrating style (b-d). An initial central updoming results from the asthenospheric uprise (topography above 2a with and without erosion, red and black curves, respectively). During the post-rift evolution (d-e) lateral heat transport results in uplift (purple arrows), erosion of the basin margins and subsidence of the basin centre (green arrow). Faults and shear zones are indicated based on the calculated strain rate results of the thermo-mechanical models. Blue horizontal arrows show the asymmetric extension velocities imposed on the model sides for 13 Myr simulating back-arc extension and then the velocities are set to 0 for the post-rift phase (d-e).

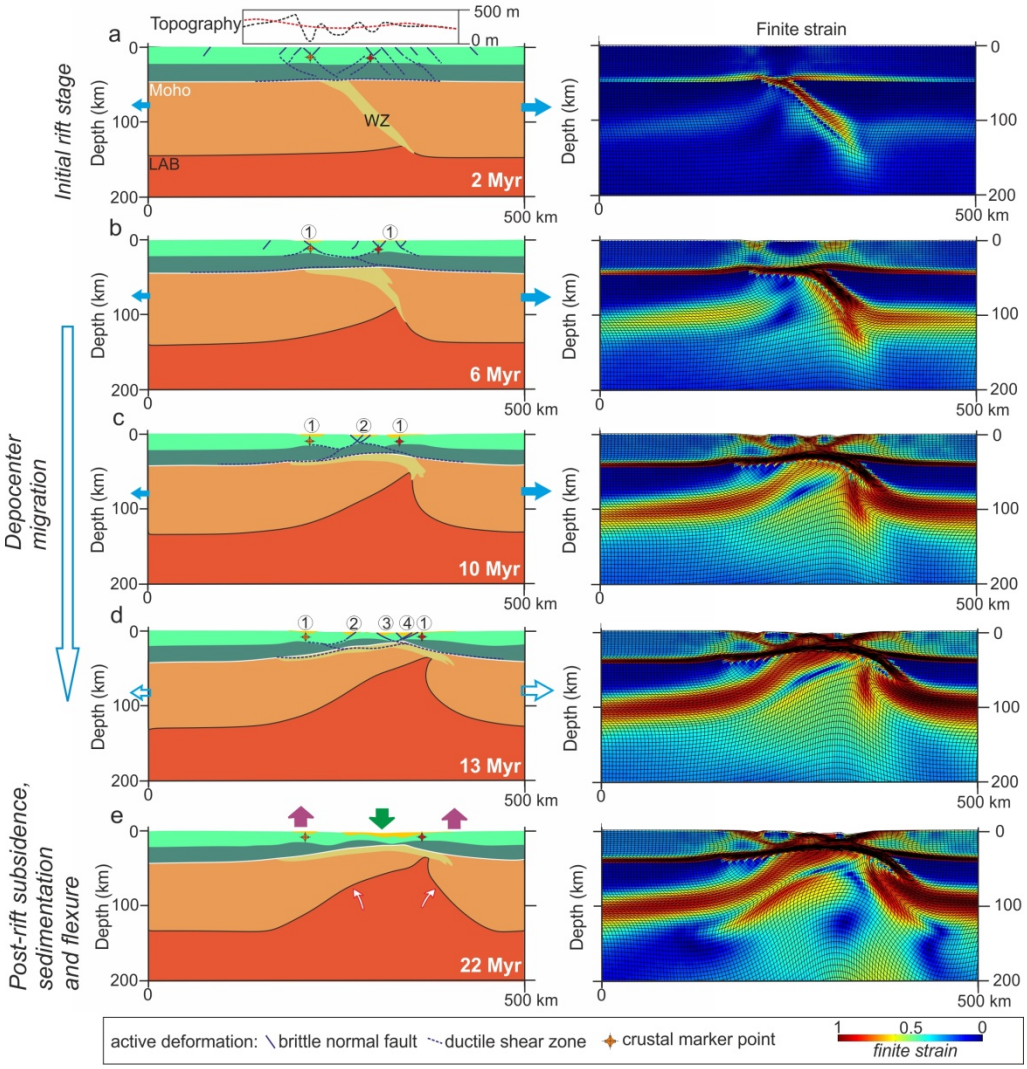

The rapid ascent of the asthenosphere is highly asymmetric, mirroring the localisation of extension along the partly re-distributed weakness zone. This localisation leads to migration of the newly formed sub-basins (direction of younging from 1 to 4 in Figure 4.2d) that follows the initial dipping direction of the weakness zone. At the end of the syn-rift phase, the location where the crust records maximum thinning is horizontally offset (with ~20 km) from the position showing the highest asthenospheric ascent. Domains of maximum and minimum thinning are opposed in the upper and lower crust.

After the extensional velocity reduces to zero, the thermal relaxation of the highly asymmetric asthenosphere uprise will be attenuated towards a more symmetric configuration due to lateral cooling. During this stage, the place recording maximum mantle lithospheric thinning is still horizontally offset from the location of the basin

depocentre. The lateral heat transfer from the asthenospheric upwelling creates flexural uplift and erosion near the margin of the area affected by crustal extension. Sediments are re-deposited in the centre of the basin. This re-distribution results in flexure of the thermally weakened lithosphere, which enhances differential vertical movements and creates minor upper crustal deformation and lower crustal flow (see also *Burov and Poliakov*, 2001).

4.3.2 Parameter sensitivity study

The effect of the initial dipping angle and dip direction of the rheologically weak zone was tested in a series of experiments, illustrated at the end of the syn-rift phase (Figure 4.3). We have tested four dip angles in the direction of the maximum lateral velocity (30°, reference model of 50°, 65° and vertical, Figures 4.3a,c,d,e) and one with opposite direction (-50°, Figure 4.3b). We have compared these results with a model where no tilted rheological weakness zone was present, but strain localisation was achieved by inserting a rectangular seed of 10 times 10 km at the base of the lithosphere in the centre of the model where the temperature is +50ºC higher than the surrounding rocks (Figure 4.3f). This thermal seed weakens the overlying lithosphere and localises the strain. When the dip of the weak zone is opposite to the direction of the maximum lateral velocity (Figure 4.3b), the lithosphere is less thinned but the width of the asthenospheric anomaly and overlying sedimentary basin is higher. In this situation, the horizontal offset between the locations of maximum crustal and lithospheric mantle thinning is higher when compared to the reference model (Figures 4.3a,b). The edge of the asthenospheric anomaly is still steeper in the initial dip direction of the rheological weak zone, implying a stronger control of the dip direction compared with the direction of maximum lateral velocity. Testing the influence of the dip angle of the rheological weakness zone (Figures 4.3a,c-e) shows that a steeper weak zone creates a more symmetric asthenospheric uprise, higher crustal and lithospheric thinning, narrower and deeper overlying sedimentary basins and lower horizontal offset between the locations of maximum crustal and mantle thinning. When the weak zone is vertical (Figure 4.3e), the model shows a more

Figure 4.3 (facing page): The influence of the initial angle of dip and dip direction of the rheological weak zone (WZ). Upper panels: phase configuration after 13 Myr of extension and initial phase configuration (upper right); lower panel: finite strain result after 13 Myr of extension. Above the panels the basement depth profiles are drawn after 13 Myr of extension. a-f) models M1, Mwr, Mwg, Mws, Mwv, Mtp (Table 4.1), respectively. a) reference model M1; b) The weak zone is dipping in the opposite direction compared to the maximum lateral velocity; c) Initial lower dipping angle of the rheological weak zone; d) Initial steeper dipping angle of the rheological weak zone; e) Initial vertical rheological weak zone; f) No weak zone, extension initiated by an initial thermal perturbation in the mantle lithosphere. Blue horizontal arrows show the asymmetric extension velocities of -0.65 + 1.35 cm yr^{-1} imposed on the model sides.

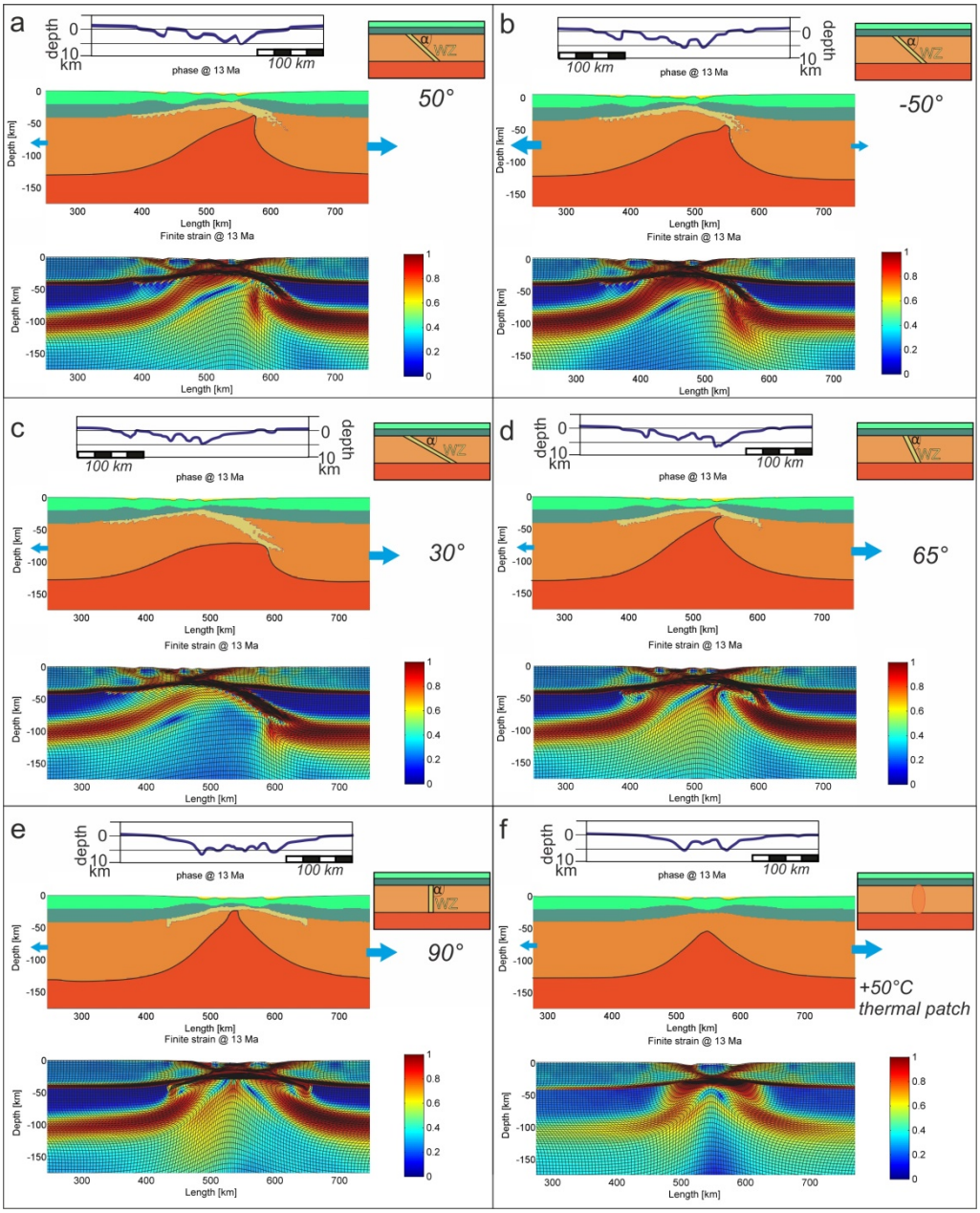

pronounced lithospheric mantle thinning when compared with models without a weak zone (Figures 4.3e,f see also *Burov and Poliakov*, 2001), and a symmetric final lithospheric geometry structure and overlying sedimentary basin. In the model without a weak zone (Figure 4.3f), the overall narrower sedimentary basin is composed of two localised depocentres that formed in the same manner and at the same time, and symmetrically overlies a significantly lower asthenospheric uprise, when compared with models containing a tilted weak zone.

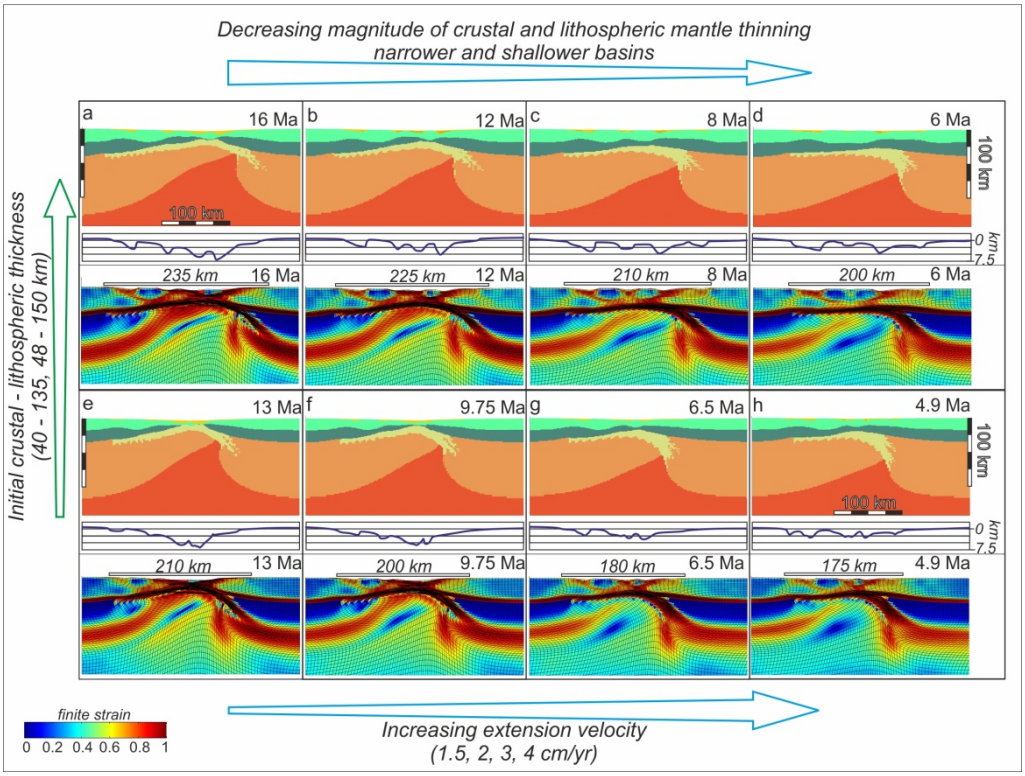

Figure 4.4: Comparison of phase configuration (upper panel), basement subsidence (middle graph) and finite strain (lower panel) results of models with different extension velocities (1.5, 2, 3 and 4 cm/yr) and initial crustal/lithospheric thicknesses. (a-d) Ms, M1, Mf experiments with higher initial crustal and lithospheric thickness after 240 km of bulk extension; (e-h) Mst, Mt, Mft, Mft2 experiments with lower initial crustal and lithospheric thickness after 195 km of bulk extension. Bars above the finite strain panels show the final width of the area affected by extensional deformation.

The effect of extension velocities was tested by comparing experiments with different extensional velocities (sum of the left and right side of the experiment) of 1.5, 2, 3, 4 cm/yr (Figure 4.4, Table 4.1) and with different crustal and lithospheric thicknesses (40 and 48 km, 135 and 150 km, Figures 4.4a-d and Figures 4.4e-h, respectively). We compare our results in such a way that the amount of lithospheric thinning is constant (at bulk extension of 195 and 240 km, respectively). All other parameters were kept constant relative to the reference model. In all experiments the right boundary velocity is double the value than on the left side. The experiments show that increasing the extensional velocity, and thus decreasing the modelled time duration, results in decreased asthenospheric uprise and lower amounts of crustal thinning, creating a narrower and shallower overlying sedimentary basin in both lithospheric thickness configurations (Figure 4.4). For instance, in the models with an initial lithospheric thickness of 150 km, the width of the crustal deformed zone decreases from 235 km to 200 km when comparing models with extension velocities

of 1.5 cm/yr and 4 cm/yr, respectively (Figures 4.4a,d). A similar decrease from 210 km to 175 km is observed in models with a lower initial lithospheric thickness (Figures 4.4e,h). Our models show that the crustal/lithospheric thinning and width of the overlying sedimentary basin is not only controlled by the amount of extension, but also by the rate of extension.

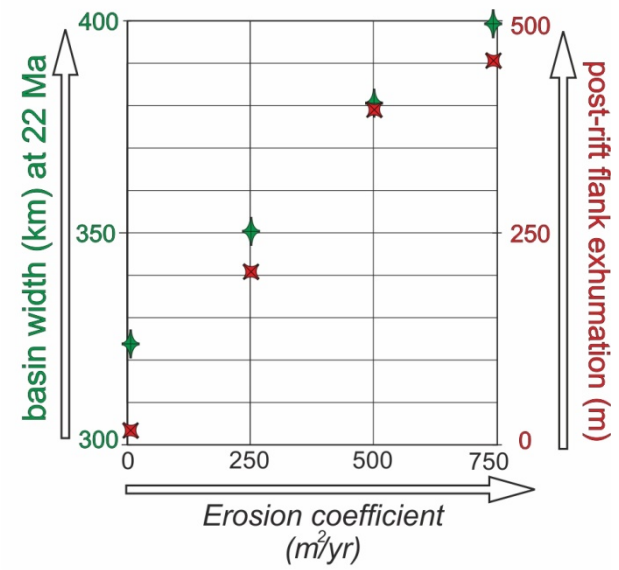

Figure 4.5: Control of different erosion rate values on the width of the extensional basin (models M1ne, M1le, M1, M1he in Table 4.1). Post-rift exhumation of the basin margins increases with higher erosion rates. Green symbols show the basin width, red symbols show values of post-rift flank exhumation after 13 Myr of extension and additional 9 Myr of thermal cooling.

For the two initial lithospheric configurations (crustal thickness 40 and 48 km, lithospheric thickness 135 and 150 km, Figures 4.4a-d and Figures 4.4e-h, respectively) the final width of the sedimentary basin can be as large as the previously thickened crustal domain amplified by the amount of bulk extension (*Brun*, 1999). Obviously, experiments with higher initial crustal and lithospheric thickness require a larger amount of total extension in order to create similar crustal and lithospheric thickness values underlying the sedimentary basin when compared with initially thinner crust and lithosphere models (240 km versus 195 km total extension, respectively, Figure 4.4). Hence, models with a thicker initial lithosphere create wider asthenospheric upwelling and overlying sedimentary basins.

The effect of surface processes has been simulated by testing variable erosional rates in our models. Four erosional coefficients have been tested by our models (0, 250, 500, 750 m^2yr^{-1}, Figure 4.5, Table 4.1). The experiments infer that the final width of the overlying sedimentary basin at the end of the model runs (syn- and post-rift period) increases with increasing erosion rate (i.e., from 315 km for zero erosion to 400 kilometres for an erosion coefficient of 750 m^2yr^{-1}, Figure 4.5). This is related to the erosion of the flanks and an additional sediment loading in the basin centre, in agreement with previous studies (e.g., *Burov and Poliakov*, 2001). Therefore, a high rate of erosion enhances exhumation of the basin margins.

4.4 Inferences from thermo-mechanical modelling

The implementation of a rheological weak zone in the mantle lithosphere drives an asymmetric evolution of the extensional system. A number of features are similar to findings by previous modelling studies, where the initiation of the rifting is induced by symmetrical weak seeds or thermal perturbations (e.g., *Huismans and Beumont*, 2003). However, the asymmetry of our model enhances some of the known effects and creates novel patterns that require interpretation.

4.4.1 Lithospheric-scale thermal evolution

Our numerical models show a similar large scale convective behaviour created by the interaction between the asthenosphere and mantle lithosphere as inferred previously (*Huismans et al.*, 2001; *Burov*, 2007; *Cloetingh et al.*, 2013; *Burov and Gerya*, 2014). The convective upwelling of the asthenosphere and lateral down welling of the mantle lithosphere is accentuated in our models because of the large amounts of extension combined with the initial thick, hot and weak orogenic lithosphere (Figure 4.6). The ultimate geometry of the asthenospheric upwelling (*Huismans et al.*, 2001) and associated surface heat flow is a combination between convective and conductive heat transport effects. The continuation of convection results in plume head interactions, where deep asthenosphere ascent is accommodated by lateral down welling and drip-off of lithospheric mantle (*Cloetingh et al.*, 2013). Furthermore, our models predict the novel possibility of a switch between thermal cooling and asthenospheric uprise during post-rift times: this is observed in the thermal evolution of the reference model (Figure 4.6), where an initial post-rift cooling of the lithosphere-asthenosphere boundary (Figure 4.6b) is followed by its ascent again due to deeper asthenospheric uprise, the latter being visible, for instance, in the 1500°C isotherm (Figures 4.6b-d).

Such convective processes also control the correlation between an increase of the extensional velocity and a decrease of both lithospheric thinning and overlying sedimentary basin width (Figure 4.4). The convective thermal erosion has a higher impact in models with lower extension rates, when there is more time to grow thermal instabilities. This is in accordance with the results of Burov (2007), who showed that positive Rayleigh-Taylor instabilities results in faster lithospheric thinning in experiments with lower extension velocities after the same amount of extension. The convective heat transport in the asthenosphere is much more effective than the conductive heat transport in the crust and associated heat loss. The accentuation of asthenospheric uprise by convection during slower extension decreases the lithospheric strength over a larger area, distributing the crustal thinning and, therefore, increasing the width of the basin. The viscosity of the ductile layers is exponentially dependent on the temperature and therefore the active upwelling of the lithosphere-

asthenosphere boundary has a higher impact in such cases than the strain rate variation. In other words, the thinning of the lithosphere is the joint result of the passive extension controlled stretching and the active upwelling of the hot asthenosphere. This is controlled by thermal effects and it is in contrast with analogue modelling inferences. Although analogue model experiments are especially suitable in general for studying 3D fault geometries (*Corti et al.*, 2003 and references therein), it should be noted that temperature evolution is not implemented in such models.

4.4.2 Sedimentary basin evolution

The evolution of the topography during extension indicates a generalised uplift during the initial extension, combined at higher resolution with the formation of footwall uplifted and hanging-wall subsided areas (Figure 4.2a). This is similar to many other active extension systems, both in nature and in experiments (e.g., *Ziegler and Cloetingh*, 2004; *Corti et al.*, 2003 and references therein). Specific in our models is the topographic asymmetry created by larger differential vertical movements in opposite direction when compared with the dip of the rheological weak zone.

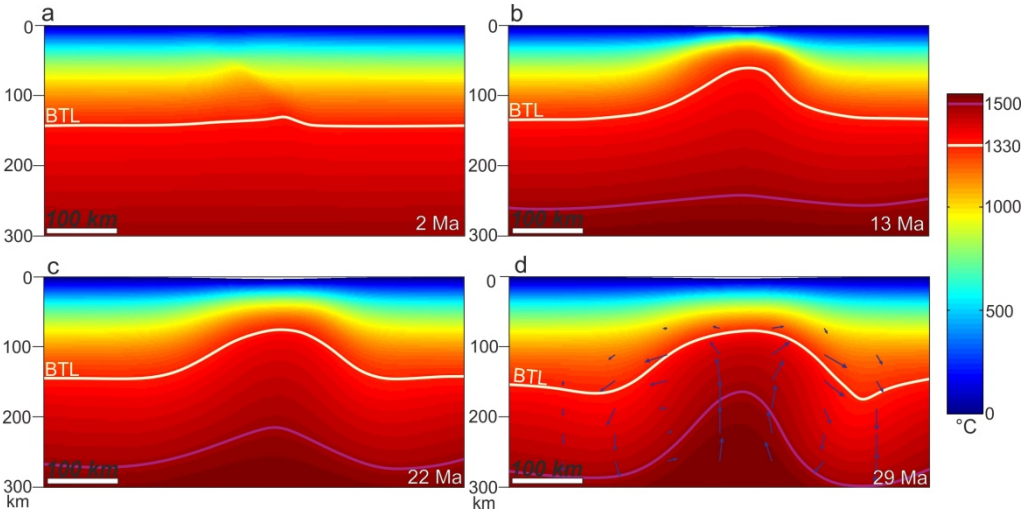

Figure 4.6: Thermal evolution of the reference model M1. a) after 2Ma; b) at the end of the 13Ma syn-rift extension; c) after 9 Myr of post-rift evolution. The conductive thermal cooling is associated with subsidence of the basin centre. The asthenospheric thermal anomaly is wider due to lateral heat transport; d) after 16 Myr of post-rift evolution. A convective upwelling of the deep asthenosphere and drip-off of the marginal mantle lithosphere are observed. BTL – base of the thermal lithosphere, purple line – 1500 °C isotherm, blue arrows indicate the velocity field.

Our asymmetric models are characterised by a lateral migration of depocentres during the syn-rift phase in the sedimentary basin (Figure 4.2). At the end of this syn-rift period, the oldest basins are located near the margins of the extensional basin system, with the youngest basin located more to the centre in an asymmetric

position, closer to the margin overlying the maximum asthenospheric uprise. This migration is controlled by the evolution of the rheologically weak zone that is gradually redistributed and elongated in a continuous sub-horizontal layer in the upper part of the lithospheric mantle. This weak layer provides an effective decoupling, enhancing the weakening effect of the asthenospheric uprise and focuses deformation. The formation and evolution of the overlying sedimentary basins are limited to the area where this layer is present at depth. While thinning is continuously focused in the weak layer of the mantle lithosphere accentuating the asymmetry during the syn-rift time, the overlying crust records distributed deformation on a much larger area. The interplay between convective and conductive processes decreases the lithospheric mantle asymmetry during post-rift times and makes it more difficult to detect at longer times after extension has ceased. Our models show a change in crustal deformation mechanics during extension. The initial extension creates half-grabens associated with footwall uplift due to the steep orientation of the rheological weak zone, favouring the initiation of large scale detachments (Figure 4.2, strain panels). The later re-orientation of the rheological weak zone to a sub-horizontal position favours more symmetric crustal deformation, where the formation of grabens is recorded.

Following the coordinates and thermal properties of marker points in the upper crust and overlying sediments we extracted the basement subsidence and surface heat flow history of our models and compared with constructed ones from the Pannonian basin (Figure 4.7). Analysis of the modelled subsidence patterns for the overlying sedimentary basin indicates that in all cases an early moderate syn-rift subsidence stage is subsequently followed by periods of fast syn-rift subsidence, stagnation or uplift (Figure 4.7a). Such variability is obviously controlled by different degrees of crustal and lithospheric mantle thinning combined with associated thermal effects. The thermal evolution of the sedimentary basins is strongly coupled with the time duration of extension. Fast extension models predict a maximum surface heat flow that is ~20 mW/m^2 lower in the most extended crustal area, when compared with the reference model (Figure 4.7d, Mf, M1). A similar pattern is observed in models with lower lithospheric thickness (Figure 4.7d, Mt, Mft). All models containing a weakness zone predict larger amounts of lithospheric thinning when compared with models where such a zone is absent (Figure 4.3). It also demonstrates that local zones of extreme thinning in the lithospheric mantle can be obtained rather by extension than attributing them to local or deep mantle plumes.

A significant uplift at the onset of the post-rift evolution is created by the rapid cessation of extension at the transition between syn- to post-rift, which simulates the transition from rapid roll-back to collision and slab-detachment affecting extensional back-arcs. Such a rapid cessation of extension works against the rift push forces still affecting the lithospheric mantle (e.g., *Huismans et al.*, 2001) and the

ductile flow of the lower crust due to gravitational loading differences (*Burov and Poliakov*, 2001). This creates a short lived inversion that induces uplift in the order of few tens to hundreds metres in the centre of the basin as observed in different model setups (Figures 4.7a,c).

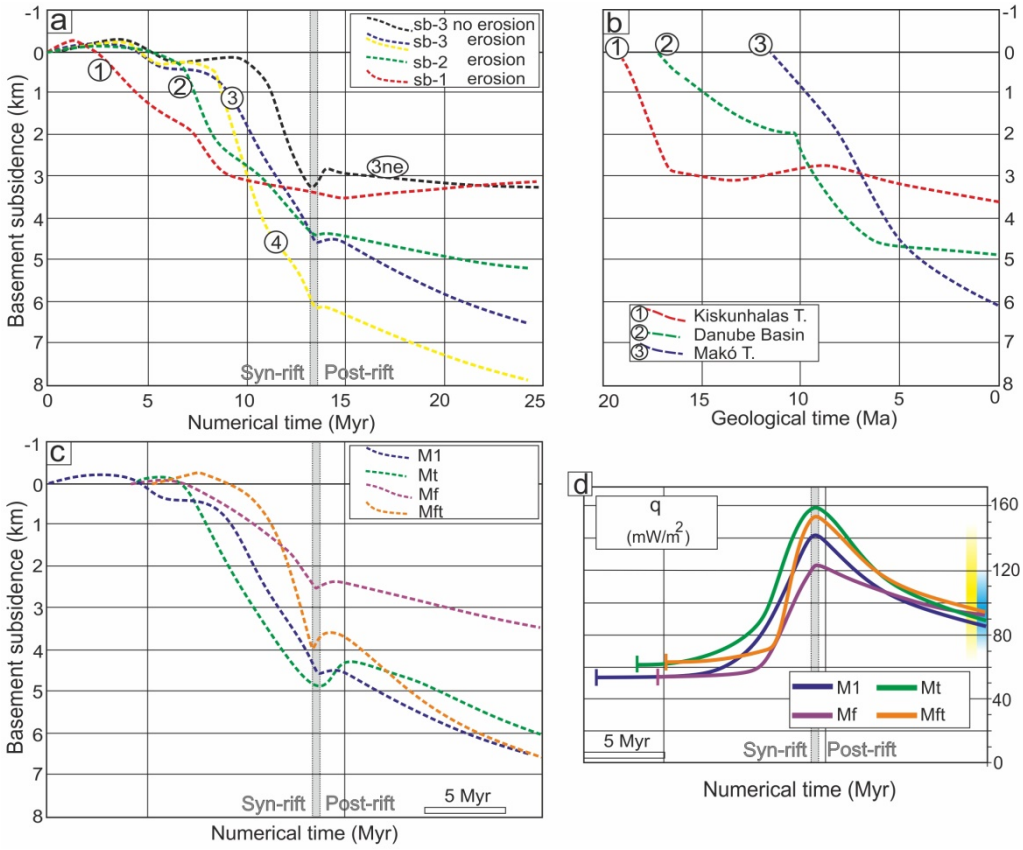

Figure 4.7: (a) Predicted basement subsidence curves from different locations of the reference model M1. Curves correspond to various sub-basins (1-4), as marked in Figure 4.2. Black curve shows the subsidence of sub-basin 3, but without any erosion applied during the modelling (model M1ne, Table 4.1); b) Reconstructed basement subsidence history of sub-basins from the Pannonian basin system (modified after Balázs et al., 2016). Peak of syn-rift subsidence varies from Early, Middle to Late Miocene in the Kiskunhalas, Danube and Makó basins, resp. (c) Basement subsidence curves of different modelling scenarios from the central part of the experiments (d) Surface heat flow evolution of thick lithospheric models with 260 km of extension, thinner lithosphere models with 195 km extension. Mf – model with higher extension velocity. Mt – model with thinner initial lithospheric thickness. Mft – model with higher extension velocity and thinner initial lithosphere. Blue and yellow signs at 0 Ma show the present day surface heat flow values of the Pannonian and Aegean basins, respectively (after *Lenkey et al*., 2002; *van Wees et al*., 2009). Grey line on various panels indicates the end of the syn-rift period.

The subsequent post-rift subsidence rates are dependent on the inherited crustal/lithospheric thinning and the rate of surface erosion active during both the syn- and post-rift times (Figures 4.5, 4.7a,c). We have implemented a simplistic 2D sedimentary transport route from the uplifted and eroded footwalls towards the basin centre. This is coupled with the flexural (un)loading of a thermally weakened lithosphere, which is further enhanced by the re-distribution of the weak zone. The overall spatial and temporal migration of depocentres in our asymmetric model combined with surface processes and lateral heat transport induces uplift and erosion reaching 400 m near the basin margins during post-rift times (Figure 4.5). High resolution 3D morphological models can specify the detailed patterns of landscape evolution (e.g., *Ellis et al.*, 1999).

4.5 Comparison with observations from extensional back-arc basins

We compare our numerical modelling results with observations in extensional back-arc basins formed in the hinterland of highly arcuated Mediterranean orogens that formed in response to the rapid retreat of a number of genetically associated slabs (e.g., *Faccenna et al.*, 2014). The Pannonian, Aegean, Alboran, Liguro-Provencal - Thyrrenian and Black Sea extensional back-arc basins formed in response to the rapid retreat of the Vrancea, Aegean, Gibraltar, Calabrian and Neotethys slabs during the formation of the Carpathians, Hellenides, Betics-Rif, Apennines and Turkey-Cyprus orogenic areas, respectively (e.g., *Wortel and Spakman*, 2000; *Faccenna et al.*, 2014). The most suitable correlation with our modelling are the thinned continental extensional back-arcs of the Pannonian and Aegean basins, where the Paleogene - Miocene extension has affected an inherited Alps, Carpathians, Dinarides and Hellenides orogenic nappe stack by reactivating primarily the inherited Neotethys/Vardar and/or Pindos suture zones (e.g., *Jolivet et al.*, 2013; *Matenco and Radivojević*, 2012).

4.5.1 The Pannonian Basin system

The orogenic area presently underlying the Miocene Pannonian basin (Figure 4.8) formed in response to the opening and closure of the Alpine Tethys and a northern branch of the Neotethys oceans. While the Neotethys branch opened during Middle Triassic and was closed by successive moments of late Jurassic - Cretaceous subduction and continental collision, the Alpine Tethys opened during the Middle Jurassic and was subsequently closed by successive moments of Cretaceous - Miocene shortening observed at the exterior of the Carpathians (e.g., *Schmid et al.*, 2008 and references therein). Towards the end of the Paleogene times these movements have created a large orogenic area with thickened crustal structure and composed of two main tectonic megaunits, i.e., ALCAPA and Tisza-Dacia (Figure 4.8). While their contact is thought to have been a large transcurrent fault zone

accommodating the change in polarity between the Carpathians and the Dinarides, the Tisza-Dacia unit was largely sutured over the Dinarides during Latest Cretaceous times along the Sava Suture Zone (*Schmid et al*., 2008; *Ustaszewski et al*., 2010). The overall orogenic area together with the inherited suture zones and nappe contact was subsequently affected by 220-270 km of Miocene extension that created the Pannonian Basin back-arc during the coeval N, NE- to E-ward retreat of a slab situated at the exterior of the Carpathians (Figure 4.9a, e.g., *Horváth et al.*, 2015). The extension ceased rapidly during the final stages of the 13-8 Ma Middle - Late Miocene collision of the Carpathians (e.g., *Matenco et al.*, 2016). The present structure indicates maximum crustal and lithospheric thinning to 20-22 km and 50-60 km (Figure 4.9a), respectively, with evidence for large scale shearing and serpentinisation in the mantle lithosphere (*Posgay et al.*, 2006; *Hetényi et al.*, 2015; *Lenkey et al*., 2002; *Horváth et al*., 2015).

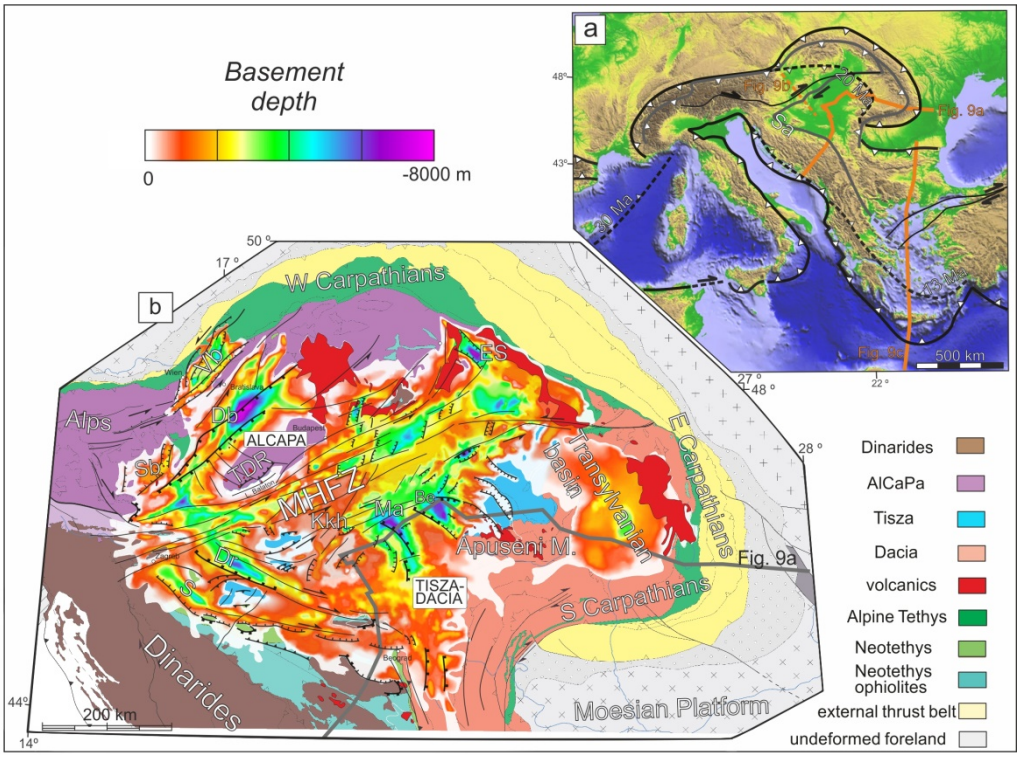

Figure 4.8: (a) Simplified tectonic outlines of plate contacts in the Mediterranean region (after *Schmid et al.*, 2008; *Faccenna et al.*, 2014). Dashed black lines show the positions of the orogenic front prior to the onset of extension in back-arc basins (modified after *Wortel and Spakman*, 2000). Sa – Sava Suture Zone. (b) Simplified tectonic map of the Alps - Carpathians Dinarides region (modified after *Schmid et al.*, 2008) overlain by the Miocene – Quaternary sedimentary thickness (in meters) of the Vienna (Vb), Pannonian and Transylvanian basins. MHFZ – Mid-Hungarian Fault Zone, Db – Danube basin, TDR – Trans-Danubian Range, Sb – Styrian basin, ES – East Slovak basin, Dr – Drava Trough, S – Sava Trough, Kkh – Kiskunhalas subbasin, Ma – Makó Trough, Be – Békés basin.

Kinematic and exhumation studies have demonstrated that the subsidence in half grabens in the large Great Hungarian Plain part of the Pannonian Basin (*Tari et al.*, 1999) was associated with significant exhumation of the Dinaridic orogenic margin, controlled by extensional detachments that largely reactivated the inherited Sava Suture Zone contact with the Tisza-Dacia unit (Figure 4.9a, e.g., *Ustaszewski et al.*, 2010). In agreement with our reference numerical model this suture zone is dipping NE-wards at the Dinaridic basin margin near the Sava Trough, similarly with the main direction of the roll-back of the Carpathian slab. In agreement with our numerical modelling results, this extension migrated in space and time during the Miocene from Early Miocene near the basin margins to maximum ~7 km deep Late Miocene structures (Figures 4.7b and 4.9a) situated asymmetrically towards the SE margin of the basin (*Balázs et al.*, 2016). Our modelling infers a large spatial shift between the crustal location of the Sava suture zone and its equivalent in the lithospheric mantle and is in agreement with the observation of opposed maximum and minimum thinning in the upper and lower crust (Figure 4.9b, see also *Hetényi et al.*, 2015). Modelled subsidence patterns are in agreement with observations in the basin during the migration of deformation (Figures 4.7a and b). More specific, sub-basins like the Styrian, Sava or East Slovakian basin situated near the margins of the area have rapid initial Early - Middle Miocene subsidence followed by stagnation or uplift, while later Middle - Late Miocene basins show a gradual acceleration during late -syn to post-rift times. The widespread unconformity recorded near the transition between the Middle and Late Miocene in the centre of the Pannonian Basin (*Balázs et al.*, 2016) is generally attributed to a short-lived inversion triggered by the Carpathian collision (*Horváth*, 1995). A similar observation in our modelling near the transition between syn- to post-rift times implies that such uplift could also be driven by the rapid cessation of the extensional forces. The extension and subsequent thermal subsidence in the Pannonian Basin was followed by a period of inversion (*Bada et al.*, 2007) characterised by shortening and uplift of the Dinarides margins and subsidence in the basin centre (*Horváth, 1995*; *Horváth et al.*, 2015 and references therein). The similarity with modelling predictions (i.e., uplift over the basin margins and subsidence in its centre during post-rift times) implies that such differential vertical movements can also be accentuated by the evolution of the extensional thermal anomaly and surface processes, combined with flexural effects of the weak Pannonian lithosphere. Large asthenospheric ascent during extension favours the onset of genetically related magmatism. The post-Miocene mafic alkaline magmatism of the Pannonian Basin is not located at the syn- to post-rift transition, but culminates with larger volumes during the onset of Pliocene times (*Kovács et al.*, 2012; *Harangi et al.*, 2015). Such a late stage post-rift magmatic peak can be explained by the switch between thermal cooling and deeper asthenospheric ascent during post-rift times predicted by our numerical models (Figure 4.6, see also *Huismans et al.*, 2001).

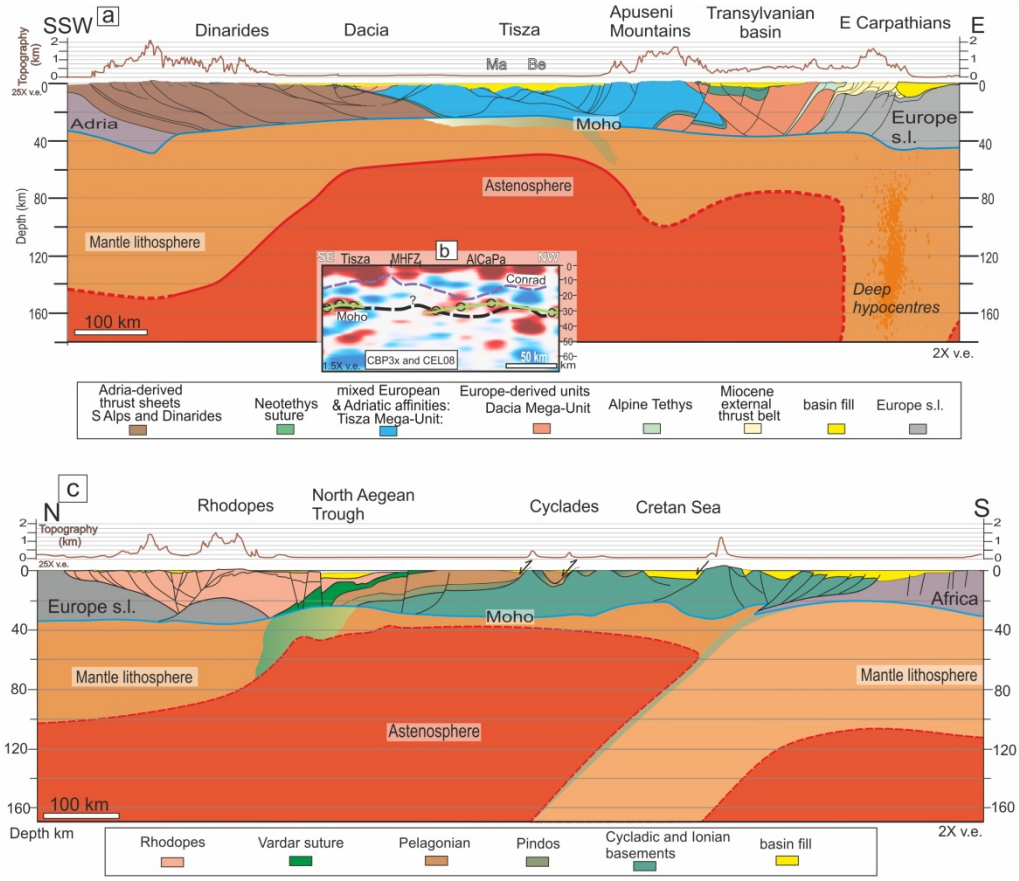

Figure 4.9: (a) Lithospheric scale cross-section over the Dinarides – Pannonian Basin - Apuseni Mountains - Transylvanian Basin – East Carpathians (compiled from *Schmid et al.*, 2008; *Balázs et al.*, 2016; *Matenco et al.*, 2016). The trace of the cross section (Figure 4.8) was chosen to approximate the curved N to NE to E direction of extension accompanying the clockwise rotation of the Tisza-Dacia unit; b) Receiver function section over the Pannonian basin (from *Hetényi et al.*, 2015). Green line shows the interpreted Moho, while purple and green lines show the interpreted Conrad and Moho surfaces based on the CEL08 deep seismic profile (*Kiss*, 2009). c) Cross section over Balkans – Rhodope – Aegean Sea – North Africa (modified after *Jolivet and Brun,* 2010; *Menant et al.*, 2016) showing the crustal and lithospheric architecture of the Aegean-Rhodope extensional system. Location of the cross section is given in Figure 4.8a.

4.5.2 The Aegean system

The Hellenides domain presently underlying the Eocene to present Rhodope-Aegean extensional system formed in response to the Middle-Late Triassic opening of the Vardar/Neotethys ocean and Pindos - Cukali - Budva thinned continental to oceanic domain followed by their subsequent and gradual Cretaceous - Eocene closure, continental collision and post-dating thrusting (*Jolivet and Brun*, 2010; *van Hinsbergen and Schmid*, 2012). These studies have suggested that the 400-600 km of back-arc extension accommodating the rapid retreat of the Aegean slab started during

Eocene times with the formation of the Rhodope system of detachments and associated large scale exhumation and deformation gradually migrated southward, resulting in asymmetric extension in the Cyclades, Corinth Gulf and Crete. This was associated with major exhumation in the footwall of detachments combined with opening of the Aegean Miocene basins, still active today (e.g., *Brun and Sokoutis*, 2007; *Jolivet and Brun*, 2010). Significant research has been dedicated to understanding the rheology and crustal coupling effects in the Aegean system (*Jolivet et al*., 2013 and references therein) and all studies agree on the strong localisation of deformation, largely reactivating the inherited Vardar, Pindos and related nappe contacts (Figures 4.8a and 4.9d, see also *Brun and Faccenna*, 2008; *Huet et al*., 2011 and references therein).

The above findings suggest that the asymmetric back-arc modelling approach of our study is partly applicable to the Aegean extension, although the extension lasted longer, had higher amplitudes and there is no real rapid cessation during a post-rift period. Our modelling is in agreement with the earlier stages of Eocene - Miocene extension (see also *van Hinsbergen and Schmid*, 2012) and suggests that the extensional geometry was primarily controlled by the lithospheric mantle rheological weakness of the Vardar and/or Pindos suture zones. The redistribution of this weakness zone in the upper part of the lithospheric mantle may have induced the gradual migration of extension southward. In other words, not only the currently strongly debated Aegean crustal rheological strain localisation and the deep mantle forcing effects (see discussion in *Jolivet et al*., 2013) have a major impact during extension, but also the re-distribution of the inherited weakness zone in the upper part of the mantle lithosphere may condition the kinematics and geometry of Aegean extension. The southward migration in time from the Eocene Rhodope margin to the Miocene North Aegean (e.g., *Brun and Sokoutis*, 2007) corresponds to our predicted migration towards the main suture zone and is in agreement with the overall reduction of asymmetric effects (amounts of exhumation against detachments versus basin subsidence) in time southward. The more S-ward migration towards the Cyclades, Gulf of Corinth and Crete (i.e. migration in time towards the margin of the basin) is not in agreement with our single weakness zone modelling predictions, but may be related to the gradual activation with time of other major weakness zones in the direction of slab retreat, such as the Pindos suture or related nappe contacts. Such a multiple distribution of weakness zones or dynamic slab-related asthenospheric flow had significant effects in the Aegean system (e.g., *Menant et al*., 2016).

4.6 Conclusions

Numerical experiments simulating back-arc asymmetric extension of an overthickened lithospheric structure by reactivating inherited orogenic contacts suggest that large scale weakness zones play a major role in syn- and post-rift basin

evolution. Such zones can be significantly re-distributed at deep crustal and mantle lithospheric depths during deformation and localise strain and associated asthenospheric convective and conductive effects. Switches between generalised post-rift asthenospheric cooling to localised upwelling may explain the delayed onset of mafic alkaline magmatism as observed, for instance, in the Pannonian back-arc system. Large-scale asthenospheric asymmetries created during syn-rift deformation may be significantly attenuated by subsequent thermal processes during the post-rift phase, creating ultimately apparent symmetric lithospheric structures. This results in contrasting deep mantle geometries when compared with overlying differential vertical movements recorded by the crust and the sedimentary basins. This plays a critical role in the spatial and temporal migration of individual basin depocentres across the extensional system, leading to variable subsidence patterns similar to reconstructed subsidence histories in Mediterranean extensional back-arcs as the Pannonian basin and the Aegean system.

Our experiments show that a steeper rheological weak zone creates a more symmetric asthenospheric uprise, higher crustal and lithospheric thinning, narrower and deeper overlying sedimentary basins and lower horizontal offset between the locations of maximum crustal and mantle thinning. Modelling suggests that thermal effects of the convective asthenospheric upwelling are more important for slower extension and it decreases the overall lithospheric strength over a larger area, distributing the crustal thinning. Therefore, lower extension rate results in wider basins and higher surface heat flow values. Our modelling also infers periods of significant uplift near the basin margins, created during the post-rift lateral heat transport, and in the basin centre, after the rapid cessation of back-arc extension driven by orogenic collision. Such processes create unconformities and differential vertical movements, such as observed during the post-rift evolution of the Pannonian basin. The subsidence rates of individual sub-basins and uplift along their flanks during the syn- and post-rift periods are controlled by the initial geometry of the lithospheric weakness zone and by surface processes. Our models are also in agreement with recent observations of a direct correlation between uplift and erosion at the margins of the basin and increased sedimentation towards its centre due to flexural and lower crustal flow effects.

Appendix 4A:

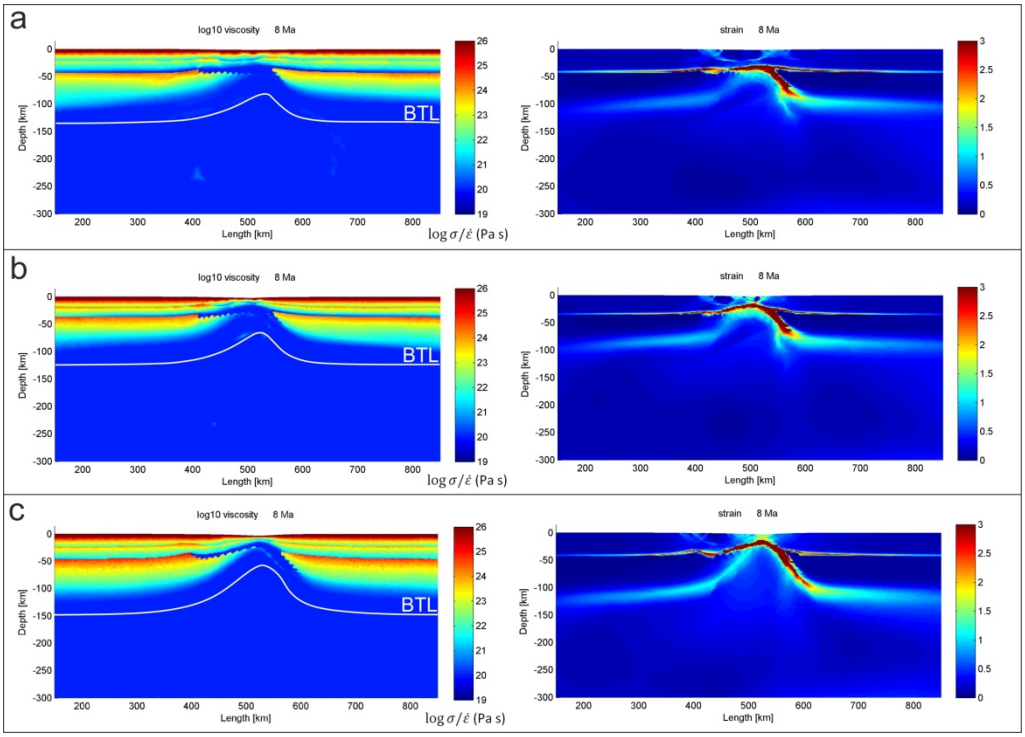

Figure 4.10: Logarithmic viscosity (left) and strain (right) fields of the models during the syn-rift extension at 8 Ma. (a) Reference model (M1, Table 4.1), (b) model with thinner initial lithosphere (Mt, Table 4.1), and (c) an additional model with lower geotherm and therefore stronger lithospheric strength (Mo, Table 4.1). The latter model with lower geotherm shows that the higher lithospheric strength and therefore an increased coupling between the lithospheric layers results in faster and accentuated crustal and lithospheric thinning. Such low initial temperature values represent an old lithosphere. BTL – base of the thermal lithosphere.

Appendix 4B: Basic equations

Flamar uses a large strain fully explicit time-marching scheme (e.g., *Francois et al*., 2013). In the Lagrangian method, incremental displacements are added to the grid coordinates allowing the mesh to move and deform with the material. This allows for the solution of large-strain problems while using locally the small-strain formulation: on each time step the solution is obtained in local coordinates, which are then updated in a large-strain mode. The code locally solves full Newtonian equations of motion in a continuum mechanics approximation, where ρ is the density, u is the displacement, σ is the stress and g is the acceleration due to body forces:

$$\langle \rho \ddot{\boldsymbol{u}} \rangle - div\, \sigma - \rho \boldsymbol{g} = 0 \qquad \text{I.}$$

Solving the previous equation is coupled with constitutive equations:

$$\frac{D\sigma}{Dt} = F(\sigma, \boldsymbol{u}, \dot{\boldsymbol{u}}, \nabla\dot{\boldsymbol{u}}, T, \dots) \qquad \text{II.}$$

and with the equations of heat transfer:

$$\rho C_p \frac{DT}{Dt} - \nabla(k\nabla T) - \sum_i^n H_i = 0 \qquad \text{III.}$$

$$\rho = f(p, T) \qquad \text{IV.}$$

where the terms t, ρ, Cp, T, and H_i designate respectively time, density, specific heat, temperature, internal heat production per unit volume. Density is a function of pressure and temperature.

The model uses visco-elasto-plastic rheologies based on Maxwell summation for deviatoric strain rate to simulate flow:

$$\dot{\varepsilon} = \dot{\varepsilon}_{vis} + \dot{\varepsilon}_{elas} + \dot{\varepsilon}_{plas} \qquad \text{V.}$$

At high confining pressure, Byerlee's law shows that maximal brittle strength is proportional to 0.6 P, where P is the total pressure. Within our formulation, we model this experimental law using the cohesion $C_0 = 20$ MPa and the internal friction angle Φ = 30°.

$$|\tau| = C_0 + \sigma_n \tan\Phi \qquad \text{VI.}$$

The elastic behavior is described by Hooke's law:

$$\sigma_{ij} = \lambda\varepsilon_{ij}\delta_{ij} + 2G\varepsilon_{ij} \qquad \text{VII.}$$

For viscous (ductile) behaviour the effective viscosity (μ_{eff}) depends on the temperature (T) and strain rate ($\dot{\varepsilon}$) and the pre-exponential factor n. R is the universal gas constant and A is a material constant (see Table 4.1):

$$\mu_{eff} = \dot{\varepsilon}^{(1-n)/n} A^{-1/n} \exp(E(nRT)^{-1}) \qquad \text{VIII.}$$

Surface heat flow is calculated according to Fourier's law based on the temperature gradient of the uppermost crustal grid cells:

$$q = -k_c \Delta T/\Delta z \qquad \text{IX.}$$

Erosion is modelled with a linear diffusion law:

$$\frac{dh}{dt} = k_e \frac{\partial^2 h}{\partial x^2} \qquad \text{X.}$$

5. Tectonic and climatic controls on asymmetric half-graben sedimentation: inferences from 3D numerical modeling[4]

[4]*This chapter is based on Balázs, A., Granjeon, D., Matenco, L., Sztanó, O., Cloetingh, S., 2017. Submitted to Tectonics*

5.1 Introduction

The evolution of extensional sedimentary basins is driven by a complex interplay between the mechanics of the system combined with external and internal forcing factors, such as tectonics, climate, source areas, surface processes, geometry of depocenters and auto-cyclic sedimentary processes (e.g., *Cloetingh et al.*, 2013). Current models of syn- and post-kinematic depositional response to extension are not directly applicable in places where series of genetically linked half-grabens, bounded by one major normal fault or detachment, control the coeval sedimentation (Figure 5.1, *Wernicke*, 1992; *Prosser*, 1993; *Ellis et al.*, 1999; *Tirel et al.*, 2008). The spatial and temporal variability of vertical movements in such asymmetric extensional systems is important also for understanding landscape evolution, changes in the location of depocenters and stratigraphic architecture (e.g., *ter Voorde et al.*, 1997; *Contreras et al.*, 1997; *Gupta et al.*, 1998; *Balázs et al.*, 2016; *Andrić et al.*, 2017).

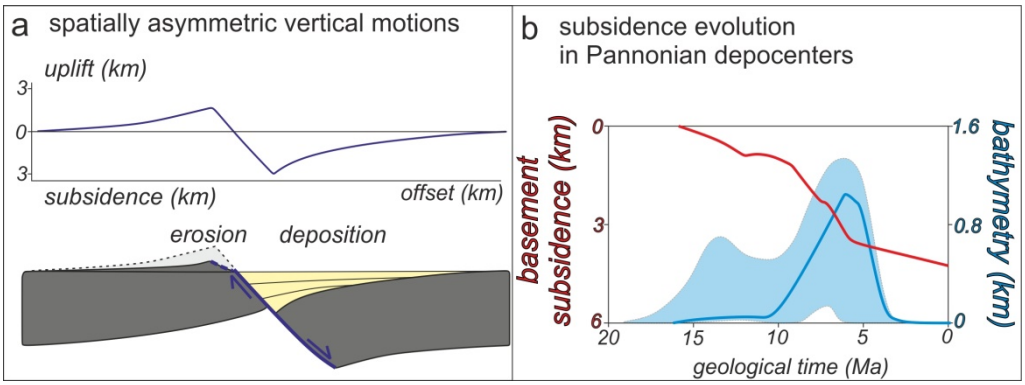

Figure 5.1: Simplified model of half-graben evolution controlled by a low-angle normal fault or detachment. a) Asymmetric hanging wall subsidence is associated with uplift and exhumation of its footwall. Differential vertical movements are enhanced and localized by footwall erosion and hanging wall sedimentation. b) Temporal evolution of depocenter subsidence (red curve) and paleo-water depth trend (blue area) generalized from half-grabens from the Pannonian Basin, derived from this study and previously published data (*Horváth et al.*, 1988; *Báldi et al.*, 2002; *Balázs et al.*, 2016). Continuous blue curve shows the paleo-water depth evolution of the Szeged sub-basin.

Observed differential vertical movements are primarily controlled by patterns of crustal and lithospheric thinning coupled with the evolution of the underlying asthenosphere, strongly influenced by rheological composition, amounts of extension, localization, rate and variability of strain (e.g., *Balázs et al.*, 2017 and references therein). Furthermore, the tectono-sedimentary evolution of extensional basins is intrinsically coupled to surface processes in terms of erosion and sedimentation, which are controlled also by climatic variations (e.g., *Burov and Poliakov*, 2003; *Cloetingh and Haq*, 2015). Internal surface processes, such as footwall erosion and hanging-wall sedimentation enhance and localize vertical movements (*Leeder et al.*,

1998; *Ellis et al.*, 1999). All these processes create a large spatial and temporal variability of extensional geometries (e.g., *van Wijk and Cloetingh*, 2002) that are often associated with a sequence of slower, faster and ultimately again slower subsidence rates in the center of half-grabens during the syn- and post- kinematic evolution (Figure 5.1). This subsidence evolution differs significantly from the rapid syn-rift followed by decreasing post-rift patterns of classical extensional models (e.g., *Baur et al*., 2014; *Balázs et al.*, 2017). In back-arc settings, rapid basin subsidence episodes are associated with variable extensional pulses created by slab roll-back and further mantle dynamics (*Faccenna et al.*, 2014). In such overall settings, the sedimentary response to extension is not sufficiently understood.

The sedimentary architecture of half-grabens is obviously the result of a balance between the rate of creating accommodation space and the external or internal sediment supply, combined with sedimentary transport processes within the basin (e.g., *Schlager*, 1993; *Postma* et al., 2008). Depositional concepts driven by the interpretation of geological and geophysical data (Figure 5.2) can be quantitatively tested by recent advances in 3D numerical modeling techniques. These 3D models provide the possibility to simulate sedimentation and related lithologies at higher resolution, accounting for the influence of tectonic and climatic forcing, such as variable subsidence and uplift rates, eustatic water-level variations, sediment and water discharge and transport processes (e.g., *Clevis et al.*, 2004; *Granjeon*, 2014).

A probably ideal case for conceptual understanding of sedimentation in asymmetric extensional systems is the Pannonian back-arc basin of Central Europe, where the extended database required to model numerically these concepts and to define generic links between extension and sedimentation is already available (Figure 5.2). Here, the Great Hungarian Plain recorded the temporal and spatial formation and migration of half-grabens during the Miocene back-arc extension related to the Carpathian slab roll-back (e.g., *Horváth et al*., 2015; *Balázs et al*., 2016; *Matenco et al*., 2016), often associated with contrasting patterns of decreasing and subsequently increasing syn-rift subsidence (Figure 5.2c). These Miocene sub-basins are flanked by large-offset low angle normal faults or detachments and are filled by up to 3.5 km of syn-kinematic sediments, deeply buried beneath the subsequent late Miocene - Quaternary post-rift deposits (Figure 5.2). The overall total sediment thickness reaches ~7 km in the main depocenters (e.g., *Tari et al*., 1999; *Horváth et al*., 2015 and references therein).

In this study, we investigate the link between tectonics, climate and sedimentation during the formation and evolution of half-grabens associated with footwall exhumation by the means of 3D numerical stratigraphic forward modeling. We analyze the evolution of one generic half-graben by defining a reference model and performing a parametric study. Subsequently, the evolution of a system of half-grabens is modeled, with a structure and sediment flux parameters inspired by the

Miocene evolution of the Pannonian Basin. These parameters have general average values observed in natural examples elsewhere. Therefore, this integrated approach yields a generic quantitative understanding of the link between tectonics and sedimentation in asymmetric extensional systems, including lithological distributions and formation of unconformities, and their connections with the main forcing factors.

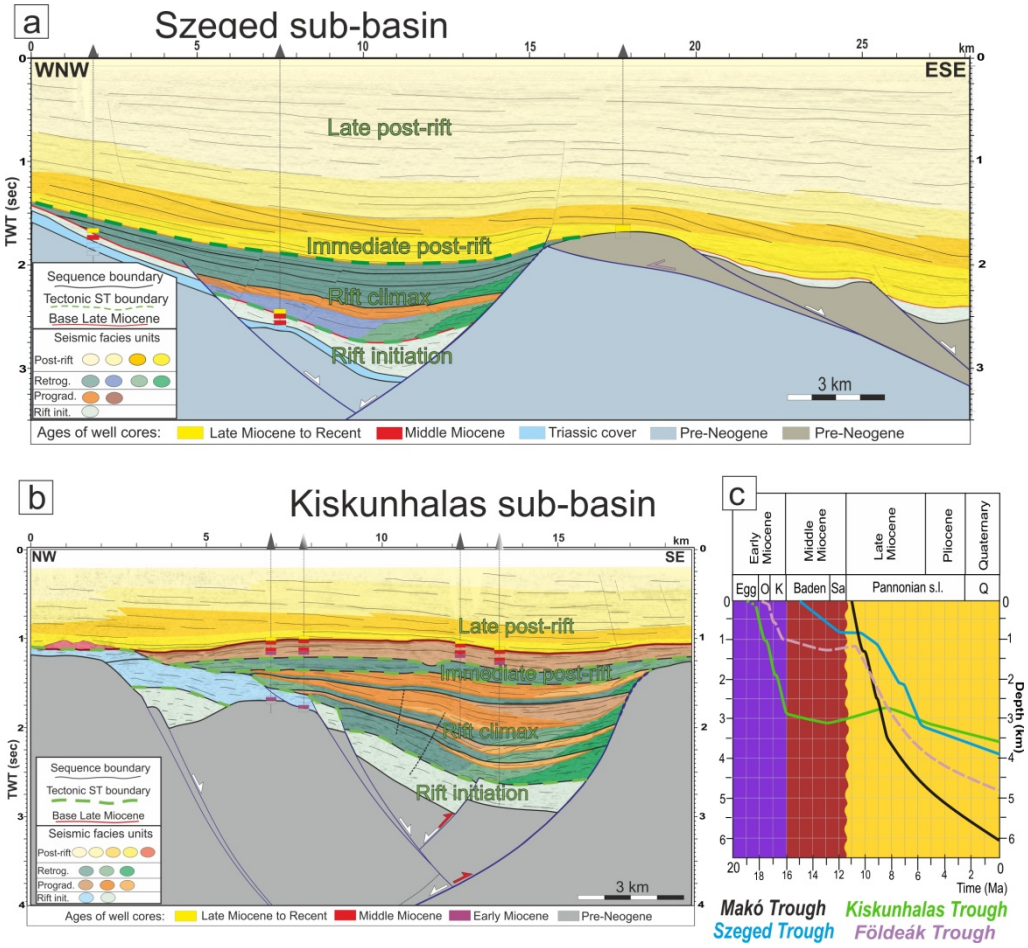

Figure 5.2: a) and b) Tectono-sedimentary evolution of the Pannonian Basin based on interpretation of reflection seismic profiles calibrated by high-resolution well data from the Szeged (a) and Kiskunhalas (b) half-grabens (modified from *Balázs et al.*, 2016) illustrating key features of the conceptual model. In the Szeged sub-basin, rift initiation (RI) sediments are overlain by a retrograding-prograding cycle followed by three retrograding facies associations. In the Kiskunhalas sub-basin, syn-rift prograding-retrograding cycles are grouped into lower order rifting phases (RC – rift climax). White arrows indicate Miocene kinematics of faults, red arrows show the latest Middle–early Late Miocene inversion. Locations are displayed in Figure 5.10. c) Basement subsidence curves calculated from seismic and well data in the main sub-basins modeled in the Pannonian Basin showing migration of extension and episodes of fast subsidence in time (adopting Paratethys endemic time-scale stages Egg - Eggenburgian; O - Ottnagian; K - Karpatian; Sa - Sarmatian).

5.2 Methodology

Numerical forward modeling is particularly well suited to understand facies distribution during the evolution of sedimentary basins. Two classes of stratigraphic and geomorphologic forward models are commonly available. Models of the first class solve small-scale physical laws, such as the Navier-Stokes equation to simulate local and complex interactions between basin deformation, water flow and sediment transport at high spatial and temporal resolutions (e.g., *Griffith et al*., 2001; *de Leeuw et al*., 2016). Models of the second class follow more regional approaches and usually solve a diffusion equation that enables the modeling of sedimentary systems at larger spatial and temporal scales, and the integrated analysis of transport processes. Such diffusion laws in various forms are commonly used to represent the large-scale, spatially averaged sediment transport (e.g., *Culling*, 1960; *Carson and Kirkby*, 1972; *Granjeon*, 1997; *Postma et al*., 2008).

5.2.1 Modeling approach

All numerical experiments were performed with the 3D deterministic forward numerical modeling software DionisosFlow (e.g., *Granjeon*, 2014). This model accounts for spatial and temporal variable subsidence and erosion rates, a sediment influx composed of different sediment classes, compaction, eustasy, water discharge, sediment supply and transport processes. The overall conceptual modeling approach is described in details elsewhere (e.g., *Csató et al*., 2013).

The numerical modeling approach combines empirical water and gravity driven diffusion equations, which include a slow slope-driven creeping law and a faster non-linear water-driven and slope-driven diffusion equation. This approach leads to the following sediment transport equation (*Granjeon*, 2014):

$$Q_{s_i} = -K_{s_i} S - K_{w_i} \hat{Q}_w^m S^n, \text{ where } \hat{Q}_w = Q_w / Q_{w_0} \quad (1)$$

where Q_{s_i} is the flux of the i-th sediment class (m^2s^{-1}), K_{s_i} is a creeping diffusion coefficient, S is the local slope gradient, K_{w_i} is a water-driven diffusion coefficient, $\hat{Q}_w$ is a local normalized water discharge with Q_{w_0} = 1 m^3s^{-1}, m and n are power coefficient constants between 1 and 2 (*Tucker and Slingerland*, 1994) and *i* is the index of the grain size fraction.

This transport equation reflects the general depositional process during erosion, transport and deposition at basin scale (*Burgess et al*., 2006). A wide range of diffusivity coefficient values (K_s and K_w in equation 1) were used in previous numerical studies. These coefficients reflect the ratio of sediment discharge and basin slope, more fine-grained sediments showing higher values than coarse-grained ones. We used average diffusion coefficients for coarse- and fine- grained fractions in our

modeling scenarios that are similar to previous DionisosFlow models (e.g., *Gvirtzman et al*., 2014), i.e., 80 and 160 km^2/kyr, and 0.08 and 0.8 km^2/kyr for sand and mud water-driven diffusion coefficients in continental and marine environments, respectively. Similar to these previous studies, the maximum erosion rate induced by water flow and sediment transport is limited to a value of 0.3 mm/yr, which is a reasonable assumption for Miocene extensional basins in the region (e.g., *Karátson et al*., 2006).

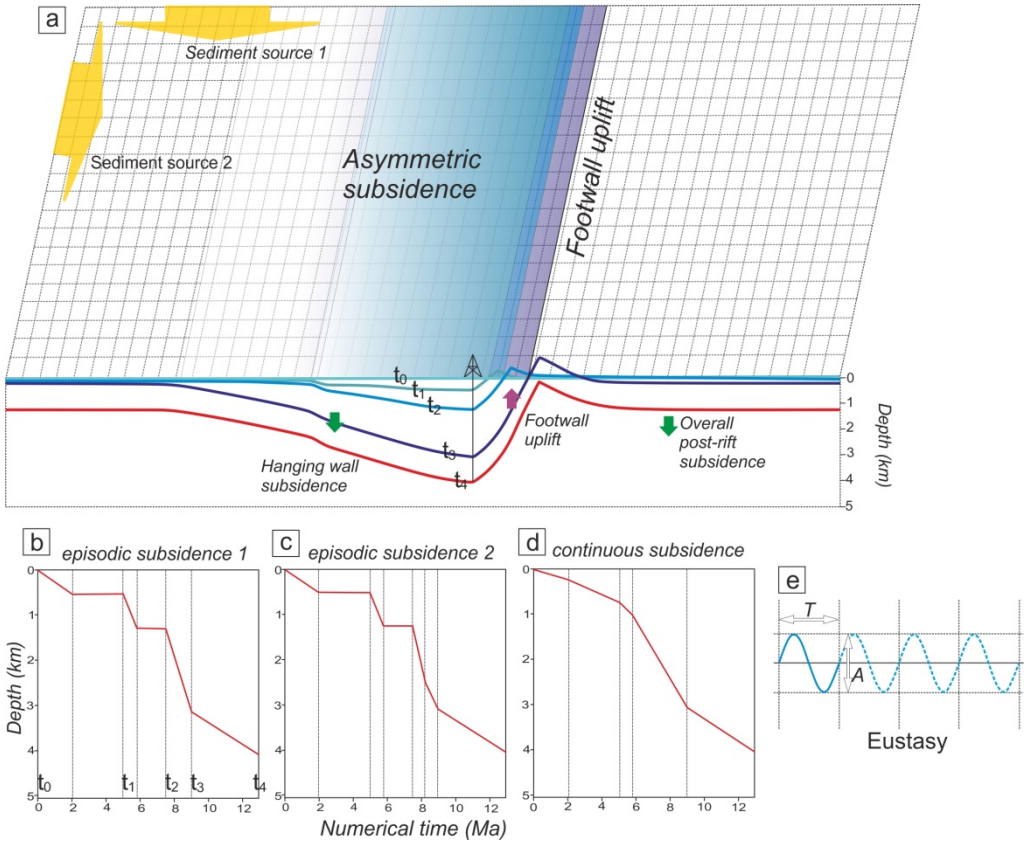

Figure 5.3: Modeling setup of sediment transport and deposition in half-grabens. a) Geometry of the numerical model. The first setup assumes 80 × 80 equally spaced cells with 0.5 km equal spacing (i.e., 40 × 40 km^2 modeled area). The second setup assumes 100 × 100 equally spaced cells with 1 km equal spacing (i.e., 100 × 100 km^2 modeled area). Water discharge and sediment flux in the model are defined parallel with and perpendicular to the strike of the half-grabens in their hanging-wall close to a corner of the model by a km-scale channel where a linear function of increasing water and sediment amounts to the center of this channel is assumed. The vertical movements recorded by the half-graben and its neighboring area are defined by pre-imposed basement subsidence maps (t_0-t_4); b-d) Illustrative basement subsidence curves for the center of the half-graben in different modeling scenarios assuming episodic (b-c) and continuous subsidence (d); e) Illustration of the assumed eustatic variation that change their time period (T) and amplitudes (A) in different scenarios.

The punctual sedimentation and erosion rate at each time step is computed from the local sediment flux assuming mass conservation in the basin. Compaction of sediments is computed following generic lithology-dependent porosity-burial depth curves taken from borehole measurements from the Pannonian Basin (*Szalay*, 1982). The calculation dynamic time step is variable from hundreds of years up to 20 kyr, while model results are saved after every 100 kyr. Therefore, the vertical resolution of our numerical model is variable from 10s of meters up to hundreds of meters, as a function of sedimentation rate.

5.2.2 Model geometries and boundary conditions

An area of 40 × 40 km^2 is modeled in a first series of experiments, where one half-graben is fed by water discharge and sediment influx defined at the boundary and close to the model corner (Figure 5.3). We defined a reference model (Figures 5.4, 5.5) that is subsequently analyzed by the means of a parametrical study, where the variability of other factors, such as subsidence rates, eustatic water-level variations (Figure 5.6) and the boundary water discharge (Figure 5.7) is tested. The geometry and evolution of the half-graben, including the final basement subsidence in the hanging wall and uplift of the footwall, are defined based on average observations in natural situations derived from seismic and well data. This is, for instance, illustrated by the half-grabens of the Corinth Rift (*Nixon et al.*, 2016) or the Pannonian Basin (*Balázs et al.*, 2016), where 3-4 km of hanging wall subsidence was associated with kilometer-scale footwall uplift. Although the same amount of total basement subsidence is applied in all models in the center of the half-graben, three different subsidence rate scenarios are compared, which assume continuous or episodic basement subsidence pulses with different subsidence rates at different rifting moments (Figures 5.3b-d). The continuous or the episodic basement subsidence pattern defines phases of sedimentation during the syn-rift evolution that takes place in all models for a total of 9 Myr. These can be generally grouped into rift initiation, rift climax, immediate- and late post-rift periods (cf., *Prosser*, 1993), although the creation of tectonic system tracts is not specifically implied. The overall chosen patterns of basement subsidence, characterized by a low rate at the onset of rifting, followed by a subsequent gradual acceleration, are specific to observations in asymmetric extensional systems (e.g., *Burov and Poliakov*, 2003; *Balázs et al*., 2017). The syn-rift phase is followed by 4 Myr of uniform basement subsidence everywhere in the model area (Figures 5.3b-d), simulating a post-rift thermal sag that takes place at a much larger scale than the one in the half-graben. Different eustatic variation amplitudes and frequencies are simulated to analyze the influence and interactions between tectonic subsidence and sea-level variations (Figure 5.3e). The boundary sediment flux is defined as constant for one syn-rift phase in such a way that a balance is kept with the rate of creating accommodation space during the same phase. The

exception is the last 2 Myr of post-rift thermal subsidence, when the sediment supply is significantly increased (doubled when compared with the rate of previous sedimentation). This increase simulates the final stage of a rapid fill in extensional basins, when deltaic influxes from major rivers are often recorded (*Sztanó et al*., 2013; *Matenco and Andriessen*, 2013). Obviously, the uplifted and gradually eroding footwall also provides a local source for the basin. Water discharge is set between 50 and 900 m^3/s, resembling different climatic conditions. Furthermore, climatic variations are also simulated by the definition of wet short-term and dry long-term intervals (Figure 5.8). This modeling approach assumes that during each time step ~20% of the sediment influx defined at the boundary of the modeling area is characterized by a higher water discharge value during wet short-term than during dry long-term intervals. This discharge ratio between dry and wet periods is analyzed in the parametric study.

Another series of experiments is applied to a larger area (100×100 km^2) that include four half-grabens, to simulate the syn-rift subsidence, erosion and sedimentation of the Great Hungarian Plain of the Pannonian Basin (Figures 5.9, 5.10). Basement subsidence histories derive from available seismic interpretations and backstripped well data (Figure 5.2, *Balázs et al*., 2016). Modeling results are presented at four representative moments of basin evolution, showing cross-sections through the sub-basins at the end of the overall syn-rift phase at 8.5 Ma. This novel syn-rift modeling applied to the Pannonian Basin complements and is calibrated by available post-rift stratigraphic modeling studies available in the same region, which use the same DionisosFlow modeling software (*Csató et al*., 2013; *Csató et al*., 2015).

5.3 Numerical modeling of sedimentation in one half-graben

The reference model is designed to simulate an asymmetric and variable basement subsidence in the hanging-wall depocenter of one half-graben (Figure 5.3b), associated with syn- and post-kinematic sedimentation (Figures 5.4 and 5.5). The 9 Myr of syn-rift evolution is subdivided into multiple syn-rift phases. The first extensional pulse assumes 2 Myr of moderate basement subsidence rate (~0.25 km/Ma), followed by 3 Myr of zero tectonic subsidence (Figure 5.3b). In this syn-rift phase, deposition keeps pace with the tectonically-induced basement subsidence (Figure 5.4a), the accommodation space is filled by alluvial and shallow delta sediments and footwall derived fans are deposited in its proximity, while the sediment flux and water flow geometry is conditioned by the opening of the half-graben (Figure 5.5).

The subsequent 4 Myr contain two rapid pulses of acceleration of the normal fault offset (higher rate of basement subsidence, 0.7 km/Ma) separated by a period of zero subsidence, which simulate a rift climax period (t2 and t3 in Figure 5.3b). The

flank of the hanging-wall at larger distances from the depocenter is dominated by alluvial and delta environments. The sediments of clastic lobes are sourced from the hanging wall and by footwall erosion and are transferred to the narrow and deep depocenter reaching high sedimentation rates (~3 km/Ma, Figure 5.5d). In more detail, the second syn-rift phase results in an overall retrogradation to a maximum water depth of ~200 meters, which is subsequently filled by rapid progradation during regression associated with the period of zero subsidence. This evolution is repeated during the third syn-rift phase, when yet again a rapid retrogradation is recorded to a maximum water depth of ~400 m, followed by progradation (Figure 5.4c). In this model setup, this progradation is enhanced by this time with a period of sea-level fall at the end of this syn-rift phase. A higher order retrograding-prograding cyclicity of small-scale delta slopes and lobes is deposited over the hanging-wall, controlled by sea-level variations and lateral auto-cyclic processes affecting the sediment flux (Figure 5.4c). Interestingly, these auto-cyclic variations create moments when sand lobes are transported into the deeper parts of basin (Figures 5.5c,d). The rapid uplift of the footwall is only partly accompanied by erosion, which forms a positive topography at the end of the syn-rift period. This topography prevents bypass and transfer of sediments from the external source area. At this time the deposition over the hanging wall is exclusively sourced by the footwall erosion.

The subsequent 4 Myr period of thermal subsidence creates an overall retrogradation at the beginning of the post-rift period. This results in maximum water depths in the order of 600 m in distal depositional areas (Figure 5.4d). The change from focused subsidence in the depocenter to regional subsidence creates an unconformity at the transition between the syn- to post-rift sedimentation, which resembles the geometry of the break-up unconformity, created at the transition between rifting and drifting during the evolution of passive continental margins (e.g., *Ziegler and Cloetingh*, 2004). The erosion of the footwall gradually decreases as it progressively submerges to later form positive seafloor morphology. This prevents bypass of coarse-grained sediments. The main sediment flux is transported in the half-graben depocenter, with only thin sand lobes deposited over the distal footwall during wet short-term intervals (Figure 5.5e). The rapid increase in sediment supply during the last 2 Myr leads to the formation of a large-scale prograding sequence, where deposition of slope sediments connects a deltaic environment with the few hundred meters deep basinal areas (Figures 5.4e,f). The height of this prograding slope is larger over the underlying half-graben depocenter due to differential compaction effects added to the overall basement subsidence. Differential compaction also obviously decreases the overall thickness of the underlying syn-rift sediments. The interplay between the low post-rift basement subsidence rate (~0.22 km/Ma) and sea-level variations controls the formation of prograding, aggrading and/or retrograding clinoforms cyclicity (Figure 5.4f). During these times, sedimentation rate reaches its

maximum at the slope, while coarse-grained sediments are partitioned between the shelf and at the toe of slope. Although, there is still minor positive morphology over the eroded footwall, the sediment transport probable by turbidity currents overcomes and the sand lobes can be deposited at much larger distances that can reach ~25 km from the shelf edge (Figure 5.5f).

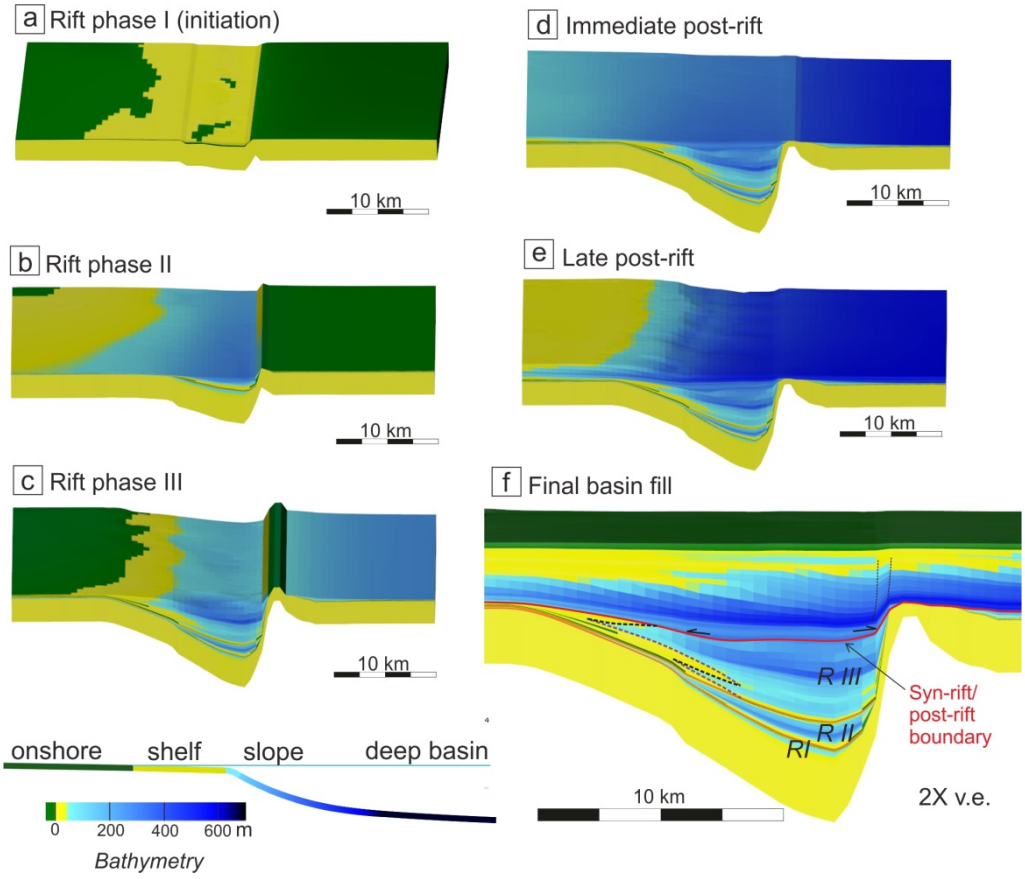

Figure 5.4: Evolution of bathymetry in the reference experiment at the initial rift phase I (a), rift phase II (b), rift phase III (c), immediate post-rift (d), late post-rift (e) and final basin fill (f). Red line indicates the syn-rift/post-rift boundary, orange lines indicate rift phase boundaries. Purple and black dashed lines at the flank of the hanging wall indicate retrograding-prograding high order cyclicity within the third rift cycle. An episodic basement subsidence was used (Figure 5.3b) with an eustatic variation period (T) of 0.7 Myr and amplitude (A) of 70 m, water discharge (Q) of 200 m^3/s, short-/long-term discharge ratio (R) of 20 and a source mud/sand ratio of 7/3. The three rift phases are reflected by a low-order change in paleobathymetry that is superposed over a higher-order change in paleobathymetry, which is driven by a combination between eustatic cycles and lateral auto-cyclic sedimentary processes. This cyclicity is well-visible in the hanging-wall area fed by the sedimentary influx, but also in the distal hanging-wall area fed by the uplifting and eroding footwall during the rift cycles. This latter source becomes buried during the post-rift phase.

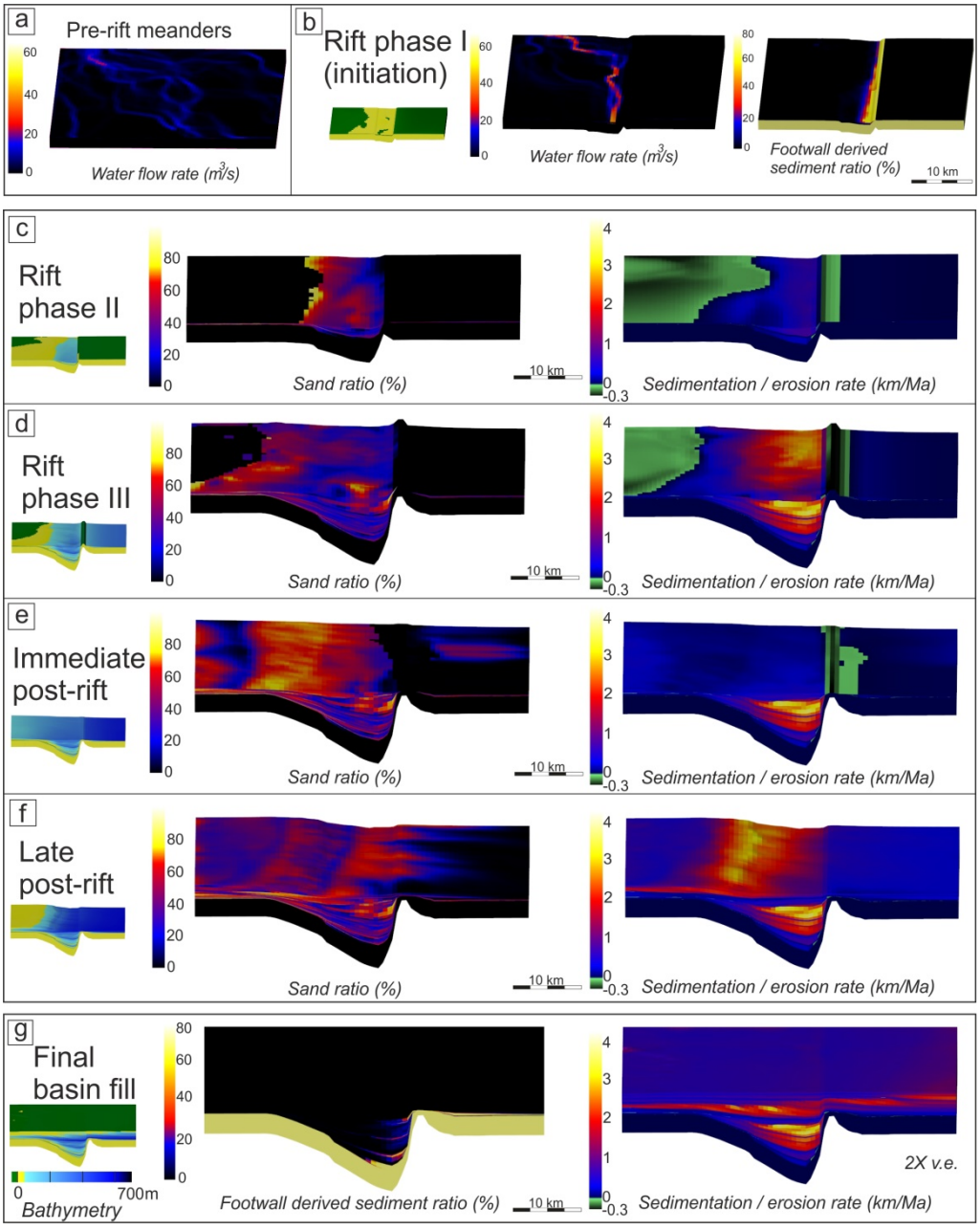

Figure 5.5: Modeled sediment composition, sedimentation rate and water flow in the reference experiment. Same parameters are applicable as in Figure 5.4. a) The distribution of the water flow rate at the beginning of the model, i.e., after the first time step and before the onset of deformation in the half graben. b) Water flow rate and footwall-derived sediment ratio at rift phase I. c-f) Sedimentary sand ratio and sedimentation or erosion rate for the subsequent rift phase II, rift phase III, immediate post-rift and late post-rift periods, respectively; g) Footwall-derived sediment ratio and sedimentation rate at the end of the model.

5.3.1 Parameter sensitivity analysis

In a series of seven experiments we have analyzed the effects of different basement subsidence scenarios combined with different eustatic frequencies and amplitudes on half-graben syn-kinematic sedimentation (Figure 5.6). The first experiment with zero eustatic variations and a continuous basement subsidence pattern (Figure 5.3d) shows a gradual increase in water depth towards the half-graben depocenter during the syn-rift phase. The minor variation in the proximity of the footwall is the result of local sourcing due to erosion and re-deposition (Figure 5.6a). In this situation, the late post-rift progradation shows a continuous prograding and aggrading pattern. When sea-level variations with amplitude of 70 m and period of 700 kyr are added in a second experiment, high order retrograding-prograding variations are observed during the entire evolution in the shallow part of the basin by moments of progradation, aggradation and retrogradation, which reflect cycles of transgression, normal and forced regression (Figure 5.6b). The comparison of these two experiments shows the impact of high-order sea-level variations.

The following four experiments follow the same pattern, analyzing the effects of the two types of episodic subsidence (Figures 5.3b,c). When sea-level variations are absent, the rift initiation and the subsequent second rift phase show similar retrogradation-progradation cycles (Figures 5.6c,d). Starting from this setup, a small modification in the basement subsidence rate at the end of the third rift phase creates a significant effect (Figures 5.3b,c). In the first scenario (Figure 5.6c), the rapid basement subsidence during the entire third phase shows a gradual overall retrogradation along the hanging-wall followed by the onset of progradation during post-rift times. In the second scenario (Figure 5.6d), the rapid basement subsidence is decreased at the end of the third syn-rift phase, which creates a retrogradation - progradation pattern (IIIa and IIIb), followed by one other retrogradation - progradation during post-rift times. In both scenarios, higher order retrogradational - progradational cycles visible in the proximal sedimentation of the hanging-wall during the third syn-rift phase reflect lateral auto-cyclic processes. These auto-cyclic processes are less visible when sea-level variations are present in our models (Figures 5.6e,f), which create a higher order retrogradation-progradation cyclicity superposed over the lower order one induced by the three rift phases. The fact that this higher order cyclicity is driven by sea-level variations is demonstrated by its dependence on the eustatic frequency, as observed when this frequency is changed in a subsequent experiment (higher frequency and higher-order cycles in Figure 5.6g). Although the sedimentation effects are always similar for the first and second-rifting phase, this gradual implementation of the sea-level variations facilitates the discrimination of tectonic and eustatic effects during the third syn-rift phase, when larger accommodation space is available near the basin margins and their effects are comparable (Figures 5.6e,f).

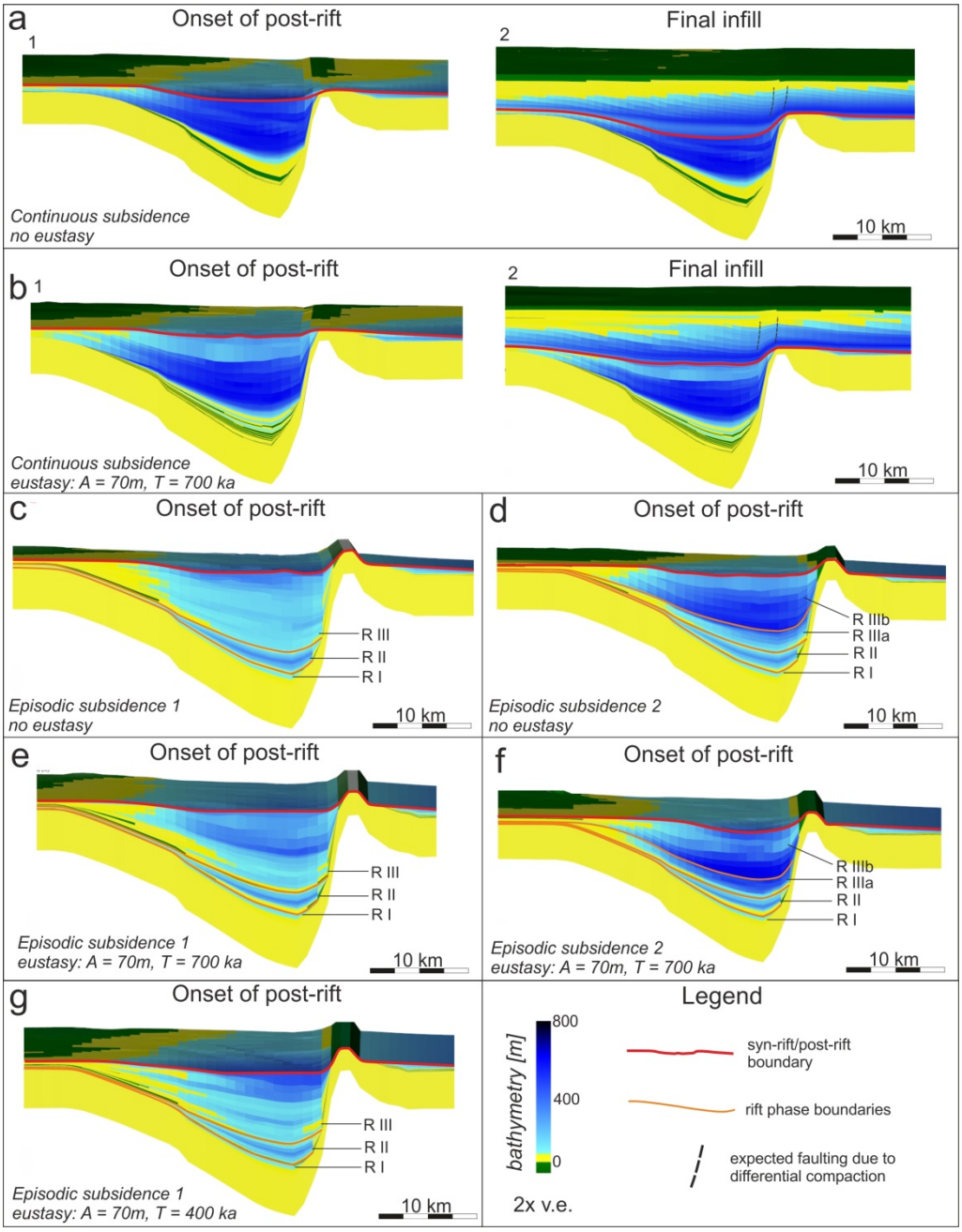

Figure 5.6: Parameter study analyzing the influence of eustatic variations, their period (T) and the influence of the type of basement subsidence (continuous versus variable episodic) on the paleobathymetric evolution of the models. The episodic subsidence 1, episodic subsidence 2 and continuous subsidence are illustrated in Figures 5.3 b,c,d, respectively. Note the retrograding-prograding pattern of low-order rift cyclicity in experiments with episodic subsidence combined with a higher-order pattern of retrogradation-progradation controlled by a combination of eustatic cycles and lateral auto-cyclic sedimentary processes.

The influence of external water influx value (Q_w) is analyzed in a series of experiments where all other parameters are kept identical with the reference model (Figure 5.7). In our diffusion modeling approach, this discharge value influences the sediment transport distance, with higher discharge values enabling transportation over larger distances (cf., *Gvirtzman et al*., 2014). Three models were conducted that simulate relatively low, medium and high water discharge values (50, 200 and 800 m^3/s, respectively, Figure 5.7a). This shows that a higher water discharge value creates a wider shallow-water shelf environment, with a lower dip angle of the shelf-margin slope and lower water depth averages in the depocenter. This dependence is best illustrated by the average water depth values of a small volume located in the same area within the deep-water part of the basin (red square Figure 5.7a). This shows a clear correlation between decreasing bathymetry with increasing water discharge.

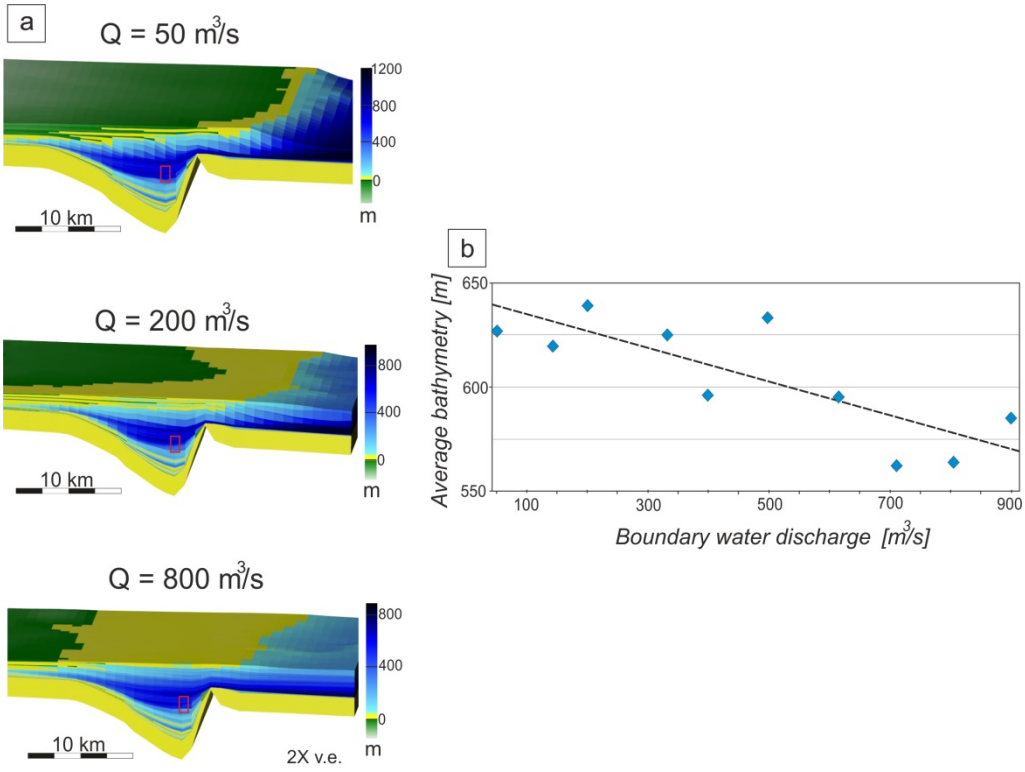

Figure 5.7: Parameter study analyzing the influence of water discharge (Q) into the model. This water discharge is associated with the same amount of sediment influx, but sediments are transported over larger distances at higher discharges. a) the paleobathymetric evolution of the model; b) Plot showing the influence of water discharge on the paleobathymetry of a selected time and space interval (red rectangles in Figure 5.7a) selected near the end of rifting in the depocenter of the basin. Note the main anti-correlation trend, while the variability is controlled by lateral auto-cyclic sedimentary processes.

The influence of climate was tested in a series of ten consecutive models, where the ratio between wet short-term and dry long-term discharge values (R) is changed (Figure 5.8). At higher ratios, simulating a more wet climate associated with a higher water discharge, sediments will be transported at larger distances, delivering more effectively the sand fraction (Figure 5.8a). At low ratios simulating a balanced, drier climate, most of the sediments remain near the shelf slope (Figure 5.8a). The influence of climate in building the clinoform geometries was studied by the average dip angle of the bottomsets during the post-rift phase. The results show that higher discharge ratios result in more elongated clinoform geometries, characterized by lower dip angles and more coarse-grained bottomsets (Figure 5.8b).

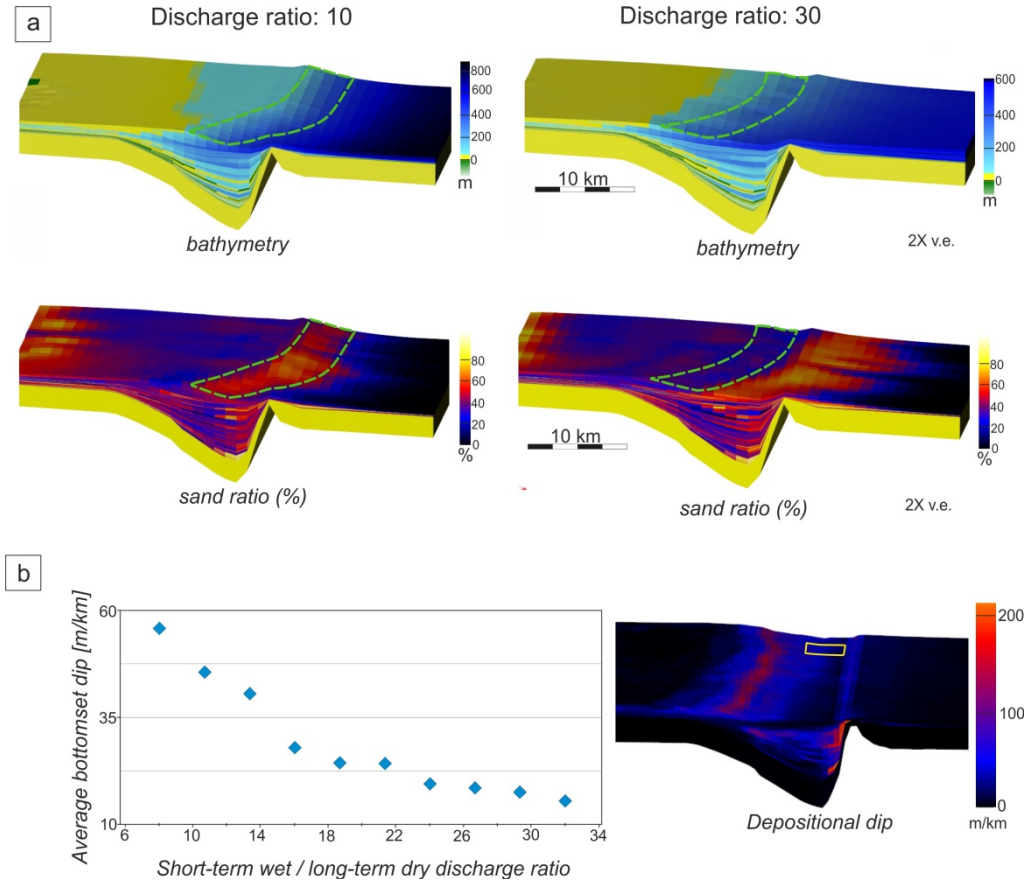

Figure 5.8: Parameter study analyzing the influence of water discharge ratio (R) between wet short-term and dry long-term intervals (see methodology description). a) paleobathymetric evolution and sedimentary sand ratio during late post-rift progradation. Note that shelf-margin slope (drawn with green dashed line) is steeper and more coarse-grained for lower discharge ratios, while the bottomsets contain a higher proportion of sands at higher discharge ratios; b) Plot (left) showing the influence of discharge ratios on the average bottomset dip paleobathymetry of a selected time and space interval (yellow rectangle on the right figure). Note the anti-correlation trend.

5.4 Syn-rift sedimentation in the Pannonian Basin system

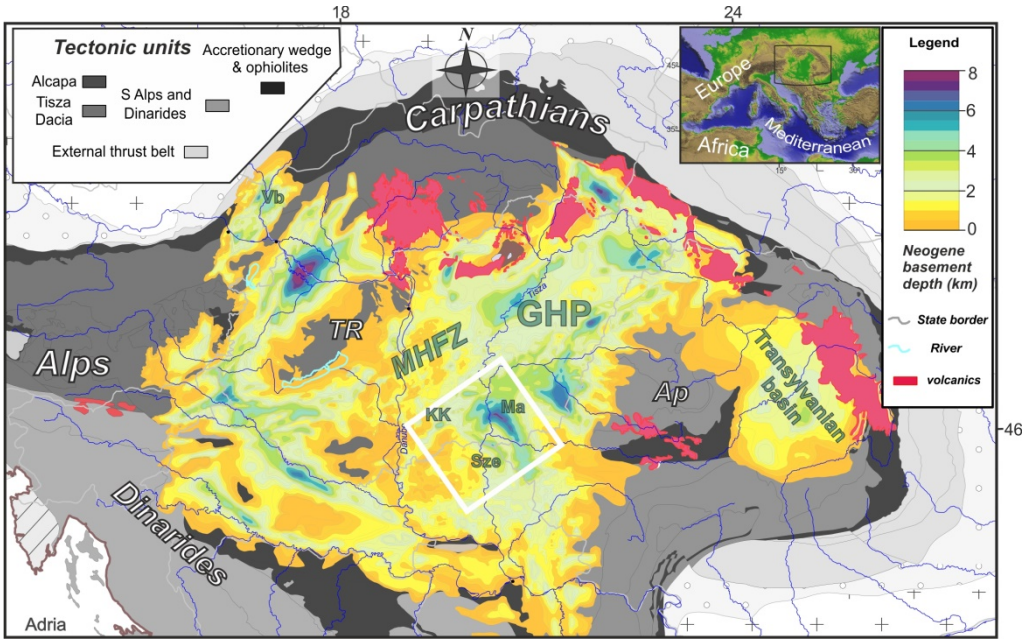

Figure 5.9: Application of our modeling to the natural case of the Miocene syn-rift evolution of the SE part of the Great Hungarian Plain of the Pannonian Basin system. Figure shows simplified basement tectonic map of the Alps - Carpathians - Dinarides region overlain by the Miocene – Quaternary sedimentary thickness (in kilometers) of the Vienna (Vb), Pannonian and Transylvanian basins (simplified after *Schmid et al*., 2008; *Balázs et al.*, 2017). MHFZ – Mid-Hungarian Fault Zone, TR - Trans-Danubian Range, KK - Kiskunhalas subbasin, Ma - Makó Trough, Sze - Szeged Basin.

The variability of the Miocene extension observed in the Great Hungarian Plain of the Pannonian Basin mirrors the evolution of back-arc extension, during the gradual clockwise rotation of the underlying Tisza-Dacia mega-unit, associated with the Carpathian slab retreat and invasion of its external embayment (Figure 5.9, see *Tari et al*., 1999; *Horváth et al*., 2015 for further details). The result is a gradual activation and evolution of extensional half-grabens that have different strikes and extensional directions during Miocene times. Therefore, these differently oriented half-grabens show also diachronous syn-rift sedimentation and transition to the post-rift phase (Figure 5.10, *Balázs et al.*, 2016). In the Great Hungarian Plain, we have selected a modeling area of 100 × 100 km^2 that includes the evolution of Kiskunhalas, Szeged, Földeák and the larger Makó half-graben (white rectangle in Figures 5.9, 5.10). The subsidence history of these half-grabens (Figure 5.2c) and the larger area is constrained by the interpretation of a dense network of seismic and well data (Figures 5.2a,b, see also *Tari et al*., 1999; *Pigott and Radivojević*, 2010; *Balázs et al*., 2016). The gradual Miocene extensional activation constrains the basement subsidence that

has an episodic or continuous pattern for each of these half-grabens (Figure 5.2c). These half-grabens were filled by sediments sourced dominantly from the neighboring orogens, such as the Dinarides, Alps and Carpathians by fluvial systems associated, for instance, with the former location of the Danube and Tisza rivers (*Magyar et al.*, 2013).

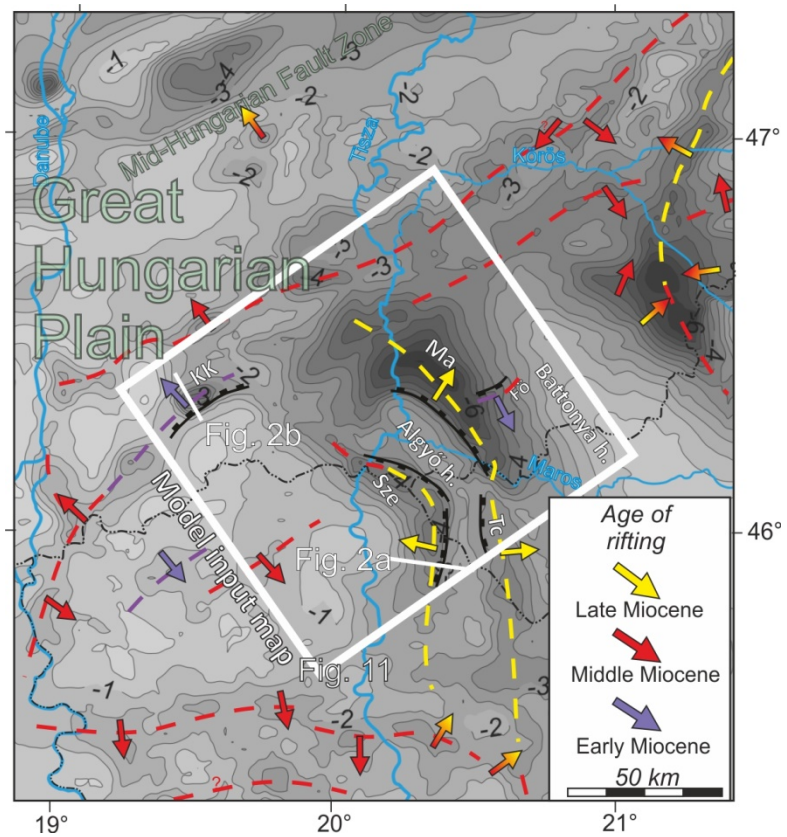

Figure 5.10: Neogene basement isopach map of the SE part of the Great Hungarian Plain with the location of the main depocenters with their strike (dashed lines), age of rifting and the main direction of extensional tectonic transport in the various sub-basins (the same color-coded arrows, after *Balázs et al.*, 2016). White lines show the locations of the interpreted seismic sections. The white square indicates the modeled area of Figure 5.11. Boundary normal faults of the modeled half-grabens are indicated.

The modeled retrograding - prograding cyclicity is constrained by recent seismic interpretations analyzing reflection terminations and the overall distribution of seismic facies units (*Balázs et al.*, 2016). These have shown, for instance, that the Kiskunhalas half-graben was controlled by a NNW-dipping low-angle normal fault with a highly-eroded footwall and was filled with ~3 km Lower Miocene syn-kinematic sediments grouped into four retrograding-prograding cycles (Figure 5.2b). This Middle Miocene immediate post-rift is separated by a gently folded erosional unconformity from the overlying Late Miocene sediments, created by inversion during latest Middle Miocene - earliest Late Miocene times. Finally, the Szeged half-

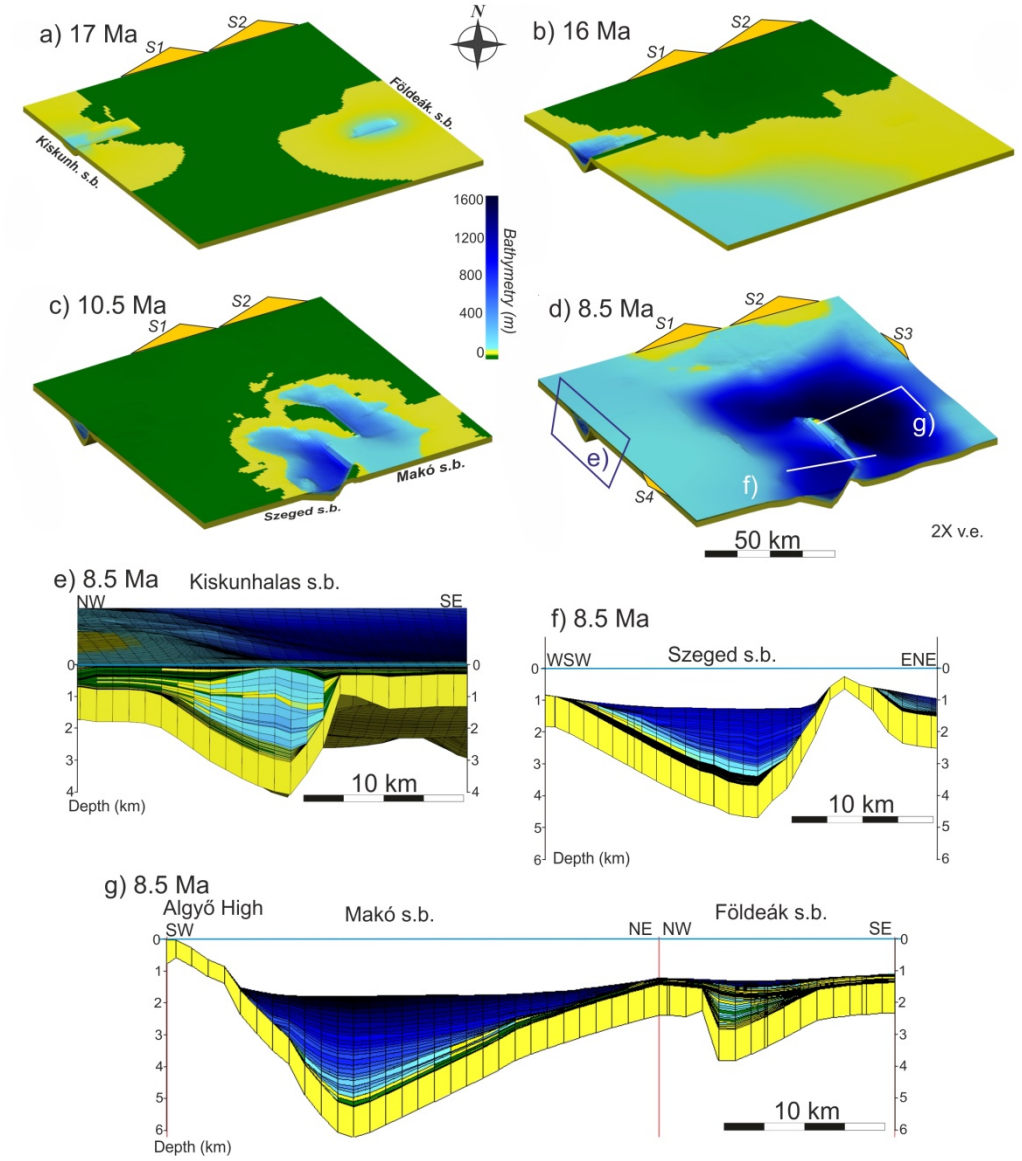

Figure 5.11: Results of the second modeling setup aimed to simulate the patterns observed in the syn-rift sedimentation of the Pannonian Basin. The post-rift patterns have already been well simulated by similar type of numerical modeling in other studies (*Csató et al.*, 2013, 2015). a-d) Evolution of bathymetry in the second modeling setup that assumes the gradual fill over multiple half-grabens. Yellow triangles illustrate the influx of water and sediments in the model. Note that the stages are displayed at stratigraphic ages with the onset of the model at 19 Ma; e-g) comparative modeled cross-sections over the four half-grabens displayed at the same stratigraphic time. Location of the cross-sections is displayed in Figure 5.11d. The onset of rifting is diachronous and the basement subsidence patterns are different in various half-grabens (see text description). Note the inverted geometry of the Kiskunhalas Trough (Figure 5.11e).

graben was controlled by a low-angle normal fault dipping W-wards with a highly-eroded footwall and 2.5 km of Middle to early Late Miocene syn-rift and Late Miocene - Quaternary post-rift sedimentation associated with retrograding-prograding cycles (Figure 5.2a). All the various half-grabens were subsequently affected by a late post-rift subsidence that took place at the much larger scale of the entire Great Hungarian Plain (see further details in *Magyar et al*., 2013; *Sztanó et al*., 2013; *Csató et al*., 2015).

5.4.1 Numerical forward modeling of syn-rift sedimentation in the Great Hungarian Plain

The onset of modeling at 19 Ma (Early Miocene) is associated with the start of the basement subsidence in the NE-SW oriented Kiskunhalas and Földeák half-grabens, which subsequently captured most of the sourced sediments (Figure 5.11a). The smaller Földeák half-graben was filled by the end of the Early Miocene by footwall derived fans and sediments sourced from the north, while the Kiskunhalas half-graben still retained shallow-water sedimentation (Figure 5.11b). The shallow-water environment was maintained during the Middle Miocene, when the Kiskunhalas half-graben was filled by immediate and late post-rift sediments. At the same time the onset of extension in the Szeged half-graben was associated with the deposition of a rift initiation cycle. The inversion observed in the Pannonian Basin at the transition to the Late Miocene (cf., Figure 5.2b, ~12-11 Ma, *Horváth*, 1995) resulted most likely in exhumation to continental conditions in most of the modeled area outside the deeper parts of the Szeged half-graben. This short quiescence of extension was followed by the activation of the Makó half-graben and the regional subsidence in the SE associated with a transgression (Figure 5.11c). Eroded and redeposited sediment remnants of the older Földeák half-graben are overlain by the younger syn-kinematic deposits of the Makó half-graben. The syn-rift deposition continued in the Szeged and Makó half-grabens until ~8.5 Ma. The regional subsidence and transgression created water depth values exceeding 1 km in these half-grabens (Figure 5.11d). The increase of sediment influx sourced by the Alps and Carpathians (*Magyar et al*., 2013, *Sztanó et al*., 2013) filled by progradation this high accommodation space during subsequent post-rift times.

Three representative cross-sections have been extracted from our 3D evolutionary model to illustrate the sedimentary architecture of the half-grabens at the end of the overall syn-rift extension in the Great Hungarian Plain (~8.5 Ma, Figures 5.11e-f). In the Kiskunhalas half-graben, the first rift initiation cycle is overlain by shallow-marine sediments. Similar to the reference model (Figure 5.4c), prograding-retrograding shallow delta cycles are deposited over the hanging-wall and are controlled by the pulses of fast subsidence during Early Miocene times (Figure 5.11e,

compare with 5.2b). The inversion and formation of the antiformal geometry followed by the Late Miocene transgression create onlaps over its flanks during the increase of water depth. In the Szeged half-graben, the shallow-water Middle Miocene rift initiation cycle is overlain by one Late Miocene retrogradational - progradational cycle above the separating unconformity (Figure 5.11f). The subsequent rapid Late Miocene subsidence combined with the location of this half-graben at larger distance from the sediment source with intervening trapping basins result in a general transgression to high water depths and distal sedimentation in the depocenter (Figure 5.11f). Similarly, the rapid Late Miocene syn-rift subsidence of the Makó half-graben outpaces the external sediment influx and the one derived from its eroding footwall (Algyő High), resulting ultimately in high water depth and distal sedimentation (Figure 5.11g). Similar with observations (*Sztanó et al*., 2013), the Algyő High and other eroding footwalls are also flooded after ~8 Ma and the local sediment re-distribution ceases.

5.5 Discussion

Our modeling yields novel insights in quantifying the tectonic and climatic controls on sedimentation in asymmetric extensional basins and proposes an evolutionary model for the distribution of fine- and coarse-grained lithologies and sedimentary facies in half-grabens and during the subsequent post-rift evolution.

5.5.1 3D evolutionary model and facies distribution during asymmetric extension

Initiation of asymmetric subsidence in half-grabens drives a reorganization of sedimentary environments (Figures 5.5a,b). Even when high sedimentation rate keeps pace with basement subsidence, sediment routing is concentrated in sourcing hanging wall depocenters, while exhuming footwalls hampers external transport but feeds internally both the hanging wall and the hinterland of the footwall. This rift initiation phase contains the largest volumes of gravity-driven re-distributed coarse sediments. Due to the asymmetric geometry of the uplifted footwall, most of the eroded materials is transported toward its hinterland and creates a low-angle pediment surface. Only one third of the material sourced by the eroding footwall is redistributed to the hanging-wall depocenter during these times (Figure 5.12). Controlled by the interplay between sedimentation rate and relative water-level variations, a rapid transition from alluvial to marine environment is recorded. Therefore, the footwall derived sediments can be transported as fan-deltas as early as the rift-initiation phase, such as is the case of the Middle Miocene Szeged half-graben (Figure 5.11f).

The subsequent rift phases are primarily controlled by larger fault offsets. Rapid subsidence rates during periods of fault activation result in an overall retrogradation, while periods of tectonic quiescence enable progradation (see also

Martins-Neto and Catuneanu, 2010). The flank of depocenters records a higher order transgressive-regressive cyclicity, which is superimposed on the lower order tectonic activity, both creating retrograding - aggrading - prograding delta slopes. Sand lobes can be transported at larger distances into the half-graben during periods of wet climate (Figures 5.5 and 5.8), due to high water discharge values and/or sediment influx (e.g., *Gong et al.*, 2016) and farther progradation of deltas towards the deep basin (e.g., *Kim et al.*, 2013). Active fault offsets are associated with moments of footwall uplift and denudation resulting in sediment re-distribution toward the depocenters. Erosion rates cannot always keep pace with footwall uplift and, therefore, the deposition of footwall derived fans may continue during periods of tectonic quiescence as well (Figure 5.5).

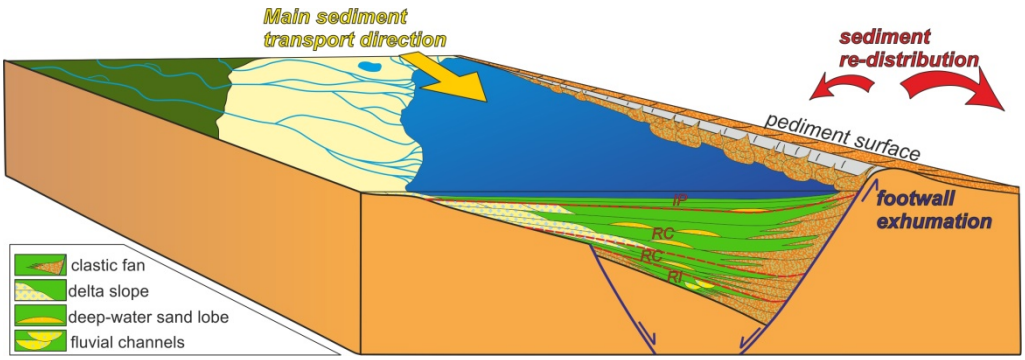

Figure 5.12: Conceptual model of tectono-sedimentary evolution of a half graben filled with syn-kinematic sediments shed from an external hanging-wall source and internal footwall erosion displayed at the onset of post-rift (IP) time.

The regional post-rift thermal subsidence progressively buries the half-grabens in our models. The footwall of the controlling normal fault may remain above sea-level during immediate post-rift times and source the depocenter with footwall fans. Subsequently, differential compaction creates gentle syncline geometry above the former hanging-wall and induces normal faulting above the footwall (Figures 5.6 and 5.2a). Coarse-grained sediments cannot initially bypass the positive morphology of the eroded remnant of the footwall located above or below sea-level (Figure 5.5e). The final bypass and basin fill is recorded only during the late post-rift times, when sedimentation rate finally outpaces the subsidence and tectonic controls are minor, when compared to climatic sea level variation or differential compaction effects. These later effects combined with sediment sourcing influence the sedimentation over the shelf and transport of coarse-grained material towards the deep basin (Figure 5.5f).

5.5.2. Tectonic versus climatic controls on building the transgressive-regressive cyclicity

A robust feature of our numerical modeling of syn-kinematic sedimentation in asymmetric extension is the evolution of sedimentation cyclicity at different orders (Figures 5.4, 5.6). The retrogradation - progradation pattern observed in our models has obvious coastal onlaps and correlative maximum regression surfaces. Therefore, the conversion to a transgressive-regressive cyclicity is direct (cf., *Embry and Johannessen*, 1992; *Helland-Hansen and Martinsen*, 1996). Low-order rift cycles are primarily driven by the variable rates of tectonic-driven subsidence in the half-graben. Moments of active normal faulting results in high subsidence rates and are associated with rapid transgression. The subsequent evolution at lower subsidence rates enables the progressive infill of the created accommodation space, resulting in an overall regression (see also *Martins-Neto and Catuneanu*, 2010). This means, obviously, that our rift phases are in fact rift cycles. Such a rift cycle starts with a rapid flooding and an initial retrogradation followed by a prograding and shallowing sequence, which drives an initial fining followed by coarsening upwards sedimentary cycle.

Higher order climatic effects and water-level variations are superimposed on this pattern and can be well discriminated over the flanks of the half-grabens, where the rates of the spatially asymmetric tectonic subsidence are lower (Figure 5.1a) and the shallower deltaic higher-order transgressive-regressive cycles are better visible than in the main depocenter. It is noteworthy by our modeling, that can discriminate auto-cyclic processes from sea level variations and tectonically-induced subsidence (cf., Figures 5.6c,e and g). This is more obvious when the accommodation space is larger, such as during our third rift phase that is characterized by a constant, high-rate of basement subsidence creating a transgressive shift of the delta environment with ~20 km landwards, which is superimposed by higher-order eustatic retrogradation-progradation cycles (Figure 5.6e). Slight variations in the subsidence pattern may significantly modify the low-order tectonic cycles, such as during the third syn-rift phase, when a minor decrease in subsidence creates an additional retrograding-prograding cycle (compare Figures 5.6e and 5.6f). The modeling also shows that lateral auto-cyclic sourcing variations of the feeding delta create even higher order cycles both by proximal sedimentation over the flank (Figure 5.6c) and by deposition of sand lobes in the deep basin (Figure 5.5). Obviously, such a discrimination of external and internal driving factors in sedimentation depends on the chosen sediment influx, the frequencies and amplitudes of sea-level and tectonic variations, and the resolution of our model. For instance, our modeling can simulate the observations at high sediment flux in the Kiskunhalas half-graben of the Pannonian Basin (Figures 5.2b and 5.11e), while the low sediment flux and high subsidence rates of the Makó half-graben situated at larger distances from the source area with intervening trapping

basins (cf., *Sztanó et al.*, 2013) creates distal sediments whose cyclicity is below the resolution of most seismic observations and numerical models (Figure 5.11g).

5.6. Conclusions

By conducting a series of 3D numerical modeling experiments, we have contributed to the understanding of sedimentary infill of asymmetric extension in half-grabens controlled by one major listric normal fault or detachment that drives the sedimentation in hanging walls and the uplift of their footwalls. Observations in key basins, such as the Pannonian back-arc of Central Europe, show that the asymmetric nature of extension drives a specific deformational pattern: footwall exhumation is associated with moments of low subsidence followed by its acceleration in the center of the half-graben, which are followed by a slower regional thermal subsidence phase. Our modeling shows that such scenarios are associated with continental alluvial to shallow-water sedimentation during the early stages of the syn-rift, followed by rapid deepening during the subsequent syn-rift evolution.

Our modeling demonstrates that forcing factors, such as tectonics, sea-level variations or climate, associated with water and sediment influx, have primary control on the sedimentary architecture and control the variability of erosion and lithologies inside the half-grabens and neighboring areas. Our modeling shows the ability to discriminate between the low-order tectonic and higher order sea-level and climatic-driven transgressive-regressive cycles from the auto-cyclic nature of the depositional system during multiple stages of the syn- and post-rift evolution. Unconformities separate these various temporal and spatial orders of the modeled and observed cyclicity. The actual sedimentation rate is linked to tectonics and to climatic variations controlling the distance and transport processes between the sources and the depocenter. A high sediment influx and water discharge during wet climate transport sand lobes at large distances in the deep part of the basin, assisted or not by moments of sea-level drop. The depocenter of such extensional structures records large water depth variations, episodic activity of normal faults and their migration in time, while the flanks record the various orders of transgressive-regressive cyclicity.

We have also modeled a system of multiple half-grabens that are activated in different locations, at different times and with different kinematics, such as observed in the Great Hungarian Plain of the Pannonian Basin. Modeling demonstrates the complex interplay between direct sediment sourcing and the ability of sediments to bypass trapping basins, compaction induced geometries and paleo-reliefs created by eroded footwall geometries. Such obstacles in the pathway of the sediment flux creates a distal, often pelagic sedimentation, where our ability to detect moments of activation of various forcing parameters is rather reduced at the standard seismic or wells observational scale.

6. Concluding remarks: integrating geological observations and numerical modelling results

The objective of the research presented in this thesis was to evaluate the role of the main tectonic and surface processes and their links providing first-order controls on the formation and evolution of extensional back-arc basins. The interpretation of a dense network of geophysical data and the use of numerical modelling demonstrate that back-arc extension in the Pannonian region took place at high rates with dominantly asymmetric mechanism. This resulted in the formation of deep half-grabens, with their formation interrupted and followed by episodes of basin inversion. The observed differential vertical movements differ from the classical concept of a rapid syn-rift and subsequent decaying post-rift evolution, such as observed in many passive continental margins (Figure 1.3). Spatial and temporal variations of subsidence and uplift rates are driven by patterns of crustal and lithospheric thinning due to back-arc extension and associated mantle dynamics and are intrinsically coupled to surface processes in terms of erosion and sedimentation (Figure 6.1). In this chapter I briefly summarize the main inferences from our seismic and well interpretation and numerical models and discuss our findings in the context of coupling between lithosphere processes and their near-surface expressions.

6.1 Links between tectonics and surface processes

Our observations from the Pannonian Basin accompanied by numerical modelling show the evolution of tectono-sedimentary cycles with different wavelengths and temporal scales. A noteworthy feature with the largest spatial scale is the re-organization of the overall sedimentary system during the transition from syn- to post-rift times. It is associated with regional differential vertical movements creating unconformities controlled by the gradual cessation of crustal extension and further active mantle dynamics.

The asymmetric nature of extension drives a specific deformation pattern of half-grabens during syn-rift times: footwall exhumation is associated with moments of low subsidence followed by its acceleration in the centre of the hanging-wall, which are followed by a regional thermal subsidence phase. The latter post-rift phase can be altered by basin inversion and/or flexural effects (*Horváth and Cloetingh*, 1996). Forcing factors, such as tectonics, sea-level and/or climatic variations associated with water and sediment flux, exert primary controls on the sedimentary architecture and determine the variability of erosion and lithologies inside the half-grabens and neighboring areas. The depocentre of such extensional structures records large water depth variations, episodic activity of normal faults and their migration with time, while the flanks record various orders of transgressive-regressive cyclicity.

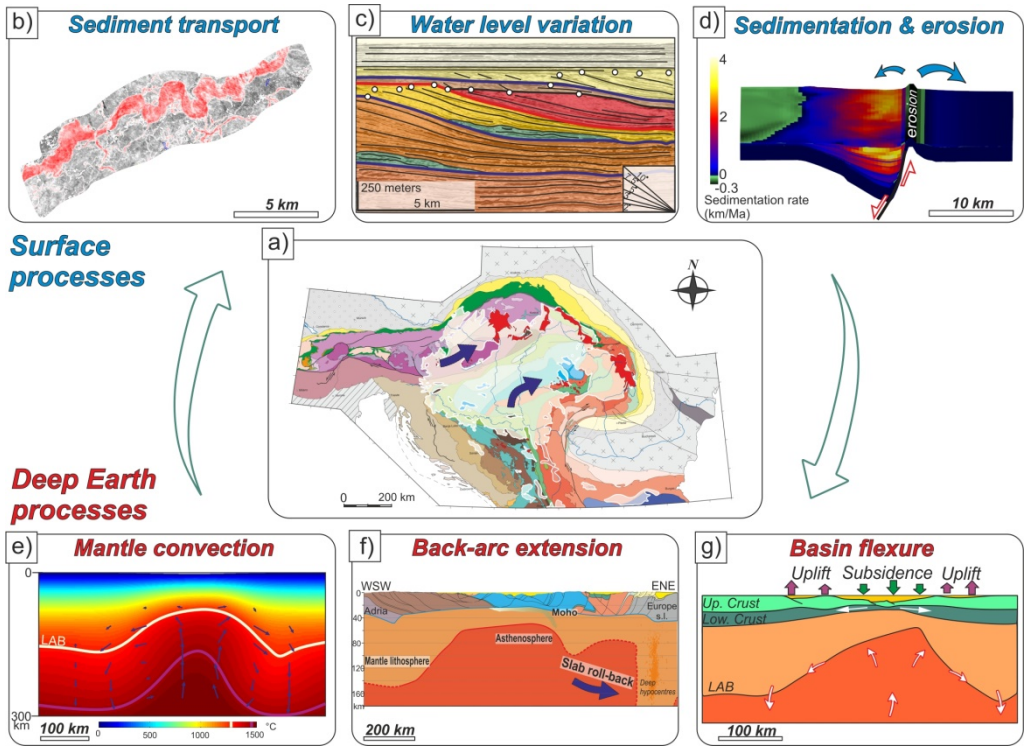

Figure 6.1: Synthesis of the main surface and tectonic processes that affect the formation and evolution of the Pannonian Basin system. a) Simplified tectonic map of the Pannonian Basin and surrounding orogens. Blue lines indicate the extrusion and rotation of the northern ALCAPA and southern Tisza-Dacia megaunits (modified after *Schmid et al.*, 2008). b) Seismic amplitude map of a meandering fluvial channel. c) Prograding-aggrading-retrograding patterns in Pannonian sediments. d) Modelled sedimentation and erosion rates in a half-graben. e) Modelled thermal evolution of an extensional basin. Note the convective asthenospheric upwelling and early drip-off of the marginal mantle lithosphere. f) Lithospheric-scale profile through the Pannonian region. Note the remnant of the Carpathian slab and associated seismicity. g) Post-rift subsidence in the centre of the basin and the uplift of the margins due to lateral heat transport resulting flexure of the thermally weakened lithosphere. This enhances sediment re-distribution and facilitates lower crustal flow from the depocentre towards the margins.

The effect of erosion rate on the overall basin architecture has been analyzed in our models in Chapters 4 and 5. Numerical experiments show that the final width of the sedimentary basin increases with increasing erosion rate due to the erosion of the flanks and an additional sediment loading in the basin centre, in agreement with previous studies (e.g., *Burov and Poliakov*, 2001). Therefore, a high rate of erosion enhances exhumation of the basin margins. Models also demonstrate that erosion rates cannot always keep pace with footwall uplift and, therefore, the deposition of footwall derived fans may continue after the cessation of local normal faulting. Asymmetric extension creates barriers, such as the eroded remnants of the footwalls. The erosion

gradually decreases as the remnant of the footwalls progressively submerge to later form positive seafloor morphology. This modifies the sedimentary transport routes (cf., *Sztanó et al.*, 2013) by preventing major bypass of coarse-grained sediments, with the main sediment flux being transported in the half-graben depocentre. Such obstacles in the pathway of the sediment flux create a distal, often pelagic sedimentation, where our ability to detect moments of activation of various forcing parameters is rather reduced at the standard seismic or wells observational scale.

Our study presented in Chapter 3 demonstrates that compaction effects creating fault systems such as the one quantified above the Dévaványa basement high are certainly significant in the sedimentary fill of the Pannonian Basin. Such effects should be similar elsewhere: by faults with variable offsets, increasing and subsequently decreasing towards the surface, reaching a maximum in the order of 150 m playing a major role in hydrocarbon migration and accumulation.

Seismic interpretation suggests that paleo-bathymetries and sedimentary transport routes of Lake Pannon were controlled by the inherited and/or local active extensional geometries. The height of the shelf-margin slope connecting the morphological shelf and deep-water environments shows higher values over the various sub-basins when compared with intervening basement highs. This means that the deposition of deep-water pelagic sediments and distal turbidites was unable to compensate the morphological differences inherited from syn-rift times before the shelf-margin slope progradation arrived to a proximal position. Highest water depth values characterized the SE latest Miocene to Pliocene remnant of the lake due to the higher subsidence rates and more distal position from the main source areas (cf., *ter Borgh et al.*, 2015).

These quantitative links between tectonics and sedimentation have allowed the definition of a novel model of sedimentation in asymmetric basins (Figure 6.1) that can be applied in other natural scenarios observed elsewhere.

6.2 Inferences for the tectonic evolution of the Pannonian Basin

Our studies demonstrate that extension in the Pannonian Basin system was diachronous and migrated in space and time across the basin between Early to Late Miocene times. The basin is superimposed on two distinct orogenic mega-units (i.e., ALCAPA and Tisza-Dacia) deriving from different paleogeographic positions (e.g., *Balla*, 1986; *Csontos and Vörös*, 2004). Their extensional collapse could have commenced at different times driven by subduction roll-back that took place in the Carpathians and Dinarides (*Matenco and Radivojević*, 2012). Extension was associated with significant exhumation of the Dinaridic orogenic margin, controlled by extensional detachments that largely reactivated the inherited Sava Suture Zone contact with the Tisza-Dacia mega-unit (e.g., *Ustaszewski et al.*, 2010). Our thermo-

mechanical numerical modelling implies an initial topographic updoming phase at the onset of extension resulting from the fast asthenospheric uprise. The oldest stratigraphic age penetrated by wells in the Pannonian Basin is dated as Lower Miocene (e.g., *Fodor et al.*, 1999; *Horváth et al.*, 2006). An earlier onset of extension and subduction roll-back associated with an initial updoming could have prevented the deposition of older syn-rift sediments. Recent thermo-chronological studies also infer that the activity of extensional sub-basins and associated detachments started near or in the Dinarides already during the Oligocene (*Matenco et al.*, 2016 and references therein).

The overall geometry of the Pannonian Basin is characterized by a series of genetically linked half-grabens, bounded by one major normal fault or detachment controlling the coeval sedimentation in the hanging wall and associated with significant uplift of the footwall. Given the amounts of footwall erosion and block tilting across the half-grabens, we can estimate an amount of exhumation ~2-6 km. These amounts are higher than the thickness of the syn-kinematic basin fill deposited in the hanging-walls and this type of exhumation increases in local detachments and core-complexes towards the Eastern Alps and Dinaridic margins of the Pannonian Basin. Therefore, the amount of extension along various controlling structures is much higher than looking solely on the syn-kinematic basin fill. This means that integrating the amounts of asymmetric extension from the Dinaridic margin in the Pannonian Basin towards the Carpathians, the total amount of crustal extension of the Tisza-Dacia mega-unit is at least 220-270 km. In agreement with previous studies, our data show that the Middle Miocene was the peak period of extensional subsidence of the Pannonian Basin, most of the half-grabens of the Great Hungarian Plain accommodating maximum hanging-wall deposition. The contrasting present-day strike of various sub-basins is the result of their gradual subsequent clockwise rotation during and after extension.

As discussed in detail in Chapter 2 extension and large-offset normal faulting in the Pannonian Basin gradually ceased between 14 ~ 8 Ma (cf., *Matenco and Radivojević*, 2012; *Balázs et al.*, 2013; *Fodor et al.*, 2013; *ter Borgh*, 2013) and therefore the onset of post-rift sedimentation appears to be diachronous, with youngest half-grabens located in the SE parts of the basin. The anomalous pattern of the distribution of late Middle Miocene (Sarmatian) sediments might be related to different processes, but one interesting feature is its ~400 km of wavelength. A widespread unconformity recorded near the transition between the Middle and Late Miocene in the centre of the Pannonian Basin is generally attributed to a short-lived inversion. A similar observation in our modelling near the transition between syn- to post-rift times implies that such uplift could also be driven by the cessation of the extensional forces, change in the patterns of lower crustal flow and additional

asthenospheric dynamics. Large-scale asthenospheric asymmetries created during syn-rift deformation may be significantly attenuated by subsequent thermal processes during the post-rift phase. Thermal convection during the classical "post-rift" times (cf., *Huismans et al.*, 2001) can explain the delayed peak of alkaline basalt magmatism in the Pannonian region as well.

Phases of basin inversion and contraction also show a variable spatial and temporal pattern, as summarized in Chapters 2 and 3. For instance, the Kiskunhalas Trough, or sub-basins in the SW part of the Pannonian Basin system underwent basin inversion during late Middle Miocene to early Late Miocene times (Figure 1.3). The cessation of extension was followed by the onset of large-scale inversion in the Pannonian Basin from late Miocene times (from 8–7.5 Ma) controlled by the counterclockwise rotation and push of the Adriatic microplate which created large-scale contractional structures near the Dinaridic margin and dominantly transcurrent kinematics elsewhere (*Bada et al.*, 2007; *Fodor et al.*, 2005; *Uhrin et al.*, 2009). The resulted tectonic topography appears to be basin scale folding process (*Horváth and Cloetingh*, 1996; *Dombrádi et al.*, 2010; *Jarosinski et al.*, 2011). Our thermo-mechanical modelling shows that the lateral heat transfer from the asthenospheric upwelling below the Pannonian Basin enhances flexural uplift and erosion near the basin margins. Areas of uplift are subject to denudation and the eroded material continuously overfill the generated accommodation space. This re-distribution results in flexure of the thermally weakened lithosphere, which enhances differential vertical movements and creates minor upper crustal deformation and lower crustal flow. Sediments up to ~6 km have been affected by this still ongoing differential vertical movement and differential compaction creating gentle fold geometries and compaction induced fault offsets.

6.3 Future perspectives

In this thesis I have presented the interpretation of a large dataset mainly built up by seismic and well data and used different modelling approaches to improve our understanding of the tectono-sedimentary evolution of the Pannonian Basin system. I have relied on the available chronostratigraphic framework (e.g., Magyar et al., 2013) constructed by the integrated analysis of biostratigraphic, magnetostratigraphic data calibrated by a few radioactive isotope age measurements. Due to the complex evolution of the Paratethys Sea, as well as the Pannonian Basin, a further refinement of this framework is crucial in order to obtain an even higher resolution evolutionary model of the basin system. This is especially true for the Early and Middle Miocene basin stratigraphy.

The thermo-mechanical modelling presented in this thesis has been conducted in 2D. Due to the recent rapid advances in 3D numerical modelling (e.g., Burov and

Gerya, 2014) a logical next step is the implementation of our modelling in 3D. This research is already in progress (Balázs et al, in prep.), using a 3D thermo-mechanical code I3VIS solving the mass, momentum and heat conservation equations based on a conservative finite-difference scheme combined with a marker-in-cell technique and includes non-Newtonian visco-plastic rheologies (e.g., Liao and Gerya, 2014).

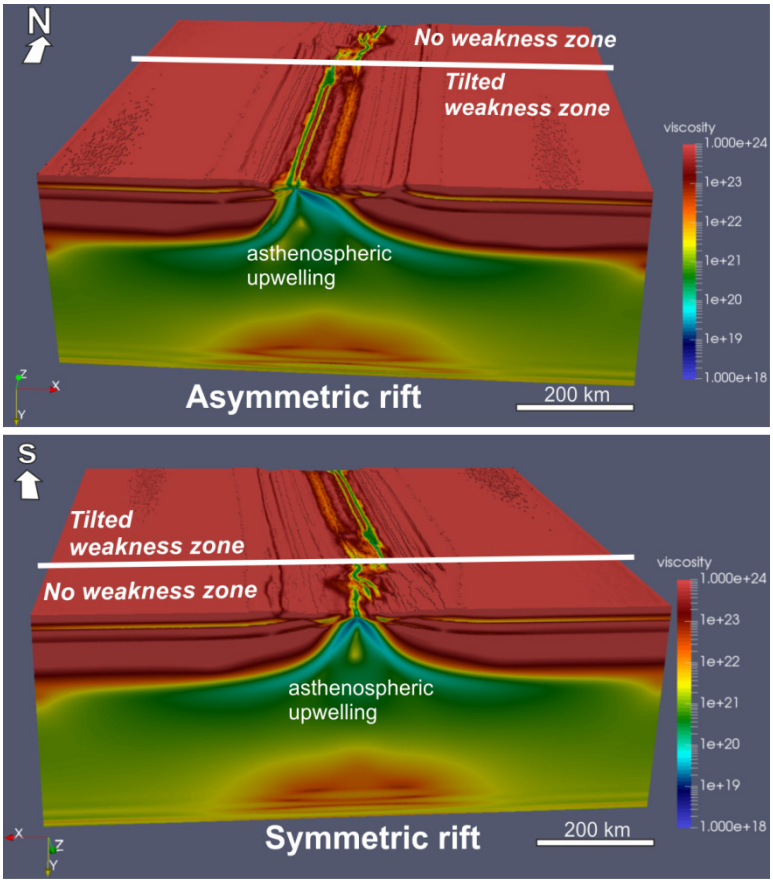

Figure 6.2: 3D thermo-mechanical extensional model result illustrated by logarithmic effective viscosity field showing the localization of deformation. A tilted weakness zone is implemented in the mantle lithosphere in the southern part of the model. Above the tilted weakness zone asymmetric rift configuration develops, while symmetric rift structures evolve in the absence of the pre-existing weakness zone. Their boundary is characterized by a wide zone of transtension (Balázs et al., in prep.).

In our first series of experiments we have implemented a tilted weakness zone in the southern part of the lithospheric mantle, while the northern part of the lithospheric mantle is homogenous. Simulating similar conditions like in the 2D models presented in Chapter 4, the modelled viscosity field (Figure 6.2) shows an asymmetric rift in the southern part, which evolution is controlled by the weakness zone, while in the northern part, in the absence of any weakness zone, a symmetric rift

structure develops. Note that between the symmetric and asymmetric rift structures, above the edge of the pre-defined mantle rheological weakness zone, a wide zone of transtension takes place. Following the procedure discussed in Chapter 4, we aim to design subsidence history and heat flow evolutionary models using this 3D code. Furthermore, the application of such a code enables to study the effects of magma generation and melt-induced rheological weakening in the crust and lithosphere. The 3D development of Rayleigh-Taylor instabilities and subduction dynamics, such as slab tearing and associated asthenospheric flow systems (e.g., *Menant et al*., 2016) have not been quantified yet for the evolution of the Pannonian back-arc basin. These large-scale geodynamic processes and their controls on more shallow geological features, such as basin geometries and their thermal evolution, organic matter maturation, or the migration toward to the surface of mantle-derived CO_2 (e.g., *Créon et al*., 2017) could be studied in future research.

Reliable modelling of such integrated systems obviously requires high-resolution geophysical observations. The AlpArray initiative (*Hetényi et al*., 2016) aims the high-resolution imaging of 3D structure and physical properties of the Alps-Appenines-Carpathians-Dinarides regions by means of seismic tomography. This could offer new constraints for the thermo-mechanical properties and geodynamic processes in the region, such as the extrusion in the Eastern Alps. There is still ongoing debate on the mode of extrusion, if it involved a lithospheric block (e.g., *Kovács et al*., 2012; *van Gelder*, 2017) or solely crustal-scale "flakes" (*Horváth et al*., 2015). My thermo-mechanical models (*Balázs et al.*, 2017) show that even an overthickened lithospheric block can be affected by fast extreme lithospheric mantle thinning assuming the ~ 220-270 km extension observed in the Pannonian region. A new generation of regional high-resolution seismic tomographic images (e.g., *Sumanovac and Dudjak*, 2016) could also address prime questions, such as the existence and development of the Dinaridic slab window below the northern Dinarides.

Finally, a better understanding of the links between tectonic and surface processes can be obtained by the continuation of integrated research, such as the application of coupled 3D geodynamic-geomorphological forward numerical models (e.g., *Ueda et al.*, 2015). Furthermore, comparison and integration of numerical and analogue tectonic modelling, with sedimentological experiments, either numerical, such as Dionisos or analogue, like the EuroTank at Utrecht University offers high potential for future research.

Summary

Understanding the formation and evolution of sedimentary basins is of paramount importance because they record the Earth's history: past changes in climate and sea or lake level, changes of sediment and water discharge. Their basin fill is not only a target of academic research, as they also show high potential for reserving mineral deposits, energy resources and fresh water. Extensional back-arc basins evolve in the hinterland of active convergent areas in response to retreating subduction boundaries. Understanding the evolution of such extensional basins in space and time requires the integrated analysis of tectonic and surface processes by linking different spatial and temporal scales.

In this thesis I aimed to study the mechanisms driving the sensitive interplay between tectonics and sedimentation in extensional back-arc basins. In such settings extensional basin formation post-dates an orogenic evolution, and is juxtaposed over an inherited nappe stack, often reactivating thrust contacts and exhuming rocks previously deeply buried. Thanks to the existing advanced knowledge from the Pannonian Basin of Central Europe and the surrounding Alpine-Carpathian-Dinaridic system, this region provides a key natural laboratory for the development and verification of a new generation of tectono-sedimentary models, which can be applied in similar highly-extended back-arc basins.

Chapter 2 presents a detailed analysis of the tectono-sedimentary evolution of the Pannonian Basin by means of interpretation of seismic and well data from the Great Hungarian Plain. It is floored by continental lithosphere and was affected by large amounts of extension driven by the subduction roll-back that took place in the Carpathians and/or Dinarides. A novel kinematic, seismic and well sequence stratigraphic interpretation allow the quantification of the link between the formation of half-grabens and coeval sedimentation in the depocentres. Our interpretation of temporal and spatial migration of extension during the entire Miocene times explains the contrasting present-day strike of various sub-basins as a result of their gradual clockwise rotation. The link between tectonics and sedimentation has allowed the definition of a novel model of sedimentation in asymmetric basins.

The post-rift phase of the Pannonian Basin is associated with the evolution of Lake Pannon: an initial underfilled, then balance fill and a final stage of overfilled giant paleo-lake. Chapter 3 focuses on the sedimentation in such a system by the interpretation of 2D and 3D seismic dataset corroborated with calibrating wells. The Late Miocene-Pliocene lake persisted for about 7-8 Myr and was progressively filled by clastic material sourced by the surrounding mountain chains and transported by large rivers, such as the paleo-Danube and paleo-Tisza. We combined sedimentological observations with a backstripping methodology facilitated by well lithology and porosity data to gradually remove the sediment overburden. This has

resulted in a morphological reconstruction of the former depositional surfaces with special focus on the prograding shelf-margin slopes. Calculations show that the paleobathymetric differences in the lake were clearly larger than 1000 metres in the deepest sub-basins of the Great Hungarian Plain. The large amount of compaction associated with lateral variations of Neogene sediment thicknesses has created non-tectonic normal fault offsets and folds.

The influence of lithospheric-scale rheological heterogeneities on the extension of an over-thickened, hot lithosphere is described in Chapter 4. Pre-existing orogenic suture zones localize extensional deformation resulting in asymmetric basins. Such crustal geometries are often in contrast with the more symmetrical regional lithospheric structure observed beneath extensional basins. Such (a)symmetries and their controlling parameters were studied by conducting a series of 2D thermo-mechanical numerical experiments. The modelling shows that syn-rift subsidence rates are low to moderate creating asymmetric half-grabens where extension migrates in space and time, grouped in an overall symmetrical appearance on a larger scale. The initial lithospheric mantle asymmetry is attenuated by the lateral heat conduction and further dynamic evolution of the thermal anomaly during the "post-rift" phase, resulting in differential vertical movements of the crust including additional 2-3 km subsidence in the basin centre. The modelling shows that the initial crustal and lithospheric thicknesses, rate of extension and surface processes strongly control the thermo-mechanical evolution of the extensional system.

The stratigraphic numerical modelling described in Chapter 5 was designed to study the sedimentation at the scale of individual half-grabens, controlled by one major normal fault focussing the coeval sedimentation in the hanging wall and comparable uplift of its footwall. The numerical experiments were performed with the 3D deterministic forward modelling software Dionisos. This model accounts for spatially and temporally variable subsidence and erosion rates, sediment flux composed of different lithologies, compaction, eustasy, water discharge and transport processes. My modelling applied to the Miocene syn-rift evolution of the Pannonian Basin highlighted the migration of active depocentres between Early to Late Miocene and its sedimentary responses. Our rift sequence model inspired by seismic and well data interpretation, described in Chapter 2, is analysed in detail with this numerical approach. This modelling can discriminate the low-order tectonic cycles driven by normal fault activity and higher order sea-level and climatic-driven transgressive-regressive cycles and the auto-cyclic nature of the depositional system.

The analysis of the studied extensional system and the performed numerical modelling were synthetized in the concluding Chapter 6. A close relationship between lithospheric to crustal deformation and surface processes has been investigated and established in the Miocene to Quaternary formation and evolution of the Pannonian Basin.

Samenvatting

Omdat sedimentaire bekkens de geschiedenis van de aarde registreren en vastleggen, onder meer waar het gaat om klimaatverandering en zeespiegelfluctuaties, veranderingen van aanvoerroutes van sedimenten en afvoer van rivierwater, is een beter begrip van hun vorming en ontwikkeling van groot belang. Onderzoek naar de invulling van bekkens is door de aanwezige mineraalafzettingen, energiebronnen en vers water, niet slechts van academisch belang. Extensiebekkens (back-arc basins) ontstaan in het achterland van actief convergerende platen als reactie op de terugtrekkende subductiegrenzen. Studie naar de evolutie van zulke bekkens in ruimte en tijd vereist een geïntegreerde analyse van tektonische en oppervlakteprocessen door verschillende ruimte- en tijdschalen te koppelen.

In dit proefschrift had ik als doel om de mechanismen te bestuderen die het delicate samenspel tussen tektoniek en sedimentatie in extensiebekkens aansturen. In dit soort tektonische regimes vindt bekkenformatie plaats na gebergtevorming tussen overerfde series dekbladen. Daarbij worden vaak al aanwezige overschuivingscontacten gereactiveerd die diep gelegen gesteente weer opstuwen naar het aardoppervlak. Door de grote hoeveelheid kennis over het Pannoonse Bekken in Centraal-Europa en het omliggende Alpen, Karpaten en Dinariden gebergtesysteem vormt deze regio een belangrijk studiegebied voor de ontwikkeling en toetsing van een nieuwe generatie van tektonisch-sedimentaire modellen, die kunnen worden toegepast op vergelijkbare sterk uitgerekte bekkens.

In Hoofdstuk 2 wordt verslag gedaan van een uitgebreide analyse van de tektonisch-sedimentaire evolutie van het Pannoonse Bekken door middel van interpretatie van seismische secties en boorgatgegevens van de Grote Hongaarse Laagvlakte. Deze vlakte is gevormd door uitrekking van de onderliggende continentale lithosfeer, veroorzaakt door het ‘terugrollen’ (roll-back) van de subductiezone die plaatsvond in de Karpaten en/of Dinariden. Een nieuwe sequentiestratigrafische interpretatie op basis van kinematische gegevens, seismische secties en boorgatgegevens, maakt het mogelijk om de koppeling te kwantificeren tussen vorming van halfgrabens en de gelijktijdige sedimentatie in de depocentra (diepste delen van het bekken waar het meeste sediment wordt afgezet). Mijn interpretatie van de migratie van extensie in ruimte en tijd gedurende het gehele Mioceen geeft een verklaring voor de contrasten in oriëntatie van verschillende subbekkens, veroorzaakt door hun geleidelijke kloksgewijze rotatie. Het verband tussen tektoniek en sedimentatie maakt het mogelijk om een nieuw model te definiëren voor sedimentatie in asymmetrische bekkens.

De fase na opbreking (post-rift) van het Pannoonse Bekken wordt in verband gebracht met de evolutie van het Pannoonse Meer. In eerste instantie werd er in het bekken relatief weinig sediment afgezet, gevolgd door een fase van evenwicht tussen

daling en sedimentatie, om uiteindelijk volledig dicht te slibben. In Hoofdstuk 3 wordt de sedimentatie in een dergelijk systeem in meer detail geanalyseerd door middel van interpretatie van 2D en 3D seismische secties en ijking met boorgatgegevens. Het Laat-Miocene tot Pliocene meer heeft voor 7 tot 8 miljoen jaar bestaan voordat het geleidelijk werd opgevuld met klastisch materiaal dat door grote rivieren zoals de paleo-Donau en paleo-Tisza werd getransporteerd vanuit het omliggend gebergte. Door sedimentologische gegevens te combineren met een reconstructie van de verticale bewegingen in het bekken (backstripping), ondersteund door boorgatgegevens over lithologie en porositeit, werd het mogelijk om het bovenliggend sediment te verwijderen. Hierdoor kon een reconstructie van het voormalig afzettingsoppervlak worden gemaakt met speciale aandacht voor de prograderende continentale marge en helling. Berekeningen tonen aan dat in de diepste subbekkens van de Grote Hongaarse Laagvlakte de paleobathymetrische verschillen in het meer duidelijk groter waren dan 1000 meter. De aanzienlijke compactie, gekenmerkt door de laterale diktevariatie van Neogene sedimenten, is de oorzaak van niet-tektonische beweging langs afschuivingsbreuken en voor het ontstaan van plooien.

Het effect van verticale en laterale variaties in reologische sterkte van de lithosfeer op de extensie van een verdikte, warme lithosfeer wordt beschreven in Hoofdstuk 4. Oude breukzones in gebergten zorgen er voor dat deformatie wordt gelokaliseerd waardoor asymmetrische bekkens ontstaan. Zulke korstgeometrieën staan in schril contrast met de meer symmetrische regionale lithosfeerstructuur, die meestal wordt waargenomen onder extensiebekkens. Zulke (a)symmetrieën en de bijbehorende parameters zijn bestudeerd in dit project door het uitvoeren van een serie 2D thermo-mechanische numerieke modelstudies. Deze modellen tonen aan dat de (syn-rift) extensie gekenmerkt wordt door lage tot matige bodemdalingssnelheden. Op plekken waar de extensie migreert ontstaan asymmetrische halfgrabens, terwijl op grotere schaal het systeem als geheel symmetrisch lijkt. De aanvankelijke asymmetrie in de mantellithosfeer wordt versterkt door laterale warmtegeleiding en dynamische evolutie van de thermische anomalie gedurende de ‘post-rift’ fase. Dit resulteert in een ongelijkmatige verdeling van verticale korstbewegingen, met bijbehorende extra bodemdaling van 2 tot 3 kilometer in het midden van het bekken. De modellen laten zien dat de thermo-mechanische evolutie van een extensiesysteem sterk wordt bepaald door de initiële korst- en lithosfeerdikte, in combinatie met de snelheden waarmee zowel de extensie als de oppervlakteprocessen plaatsvinden.

De (numerieke) stratigrafische modellen, beschreven in Hoofdstuk 5, zijn opgezet voor het bestuderen van sedimentatie op de schaal van individuele halfgrabens, die gevormd worden door een enkele grote afschuivingsbreuk. In de analyse wordt met name gekeken naar de gelijktijdige afzetting van sedimenten in het neerwaartse bewegende blok en de vergelijkbare opheffing van het opwaarts bewegende blok. Deze numerieke experimenten zijn uitgevoerd met Dionisos, een

softwarepakket voor 3D deterministische voorwaartse modellen. Bij de experimenten werd rekening gehouden met ruimtelijke en temporele variaties in bodemdaling, erosie, sedimentflux van verschillende soorten sediment, compactie, globale zeespiegelfluctuaties, waterafvoer en transportprocessen. De modellen van de Miocene syn-rift evolutie van het Pannoonse Bekken laten onder andere zien hoe migratie van actieve depocentra tussen het Vroeg- tot Laat-Mioceen invloed heeft op sedimentatie. Hiermee is het in Hoofdstuk 2 beschreven model van riftopeenvolging, gebaseerd op interpretatie van seismische secties en boorgatgegevens, in meer detail geanalyseerd, waarbij onderscheid gemaakt is tussen lagere orde tektonische cycli, gedreven door activiteit van afschuivingsbreuken, hogere orde transgressieve-regressieve cycli, gedreven door zeespiegel- en klimaatverandering, en cycli die worden veroorzaakt door de autocycliciteit van het afzettingsmilieu.

Na analyse van het bestudeerde extensiesysteem en de uitgevoerde numerieke modellen, samengevat in Hoofdstuk 6, kan worden geconcludeerd dat er een sterk verband is aangetoond tussen lithosfeer- en korstdeformatie en oppervlakteprocessen voor het ontstaan van het Pannoonse Bekken en de evolutie gedurende het Mioceen tot Kwartair.

Acknowledgements

There and back again… the story of my life from the last few years. I am lucky because on my journey in Hungary, in the Netherlands and in France I had the chance to meet so many great people who inspired and supported me to write this thesis.

First I would like to thank my promoters Sierd and Frank for giving me the opportunity to carry out this exciting research and defend my thesis in Utrecht. The stimulating working environment and the scientific support – occasionally coupled with a glass of decent red wine in Budapest or in the Faculty Club of Utrecht– are very much appreciated.

Liviu, your enthusiasm, encouraging advice and critical supervision kept me motivated to progress with my project. I really appreciated that your door was always open for lively discussions. Great thanks for everything!

My great appreciation goes to Professor Evgueni Burov and Dr. Didier Granjeon who helped me to make my first steps in the field of numerical modelling with Flamar and Dionisos.

I would like to express my gratitude to the members of the reading committee: Prof. Taras Gerya, Prof. Carmen Gaina, Prof. Magdalena Scheck-Wenderoth, Prof. Giovanni Bertotti and Dr. Didier Granjeon. Thank you for taking the time to review my thesis.

Special thanks go to Orsolya Sztanó and Imre Magyar for all the fruitful discussions and collaboration. Sharing your opinion on many things in the last few years is really appreciated.

It has been a great pleasure to discuss the evolution of the Pannonian region and enjoy many field trips including the Atlas, the Alps or the fabulous Bükk with László Fodor and Szilvia Kövér. Thank you!

Thanks to Gábor Bada, Endre Dombrádi, László Lenkey and Viktor Lemberkovics for the helpful talks.

The completion of this thesis would not have been possible without the support of many friends and colleagues from ELTE, thank you for all the good times: TG, Laci (×2), Mammut, Dezső, Zoli, Gali, Károly, Judit, Andy, Balázs, Robi, Feri, Gábor, Surda, Lilla, Nóri, Ági, Barbi, Herki, Misi, Soma, Jani, Gina… and many others.

I definitely found a lot of fun as well as an inspiring atmosphere to work in the Tectonics Group of Utrecht, this is thanked to you: Shang Yu, Jan-Diederik, Milos, Marten, Thomas, Antoine, Anouk, Alessio, Derya, Magdala, Fred, Damien, Marius, Dimitrios, Marianne, Lindsay, and to the honorary leader of the Tectonics Climbing and Skiing Group, Ernst! Great thanks for the excellent company Nevena and Jeroen!

I also always enjoyed my “refreshment” time with the magyar friends here with Eszti, Erzsébet, Dani and Kristóf. Inge and Elisa, I would like to thank you for all your help from the very beginning. I have very pleasant memories about discussions on the evolution of the Alps or intraplate deformation with a slice of cheese cake or a stroopwafel. It was a pleasure to share my time in Utrecht with you Katharina and Jon. Here I also would like to thank for being my paranymphs, I really learned a lot from all of you: I guess we will never forget that “you cannot have fun if you are not serious, but you cannot be serious if you don’t have fun”…

I enjoyed the time I spent with my bachelor and master students, thanks Zsófi, Youri and Benjamin.

Seismic interpretation was carried out by Kingdom, Petrel and OpendTect software, which we could use as participants of the IHS, Schlumberger and dGB University Software Grant Programs. I thank Beicip-Franlab for providing an academic license for DionisosFlow and CougarFlow.

Finally, I honestly would like to say thanks to all of my friends, girlfriend and family for the permanent support. Köszönet!

References

Andrić, N., Sant, K., Matenco, L., Mandic, O., Tomljenović, B., Pavelić, D., Hrvatović, H., Demir, V., Ooms, J., 2017. The link between tectonics and sedimentation in asymmetric extensional basins: inferences from the study of the Sarajevo-Zenica Basin, *Mar. Petroleum Geol*. 83, 305-332.

Angevine, C.L., Heller, P.L., Paola, C., 1990. Quantitative sedimentary basin modelling, *AAPG Course Note Series* 32, 133 pp.

Árkai, P., A. Bérczi-Makk, D. Hajdu, 1998. Alpine prograde and retrograde metamorphism in an overthrusted part of the basement, Great Plain, Pannonian Basin, Eastern Hungary, *Acta Geol. Hung*., 41, 179–210.

Artemieva, I., H., Thybo, and M.K., Kaban, 2006. Deep Europe today: Geophysical synthesis of the upper mantle structure and lithospheric processes over 3.5 Ga, in European Lithosphere Dynamics, vol. 32. Gee, D. and Stephenson, R. (Eds.), *Geological Society, London, Memoirs*, pp. 11-41.

Bada, G., Horváth, F., Dövényi, P., Szafián, P., Windhoffer, G., Cloetingh, S., 2007. Present-day stress field and tectonic inversion in the Pannonian Basin. *Global Planet. Change* 58, 165–180. doi:10.1016/j.gloplacha.2007.01.007.

Balázs, A., Burov, E., Matenco, L., Vogt, K., Francois, T., Cloetingh, S., 2017. Symmetry during the syn- and post-rift evolution of extensional back-arc basins: the role of inherited orogenic structures. *Earth Planet. Sci. Lett*. 462, 86-98.

Balázs, A., Magyar, I., Horváth, F., 2013. Stratigraphic and structural interpretation of regional seismic sections from the Pannonian Basin, 14th RCMNS congress, Istanbul, abstract book pp.191.

Balázs, A., Matenco, L., Magyar, I., Horváth, F., Cloetingh, S., 2016. The link between tectonics and sedimentation in back-arc basins: new genetic constraints from the analysis of the Pannonian Basin. *Tectonics* 35, 1526–1559. doi: 10.1002/2015TC004109

Balázs, A., Tőkés, L., Magyar, I., 2015. 3D analysis of compaction related tectonic and stratigraphic features of the Late Miocene succession from the Pannonian Basin. Abstract Book of 31st IAS Meeting of Sedimentology 1–52.

Báldi, K., L. Benkovics and O. Sztanó, 2002. Badenian (Middle Miocene) basin development in SW Hungary: subsidence history based on quantitative paleobathymetry of foraminifera.– *Int. J. Earth. Sci.*, 91, 490–504.

Báldi, T., 1986. Mid-Tertiary stratigraphy and Paleogeographic evolution of Hungary. Budapest, Akadémiai Kiadó, 201.

Balla, Z., 1986. Palaeotectonic reconstruction of the central Alpine-Mediterranean belt for the Neogene, *Tectonophysics*, *127*, 213-243.

Balla, Z., 1987. Tertiary palaeomagnetic data for the Carpatho-Pannonian region in the light of Miocene rotation kinematics, *Tectonophysics*, *139*, 67-98.

Baur, J., Sutherland, R., Stern, T., 2014. Anomalous passive subsidence of deep-water sedimentary basins: a prearc basin example, Southern New Caledonia trough and Taranaki Basin, New Zealand. *Basin Res*. 26, 242–268.

Bennett, R. A., S. Hreinsdóttir, G. Buble, T. Bašic, Ž. Bacic, M. Marjanović, G. Casale, A. Gendaszek, and D. Cowan, 2008. Eocene to present subduction of southern Adria mantle lithosphere beneath the Dinarides, *Geology*, 36, 3-6.

Bérczi, I., Phillips, R.L., 1985. Process and depositional environments within Neogene deltaic–lacustrine sediments, Pannonian Basin, Southeast Hungary. *Geophysical Transactions* 31, 55–74.

Bérczi, I., V. Dank, S. Gajdos, S. Pap, I. Révész, K. Szentgyörgyi, and L. Völgyi, 1987. Ablagerungen der Kunság-Stufe (Pannonien s. str.) auf der Grossen Ungarischen Tiefebene (Translated title: Depositional environments of the Kunság stage of the Great Hungarian Plain), *Annals of the Hungarian Geological Institute 69*, 179–211.

Brun, J.-P., 1999. Narrow rifts versus wide rifts: inferences for the mechanics of rifting from laboratory experiments. *Philosophical Transaction of the Royal Society London* 357, 695–710.

Brun, J.P., Faccenna, C., 2008. Exhumation of high-pressure rocks driven by slab rollback. *Earth Planet. Sci. Lett*. 272, 1–7. doi: 10.1016/j.epsl.2008.02.038.

Brun, J.P., Sokoutis, D., 2007. Kinematics of the southern Rhodope core complex (north Greece). *International Journal of Earth Sciences* 96, 1079-1099. doi: 10.1007/s00531-007-0174-2.

Brune, S., Heine, C., Perez-Gussinye, M., Sobolev, S.V., 2014. Rift migration explains continental margin asymmetry and crustal hyper-extension. *Nat. Commun*. 5 doi: 10.1038/ncomms5014

Burg, J.-P., Gerya, T., 2005. The role of viscous heating in Barrovian metamorphism of collisional orogens: thermomechanical models and application to the Lepontine Dome in the Central Alps. *J. Metamorph. Geol*.23, 75–95.

Burgess, P.M., Lammers, H., Van Oosterhout, C., Granjeon, D., 2006. Multivariate sequence stratigraphy: tackling complexity and uncertainty with stratigraphic forward modelling, multiple scenarios and conditional frequency maps. AAPG Bull. 90, 1883–1901.

Burov E., Poliakov A., 2001. Erosion and rheology controls on syn- and post-rift evolution: verifying old and new ideas using a fully coupled numerical model. – *J. Geophys. Res*. 106, 16461-16481.

Burov, E. B., and S. A. P. L. Cloetingh, 2009. Controls of mantle plumes and lithospheric folding on modes of intraplate continental tectonics: Differences and similarities, *Geophys. J. Int*., 178, 1691–1722.

Burov, E., 2007. The role of gravitational instabilities, density structure and extension rate in the evolution of continental margins. *Geol. Soc. London Spec. Publ*. 282, 139–156.

Burov, E., 2011. Rheology and strength of the lithosphere. *Marine and Petroleum Geology* 28, 1402-1443.

Burov, E., and L. Guillou-Frottier, 2005. The plume-head continental lithosphere interaction using a tectonically realistic formulation for the lithosphere, *Geophys. J. Int*., 58, doi:10.1111/j.136.-246x.2005.02588.x

Burov, E., Gerya, T., 2014. Asymmetric three-dimensional topography over mantle plumes. *Nature* 513, 85-89, doi:10.1038/nature13703

Burov, E., Poliakov, A., 2003. Erosional forcing of basin dynamics: new aspects of syn- and post-rift evolution. *Geol. Soc. Spec. Pub. London*, 212, 209-223.

Carroll, A. R., Bohacs, K. M., 1999. Stratigraphic classification of ancient lakes: balancing tectonic and climatic controls. *Geology* 27, 99-102.

Carson, M.A., Kirkby, M.J., 1972. Hillslope Form and Process. *Cambridge University Press*, Cambridge. 475 p.

Cartwright, J., Huuse, M., 2005. 3D seismic technology: the geological 'Hubble'. *Basin research,* 1-20.

Catuneanu, O., 2002. Sequence stratigraphy of clastic systems: Concepts, merits, and pitfalls, *Journal of African Earth Sciences*, 35, 1-43.

Catuneanu, O., V. Abreu, J.P. Bhattacharya, M.D. Blum, R.W. Dalrymple, P.G. Eriksson, C.R. Fielding, W.L. Fisher, W.E. Galloway, M.R. Gibling, K.A. Giles, J.M. Holbrook, R. Jordan, C.G.S.C. Kendall, B. Macurda, O.J. Martinsen, A.D. Miall, J.E. Neal, D. Nummedal, L. Pomar, H.W. Posamentier, B.R. Pratt, J.F. Sarg, K.W. Shanley, R.J. Steel, A. Strasser, M.E. Tucker, and C. Winker, 2009. Towards the standardization of sequence stratigraphy, *Earth-Science Reviews,* 92, 1–33.

Catuneanu, O., W.E. Galloway, C.G.S.C. Kendall, A.D. Miall, H.W. Posamentier, A. Strasser, and M.E. Tucker, 2011. Sequence Stratigraphy: Methodology and Nomenclature. *Newsletters on Stratigraphy,* 44, 173-245.

Chopra, S. and K. Marfurt, 2005. Seismic attributes- a histor ical perspective, *Geophysics*, 70, 3SO-28SO.

Clevis, Q., De Boer, P.L., Nijman, W., 2004. Differentiating the effect of episodic tectonism and eustatic sea-level fluctuations in foreland basins filled by alluvial fans and axial deltaic systems: insights from a three-dimensional stratigraphic forward model. *Sedimentology* 51, 809–835. doi:10.1111/j.1365-3091.2004.00652.x.

Cloetingh, S., Bada, G., Matenco, L., Lankreijer, A., Horváth, F., and Dinu, C., 2006. Modes of basin (de)formation, lithospheric strength and vertical motions in the Pannonian–Carpathian system: inferences from thermo-mechanical modelling. In Gee, D. and Stephenson, R., editors, European Lithosphere Dynamics, *Geological Society of London*, 207–221.

Cloetingh, S., Burov, E., Matenco, L., Beekman, F., Roure, F., Ziegler, P.A., 2013. The Moho in extensional tectonic settings: Insights from thermo-mechanical models. *Tectonophysics* 609, 558-604.

Cloetingh, S., Haq, B.U., 2015. Inherited landscapes and sea level change. *Science* 347(6220).

Cloetingh, S., Van Wees, J. D., Ziegler, P., Lenkey, L., Beekman, F., Tesauro, M., Förster, A., Norden, B., Kaban, M., Hardebol, N., Bonté, D., Genter, A., Guillou-Frottier, L., Voorde, M. T., Sokoutis, D., Willingshofer, E., Cornu, T., and Worum, G., 2010. Lithosphere tectonics and thermo-mechanical properties: An integrated modelling approach for Enhanced Geothermal Systems exploration in Europe, *Earth-Sci. Rev*. 102, 159–206, 2010.

Cloetingh, S., Willett, S.D., 2013. TOPO-EUROPE: Understanding of the coupling between the deep Earth and continental topography, *Tectonophysics*, 602, 1-14.

Comas, M. C., V. Garcias, and M. J. Jurado, 1992. Neogene extensional tectonic evolution of the Alboran Basin from MCS data, *Geomarine Letters*, *12*. 157-164.

Contreras, J., Scholz, C.H., King, G.C.P., 1997. A model of rift basin evolution constrained by first-order stratigraphic observations. *J Geoph. Res*. 102, 7673-7690.

Corti, G., Bonini, M., Conticelli, S., Innocenti, F., Manetti, P., Sokoutis, D., 2003. Analogue modelling of continental extension: a review focused on the relations between the patterns of deformation and the presence of magma. *Earth-Sci. Rev*. 63, 169–247.

Créon, L., Rouchon, V., Youssef, S., Rosenberg, E., Delpech, G., Szabó, Cs., Remusat, L., Mostefaoui, S., Asimow, P.D., Antoshechkina, P.M., Ghiorso, M.S., Boller, E., Guyot, F., 2017. Highly CO2-supersaturated melts in the Pannonian lithospheric mantle – A transient carbon reservoir?, *Lithos*, in press.

Csató, I., 1993. Neogene sequences in the Pannonian Basin, Hungary. *Tectonophysics,* 226, 377–400.

Csató, I., Granjeon, D., Catuneanu, O., Baum, G.R., 2013. A three-dimensional stratigraphicmodel for the Messinian crisis in the Pannonian Basin, eastern Hungary. *Basin Res*. 25, 121-148.

Csató, I., Toth, S., Catuneanu, O., Granjeon, D., 2015. A sequence stratigraphic model for the Upper Miocene-Pliocene basin fill of the Pannonian Basin, eastern Hungary. Mar. Petroleum Geol. 66, 117-134.

Csontos, L., 1995. Tertiary tectonic evolution of the Intra-Carpathian area: a review, *Acta Vulcanologica*, *7*, 1-13.

Csontos, L., and A. Vörös, 2004. Mesozoic plate tectonic reconstruction of the Carpathian region, *Palaeogeography, Palaeoclimatology, Palaeoecology*, *210*, 1-56.

Csontos, L., Nagymarosy, A., 1998. The Mid-Hungarian line: a zone of repeated tectonic inversions, *Tectonophysics* 29, 51-71.

Culling, W., 1960. Analytical theory of erosion. *J. Geol*. 68, 366–344.

Cvetkovic, V., H. Downes, D. Prelevic, M. Lazarov, and K. Resimic-Saric, 2007. Geodynamic significance of ultramafic xenoliths from Eastern Serbia: Relics of sub-arc oceanic mantle?, *Journal of Geodynamics*, *43*, 504-527.

de Leeuw, A., Mandic, O., Krijgsman, W., Kuiper, K., Hrvatović, H., 2012. Paleomagnetic and geochronologic constraints on the geodynamic evolution of the Central Dinarides. *Tectonophysics* 530—531, 286—298.

de Leeuw, A., S. Filipescu, L. Maţenco, W. Krijgsman, K. Kuiper, and M. Stoica, 2013. Paleomagnetic and chronostratigraphic constraints on the Middle to Late Miocene evolution of the Transylvanian Basin (Romania): Implications for Central Paratethys stratigraphy and emplacement of the Tisza–Dacia plate, *Global and Planetary Change*, *103*, 82-98.

de Leeuw, J., Eggenhuisen, J.T., Cartigny, M.J.B., 2016. Morphodynamics of submarine channel inception revealed by new experimental approach. *Nature Com*., 7, 10886. doi:10.1038/ncomms10886

Dewey, J. F., 1980. Episodicity, sequence and style at convergent plate boundaries, in *The Continental Crust and Its Mineral Deposits*, edited by D. W. Strangway, pp. 553-573, *Geol. Assoc. Canada*, Waterloo, Ontario.

Dimitrijević, M. D., 1997. Geology of Yugoslavia, 2nd ed., 187 pp., Geoinstitute, Belgrade.

Dombrádi, E., Sokoutis, D., Bada, G., Cloetingh, S., Horváth, F., 2010. Modelling recent deformation of the Pannonian lithosphere: Lithospheric folding and tectonic topography, *Tectonophysics* 484, 103-118.

Dövényi, P., 1994. Geofizikai vizsgálatok a Pannon-medence litoszférafejlődésének megértéséhez. Candidate thesis, Hungarian Academy of Sciences, Budapest, 127 p.

Dunbar, J.A., Sawyer, D.S., 1988. Continental rifting at pre-existing lithospheric weakness. *Nature* 333, 450–452.

Dunkl, I., B. Grasemann, and W. Frisch, 1998. Thermal effects of exhumation of a metamorphic core complex on hanging wall syn-rift sediments: an example from the Rechnitz Window, Eastern Alps, *Tectonophysics*, *297*, 31-50.

Ellis, G.A., Densmore, A.L., Anderson, R.S., 1999. Development of mountainous topography in the Basin Ranges, USA. *Basin Res.* 11, 21–41.

Ellouz, N. and E. Rocca, 1994. Palinspastic reconstruction of the Carpathians and adjacent areas since the Cretaceous: a quantitative approach. In: Roure, F. (ed.) Peri-Tethyan Platforms. *Editions Technip*, Paris, 51-78.

Embry, A.F., Johannessen, E., 1992. T-R Sequence Stratigraphy, Facies Analysis and Reservoir Distribution in the Uppermost Triassic-Lower Jurassic Succession, Western Sverdrup Basin, Arctic Canada. In: Arctic Geology and Petroleum Potential (Ed. by T. Vorren), 2. *Norwegian Petroleum Society Special Publication*.

Faccenna, C., Becker, T. W., Auer, L., Billi, A., Boschi, L., Brun, J. P., Capitanio, F. A., Funiciello, F., Horvàth, F., Jolivet, L., 2014. Mantle dynamics in the Mediterranean. *Rev. Geophys*. 52, 283–332, doi:10.1002/2013RG000444.

Faccenna, C., L. Civetta, M. D'Antonio, F. Funiciello, L. Margheriti, and C. Piromallo, 2005. Constraints on mantle circulation around the deforming Calabrian slab, *Geophysical Research Letters*, *32*, L06311, doi:06310.01029/02004GL021874.

Fodor, L., A. Gerdes, I. Dunkl, B. Koroknai, Z. Pécskay, M. Trajanovas, P. Horváth, M. Vrabec, B. Jelen, K. Balogh, and W. Frisch, 2008. Miocene emplacement and rapid cooling of the Pohorje pluton at the Alpine-Pannonian-Dinaridic junction, Slovenia, *Swiss Journal of Geosciences*, *101*, 255-271.

Fodor, L., B. Jelen, E. Márton, D. Skaberne, J. Čar, and M. Vrabec, 1998. Miocene-Pliocene tectonic evolution of the Slovenian Periadriatic fault: Implications for Alpine-Carpathian extrusion models, *Tectonics, 17*, 690-709.

Fodor, L., Bada, G., Csillag, G., Horvath, E., Ruszkiczay-Rudiger, Z., Palotas, K., Sikhegyi, F., Timar, G., Cloetingh, S., 2005. An outline of neotectonic structures and morphotectonics of the western and central Pannonian Basin, *Tectonophysics* 410, 15-41.

Fodor, L., L. Csontos, G. Bada, I. Györfi, and L. Benkovics, 1999. Tertiary tectonic evolution of the Pannonian basin system and neighbouring orogens: a new synthesis of paleostress data, in B. Durand, L. Jolivet, F. Horvath and M. Seranne (Eds.) *The Mediteranean basins: Tertiary extension within the Alpine orogen*, pp. 295-334, The Geological Society, London.

Fodor, L., O. Sztanó, I. Magyar, B. Törő, A. Uhrin, A. Várkonyi, G. Csillag, Sz. Kövér, Z. Lantos, and L. Tőkés, 2013. Late Miocene depositional units and syn-sedimentary deformation in the western Pannonian basin, Hungary, 11th Workshop on Alpine Geological Studies abstract book, Schuster, R. (eds), *Berichte der Geologischen Bundesanstalt*, 99, 33–34.

Francois, T., Burov, E., Meyer, B., Agard, P., 2013. Surface topography as key constraint on thermo-rheological structure of stable cratons. *Tectonophysics* 602, 106–123, doi:10.1016/j.tecto.2012.10.009.

Fügenschuh, B., and S. M. Schmid, 2005. Age and significance of core complex formation in a very curved orogen: Evidence from fission track studies in the South Carpathians (Romania), *Tectonophysics*, 404, 33–53, doi:10.1016/j.tecto.2005.03.019.

Fügenschuh, B., D. Seward, and N. Mancktelow, 1997. Exhumation in a convergent orogen: the western Tauern window, *Terra Nova*, *9*, 213-217.

Funiciello, F., M. Moroni, C. Piromallo, C. Faccenna, A. Cenedese, and H. A. Bui, 2006. Mapping mantle flow during retreating subduction: Laboratory models analyzed by feature tracking, *J. Geophys. Res*., 111, B03402, doi:10.1029/2005JB003792.

Gagała, Ł., J. Verges, E. Saura, T. Malata, J.C. Ringenbach, P. Werner, and P. Krzywiec, 2012. Architecture and orogenic evolution of the northeastern Outer Carpathians from cross-section balancing and forward modeling, *Tectonophysics*, 532–535, 223–241.

Gálfi, J., Stegena, L., 1955. Deep reflections in the region of Hajdúszoboszló. *Geofizikai közlemények* 6, 53-60. (in Hungarian with English abstract).

Garcia-Castellanos, D., Verges, J., Gaspar-Escribano, J., Cloetingh, S., 2003. Interplay between tectonics, climate, and fluvial transport during the Cenozoic evolution of the Ebro Basin (NE Iberia). *J. Geophys. Res*. 108, 2347.

Gong, C., Steel, R., Wang, Y., Lin, C., Olariu, C., 2016. Shelf-margin architecture variability and its role in sediment-budget partitioning into deep-water areas. *Earth-Science Reviews* 154, 72-101.

Govers, R., and M. J. R. Wortel, 2005. Lithosphere tearing at STEP faults: Response to edges of subduction zones, *Earth Planet. Sci. Lett., 236*, 505–523.

Granjeon, D., 1997. Modelisation stratigraphique deterministe: conception et applications d'un modele diffusif 3D multilithologique. These de Doctorat. Universite de Rennes 1.

Granjeon, D., 2014. 3D forward modelling of the impact of sediment transport and base level cycles on continental margins and incised valleys. *Int. Assoc. Sedimentol. Spec. Publ*. 46, 453–472.

Griffiths, C.M., Dyt, C., Paraschivoiu, E. and Liu, K., 2001. Sedsim in hydrocarbon exploration. In: Geologic Modelling and Simulation (Eds. D. Merriam and J.C. Davis), pp 71–97. Kluwer Academic, New York.

Grow J.A., Mattick R.E., Bérczi-Makk A., Péró Cs., Hajdú D., Pogácsás Gy., Várnai P., Varga E., 1994. Structure of the Békés Basin Inferred from Seismic Reflection, Well and Gravity Data. In: Teleki, et al. (Eds.), Basin Analysis in Petroleum Exploration. Kluwer Academic Publishers, Dordecht, 201–218.

Gupta, S., Cowie, P.A., Dawers, N.H., Underhill, J.R., 1998. A mechanism to explain rift-basin subsidence and stratigraphic patterns through fault array evolution. *Geology* 26, 595–598.

Gvirtzman, Z., Csató, I., Granjeon, D., 2014. Constraining sediment transport to deep marine basins through submarine channels: the Levant margin in the Late Cenozoic. *Mar. Geol*. 347, 12–26.

Haas, J., and C. Péró, 2004. Mesozoic evolution of the Tisza Mega-unit, *International Journal of Earth Sciences*, *93*, 297-313.

Haas, J., T. Budai, L. Csontos, L. Fodor, Gy. Konrád (eds.), 2010. Magyarországprekainozoos földtani térképe 1:500000 (Translated title: Pre-Cenozoic geological map of Hungary 1:500000), Geological Institute of Hungary (in Hungarian).

Hámor, G., 1985. Geology of the Nógrád–Cserhát area, *Geologica Hungarica*, *22*, 1-307.

Handy, M.R., K. Ustaszewski, and E. Kissling, 2015. Reconstructing the Alps–Carpathians–Dinarides as a key to understanding switches in subduction polarity, slab gaps and surface motion, *International Journal of Earth Sciences, 104*, 1-26, DOI 10.1007/s00531-014-1129 1060-3

Harangi, Sz., Jankovics, M.É., Sági, T., Kiss, B., Lukas, R., Soós, I., 2015. Origin and geodynamic relationships of the late Miocene to quaternary alkaline basalt volcanism in the Pannonian basin, eastern-central Europe. *International Journal of Earth Sciences* 104. doi:10.1007/s00531–014–1105-7.

Harangi, Sz., Lenkey, L., 2007. Genesis of the Neogene to Quaternary volcanism in the Carpathian-Pannonian region: Role of subduction, extension, and mantle plume, *Geological Society of America Special Papers*, *418*, 67-92.

Helland-Hansen, W., Hampson, G.J., 2009. Trajectory analysis: concepts and applications. *Basin Research* 21, 454–483.

Helland-Hansen, W., Martinsen, O.J., 1996. Shoreline trajectories and sequences: description of variable depositional-dip scenarios. *J. Sediment. Res*. 66, 670-688.

Henriksen, S., Helland-Hansen, W., Bullimore, S., 2011. Relationship between shelfedge trajectories and sediment dispersal along depositional dip and strike: a different approach to sequence stratigraphy. *Basin Research* 23, 3–21.

Hetényi, Gy., Molinari, I., Clinton, J., Kissling, E., 2016. The AlpArray Seismic Network: current status and next steps. *Geophysical Research Abstracts* Vol. 18, EGU2016-11744, 2016, EGU General Assembly 2016.

Hetényi, Gy., Renc, Y., Dando, B., Stuart, G.W., Hegedűs, E., Kovács, A.Cs., Houseman, G.A., 2015. Crustal structure of the Pannonian Basin: The AlCaPa and Tisza Terrains and the Mid-Hungarian Zone. *Tectonophysics* 646, 106-116. doi: 10.1016/j.tecto.2015.02.004

Hinsken, S., K. Ustaszewski, and A. Wetzel, 2007. Graben Width Controlling Syn-Rift Sedimentation: The Palaeogene Southern Upper Rhine Graben as an Example. *International Journal of Earth Sciences*, 96, 979-1002.

Horváth, F., 1995. Phases of compression during the evolution of the Pannonian basin and its bearing on hydrocarbon exploration. *Marine and Petroleum Geology* 12, 837-844.

Horváth, F., and J. Rumpler, 1984. The Pannonian basement: extension and subsidemce of an Alpine orogen, *Acta Geologica Hungaria*, *27*, 229-235.

Horváth, F., Bada, G., Windhoffer, G., Csontos, L., Dombrádi, E., Dövényi, P., Fodor, L., Grenerczy, Gy, Síkhegyi, F., Szafián, P., Székely, B., Timár, G., Tóth, L., Tóth, T., 2006. A Pannon-medence jelenkori geodinamikájának atlasza: Euro-konform térképsorozat és magyarázó. *Magyar Geofizika* 47, 133–137.

Horváth, F., Berckhemer, H., 1982. Mediterranean backarc basins, in Alpine-Mediterranean Geodynamics, *Geodyn. Ser*., vol. 7, edited by H. Berckhemer, K. Hsü, pp. 141–173, AGU, Washington, D. C.

Horváth, F., Cloetingh, S., 1996. Stress-induced late-stage subsidence anomalies in the Pannonian basin, *Tectonophysics* 266, 287-300.

Horváth, F., G. Bada, P. Szafian, G. Tari, A. Adam, and S. Cloetingh, 2006. Formation and deformation of the Pannonian Basin: constraints from observational data, *Geological Society, London, Memoirs*, *32*(1), 191-206.

Horváth, F., Musitz, B., Balázs, A., Végh, A., Uhrin, A., Nádor, A., Koroknai, B., Pap, N., Tóth, T., Wórum, G., 2015. Evolution of the Pannonian basin and its geothermal resources. *Geothermics* 53, 328-352.

Houseman, G.A., and L. Gemmer, 2007. Intra-orogenic extension driven by gravitational instability: Carpathian–Pannonian orogeny, *Geology, 35,* 1135–1138.

Huet, B., Pourhiet, L.L., Labrousse, L., Burov, E., Jolivet, L., 2011. Post-orogenic extension and metamorphic core complexes in a heterogeneous crust, the role of pre-existing nappes. *Geophys. J. Int*. 184, 611–625. http://dx.doi.org/10.1111/j.1365-246X.2010.04849.x.

Huismans, R. S., Beaumont, C., 2003. Symmetric and asymmetric lithospheric extension: Relative effects of frictional-plastic and viscous strain softening. *J. Geophys. Res*. 108, 2496. doi:10.1029/2002JB002026.

Huismans, R., and C. Beaumont, 2011. Depth-dependent extension, two-stage breakup and cratonic underplating at rifted margins, *Nature*, *473*(7345), 74-78.

Huismans, R.S., Podladchikov, Y.Y., Cloetingh, S., 2001. Dynamic modelling of the transition from passive to active rifting, application to the Pannonian basin. *Tectonics* 20, 1021–1039.

Janik, T., M. Grad, A. Guterch, J. Vozár, M. Bielik, A. Vozárova, E Hegedus, A. Kovacs,I. Kovács, and G.R. Keller, 2011. CELEBRATION 2000 Working Group, Crustalstructure of the Western Carpathians and Pannonian Basin: Seismic modelsfrom CELEBRATION 2000 data and geological implications. *J. Geodynamics* 52,97–113.

Jarosinski, M., Beekman, F., Matenco, L., Cloetingh, S., 2011. Mechanics of basin inversion: Finite element modelling of the Pannonian Basin System, *Tectonophysics* 502, 121-145.

Johannessen, E.P., and Steel, R.J., 2005. Shelf-margin clinoforms and prediction of deepwater sands. *Basin Res*. 17, 521–550.

Johnson, J.G. and M.A. Murphy, 1984. Time-Rock Model for Siluro-Devonian Continental Shelf, Western United States, *Geological Society of America Bulletin*, 95, 1349-1359.

Jolivet, L., Faccenna, C., Huet, B., Labrousse, L., Le Pourhiet, L., Lacombe, O., Lecomte, E., Burov, E., Denele, Y., Brun, J.P., Philippon, M., Paul, A., Salaun, G., Karabulut, H., Piromallo, C., Monie, P., Gueydan, F., Okay, A.I., Oberhansli, R., Pourteau, A., Augier, R., Gadenne, L., Driussi, O., 2013. Aegean tectonics: strain localisation, slab tearing and trench retreat. *Tectonophysics* 597, 1–33.

Jolivet, L., J.P., Brun, 2010. Cenozoic geodynamic evolution of the Aegean region. *International Journal of Earth Sciences* 99, 109–138. doi:10.1007/s00531-008-0366-4.

Juhász Gy., Pogácsás Gy., Magyar I., Hatalyák P. 2013. The Alpar canyon system in the Pannonian Basin, Hungary – its morphology, infill and development. *Global Planet. Change*, 103, 174–192.

Juhász, Gy, Pogácsás, Gy, Magyar, I., Vakarcs, G., 2007. Tectonic versus climatic control on the evolution of fluvio–deltaic systems in a lake basin, Eastern Pannonian Basin. *Sedimentary Geology* 202, 72–95.

Juhász, Gy., 1991. Lithostratigraphical and sedimentological framework of the Pannonian (s.l.) sedimentary sequence in the Hungarian Plain (Alföld), Eastern Hungary, *Acta Geologica Hungarica* 34, 53–72.

Karamata, S., 2006. The geological development of the Balkan Peninsula related to the approach, collision and compression of Gondwanan and Eurasian units, in *Tectonic Development of the Eastern Mediterranean Region*, edited by A. H. F. Robertson and D. Mountrakis, pp. 155-178, *Geological Society, London, Special Publications*.

Karátson, D., Németh, K., Székely, B., Ruszkiczay-Rudiger, Zs., Pécskay, Z., 2006. Incision of a river curvature due to exhumed Miocene volcanic landforms: Danube Bend, Hungary. *Int. J. Earth Sci*., 95, 929–944.

Katz, B.J., 1990. Lacustrine basin exploration – Case Studies and Modern Analogues: *American Association of Petroleum Geologists Memoir* 50, 340p.

Kim, Y., Kim, W., Cheong, D., Muto, T., Pyles, D.R., 2013. Piping coarse-grained sediment to a deep water fan through a shelf-edge delta bypass channel: Tank experiments. *J Geophys. Res.: Earth Surface* 118, 2279-2291., doi:10.1002/2013JF002813

Király, Á., F. Horvath, and G. Tari, 2012. Revisiting the anomalous crustal structure of the Pannonian Basin, 29th IAS Meeting of Sedimentology, Schladming

Kiss, J., 2006. Magyarország gravitációs Bouguer-anomália térképe, Bouguer gravity map of Hungary, *Geophysical Transactions* 45/2, 99–104

Kiss, J., 2009. A CEL08 szelvény geofizikai vizsgálata. Magyar Geofizika (Translated title: Study of the geophysical data along the CEL08 deep seismic litospheric profile). *Hungarian Geophysics* 50, 59–74.

Kiss, J., and A. Gulyás, 2006. Magyarország mágneses DZ-anomália térképe, 1:500 000 (Translated title: Magnetic DZ anomaly map of Hungary 1:500000), *ELGI*, www.mfgi.hu (in Hungarian)

Koroneos, A., G. Poli, V. Cvetkovi, G. Christofides, D. Krsti, and Z. Pécskay (2011), Petrogenetic and tectonic inferences from the study of the Mt Cer pluton (West Serbia), *Geological Magazine*, *148*, 89-111.

Kőrössy, L., 1992. A Duna-Tisza koze koolaj- es foldgazkutatasanak foldtani eredmenyei (Translated title: Hydrocarbon geology of the Duna–Tisza interfluve, Hungary), *Általános Földtani Szemle*, 26, 3–162. (in Hungarian)

Kovác, M., Andreyeva-Grigorovich, A., Bajraktarevic, Z., Brzobohatý, R., Filipescu, S., Fodor, L., Harzhauser, M., Nagymarosy, A., Oszczypko, N., Pavelic, D., 2007. Badenian evolution of the Central Paratethys Sea: paleogeography, climate and eustatic sea-level changes, *Geologica Carpathica* 58, 579-606.

Kováč, M., P. Kováč, F. Marko, S. Karoli, and J. Janočko 1995. The East Slovakian Basin: A complex back-arc basin, *Tectonophysics*, 252, 453–466, doi:10.1016/0040-1951(95)00183-2.

Kovács, I., Falus, G., Stuart, G., Hidas, K., Szabó, Cs., Flower, MFJ., Hegedus, E., Posgay, K., Zilahi-Sebess, L., 2012. Seismic anisotropy and deformation patterns in upper mantle xenoliths from the central Carpathian–Pannonian region: asthenospheric flow as a driving force for Cenozoic extension and extrusion? *Tectonophysics* 514–517, 168–179.

Krézsek, C., Filipescu, S., Silye, L., Matenco, L., Doust, H., 2010. Miocene facies associations and sedimentary evolution of the Southern Transylvanian Basin (Romania): Implications for hydrocarbon exploration. *Marine and Petroleum Geology* 27, 191-214.

Krstić, N., L. Savić, G. Jovanović, and E. Bodor, 2003. Lower Miocene lakes of the Balkan Land, *Acta Geologica Hungarica*, 46, 291-299.

Lankreijer, A., M. Kovac, S. Cloetingh, P. Pitonak, M. Hloska, and C. Biermann, 1995. Quantitative subsidence analysis and forward modelling of the Vienna and Danube basins; thin-skinned versus thick-skinned extension, *Tectonophysics*, *252*, 1-4.

Le Pourhiet, L., Burov, E., Moretti, I., 2004. Rifting through a stack of inhomogeneous thrusts (the dipping pie concept). *Tectonics* 23, TC4005, doi:10.1029/2003TC001584.

Leeder, M., Harris, T., Kirkby, M., 1998. Sediment supply and climate change: implications for basin stratigraphy. *Basin Res*. 10, 7–18.

Leever, K.A., Matenco, L., Garcia-Castellanos, D., Cloetingh, S.A.P.L., 2011. The evolution of the Danube gateway between Central and Eastern Paratethys (SE Europe): insight from numerical modelling of the causes and effects of connectivity between basins and its expression in the sedimentary record. *Tectonophysics* 502, 175–195.

Lelkes-Felvári, G., R. Schuster, W. Frank, and R. Sassi 2005. Metamorphic history of the Algyo High (Tisza Mega-unit, basement of Great Hungarian Plain)—A counterpart of crystalline units of the Koralpe–Wölz nappe system (Austroalpine, Eastern Alps), *Acta Geol. Hung*., 48(4), 371–394, doi:10.1556/AGeol.48.2005.4.2.

Lemberkovics, V., 2014. Lessons from combination of modern 3D seismic and historical well data: development of a gilbert-delta, late Early Miocene Trough, Hungary, *CEMSEG conference abstract book*

Lemberkovics, V., Á. Bárány, I. Gajdos, and M. Vincze 2005. A szekvencia-sztratigrafiai esemenyek es a tektonika kapcsolata a Derecskei-arok pannoniai retegsoraban (Translated title: Connection of sequence stratigraphy and tectonics in the Pannonian strata of the Derecske Trough), *Földtani Kutatás*, 42, 16-24. (in Hungarian)

Lenkey, L., 1999. Geothermics of the Pannonian Basin and its bearing on the tectonics of basin evolution, PhD thesis, 215 pp, Vrije Universiteit Amsterdam.

Lenkey, L., Dovenyi, P., Horvath, F., Cloetingh, S.A.P.L., 2002. Geothermics of the Pannonian Basin and its bearing on neotectonic, in: Cloetingh, S., Horvath, F., Bada, G., Lankreijer, A. (Eds.), Neotectonics and surface processes: the Pannonian Basin and Alpine/Carpathians System. European Geosciences Union, *Stephan Mueller Special Publications* 3, pp. 29-40.

Li, Z.H., Xu, Z.Q., Gerya, T.V., 2011. Flat versus steep subduction: contrasting modes for the formation and exhumation of high- to ultrahigh-pressure rocks in continental collision zones. *Earth Planet. Sci. Lett*. 301, 65–77.

Liao, J, Gerya, T., 2014. Influence of lithospheric mantle stratification on craton extension: Insight from two-dimensional thermo-mechanical modelling. *Tectonophysics* 631, 50-64

Magara, K., 1978. Compaction and fluid migration. Amsterdam/New York, Elsevier, p. 1-349.

Magyar I., Radivojević D., Sztanó O., Synak R., Ujszászi K., Pócsik M., 2013. Progradation of the paleo-Danube shelf margin across the Pannonian Basin during the Late Miocene and Early Pliocene. *Global Planet. Change* 103, 168–173.

Magyar, I., A. Fogarasi, G. Vakarcs, L. Bukó, and G.C. Tari, 2006. The largest hydrocarbon field discovered to date in Hungary: Algyő. In: Golonka, J., Picha, F.J. (Eds.), The Carpathians and their foreland: geology and hydrocarbon resources: *AAPG Memoir* 84, pp. 619–632.

Magyar, I., Geary, D. H., Müller, P., 1999. Paleogeographic evolution of the Late Miocene Lake Pannon in Central Europe, *Palaeogeography, Palaeoclimatology, Palaeoecology* 147, 151-167.

Magyar, I., Sztanó, O., 2008. Is there a Messinian unconformity in the Central Paratethys?, *Stratigraphy* 5(3-4), 245-255.

Malinowski. M, A. Guterch, M. Narkiewicz, J. Probulski, A. Maksym, M. Majdanski, P. Sroda, W. Czuba, E. Gaczynski, M. Grad, T. Janik, L. Jankowski, A. Adamczyk, 2013. Deep seismic reflection profile in Central Europe reveals complex pattern of Paleozoic and Alpine accretion at the East European Craton margin, *Geophys Research Letters*, 40, 3841–3846.

Manatschal, G., L. Lavier, and P. Chenin, 2015. The role of inheritance in structuring hyperextended rift systems: Some considerations based on observations and numerical modeling, *Gondwana Res.*, 27, 140-164.

Martin, M., and F. Wenzel, 2006. High-resolution teleseismic body wave tomography beneath SE-Romania - II. Imaging of a slab detachment scenario, *Geophysical Journal International*, 164, 579-595.

Martins-Neto, M.A., Catuneanu, O., 2010. Rift Sequence Stratigraphy. *Mar. Pet. Geol*. 27, 247-253.

Márton, E., M. Tischler, L. Csontos, B. Fügenschuh, and S. Schmid, 2007. The contact zone between the ALCAPA and Tisza-Dacia mega-tectonic units of Northern Romania in the light of new paleomagnetic data, *Swiss Journal of Geosciences*, *100*, 109-124.

Márton, E.,. Fodor, L., 2003. Tertiary paleomagnetic results and structural analysis from the Transdanubian Range (Hungary): rotational disintegration of the Alcapa unit, *Tectonophysics* 363, 201-224.

Matenco, L., and G. Bertotti, 2000. Tertiary tectonic evolution of the external East Carpathians (Romania), *Tectonophysics*, *316*, 255-286.

Matenco, L., Andriessen, P., the SourceSink Network, 2013. Quantifying the mass transfer from mountain ranges to deposition in sedimentary basins: source to sink studies in the Danube Basin–Black Sea system. *Glob. Planet. Chang*. 103, 1–18.

Matenco, L., C. Krézsek, S. Merten, S. Schmid, S. Cloetingh, and P. Andriessen, 2010. Characteristics of collisional orogens with low topographic build-up: an example from the Carpathians, *Terra Nova*, *22*, 155-165.

Matenco, L., Munteanu, I., ter Borgh, M., Stanica, A., Tilita, M., Lericolais, G., Dinu, C., Oaie, G., 2016. The interplay between tectonics, sediment dynamics and gateways evolution in the Danube system from the Pannonian Basin to the western Black Sea, *Science of The Total Environment* 543, 807-827. doi: 10.1016/j.scitotenv.2015.10.081

Matenco, L., Radivojević, D., 2012. On the formation and evolution of the Pannonian Basin: Constraints derived from the structure of the junction area between the Carpathians and Dinarides, *Tectonics* 31(6), TC6007.

Menant, A., Sternai, P., Jolivet, L., Guillou-Frottier, L., Gerya, T., 2016. 3D numerical modeling of mantle flow, crustal dynamics and magma genesis associated with slab roll-back and tearing: The eastern Mediterranean case. *Earth Planet. Sci. Lett*. 442, 93-107.

Merten, S., L. Matenco, J. P. T. Foeken, F. M. Stuart, and P. A. M. Andriessen, 2010. From nappe stacking to out-of-sequence postcollisional deformations: Cretaceous to Quaternary exhumation history of the SE Carpathians assessed by low-temperature thermochronology, *Tectonics*, *29*, TC3013.

Mészáros, F. Zilahi-Sebess, L., 2001. Compaction of sediments with great thickness in the Pannonian Basin, *Geophysical Transactions* 44, 21 – 48.

Miall, A.D. and C.E. Miall, 2001. Sequence Stratigraphy as a Scientific Enterprise: The Evolution and Persistence of Conflicting Paradigms, *Earth-Science Reviews*, 54, 321-348.

Nagymarosy, A., Hámor, G., 2012. Genesis and evolution of the Pannonian Basin, in Geology of Hungary, *Regional Geology Reviews*, edited by J. Haas, pp. 149-200, Springer.

Nagymarosy, A., Müller, P., 1988. Some aspects of the Neogene biostratigraphy in the Pannonian Basin. in: The Pannonian Basin, a study in basin evolution, edited by L. H. Royden and F. Horvath, pp. 58-68.

Naliboff, J., Buiter, S.J.H., 2015. Rift reactivation and migration during multiphase extension. *Earth Planet. Sci. Lett*. 421, 58–67.

Nixon, C.W. et al., 2016. Rapid spatiotemporal variations in rift structure during development of the Corinth Rift, central Greece. *Tectonics* 35, doi: 10.1002/2015TC004026.

Nottvedt, A. R.H. Gabrielsen, and R.J. Steel, 1995. Tectonostratigraphy and Sedimentary Architecture of Rift Basins, with reference to the Northern North Sea. *Marine and Petroleum Geology*, 12**,** 881-901.

Pálfy, J., R. Mundil, P. R. Renne, R. L. Bernor, L. Kordos, and M. Gasparik 2007. U–Pb and 40Ar/39Ar dating of the Miocene fossil track site at Ipolytarnóc (Hungary) and its implications, *Earth and Planetary Science Letters*, *258*, 160-174.

Partyka, G., Gridley, J., Lopez, J., 1999. Interpretational applications of spectral decomposition in reservoir characterization. *The Leading Edge* 18, 353–360.

Pavelić, D., 2001. Tectonostratigraphic model for the North Croatian and North Bosnian sector of the Miocene Pannonian Basin System, *Basin Research*, *13*, 359-376.

Pavelic, D., R. Avanic, K. Bakrac, and D. Vrsaljko, 2001. Early Miocene braided river and lacustrine sedimentation in the Kalnik Mountain area (Pannonian Basin System, NW Croatia), *Geologica Carpathica*, *52*, 375-386.

Pécskay, Z., Lexa, J., Szakács, A., Seghedi, I., Balogh, K., Konecny, V., Zelenka, T., Kovacs,M., Póka, T., Fülöp, A., Márton, E., Panatiotu, C., Cvetkovic, V., 2006. Geochronol-ogy of Neogene magmatism in the Carpathian arc and intra-Carpathian area. *Geol. Carpathica* 57, 511–530.

Pereira, R. and T.M. Alves, 2012. Tectono-Stratigraphic Signature of Multiphased Rifting on Divergent Margins (Deep-Offshore Southwest Iberia, North Atlantic), *Tectonics*, 31**,** TC4001

Petersen, K.D., Nielsen, S.B., Clausen, O.R., Stephenson, R., Gerya, T., 2010. Small-scale mantle convection produces stratigraphic sequences in sedimentary basins. *Science* 329, 827–830.

Pezelj, D., O. Mandic and S. Coric, 2013. Paleoenvironmental dynamics in the southern Pannonian Basin during initial Middle Miocene marine flooding, *Geologica Carpathica*, 64, 1, 81—100, doi: 10.2478/geoca-2013-0006

Pharaoh, T.C., 1999. Paleozoic terranes and their lithospheric boundaries within the Trans-European Suture Zone (TESZ): a review, *Tectonophysics*, 314, 17-41.

Pigott, J., Radivojević, D., 2010. Seismic stratigraphy based chronostratigraphy (SSBC) of the Serbian Banat region of the Pannonian Basin. *Cent. Eur. J. Geosci*. 2, 481–500, doi:10.2478/v10085-010-0027-2.

Piller, W. E., M. Harzhauser, and O. Mandic, 2007. Miocene Central Paratethys stratigraphy - current status and future directions, *Stratigraphy*, *4*(2-3), 151-168.

Pinter, N., Grenerczy, G., Weber,, J., Stein, S., Medak D., (Eds.), 2005. The Adria Microplate: GPS Geodesy, Tectonics and Hazards (Nato Science Series: IV: Earth and Environmental Sciences), 413 pp., Springer.

Pogácsás, Gy., Lakatos, L., Révész, I., Ujszászi, K., Vakarcs, G., Várkonyi, L., Várnai, P., 1988. Seismic facies, electro facies and Neogene sequence chronology of the Pannonian Basin. *Acta Geologica Hungarica* 31, 175–207.

Poliakov, A., Cundall, P., Podladchikov, Y., Lyakhovsky, V., 1993. An explicit inertial method for the simulation of viscoelastic flow: An evaluation of elastic effects on diapiric flow in two-and three-layers models, in Flow and Creep in the Solar System: Observations, Modeling and Theory, pp. 175–195, Kluwer Acad, Dordrecht, Netherlands.

Porebski, S.J., and Steel, R.J., 2003. Shelf-margin deltas: their stratigraphic significance and relation to deepwater sands. *Earth-Science Reviews* 62, 283–326.

Posamentier, H.W. and G.P. Allen, 1993. Variability of the Sequence Stratigraphic Model: Effects of Local Basin Factors, *Sedimentary Geology*, 86, 91-109.

Posamentier, H.W., Walker, R.G., 2006. Deep water turbidites and turbiditic fans, in: Posamentier, H.W., Walker, R.G. (Eds.), Facies models revisited. *Society for Sedimentary Geology* pp. 339-527.

Posgay, K., Bodoky, T., Hajnal, Z., Toth, T.M., Fancsik, T., Hegedus, E., Kovacs, A.C., Takacs, E., 2006. Interpretation of subhorizontal crustal reflections by metamorphic and rheologic effects in the eastern part of the Pannonian Basin. *Geophys. J. Int*. 167, 187–203.

Postma, G., Kleinhans, M.G., Meijer, P.T. and Eggenhuisen, J.T., 2008. Sediment transport in analogue flume models compared with real-world sedimentary systems: a new look at scaling evolution of sedimentary systems in a flume. *Sedimentology* 55, 1541–1557.

Prosser, S., 1993. Rift related depositional system and their seismic expression, in Tectonics and Seismic Sequence Stratigraphy, edited by G. D. Williams and A. Dobb, *Geol. Soc. Spec. Publ*., 71, 35–66, doi:10.1144/GSL.SP.1993.071.01.03.

Puchnerová, M., J. Šefara, V. Szalaiová, H. Tkáčová, J. Gretsch, M. Bielik, J. Kiss, and S. Kovácsvölgyi, 2002. Results of the Geophysical survey within the framework of the Triberg project, *Geologica Carpathica*, 53, Special Issue

Răbăgia, A., L. Matenco, and S. Cloetingh, 2011. The Interplay between Eustacy, Tectonics and Surface Processes During the Growth of a Fault-Related Structure as Derived from Sequence Stratigraphy: The Govora–Ocnele Mari Antiform, South Carpathians. *Tectonophysics*, 502, 196-220.

Răbăgia, A.-M., 2009. Sequential stratigraphic studies in the northern part of the Pannonian Basin for deriving the tectono-stratigraphic evolution, PhD thesis, 98 pp, Fac. of Geol. and Geophys., Univ. of Bucharest, Bucharest.

Ranalli, G., 1995. Rheology of the Earth (second edition). Chapman & Hall, London, 413 pp.

Ratschbacher, L., H. G. Linzer, F. Moser, R. O. Strusievicz, H. Bedelean, N. Har, and P. A. Mogos, 1993. Cretaceous to Miocene thrusting and wrenching along the central South Carpathians due to a corner effect during collision and orocline formation, *Tectonics*, 12, 855-873.

Ratschbacher, L., W. Frisch, H. G. Linzer, and O. Merle 1991. Lateral extrusion in the Eastern Alps; Part 2, Structural analysis, *Tectonics*, *10*, 257-271.

Ravnas, R. and R.J. Steel 1998. Architecture of Marine Rift-Basin Successions, *AAPG Bulletin*, 82, 110-146.

Rögl, F., Daxner-Höck, G., 1996. Late Miocene Paratethys Correlations. In: Bernor R.L., Fahlbusch, V., Mittmann, H-W. (eds.), The evolution of western Eurasian Neogene mammal faunas. Columbia University Press, New York, 47-55

Roure, F., E. Roca, W. Sassi, 1993. The Neogene evolution of the outer Carpathian flysch units (Poland, Ukraine and Romania): kinematics of a foreland/fold-and-thrust belt system. Sedimentary Geology 86, 177–201.

Royden, L. H., Horváth, F. (eds), 1988. The Pannonian Basin: a Case Study in Basin Evolution. *Amer. Assoc. Petr. Geol. Mem.* 45.

Royden, L. H., Dövényi, P, 1988. Variations in extensional styles at depth across the Pannonian basin system, in: Royden, L. H. and Horváth, F. (eds.): The Pannonian Basin, a Study in Basin Evolution, *Amer. Assoc. Petr. Geol. Mem*. 45, 235–255, 1988

Royden, L., and B.C., Burchfiel, 1989. Are systematic variations in thrust belt style related to plate boundary processes? (the Western Alps versus the Carpathians), *Tectonics,* 8, 51–61.

Rumpler, J., and F. Horváth, 1988. Some representative seismic reflection lines from the Pannonian basin and their structural interpretation, in L. H. Royden and F. Horváth *(Eds.)* The Pannonian Basin, a study in basin evolution, pp. 153-169.

Ruszkiczay-Rüdiger, Zs., Fodor, L., Bada, G., Leél-Össy, Sz., Horváth, E., Dunai, T.J., 2005. Quantification of Quaternary vertical movements in the central Pannonian Basin: a review of chronologic data along the Danube River, Hungary. *Tectonophysics* 410, 157–172.

Sacchi, M., Horváth, F., Magyari, O., 1999. Role of unconformity-bounded units in the stratigraphy of the continental record: A case study from the late Miocene of the western Pannonian Basin, Hungary, in The Mediterranean Basins: Extension Within the Alpine Orogen, edited by B. Durand et al., *Geol. Soc. Spec. Publ*., 156, 357–390.

Saftic, B., Velic, J., Sztanó, O., Gy, Juhász, Ivkovic, Z., 2003. Tertiary subsurface facies, source rocks and Hydrocarbon reservoirs in the SW part of the Pannonian Basin (Northern Croatia and South-Western Hungary). *Geologica Croatica* 56, 101–122.

Săndulescu, M., 1988. Cenozoic tectonic history of the Carpathians, in L. H. Royden, and F. Horváth *(Eds.)* The Pannonian Basin, a Study in Basin Evolution*, AAPG Memoir*, 45, 17–25.

Scharf, A., M. R. Handy, S. Favaro, S. M. Schmid, and A. Bertrand, 2013. Modes of orogen-parallel stretching and extensional exhumation in response to microplate indentation and roll-back subduction (Tauern Window, Eastern Alps), *International Journal of Earth Sciences*, *102*, 1627-1654.

Schefer, S., V. Cvetković, B. Fügenschuh, A. Kounov, M. Ovtcharova, U. Schaltegger, and S. Schmid, 2011. Cenozoic granitoids in the Dinarides of southern Serbia: age of intrusion, isotope geochemistry, exhumation history and significance for the geodynamic evolution of the Balkan Peninsula, *International Journal of Earth Sciences*, *100*, 1181-1206.

Schlager, W., 1993. Accommodation and supply - a dual control on stratigraphic sequences, Sedimentary Geology 86, 111-136.

Schmid, S. M., B. Fugenschuh, E. Kissling, and R. Schuster, 2004. Tectonic map and overall architecture of the Alpine orogen, *Eclogae Geologicae Hervetiae*, *97*, 92-117.

Schmid, S.M., Bernoulli, D, Fugenschuh, B., Matenco, L., Schefer, S., Schuster, R., Tischler, M., Ustaszewski, K., 2008. The Alpine–Carpathian–Dinaridic orogenic system: correlation and evolution of tectonic units. *Swiss J Geosci*. 101, 139–183.

Sclater, J. G., L. Royden, F. Horvath, B. C. Burchfiel, S. Semken, and L. Stegena, 1980. The formation of the intra-Carpathian basins as determined from subsidence data, *Earth and Planetary Science Letters*, *51*, 139-162.

Seghedi, I., L. Matenco, H. Downes, P. R. D. Mason, A. Szakács, and Z. Pécskay, 2011. Tectonic significance of changes in post-subduction Pliocene-Quaternary magmatism in the south east part of the Carpathian-Pannonian Region, *Tectonophysics*, *502*, 146-157.

Sokoutis, D., Corti, G., Bonini, M., Brun, J.P., Cloetingh, S., Mauduit, T., Manetti, P., 2007. Modeling the extension of heterogeneous hot lithosphere. *Tectonophysics* 444, 63–79. doi:10.1016/j.tecto.2007.08.012.

Steckler, M.S., Mountain, G.S., Miller K.G., Christie-Blick, N., 1999. Reconstruction of Tertiary progradation and clinoform development on the New Jersey passive margin by 2-D backstripping. *Marine Geology* 154, 399-420.

Steininger, F. F., and F. Rögl, 1984. Paleogeography and palinspastic reconstruction of the Neogene of the Mediterranean and Paratethys, *Geological Society, London, Special Publications*, *17*, 659-668.

Stojadinovic, U., L. Matenco, P. A. M. Andriessen, M. Toljić, and J. P. T. Foeken, 2013. The balance between orogenic building and subsequent extension during the Tertiary evolution of the NE Dinarides: Constraints from low-temperature thermochronology, *Global and Planetary Change*, *103*, 19-38.

Sumanovac, F., 2010. Lithosphere structure at the contact of the Adriatic microplate and the Pannonian segment based on the gravity modeling, *Tectonophysics*, 485, 94-106.

Sumanovac, F., Dudjak, D., 2016. Descending lithosphere slab beneath the Northwest Dinarides from teleseismic tomography. *J. Geodyn*. 102., 171-184.

Szafián, P. and F. Horváth 2006. Crustal structure in the Carpatho-Pannonian region: Insights from three-dimensional gravity modelling and their geodynamic significance, *International Journal of Earth Sciences*, 95, 50-67.

Szalay, Á., 1982. A rekonstrukciós szemléletű földtani kutatás lehetőségei a szénhidrogénperspektívák előrejelzésében. Kandidátusi dolgozat, Hungarian Academy of Sciences, Budapest, 146 p. (in Hungarian)

Szalay, Á., Szentgyörgyi, K., 1988. A Method for Lithogenetic Subdivision of Pannonian (s. l.) Sedimentary Rocks. in: The Pannonian Basin, a study in basin evolution, edited by L. H. Royden and F. Horvath, pp. 89-96.

Székyné Fux, V., Pap, S., Barta, I., 1985. A nyírségi Nagyecsed-I. és Komoró-I. fúrások földtani eredményei. *Földtani Közlöny* 115., 63-77.

Szepesházy, K. (1971), A Tiszantul kozepso reszenek miocen kepzodmenyei a szenhidrogenkutato melyfurasok adatai alapjan (Translated title: Miocene formations of the central Great Hungarian Plain. Inferences from well data). *Annu. Rep. Hung. Geol. Inst*. 1968, 297–325. (in Hungarian)

Sztanó, O., Magyar, I., Horváth, F., 2007. Changes of water depth in the Late Miocene Lake Pannon revisited: the end of an old legend. *Geophysical Research Abstracts*, 9, 38897836.

Sztanó, O., Sebe, K., Csillag, G., Magyar, I., 2015. Turbidites as indicators of paleotopography, Upper Miocene Lake Pannon, Western Mecsek Mountains (Hungary). *Geologica Carpathica* 66, 331-344.

Sztanó, O., Szafián P., Magyar I., Horányi A., Bada G., Hughes D.W., Hoyer, D.L., Wallis R. J., 2013. Aggradation and progradation controlled clinothems and deep-water sand delivery model in the Neogene Lake Pannon, Makó Trough, Pannonian Basin, SE Hungary. *Global and Planetary Change* 103, 149–167.

Szuromi-Korecz, A., M. Sütő-Szentai, and I. Magyar, 2004. Biostratigraphic revision of the Hód-I well: Hungary's deepest borehole failed to reach the base of the Upper Miocene Pannonian Stage. *Geologica Carpathica 55*, 475–485.

Tari, G., F. Horváth, and J. Rumpler, 1992. Styles of extension in the Pannonian basin, *Tectonophysics*, *208*, 203-219.

Tari, G., P. Dovenyi, I. Dunkl, F. Horvath, L. Lenkey, M. Ştefănescu, P. Szafian, Toth, T., 1999. Lithospheric structure of the Pannonian basin derived from seismic, gravity and geothermal data, in The Mediterranean Basins: extension within the Alpine Orogen, edited by B. Durand, L. Jolivet, F. Horvath and M. Serrane, pp. 215-250, *Geol. Soc. London Spec. Publ*. 156.

Tari, G.C., Horváth, F., 2006. Alpine evolution and hydrocarbon geology of the Pan-nonian Basin: An overview. In: Golonka, J., Picha, F.J. (Eds.), The Carphathiansand their foreland: Geology and hydrocarbon resources. *AAPG Memoir* 84,605–618.

Tašárová, A., J.C. Afonso, M. Bielik H.-J. Götze, and J. Hók, 2009. The lithospheric structure of the Western Carpathian–Pannonian Basin region based on the CELEBRATION 2000 seismic experiment and gravity modeling, *Tectonophysics*, 475, 454-469.

Teleki, P.G., R.E. Mattick and J. Kokai (Eds.), 1994, Basin Analysis in Petroleum Exploration. A case study from the Bekes basin, Hungary, *Kluwer Academic Publishers*, 330 pp, Dordecht.

ter Borgh, M., 2013. Connections between sedimentary basins during continental collision: how tectonic, surface and sedimentary processes shaped the Paratethys, PhD thesis, 212 pp, Utrecht University, Utrecht.

ter Borgh, M., Radivojević, D., Matenco, L., 2015. Constraining forcing factors and relative sea-level fluctuations in semi-enclosed basins: the Late Neogene demise of Lake Pannon, *Basin Research* doi: 10.1111/bre.12094.

ter Borgh, M., Vasiliev, I., Stoica, M., Knežević, S., Matenco, L., Krijgsman, W., Rundić, L., Cloetingh, S., 2013. The isolation of the Pannonian basin (Central Paratethys): New constraints from magnetostratigraphy and biostratigraphy, *Global & Planet. Change* 103, 99-118.

ter Voorde, M., Ravnas, R., Faerseth, R., Cloetingh, S., 1997. Tectonic modelling of the Middle Jurassic synrift stratigraphy in the Oseberg–Brage area, northern Viking Graben. *Basin Research* 9, 133–150.

Tesauro, M., Kaban, M.K., Cloetingh, S., 2009. A new thermal and rheological model of the European lithosphere. *Tectonophysics* 476, 478–495.

Tirel, C., Brun, J.P., Burov, E., 2008. Dynamics and structural development of metamorphic core complexes. *J. Geophys. Res*. 113, 215-250.

Toljić, M., L. Matenco, M. N. Ducea, U. Stojadinović, J. Milivojević, and N. Đerić, 2013. The evolution of a key segment in the Europe–Adria collision: The Fruška Gora of northern Serbia, *Global and Planetary Change*, *103*, 39-62.

Törő B., Sztanó O., Fodor L., 2012. Aljzatmorfológia és aktív deformáció által befolyásolt pannóniai lejtőépülés Észak-Somogyban. *Földtani Közlöny* 142/4, 445-468.

Tucker, G.E., Slingerland, R., 1994. Erosional dynamics, flexural isostasy and long-lived escarpments: a numerical modelling study. *J. Geophys. Res*. 10, 12, 229–243.

Tugend, J., G. Manatschal, N. J. Kusznir, E. Masini, G. Mohn, and I. Thinon, 2014. Formation and deformation of hyperextended rift systems: Insights from rift domain mapping in the Bay of Biscay-Pyrenees, *Tectonics*, *33*, 1239-1276.

Tulucan, A., 2007. Complex geological study of the Romanian sector of the Pannonian Depression with special regard to hydrocarbon accumulation, PhD thesis, pp., 220. Fac. of Geol. and Geophys., Univ. of Bucharest, Bucharest.

Ueda, K., Willett, S.D., Gerya, T., Ruh, J., 2015. Geomorphological–thermo-mechanical modeling: Application to orogenic wedge dynamics. *Tectonophysics* 659, 12–30.

Uhrin, A., Magyar, I., Sztanó, O., 2009. Effect of basement deformation on the Pannonian sedimentation of the Zala Basin, SW Hungary., *Földtani Közlöny* 139, 273-282.

Uhrin, A., Sztanó, O., 2011. Water-level changes and their effect on deepwater sand accumulation in a lacustrine system: a case study from the Late Miocene of western Pannonian Basin, Hungary. *International Journal of Earth Sciences*. dx.doi.org/10.1007/s00531-011-0741-4.

Ustaszewski, K., Herak, M., Tomljenović, B., Herak, D., Matej, S., 2014. Neotectonics of the Dinarides-Pannonian Basin transition and possible earthquake sources in the Banja Luka epicentral area, *J. Geodyn*. 82, 52–68.

Ustaszewski, K., Kounov, A. Schmid, S. M. Schaltegger, U. Krenn, E. Frank, W., Fügenschuh, B., 2010. Evolution of the Adria-Europe plate boundary in the northern Dinarides: From continent-continent collision to back-arc extension. *Tectonics* 29, TC6017, doi: 6010.1029/2010tc002668.

Ustaszewski, K., S. Schmid, B. Fügenschuh, M. Tischler, E. Kissling, and W. Spakman, 2008. A map-view restoration of the Alpine-Carpathian-Dinaridic system for the early Miocene, *Swiss, J. Geosci*. Prague, 101(0), 273–294, doi:10.1007/s00015-008-1288-7.

Uyeda, S., and H. Kanamori, 1979. Back-arc opening and the mode of subduction, *Journal of Geophysical Research*, *84*, 1049-1061.

Vail, P.R., R.M. Mitchum, K.M. Campion, V.D. Rahmanian, 1977. Seismic Stratigraphy and Global Changes of Sea Level, Part 3: Relative Changes of Sea Level from Coastal Onlap. In by C. E. Payton, (Ed.) Seismic Stratigraphy-Application to Hydrocarbon Exploration, *AAPG Memoir*, 26, 83-97.

Vakarcs, G., Vail, P. R., Tari, G., Pogácsás, Gy., Mattick, R. E., Szabó, A., 1994. Third-order Middle Miocene-Early Pliocene depositional sequences in the prograding delta complex of the Pannonian Basin, *Tectonophysics* 240, 81-106.

van Gelder, I. E., 2017. Interfering orogenic processes derived from Alps-Adria interactions, PhD thesis, 212 pp, Utrecht University, Utrecht.

van Gelder, I. E., L. Matenco, E. Willingshofer, B. Tomljenovic, P. A. M. Andriessen, M. N. Ducea, A. Beniest, and A. Gruic, 2015. The tectonic evolution of a critical segment of the Dinarides-Alps connection: Kinematic and geochronological inferences from the Medvednica Mountains, NE Croatia, *Tectonics*, 34, 1952-1978.

van Hinsbergen, D.J.J., E. Hafkenscheid, W. Spakman, J. E. Meulenkamp, and R. Wortel, 2005. Nappe stacking resulting from subduction of oceanic and continental lithosphere below Greece, *Geology*, 33, 325-328.

van Hinsbergen, D.J.J., Schmid, S.M., 2012. Map view restoration of Aegean–West Anatolian accretion and extension since the Eocene. *Tectonics*, 31, TC5005, doi: 10.1029/2012TC003132.

van Wagoner, J.C., R.M. Mitchum, K.M. Campion, and V.D. Rahmanian, 1990. Siliciclastic Sequence Stratigraphy in Well Logs, Core, and Outcrops. Siliciclastic sequence stratigraphy in well logs, core, and outcrops: concepts for highresolution correlation of time and facies, *American Association of Petroleum Geologists Methods in Exploration Series,* 7, 55 pp.

van Wees, J.-D., van Bergen, F., David, P., Nepveu, M., Beekman, F., Cloetingh, S.A.P.L., Bonte, D., 2009. Probabilistic tectonic heat flow modelling for basin maturation: assessment method and applications. *Marine and Petroleum Geology* 26, 536–551.

van Wijk, J.W., Cloetingh, S.A.P.L., 2002. Basin migration caused by slow lithospheric extension. *Earth Planet. Sci. Lett*. 198, 275-288.

Várkonyi A, Törő B, Sztanó O, Fodor L., 2013. Late Cenozoic deformation and tectonically controlled sedimentation near the Balaton zone (central Pannonian basin, Hungary). *Occasional Papers of the Geological and Geophysical Institute of Hungary*, 72–73, ISSN 2064-0293, ISBN 978-963-671-294-5

Vergés, J., and M. Fernàndez, 2012. Tethys–Atlantic interaction along the Iberia–Africa plate boundary: The Betic–Rif orogenic system, *Tectonophysics*, *579*, 144-172.

Visnovitz F., Horváth F., Fekete N., Spiess V., 2015. Strike-slip tectonics in the Pannonian Basin based on seismic surveys at Lake Balaton. *Int. J. Earth Sci*. 2273-2285.

Vissers, R. L. M., 2012. Extension in a convergent tectonic setting: a lithospheric view on the Alboran system of SW Europe, *Geologica Belgica*, *15*, 53-72.

Wernicke, B., 1985. Uniform-sense normal simple shear of the continental lithosphere, *Can. J. Earth Sci*., 22, 108–125, doi:10.1139/e85-009.

Wernicke, B., 1992. Cenozoic extensional tectonics of the U.S. Cordillera, in: B.C., B., Lipman, P.W., Zoback, M.L. (Eds.), The Cordilleran orogen: Conterminous U.S.: Boulder, Colorado. *Geological Society of America*, pp. 553-581.

Williams, S.R.J., 1987. Faulting in abyssal-plain sediments, Great Meteor East, Madeira Abyssal Plain. *Geol. Soc. Lond. Spec. Publ*. 31, 87–104.

Windhoffer, G., G. Bada, D. Nieuwland, G. Worum, F. Horvath, and S. Cloetingh, 2005. On the mechanics of basin formation in the Pannonian basin: Inferences from analogue and numerical modelling, *Tectonophysics*, *410*, 389-415.

Wortel, M.J.R., Spakman, W., 2000. Subduction and slab detachment in the Mediterranean-Carpathian region. *Science* 209, 1910-1917.

Xie, X., Heller, P.L., 2009. Plate tectonics and basin subsidence history. *GSA Bulletin* 121, 55–64. doi:10.1130/B26398.1.

Xu, S., Hao, F., Xu, C.,Wang, Y., Zou, H., Gong, C., 2015. Differential compaction faults and their implications for fluid expulsion in the northern Bozhong Sub-basin, Bohai Bay Basin, China. *Marine and Petroleum Geology* 63, 1–16.

Ziegler, P.A., Cloetingh, S., 2004. Dynamic processes controlling evolution of rifted basins. *Earth-Science Reviews* 64, 1–50.

About the author

The author of this thesis was born on January 20, 1989 in Szeged, Hungary. In 2011 he earned his Bachelor's degree in Earth Sciences, in 2013 his Master's degree in Geophysics (with Honours) from Eötvös Loránd University, Budapest, Hungary. Following his graduation he was teaching and working on his PhD project in the Department of Geophysics and Space Sciences of Eötvös Loránd University and in the Tectonics Research Group of the Department of Earth Sciences of Utrecht University since November 2013.